Synthesis, chemical kinetics, thermodynamic and structural properties of phenyl-containing beta-diketonato complexes of rhodium(I)

A dissertation submitted to meet the requirements for the degree of

Magister Scientiae

in the

Department of Chemistry
Faculty of Natural and Agricultural Science

at the

University of the Free State

By
Nomampondomise Flaurette Stuurman
(Mpondi)

Supervisor
Dr. Jeanet Conradie

Date
January 2007

Contents.

CHAPTER 3

Results and discussion. 61

CHAPTER 4

Experimental. 119

List of Abbreviations

^{1}H NMR	nuclear magnetic resonance spectroscopy
Å	angstrom
AVK	β-aminvinylketonato
b-dik 31	n-hentriacontan-14,16-dione
b-dik 33	n-tritriacontan-16,18-dione
CO	carbon monoxide or carbonyl
Cod	1,5-cyclooctadiene
D	electron donors such as CO, ethylene and dienes
DMF	dimethylformamide
Et	ethyl
Fc	ferrocene
Hacac	2,4-pentanedione, acetylacetone, ($CH_3COCH_2COCH_3$)
Hache	2-acetylcyclohexane
Hba	1-phenyl-1,3-butanedione
Hba	1-phenylbutane-1,3-dione,benzoylacetone, [$PhCOCH_2COCH_3$]
Hbab	1- phenylhexane-1,3-dione, butyrylacetophenone
Hbap	1-phenylpentane-1,3-dione, propanylacetophenone
Hbav	1-phenylheptane-1,3-dione, valerylacetophenone
Hbfcm	1-ferrocenyl-3-phenylpropane-1,3-dione, benzoylferrocenylmethane
Hbzaa	3-benzyl-2,4-pentanedione, diacetylbenzylmethame
Hcacsm	methyl(2-cyclohexylamino-1-cyclopentene-1-dithiocarboxylate).
Hdbm	1,3-diphenylprop-1,3-dione, dibenzoylmethane [$PhCOCH_2COPh$]
Hdfcm	1,3-diferrocenylpropane-1,3-dione, diferrocenoylmethane
Hfca	1-ferrocenylbutane-1,3-dione, ferrocenoylacetone
Hfca	1-ferrocenylbutane-1,3-dione, ferrocenylacetone
Hfctfa	1-ferrocenyl-4,4,4-trifluorobutane-1,3-dione, ferrocenoyltrifluoroacetone
Hhfaa	1,1,1,5,5,5-hexafluoro-2,4-pentanedione, hexafluoroacetylacetone
Htfaa	trifluoroacetylacetone
Hthdmaa	1,1,1-trifluoro-5-methyl-2,4-hexanedione
Htmhd	
i-Pr	isoprppyl
IR	infrared spectroscopy
L	one or two donor atoms of the bidentate ligand L,L'-BID
L,L'-BID	mono anionic bidentate ligand

L’	the second donor atom of the bidentate ligand L,L’-BID
$La(thd)_3$	lanthanum(III)-2,2,6,6-tetramethyl-3,5-heptandionate
M	central metal atom
Me	methyl
n-Pr	propyl
$P(OPh)_3$	triphenyl phosphate
Ph	phenyl, (C_6H_5)
pK_a	-log K_a, K_a = acid dissociation constant
PPh_3	triphenyl phosphine
$Pr(thd)_3$	praseodym (III)-2,2,6,6-tetramethyl-3,5-heptandionate
PR_3	tertiary phosphine with substituents R
t-but	tertiary butyl
THF	tetrahydrofuran
THF	tetrahydrofuran
TTA	thenoyltrifluoroacetone
UV/Vis	ultraviolet/visible spectroscopy
v(C=O)	infrared carbonyl stretching frequency
X	halogen or alkoxide
$Yb(fod)_3$	ytterbium (III)-7,7-dimethyl-1,1,1,2,2,3,3-heptafluoro-4,6-octandionate
ΔS^*	entropy of activation
ΔV^*	volume of activation

1 Introduction and Aim of Study

1.1 Introduction.

Rhodium complex compounds are one of the most widely spread industrial homogeneous catalysts for organic raw material processing. Classic examples of efficacious catalyst systems are: methanol carbonylation to give acetic acid in the presence of $[Rh(CO)_2I_2]^-$ complex (Monsato prosess),[1] alkene hydroformylation on $RhHCO(PPh_3)_2$ catalyst, hydrogenation of olefins and acetylenes with the help of $RhCl(PPh_3)_3$ (Wilkinson's catalyst)[2,] and the use of $[Rh(acac)(CO)_2]$ in the hydroformylation of olefins.[3] In the field of olefin polymerization, metal complexes with a coordinatively unsaturated Lewis acid metal centre are generally required, whereas for transformations such as the carbonylation of methanol, electron-rich metal centres are necessary to favour oxidative addition of MeI to Rh(I).[4, 5] High catalytic reactivity of these rhodium complexes is in many respects due to the nature of ligand surroundings.[6] Supported rhodium carbonyl complexes form an important class of catalysts and precursors for the preparation of different supported rhodium species.[7] Reactivity of rhodium(I) dicarbonyl complexes, and in particular, the rate of carbonyl ligand substitution, is defined by the electron state of the rhodium centre.[6] The latter ultimately depends on donor-acceptor characteristics of chelated ligand atoms bound up directly with the metallic centre.[6] Kinetic and thermodynamic studies on the octahedral rhodium(III) complexes has gained momentum. This field has also given rise to the important discovery of the photosensitivity of rhodium complexes. β-diketone complexes of Rh(I) of the type $[Rh(\beta\text{-diketone})(D)_2$ (where D are electron donors such as CO, ethylene and dienes) undergo substitution reactions with a large variety of ligands. To examine these reactions, knowledge of the relative *trans*-effect of these ligands is necessary.[8]

The unexpected discovery of the antitumor activity of *cisplatin* has opened up the 'era of inorganic cytostatics'.[9] In the search for new organometallic compounds or inorganic coordination complexes with antitumor properties, it was found that some rhodium(I) complexes, for example [Rh(acac)(cod)] (acetylacetonate-1,5-cyclooctadienerhodium(I)), showed antineoplastic activity comparable to, or ever better than that of *cisplatin*.[10, 11]

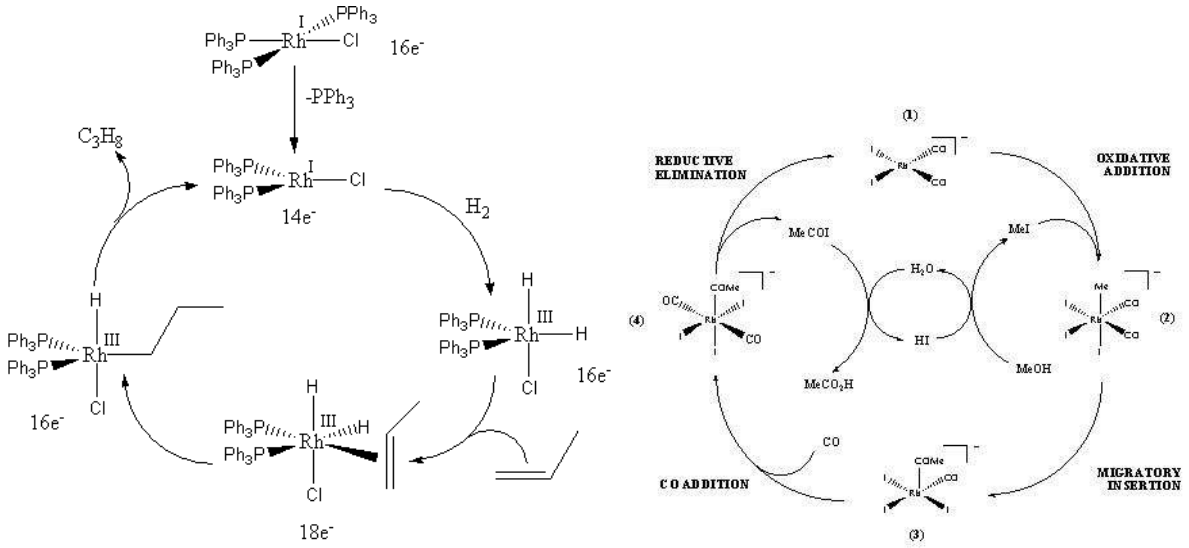

(a) **(b)**

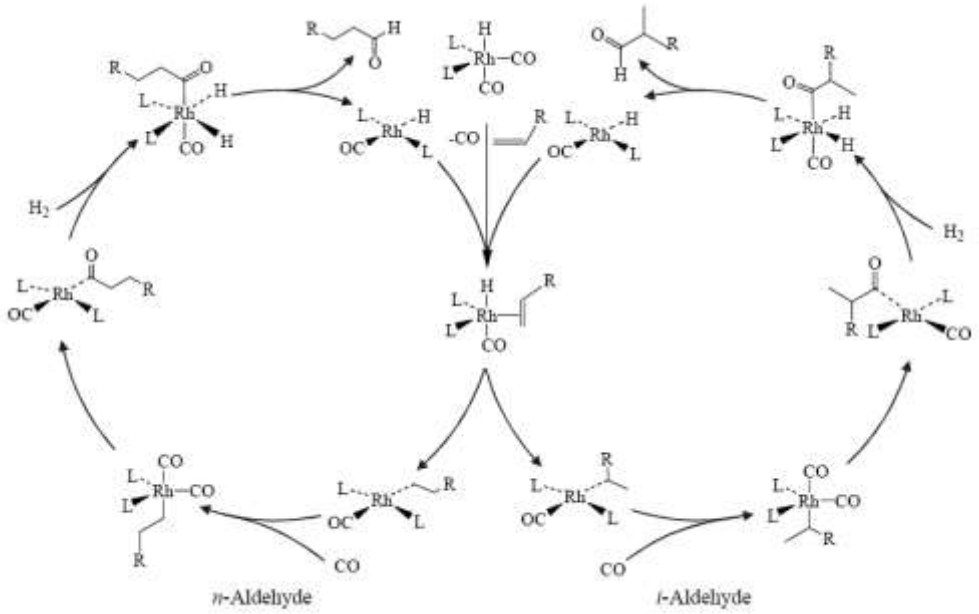

(c)

Figure 1.1: Examples of the catalytic cycles with rhodium catalyst: (a) Wilkinson's catalyst, $RhCl(PPh_3)_3$, catalyzes the hydrogenation of alkenes e.g. propylene (b) The Monsanto process for the $[Rh(CO)_2I_2]^-$ catalyst carbonylation of methanol to yield acetic acid (c) Alkene hydroformylation with $RhHCO(PPh_3)_2$ catalyst.

β-diketone compounds feature a class of important and extensively employed ligands.[12] They are very versatile and, besides the usual bidentate behaviour of monoanions, exhibit a great variety of coordination modes.[13] Equilibrium mixtures of the tautomeric keto and enol forms obtainable in β-diketones could be favoured by replacement of the terminal groups by electron-

withdrawing or electron-releasing substituents.[14] Specific stabilization, achieved by intramolecular hydrogen bonds[15] in the symmetric structure of the enol molecule, facilitates formation of a metal-ion-ligand π-bond with respect to the delocalization of the pseudo aromatic ring on the chelate ligand.[13] Along with the self-associated binary compounds[13], the bridging nature of β-diketones results in dinuclear structure complexes.[13, 16] Here, two oxygen atoms of the chelating ligand serve as the bridging donor atoms. The coordination behaviour of β-diketones also significantly influences the relative stabilities of the mixed-ligand complexes[17, 18] as well as their use in biomedicine.[19] The phenyl-containing β-diketone dibenzoylmethane (Hdbm) has been shown to exhibit antineoplastic effects in chemically induced skin and mammary cancers in several animal models.[20]

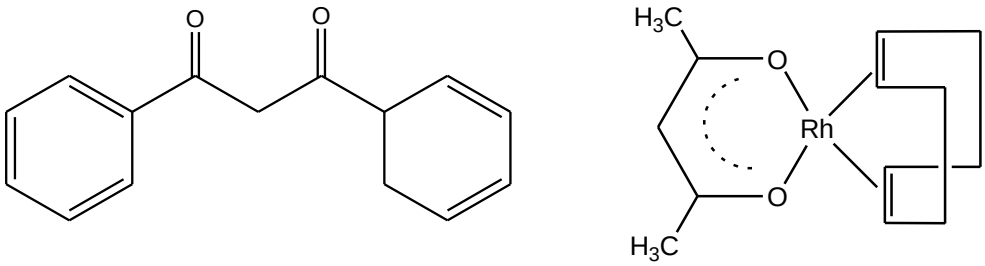

(a) **(b)**

Figure 1.2: Examples of β-diketone and rhodium- β-diketonato complexes exhibiting antineoplastic properties: (a) dibenzoylmethane (b) [Rh(acac)(cod)][21]

1.2 Aims and goals of this study.

With this exciting background the following goals were set for this study:

1. Synthesis and characterisation of β-diketonato ligands: 1-phenyl-1,3-butanedione ($C_6H_5COCH_2COCH_3$), 1-phenylpentane-1,3-dione ($C_6H_5COCH_2COCH_2CH_3$, Hbap), 1-phenylhexane-1,3-dione ($C_6H_5COCH_2COCH_2CH_2CH_3$, Hbab) and 1-phenylheptane-1,3-dione ($C_6H_5COCH_2COCH_2CH_2CH_2CH_3$, Hbav). Characterization includes pK_a value determination and the keto-enol equilibrium of the synthesised β-diketones.
2. Determination of the group electronegativity of the CH_2CH_3, $CH_2CH_2CH_3$ and $CH_2CH_2CH_2CH_3$ groups.
3. Synthesis and characterisation three new dicarbonyl rhodium(I) complexes of the type [Rh(β-diketonato)$(CO)_2$] with β-diketonato = ba (1-phenyl-1,3-butanedionato, $C_6H_5COCH_2COCH_3^-$) bap (1-phenylpentane-1,3-dione, $C_6H_5COCHCOCH_2CH_3^-$), bab (1-phenylhexane-1,3-dione, $C_6H_5COCHCOCH_2CH_2CH_3^-$) and bav (1-phenylheptane-1,3-dione, $C_6H_5COCHCOCH_2CH_2CH_2CH_3^-$). Characterization includes techniques such as IR,

NMR and the use of X-ray crystallography to determine the molecular structure of selected synthesised dicarbonyl complexes.

4. Synthesis and characterisation of 3 new triphenylphosphine mono-carbonyl complexes of rhodium(I) of the type [Rh(β-diketonato)(CO)(PPh_3)], β-diketonato = bap, bab and bav. Characterization includes techniques such as IR, NMR (^{1}H, ^{13}C and ^{31}P), determination of the thermodynamic properties of the synthesised rhodium complexes and single crystal X-ray determination of the structure all new triphenylphosphine mono-carbonyl complexes.
5. The determination of a mechanism for the oxidative addition of MeI to [Rh(β-diketonato)(CO)(PPh_3)] complexes where β-diketonato = bap, bab and bav, by means of detailed kinetic studies utilising UV, IR and ^{1}H NMR techniques.
6. The determination of the relationships (if any) between the physical quantities rate constants, pK_a-values, IR stretching frequencies, NMR data and crystallographic bond lengths and angles.

1.3 References.

[1] P. M. Maitlis, A. Haynes, G. J. Sunley, M. J. Howard. *J. Chem. Soc., Dalton Trans.* 2187 (1996).

[2] C. Masters, *Homogeneous Transition-Metal Catalysis*: A Gentle Art, Chapman&Hall, London (1981).

[3] M. G. Pedrós, A. M. Masdeu-Bultó , J. Bayardon and D. Sinou, *Catalyst Letters*, **107**, 205, (2006)

[4] V. C. Gibson, S. K. Spitzmesser. *Chem. Rev.* **103**, 283 (2003).

[5] L. Gonslavi, H. Adams, G. J. Sunley, E. Ditzel, A. Haynes. *J. Am. Chem. Soc*. **124**, 13597 (2002).

[6] E. A. Shor, A. M. Shor, V.A. Nasluzov, and A. I. Rubaylo. *J. Struct. Chem.* **46**, 220-229 (2005).

[7] G. N. Vayssilov and N. Rosch. *J. Am. Chem. Soc.* **124**, 3783-3786

[8] J. G. Leipoldt, S. S. Basson, G. J. Lamprecht, L. D. C. Bok and J. J. J. Schelebusch. *Inorg. Chim. Acta.* **40**, 43-46 (1980).

[9] P. Köpf-Maier, H. Köpf,. and E.W. Neuse,., *J. Cancer Res. Clin. Oncol.*, **108**, 336 (1984).

[10] G. Sava, S. Zorzet,, L. Perissin., G. Mestroni., G. Zassinovich and A. Bontempi,., *Inorg. Chim. Acta*, **137**, 69 (1987).

[11] T. Giraldi, G. Sava, G. Bertoli, G. Mestroni and G. Zassinovich, *Cancer Res.*, **37**, 2662 (1977).

[12] R.C. Mehrotra, R. Bohra and D.P. Gaur. *Metal β-diketoneates and allied derivatives*, Academic Press, New York (1978)

[13] S. Kawaguchi. *Coord.Chem.Rev*. **70**, 51 (1986)

[14] S. J. Eng , R. J. Motekaitis and A. E. Maetell. *Inorg.Chem.Acta* **278**, 170, (1998)

[15] S. Umetani, Y. Kawase, Q. T. H. Le and M. Matsui. *Inorg.Chim.Acta* **267**, 201, (1998).

[16] M.B. Hurthouse, M. A. Laffey, P. T. Moore, D. B. New, P. R. Raithby and P. Thornton. *J. Chem. Soc. Dalton Trans.* 307 (1982).

[17] M. Seco. *J. Chem. Educ.* **66**, 779 (1989)

[18] S.P. Sovilj, K. Babic-Samardzija and D. Stojsic. *Spectrosc. Lett.* **36**,183 (2003)

[19] T. M. Aminabhavi, N. S. Biradar and M. C. Divakar. *Inorg. Chim. Acta* **92**, 99 (1984).

[20] K. M. Jackson, M. DeLeon, C. R. Verret, W. B. Harris, Cancer Letters **178**, 161, (2002).

[21] S. T. Trzaska, H. Zheng., T. M. Swager, *Chem. Mater.* **11**, 130 (1999)

2 Literature survey and fundamental aspects.

2.1 Chemistry of β-diketones

2.1.1 Introduction.

1,3-Diketones are important intermediates not only as key building blocks for the synthesis of core heterocycles such as pyrazole,[1] isoxazole,[2] and triazole[3] in medicinal chemistry, but also as invaluable chelating ligands for various lanthanide and transition metals in material chemistry.[4]

The β-diketone dibenzoylmethane (Hdbm) has been found to be a minor constituent of licorice and sunscreens.[5] Dietary Hdbm has been reported to inhibit growth in 7,12-dimethylbenzanthracene-induced mammary tumors and lymphomas/leukemias and 7,12-tetradecanoylphorbol-13-acetate-induced skin tumors in mice.[5] K.M Jackson *et al.,*[6] reports findings of growth inhibition in prostate cancer cell lines exposed to Hdbm.

Long chain β-diketones are found to be the major class of compounds of leaf waxes of a plant named *Eucalyptus gunii*, amounting to 53% and 65% wax of the glaucous and green phenotypes respectively. The homologue range was from C31 to C37 (see **Figure 2.1)**.[7]

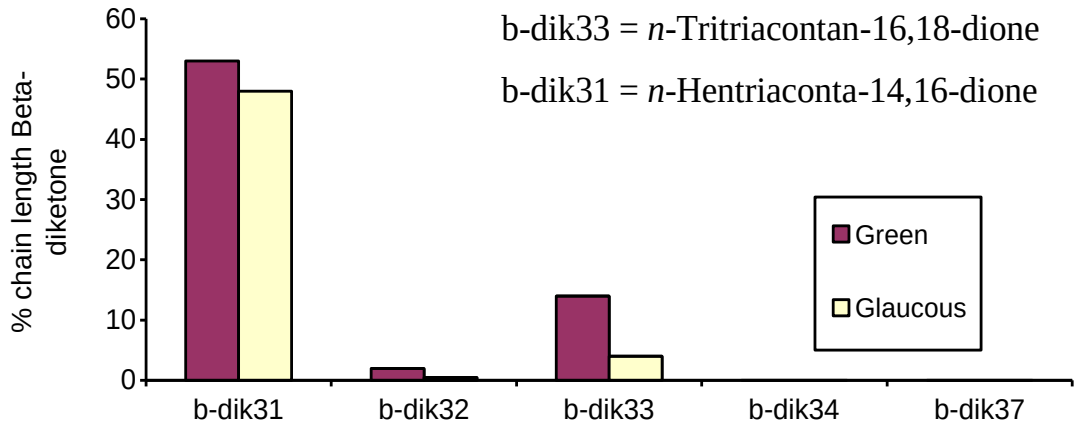

Fig. 2.1: Percentage composition (%) of β-diketones from leaf waxes of green and glaucous *Eucalyptus gunnii.* X-axis legend: the numbers on the x-axis denote carbon number of long chain β-diketone. The graph is adopted with style changes.[7]

J. A. Kenar[8] also found that long-chain β-diketone compounds are relatively common constituents of some plant waxes. The overall procedure starting from soybeans methyl esters provides a complementary approach to prepare these types of compounds.

2.1.2 Synthesis of β-diketones.

β-diketones exist in solution and in the vapour phase as mixtures of keto and enol tautomers. In the solid state, the enol form is most abunand. The methane proton in the keto form and the hydroxyl proton in the enol form of the β-diketones are acidic and their removal generates 1,3-diketonate anions which are the source of coordination compounds (**Scheme 2.1**).[9] If H in the keto compound is replaced by an alkyl or any other group, enolisation is not possible anymore. Substituents R^1, R^2 and R^3 are aliphatic or aromatic hydrocarbons. R^3 can also be H.

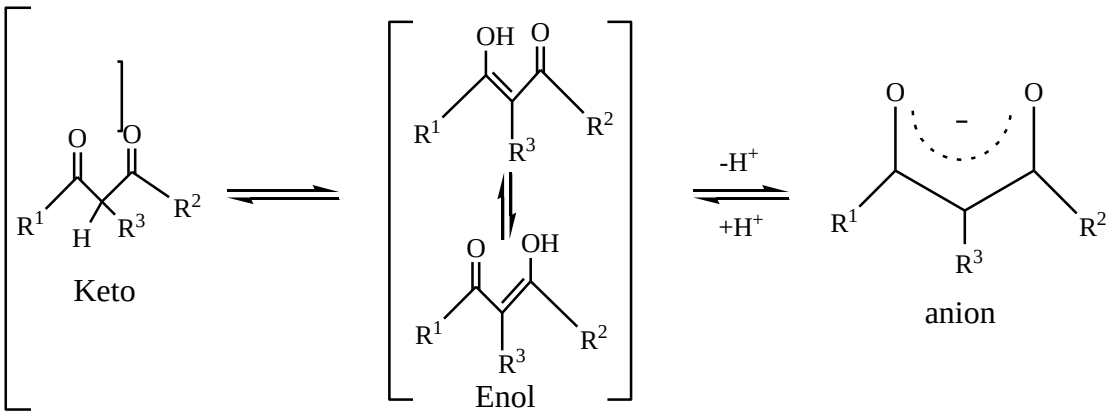

Scheme 2.1: Schematic presentation of the keto and enol tautomers of β-diketones as well as the 1,3-diketonate anion.

CHAPTER 2

Beta-diketones are normally prepared by Claisen condensation of appropriate carbonyl containing compounds. Acylation of a ketone having an α-hydrogen atom with an ester, an acid anhydride, or an acid chloride, forms a β-diketone under certain conditions.[10]

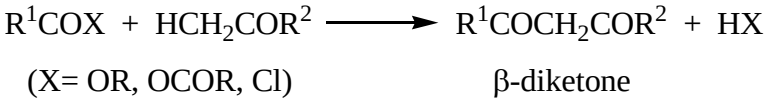

As ketones are acylated they sometimes produce the acyl derivative of an enolic form of the ketone, the O-acyl derivative which may also be rearranged thermally to give the β-diketone.[11] This process has been employed for the commercial preparation of acetylacetone.

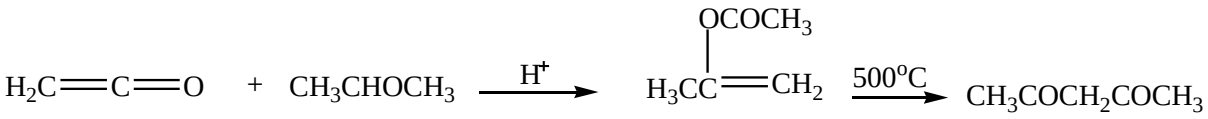

The acylation of ketones with esters has generally been accomplished by means of basic reagents such as sodium ethoxide, sodium amide or sodium hydride. Acylation may also be accomplished with acid anhydrides in the presence of an acidic reagent such as boron trifluoride. For example, the acylation of acetone with ethyl acetate and sodium ethoxide or sodium amide involves as first step the removal of an α-hydrogen (by the base) of the ketone as a proton forming acetone anion $(CH_2COCH_3)^-$, which is a hybrid of the resonance structures:

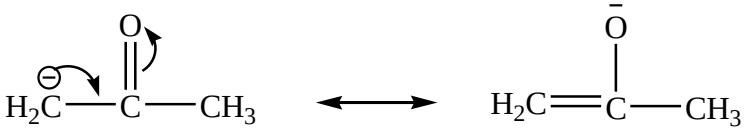

The second step may be formulated as the addition of the acetone anion to the carbonyl carbon of the ethyl acetate, accompanied by the release of ethoxide ion forming ethylacetone. The third step consists of the removal of methylenic hydrogen of the β-diketone as a proton to form the acetylacetone anion. A fourth step involves the acidification of the β-diketone.

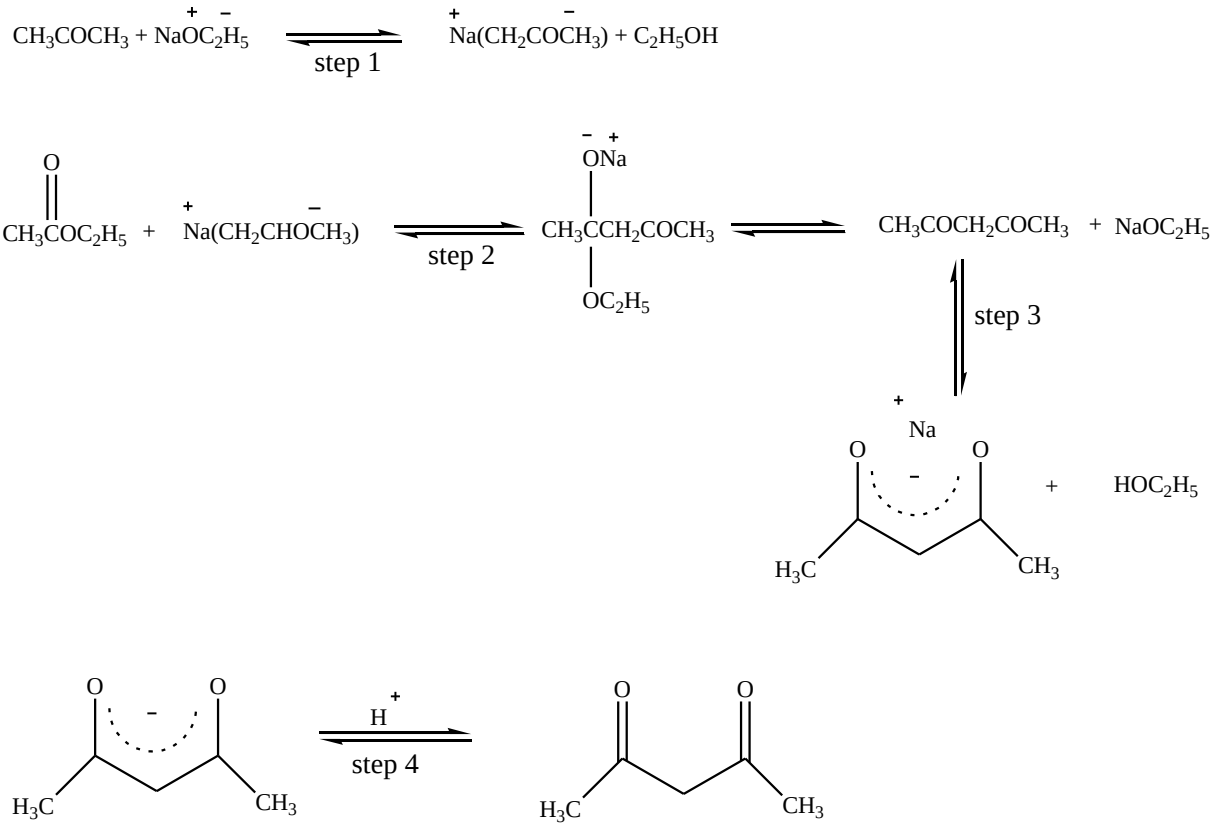

Scheme 2.2: Synthesis of β-diketone.

With the ethoxide ion, the equilibrium in the first step is probably on the side of unchanged ketone, and the third step may be considered to be normaly effected by an ethoxide ion[11]. When sodium ethoxide is used as the condensing agent, the equilibrium may be shifted futher to the right through the removal of the alcohol formed during the reaction by distillation. **Table 2.1** illustrates the yields of β-diketones formed when sodium ethoxide is used as the condensing agent[12].

Table 2.1: Yields of β-diketones from the acylation of ketones with ethyl esters in the presence of sodium ethoxide.[12]

Ethyl Ester, moles	Ketone, moles	Sodium Ethoxide, moles	β-diketone	Yield, %
Acetate, 3	Methyl isopropyl, 1	1	Isobutyrylacetone 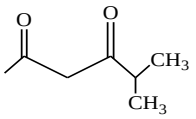	40
Acetate, 8	Methyl isobutyl, 4	4	Isovalerylacetone 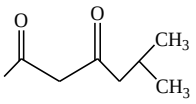	60
Acetate, 4	Acetophenone, 2	2	Benzoylacetone 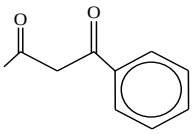	65-70
Acetate, 1.5	Acetomesitylene, 0.5	0.5	Mesitoylacetone 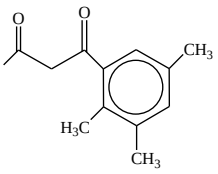	70
Acetate, 7	*p*-Phenylacetophenone, 0.5	0.5	*p*-Phenylbenzoylacetone 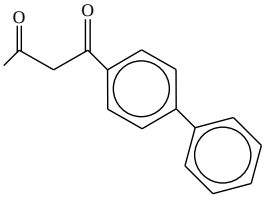	50
Furoate, 2	Acetone, 2	2	Furoylacetone 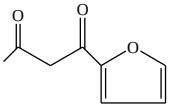	40-45
Furoate, 1	Acetophenone, 1	1	Furoylbenzoylmethane 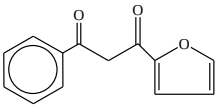	55
Tetrahydrofuroate, 0.4	Acetone, 0.4	0.4	Tetrahydrofuroylacetone 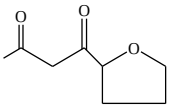	60

There are many reports on the synthesis of 1,3-diketone and its derivatives from solution chemistry,[13] but only a few routes using solid phase are known. Marzinzik *et al*[14] constructed 1,3-diketones in Wang or Rink amide resin through Claisen condensation. However, upon cleavage from solid-phase, unwanted tether such as amide or hydroxy functional group formed in the product. This unwanted functional group negatively influences the formation of β-diketone-metal complexes for various materials. Kyung-Ho and others[15] developed a traceless synthetic strategy for 1,3-diketones from solid-phase, a combination approach. A polymer supported piperazine is used as a linker for enamine acylations for example, in the synthesis of α,β unsaturated methyl ketones. The reaction is illustrated by the preliminary solution phase reaction in **Scheme 2.3** where the β-diketone **2** was obtained from *N*-methylpiperazine through its enamine intermediate **1**.[15]

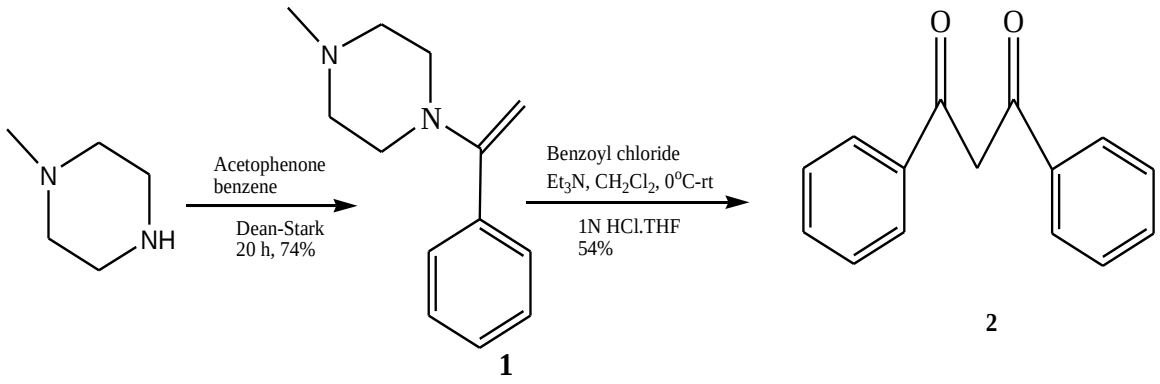

Scheme 2.3 Synthesis of a β-diketone dibenzoylmethne (DBM).

The solid-phase route, utilizing commercially available polymer bound piperazinomethylpolystyrene **3** is illustrated in **Scheme 2.4**. Several methyl ketones were succesfully attached to **3** through azeotropic dehydration to afford the polymer-bound enamine **4**. Subsequent reaction of this polymeric enamine intermediate with substituted acyl halides provided acylated enamines **5**. A hydrolysis of the polymer bound acylated enamine, afforded traceless β-diketones **6 (Scheme 2.4 and Table 2.2).**

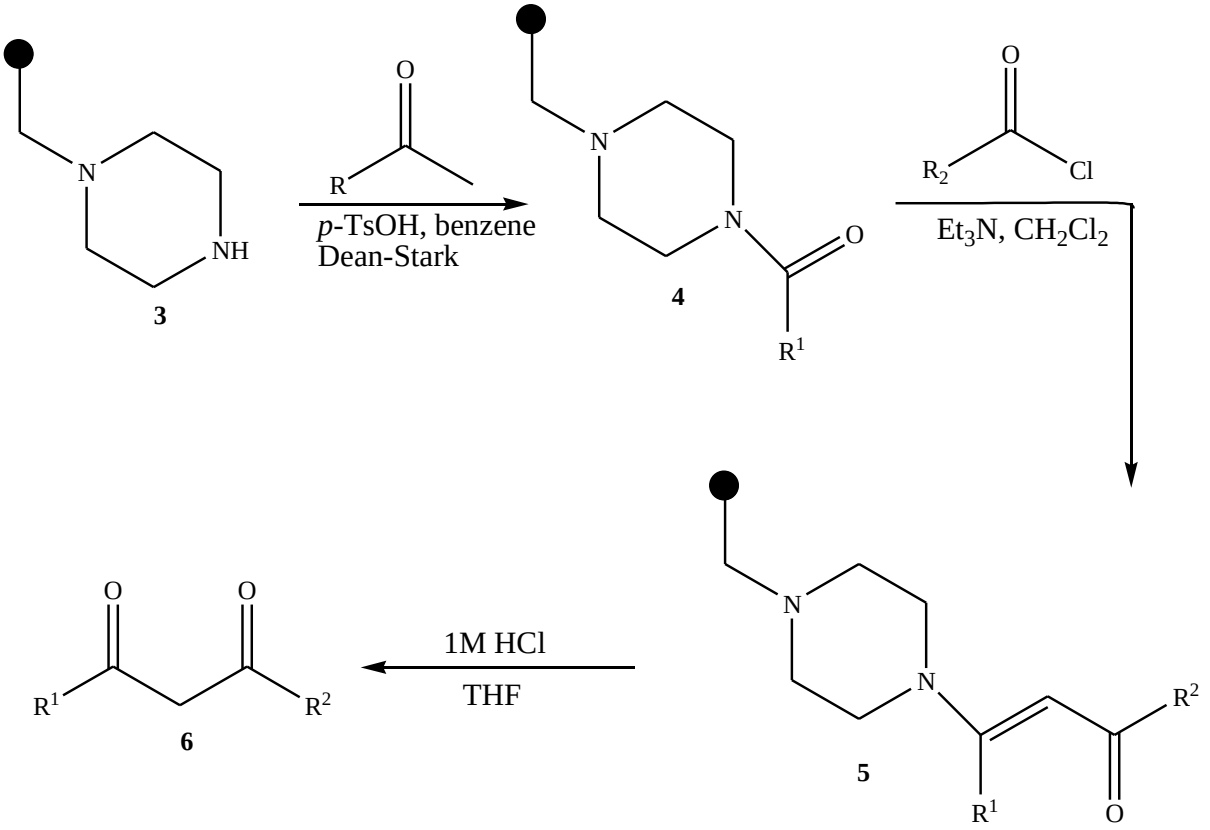

Scheme 2.4 Synthesis of a β-diketone.

The solid-phase synthesis of β-diketones of the type **11** is illustrated in **Scheme 2.5.**[15] Enamine bound resin **7**, which was made from cycloalkanones, provided polymer bound ester **9** exclusively when reacted with electron withdrawing group substituted acyl halides. The released enol ester **10** from hydrolysis of the resin **9** was quantitatively saponified (a reaction in which an ester is heated with an alkali, such as sodium hydroxide, producing a free alcohol and an acid salt, especially alkaline hydrolysis of a fat or oil to make soap) to afford the desired β-diketones **11** (**Scheme 2.5 and Table 2.2**).[15]

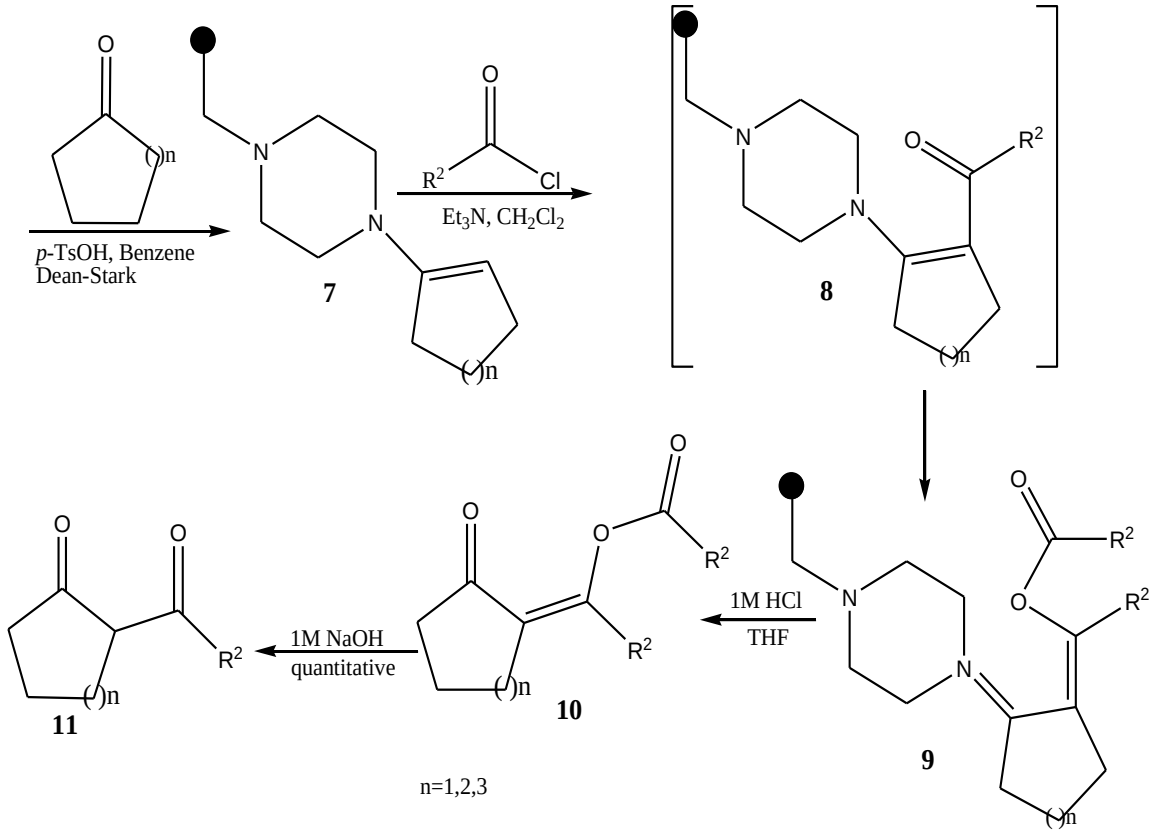

Scheme 2. 5. Synthesis of a β-diketone. n = 1, 2, 3

Table 2.2: 1,3-Diketones (6 or 11) from solid-phase synthesis.[15]

Structure	Entry	R^1 or *n*	R^2	Yield[a] (%)
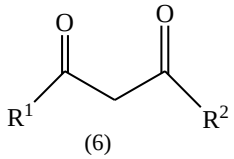 (6)	6-1	$C_6H_5^-$	$C_6H_5^-$	36
	6-2	$C_6H_5^-$	*o*-F-$C_6H_4^-$	53
	6-3	$C_6H_5^-$	*p*-CF_3- $C_6H_4^-$	40
	6-4	$C_6H_5^-$	$C_6F_5^-$	42
	6-5	*p*-CH-$C_6H_4^-$	*p*-Cl- $C_6H_4^-$	29
	6-6	*p*-F-$C_6H_4^-$	$C_6H_5^-$	38
	6-7	Biphenyl	$C_6H_5^-$	57
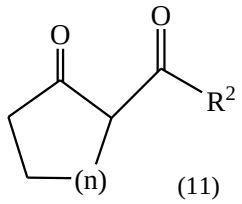 (11)	11-1	*n*=1 (Cyclopentane)	*p*-F-$C_6H_4^-$	35
	11-2	*n*=2 (Cyclohexane)	*o*-Cl- $C_6H_4^-$	66
	11-3	*n*=3 (Cycloheptane)	*p*-F-$C_6H_4^-$	50

[a]Overall yield after purification from short silica column chromatography.

2.1.3 Tautomerisation of β-diketones

2.1.3.1 Introduction

Although β-diketones are commonly represented in the ketonic form, most of them exist as keto and enol isomers, which are in equilibrium with each other. The enol isomer can exist as two tautomers. Diketonato anions are powerful chelating species and form complexes with virtually every transition and main group element.[16] Different tautomers of β-diketones may react with metal ions at quite different rates. The reactivity order generally appears to be keto < enol < enolate ion. For example, the keto form of thenoyltrifluoroacetone does not react at all, while the enol form reacts in two pathways, one independent and one inversely dependent on hydrogen ion concentration[17].

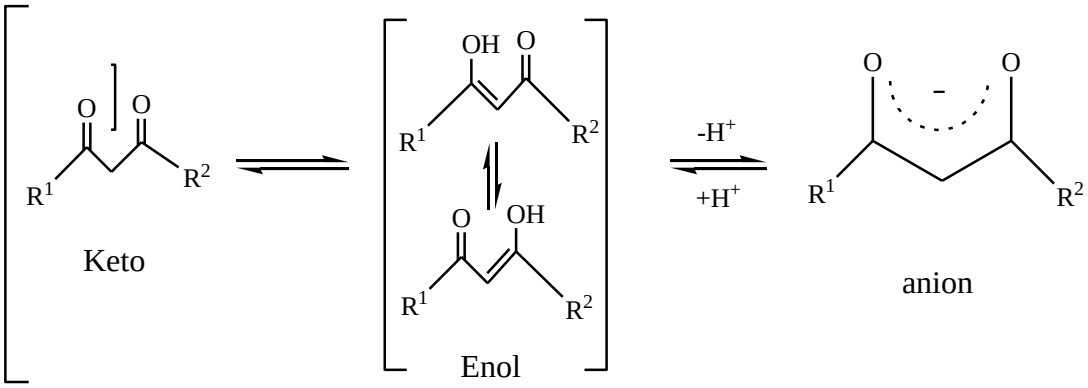

β-diketones are known to exist as two fast interchanging enolic tautomers which in addition participate in a slower keto-enol tautomerism.[18] Nuclear magnetic resonance spectroscopy (NMR), like other spectroscopic methods, provides the opportunity of investigating the tautomeric equilibrium without affecting the position of the equilibrium itself.[19]

2.1.3.2 Keto-enol tautomerism

Since the keto and enol isomers each give rise to a set of peaks in the NMR spectrum, intergration of the areas of these peaks provides a method for analysis of the mixtures without disturbing the equilibrium or requiring that either tautomer be isolated.[20] The enol form is more stable than the keto form in the gas phase, and in solution the equilibrium shifts toward the keto one as the solvent polarity increases.[21] From a ^{1}H NMR study recently performed by

Du Plessis,[22] the percentages of enolised tautomers in deuterated chloroform solutions of some β-diketones were found to be very high (> 85%)(**Table 2.3**).

Table 2.3: % enol tautomers of various β-diketones $R^1COCH_2COR^2$.

β-Dike-tone	R^1	R^2	% Enol	β-Dike-tone	R^1	R^2	% Enol
Hacac	CH_3	CH_3	91	Htmhd	$CH(CH_3)_2$	$CH(CH_3)_2$	98
Htfaa	CH_3	CF_3	>99	Hfca	Fc [(a)]	CH_3	86
Hba	CH_3	C_6H_5	92	Hfctfa	Fc	CF_3	>99
Hdbm	C_6H_5	C_6H_5	>99	Hbfcm	Fc	C_6H_5	≈95
Hhfaa	CF_3	CF_3	100	Hdfcm	Fc	Fc	>99

(a) Fc = ferrocenyl

The proportion of the enol tautomers generally increases when an electron withdrawing group, for example, fluorine, is substituted for hydrogen at an α-position relative to a carbonyl group in β-diketones, or when the ligands contain an aromatic ring.[23] Substitution by a bulky group such as an alkyl at α-position, tend to produce steric hindrance between R^3 and R^1 (or R^2) groups particularly in the enol tautomer. This, together with inductive effects of the alkyl groups often brings about a large decrease in the enol proportion.[24]

Yamabe *et al*[25] investigated the reaction path of the keto-enol tautomerism of $R^1COCH_2COR^2$, where R^1 and R^2 are H (malonaldehyde); CH_3 (acetylacetone) and OH (a dicarboxylic acid) by Density Functional Theory calculations. Results indicated that the direct proton shift from keto to enol form seem to be unlikely. The calculated (B3LYP/6-311+G(2d,p) as implemented in Gaussian 98) C-H bond energies of the keto-form of β-diketones are too high, *viz* 84.5, 87.6, and 93.0 kcal/mol, respectively. High activation energies are needed to cleave these tight C-H bond in keto form. Proton relays (reactions where a chemical species acts as both base and acid during the course of the reaction) via auxiliary (solvent) molecules were required to attain the tautomerization with small activation energies. Water clusters are known to enhance proton relays when they are bound appropriately to substrate molecules.[26] Proton relay paths of the keto-enol tautomerism via water molecules $(H_2O)_n$ n = 1 - 4 (see **Scheme 2.6**), gave much smaller activation energies than the direct proton transfer route without solvent-assistance.

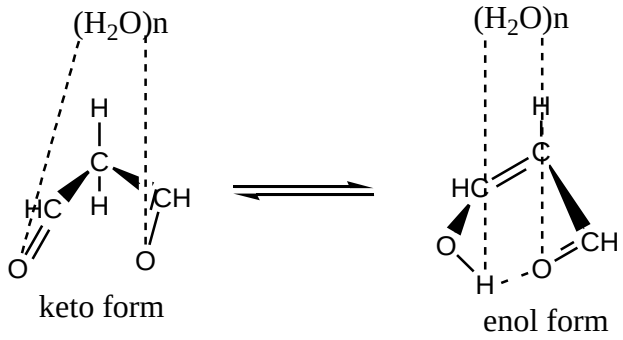

Scheme 2.6: Solvent-assisted keto-enol tautomerisation of Malonaldehyde by water molecules where n is the number of water molecules.[21]

A combination of two reactant (H_2O^{13} and H_2O^{10}) and two catalytic (H_2O^{19} and H_2O^{17}) water molecules in the above tautomerism has given a significantly nucleophilic oxygen atom (O^{10} in **Scheme 2.7 (a)**) leading to even lower activation energy for the keto-enol tautomerism, see **Scheme 2.7 (b)** for the proposed reaction model.

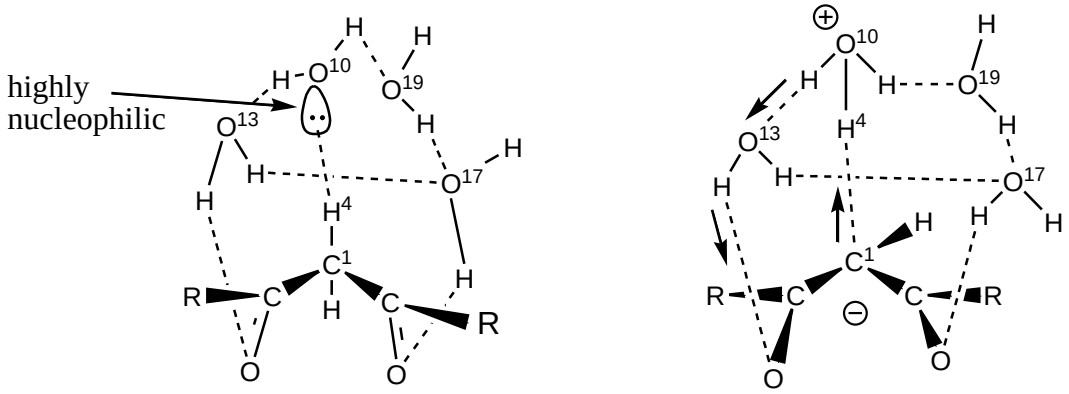

(a) keto form + $2H_2O$ + $2H_2O$ (b) a proton relay

Scheme 2.7: (a) A water tetramer makes an oxygen O^{10} highly nucleophilic. (b) A proton relay via a water dimer promoted by the ion-pair-like electronic charge distribution and a catalytic water dimer.[21]

The *cis* enol form is the consequence of proton relays along the hydrogen-bond network. The *cis* enol form can hardly contain the intramolecular hydrogen bond owing to them. This result suggests that the water content is needed for ready tautomerisation and the keto-enol tautomerization may have analogy to the E2 mechanism (**Scheme 2.8).** A C-H bond is cleaved by a nucleophile (here O^{10} in **Scheme 2.7)**. A C-C single bond is converted to a C=C double bond. The C-L heterolytic scission corresponds to conversion of the C=O bond to C-O bond. The ion-pair product ($Nu\text{-}H^+$ and L^-) in E2 mechanism is absent in the present reaction via neutralisation by proton relays.[21]

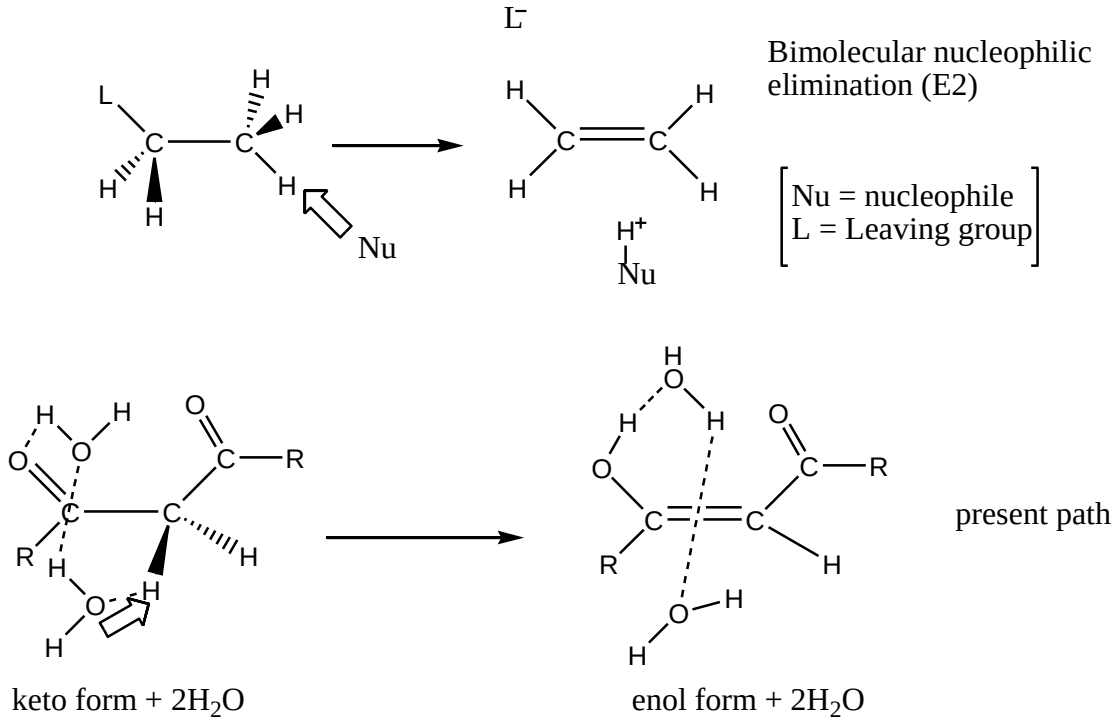

Scheme 2.8: Anology between E2 mechanism (top) and the present path (bottom) for tautomerisation.[21]

In contrast to the low enol content of monocarbonyl compounds, the enol form of the tautomeric species of 1,3-diketones sometimes predominates over the corresponding keto form. Solvent effects on the equilibrium position of these compounds are pronounced, due to the enol form which is stabilised by intramolecular O-H…O hydrogen bonds.[26]

Iglesias[27] studied the keto-enol tautomerisation of 2-acetylcyclohexanone (Hache) in water under different experimental conditions. In alkaline medium Hache undergoes rapid ionisation to give the enolate. The overall measured pK_a was 9.85. When the alkaline solution is made acidic, the enol tautomer is rapidly recovered with a yield of 100%, but subsequently the Hache enol ketonises slowly in aqueous acid medium until to reach a 57% keto content at equilibrium. Both ketonisation and enolisation are acid and general-base catalysed reactions. The base catalysis is stronger than the acid catalysis and increases with the strength of the base. Work done on Hache showed that keto-enol interconversion is a slow reaction as such detailed kinetic studies were easily done by analysing several parameters. In aprotic solvents, such as dioxane, the enolic form of Hache is the majority species, whereas in water, a mixture of both the keto and enol tautomers exists. The conversion of the enol tautomer of a β-dicarbonyl compound to its keto isomer requires the removal of hydrogen from the carbonyl oxygen and placement of hydrogen on the carbon. The reverse applies for the conversion of the keto into enol isomer. The two processes are catalysed by both acids

and bases, which fact indicates that the hydrogens move as protons in the rate-determining step.

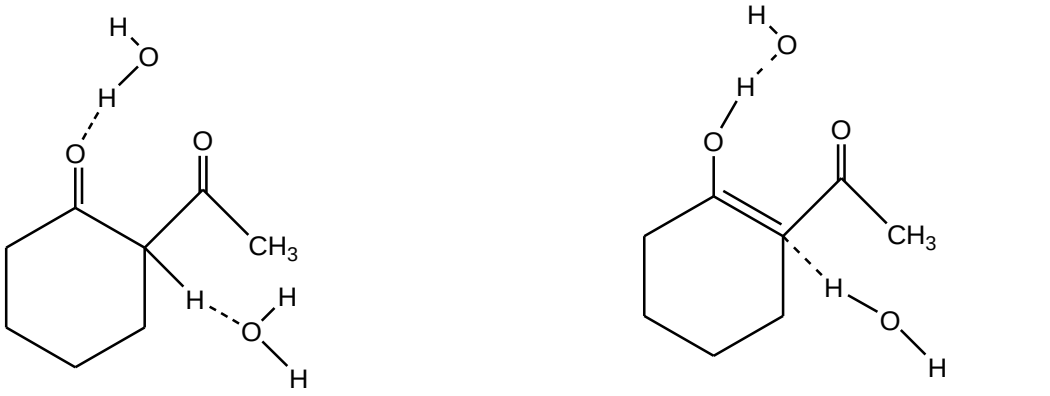

sp^3--> sp^2: keto-enolisation

sp^2--> sp^3: enol-ketolisation

Scheme 2.9: Postulated transition state for keto-enol conversion in Hache system.[27]

The reaction mechanism of keto-enolisation (**Scheme 2.10**) involves rate-determining H^+-transfer from any available acid to the β-carbon atom of the enol or its enolate ion. The general base catalysis observed (**Scheme 2.10**) in enol-ketonisation indicates that the reaction is proceeding through base ionisation of the enol in a rapid preequilibrium step followed by rate-determining carbon protonation of the enolate ion by the conjugate acid of the general base.

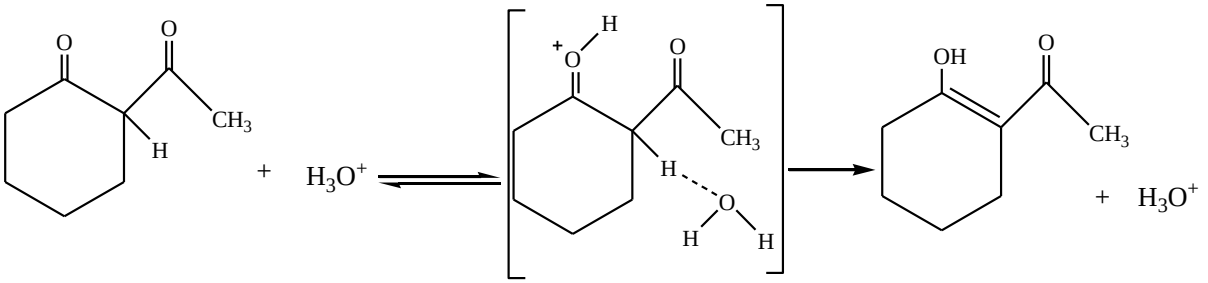

Reaction mechanism of acid-catalysed enolisation in Hache system

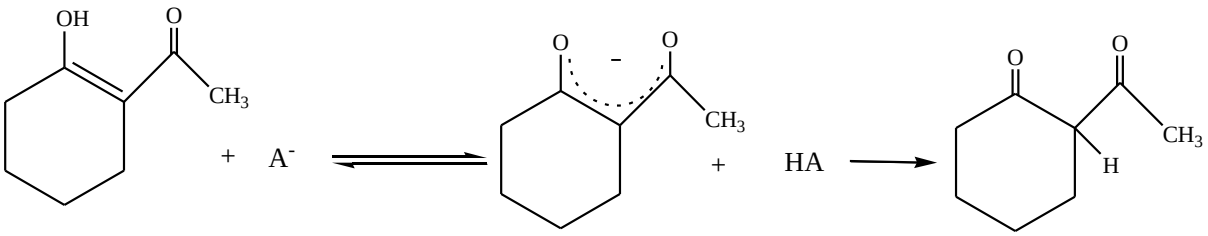

Reaction mechanism of base-catalysed enol-ketonisation in Hache system

Scheme 2.10 Synthesis of a β-diketone 2-acetylcyclohexanone (Hache)[27]

2.1.3.3 Enol-enol tautomerisation

^{1}H, ^{13}C and ^{17}O NMR chemical shifts are seen for the keto and enol forms. The *trans*-enolic form is rarely observed, as the *cis*-enolic form is more stable owing to the presence of an intramolecular hydrogen bond. The NMR spectra of the *cis*-enolic tautomer is a weighted average of the two *cis*-enolic forms (**Scheme 2.11**).

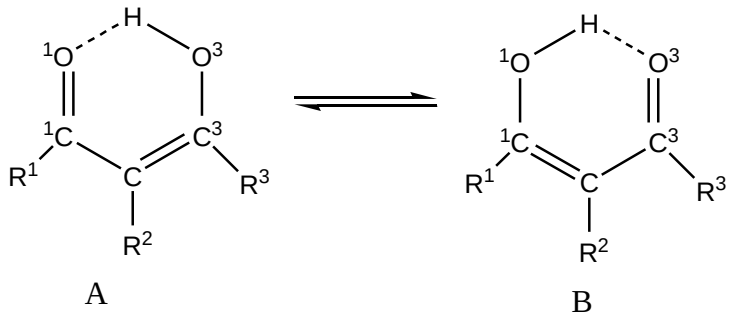

Scheme 2.11: Tautomerism of enolic β-diketones.[28]

Carbon chemical shifts show that the β-carbon primarily on the enolic form generally moves to low frequency and the β-carbon primarily on the carbonyl form moves to higher frequency when the temperature is lowered. This means that the tautomeric equilibrium is shifted further in the direction of the form most stable at room temperature.[28] Equilibrium distribution of the cis-enolic tautomer of β-diketones can be determined by means of deuterium isotope effect on ^{13}C nuclear shielding and $\delta(O^{1}H)$. ^{13}C chemical shifts for non-symmetrical β-diketones show a linear change as a function of temperature for enolic β-diketones $R^{1}COCHR^{2}COR^{3}$, R^{1}=Me, Et, iPr, t-But, Ph, C_3F_7. R^2 and R^3 are $(CH_2)_n$ for cyclic compounds, for open compounds R^{1}=H and R^{2}=Me, Et, n-Pr, t-But.[28]

Recently, two driving forces, the electronic and the resonance driving force, determining the preferred enol isomer of a β-diketone in solution, were defined.[22] Regarding Hfca (1-ferrocenylbutane-1,3-dione, see **Table 2.3**), the apparent absence of more than one set of signals in ^{1}H NMR for the ferrocenenyl substituent as well as the two observed signals for the methyl side group indicate that, as in the solid state,[29] enolisation in solution is predominantly away from the aromatic ferrocenyl group, (see **Scheme 2.12**).[22] Electronic consideration in terms of electronegativity, χ (χ_{methyl} = 2.34, $\chi_{ferrocenyl}$ = 1.87) favour **I** as the enol form of Hfca. However, structure **II** was shown by crystallography[30] and NMR spectroscopy[22] to be

dominant, implying that the equilibrium between **I** and **II** lies far to the right. A dihedral angle of $4.9(2)^0$ between the aromatic ferrocenyl group and the pseudo-aromatic β-diketone core suggests that the energy lowering conical forms such as **IV** make a noticeable contribution to the overall existence of Hfca. For clarity, the ferrocenyl group in **II** and **IV** is shown just in canonical forms but in both cases the iron atom can be bound to any of the five cyclopentadienyl carbon atoms as indicated in **I**. Likewise, the positive charge of **IV** is not confined to the single position shown, but rather oscillates between C(2) and C(5) (it cannot be on C(1). Atom numbers are indicated to individual atoms) to give rise to four different canonical forms shortly indicated as in **III** (**Scheme 2.12**). This solution behaviour is also observed for other β-diketones.[31]

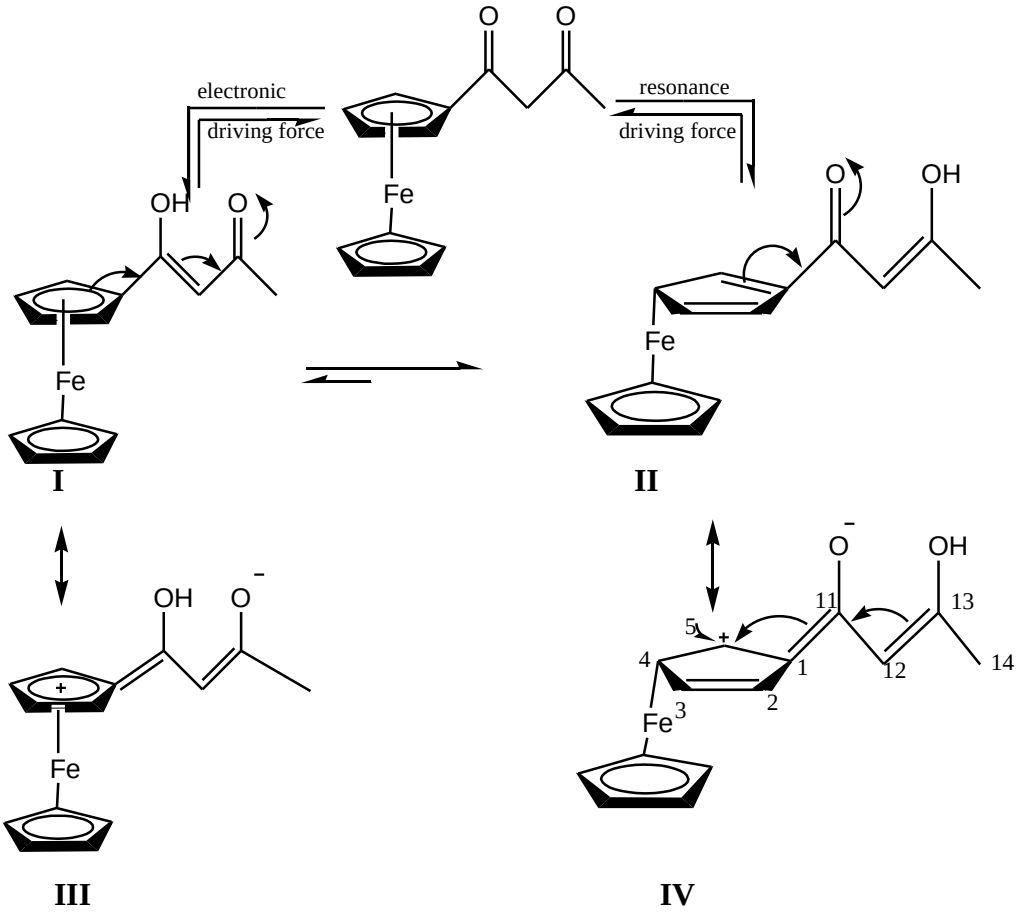

Scheme 2.12: The two driving forces, electronic and resonance, determining the preferred enol isomer of a β-diketone where aromatic side groups are present.

Enolisation for Hbfcm (1-ferrocenyl-3-phenylpropane-1,3-dione) in solution, predominantly took place towards the phenyl group as demonstrated by two distinct sets of ^{1}H NMR signals for the phenyl group *versus* the single set of signals for the ferrocenyl group. In the case of 1-

phenylbutane-1,3-dione (benzoylacetone, Hba), the lack of more than one set of phenyl ^{1}H NMR signals and two methyl signals indicate enolisation in solution took place in the direction away from the aromatic phenyl group. In order to explain the dominance of the observed enol isomer in each case, two different driving forces that control the conversion from β-diketone into an enolic isomer may be defined namely an electronic and a resonance driving force. The electronic driving force in which the formation of the preferred enol isomer is controlled by the electronegativity of the R^1 and R^2 substituents in the β-diketone $R^1COCH_2COR^2$. When the electronegativity of R^1 is greater than that of R^2 the carbon atom of the carbonyl group adjacent to R^2 will be less positive in character than the carbon atom of the other carbonyl group. Consequently, from an electronic point of view, the dominant enol isomer should be $R^1COCH=C(OH)R^2$. If the documented group electronegativities are correct, from the viewpoint of an electronic driving force as just described, only Hba of all the β-diketones just discussed exhibits the expected dominant enol isomer. For all the other β-diketones, Hfca and Hbfcm one would expect from an electronic point of view enolisation to take place predominantly in the direction of the aromatic substituent.[22]

Clearly there is a different driving force other than the suggested electronic driving force that determines the observed preferred enol configuration in β-diketones where aromatic side groups are present. To explain this observation the existence of the second driving force, the resonance driving force implies that the formation of different canonical forms of a specific isomer with low enough energy allow it to dominate over the existence of other isomers.[32]

2.1.4 pK_a

Acidity parameter, pK_a is of utmost importance to predict physiochemical, material, and biological properties of individual members of a congeneric series of compounds. Specifically, pharmacokinetics and toxicity (ADMET: absorption, distribution, metabolism, excretion, toxicity) of xenobiotics depend on their pK_a.[33] pH-metric titrations and spectrophotometric analysis are routinely used for pK_a determination.[34]

The acid dissociation constant, pK_a, characterises the charge state of an analyte at particular pH of its environment. For many compounds sparingly soluble in water, the determination of

pK_a in aqueous solution can be problematic and this is overcome by using an organic solvent or a mixed-solvent.[35] Wiczling *et.al.*[35] used reversed-phase high-performance chromatography to overcome the said problem for the determination of pK_a.

pK_a is mathematicaly defined from

$$HA \overset{K_a}{\rightleftharpoons} H^+ + A$$

where $K_a = \dfrac{[H^+][A^-]}{[HA]}$

$$pK_a = -\log K_a = \log\left(\frac{[HA]}{[A^-]}\right) - \log H^+ = \log\left(\frac{[HA]}{[A^-]}\right) + pH$$

Because this dissociation constant differs for each acid and varies over many degrees of magnitude, the acidity constant is often represented by the additive inverse of its common logarithm, represented by the symbol pK_a.

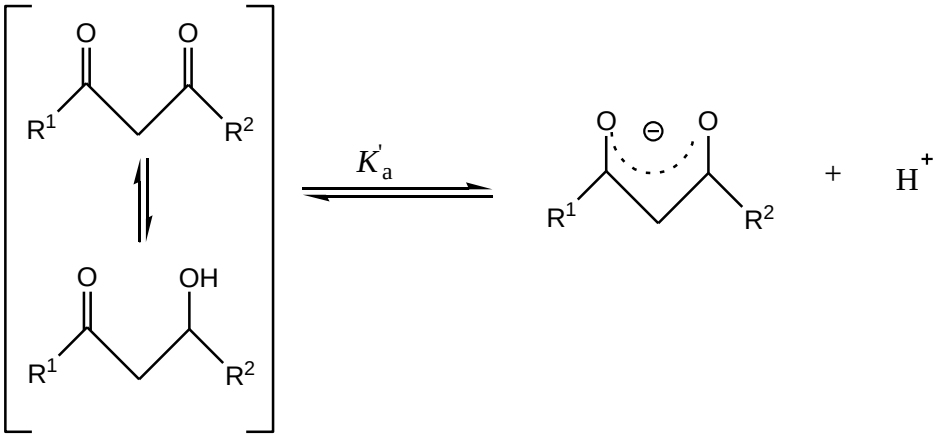

In the above reaction the concentration-based equilibrium constant $K_a^{/}$ is used commonly indicated by the addition of a prime mark[36] and also refers to the conjugated keto-enol system. The term "apparent" pK_a is used in this case since no attempt is made to partition the experimentally obtained p$K_a^{/}$ value between separate pK_a values for the enol and the keto tautomers. Observed p$K_a^{/}$ values for several β-diketones are listed in **Table2.4**.

Table2.4: pK_a' values of various β-diketones.

β-Dike-tones	**R^1**	**R^2**	**pK_a' (a)**	**β-Dike-tones**	**R^1**	**R^2**	**pK_a' (a)**
Hacac	CH_3	CH_3	8.95	Htmhd	$CH(CH_3)_2$	$CH(CH_3)_2$	11.77
Htfaa	CH_3	CF_3	6.30	Hfca	Fc	CH_3	10.01
Hba	CH_3	C_6H_5	8.55	Hfctfa	Fc	CF_3	6.53
Hdbm	C_6H_5	C_6H_5	9.35	Hbfcm	Fc	C_6H_5	10.41
Hhfaa	CF_3	CF_3	4.43	Hdfcm	Fc	Fc	13.1

(a) pK_a' values from reference37, 22 (ferrocene-containing β-diketones) and 38 (Hhfaa).

pK_a' values of the β-diketones can be obtained from a least-squares fit of UV absorbance/pH data using equation (**1**).[32]

$$A_T = \frac{A_{HA}10^{-pH} + A_A 10^{-pK'_a}}{10^{-pH} + 10^{-pK'_a}} \quad \text{.....(1)}$$

A_T = total absorbance, A_{HA} = the absorbance of the β-diketone in the protonated form, and A_A = the absorbance of the deprotonated (basic) form.[32]

2.2 Metal β-diketonato complexes

2.2.1 Introduction

The coordination chemistry of metal β-diketones has been studied extensively.[39] Metal complexes of β-diketones have been used as fuel additives,[40] as supercritical fluids for waste cleanup,[41] in superconducting thin film manufacturing,[42] and in production of homogeneous and heterogeneous catalysts.[43]

Lanthanide β-diketone complexes have long been known to give bright emission under UV irradiation because of the effective energy transfer from ligands to central ions called antenna effect. These complexes have been found in some applications such as optical devices, luminescence probes in biomedical assays, luminescence sensors for chemical species, fluorescent lighting and electroluminescent devices, particularly europium and terbium β-diketone complexes due to their high fluorescence efficiency. Their general synthesis is also

by Claisen condensation in the presence of sodium ethoxide.[44] Lanthanide elements, in their complexes with β-diketones, tend to adopt interesting higher coordination geometries. These compounds frequently crystallize as hydrates from which water removal without decomposition of the compound is difficult.[45]

β-Diketone complexes of transition metals have been the subject for different studies and application ranging from synthetic[46], kinetic[47] and structural[48] topics to catalyses[49] and others.[50] They are classified based on the mode of binding between the ligand and metal cation. The β-diketones may be bonded to the metal through the oxygen, carbon, both carbon and oxygen, and through the olefinic bond. The difference in the affinity of the metal for carbon or for oxygen is the main factor that determines the formation of different types of metal β-diketonato complexes.[51]

The use of β-diketonate chelate complexes of scandium, yttrium, and some f-block elements in effectively scrubbing H_2S from a gas stream has been described. Example of compounds used are lanthanum(III)-2,2,6,6-tetramethyl-3,5-heptandionate ($La(thd)_3$), praseodym (III)-2,2,6,6-tetramethyl-3,5-heptandionate ($Pr(thd)_3$), ytterbium (III)-7,7-dimethyl-1,1,1,2,2,3,3-heptafluoro-4,6-octandionate ($Yb(fod)_3$), or blends thereof.[52]

S. Peter[52] says that iron β-diketonate complexes are possible catalysts in hydrodesulfurization from a sour gas steam, and these complexes are possibly resistant to radical attack, which causes oxidative degradation in redox catalysts.

2.2.2 Chemistry of metal β-diketonato complexes

Specific properties such as colour, paramagnetism, electric conductivity, etc, can be obtained more easily in metal-organic complexes than in purely organic compounds.[53] Furthermore, other molecular properties such as polarizability or hyperpolarizability can be enhanced by the presence of metals.[53]

β-diketonato complexes of the first-row transition metals are of interest as structural archetypes and because of the tendency of compounds containing elements on the right-hand side of the periodic table to adopt originally unanticipated oligomeric structures so that, by

means of oxygen-bridging diketonate ligands, the central metal atom achieves a coordination number greater than or equal to four. Complexes of metals at each end of the first row are mononuclear.[45]

The simplest and most generally useful synthetic method suggested for metal diketonates is from the diketone and a metal in a variety of solvents such as water, alcohol, carbon tetrachloride or neat diketone. Since many β-diketones are poorly soluble in water, use of an organic solvent or co-solvent is seen helpful. Optionally, a base such as sodium carbonate, triethylamine or urea may be added. Addition of a base early in the reaction converts the diketone to its conjugate base, which is more reactive and usually has greater solubility in aqueous media.[54]

Metal alkoxides constitute a useful class of starting materials for the synthesis of the metal β-diketonates.[45] Similar reactions with lanthanide alkoxides, however, provide pure, unsolvated lanthanide tris(diketonates). The virtue of such synthesis lies in their ability to yield anhydrous diketonate complexes. Removal of water from the hydrates without decomposition is sometimes difficult.[55]

Electrophilic substitution at the methane carbon atom (C-3) of β-diketonates is, in many cases, a facile reaction.

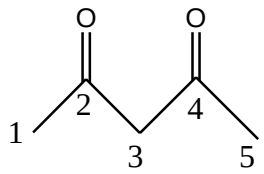

The process is of interest as a synthetic method for new diketonate complexes as well as from a mechanistic standpoint, for it is considered that such reaction imply, by their similarity to aromatic substitutions, significant bond delocalization in the C_3O_2M ring (M=metal).

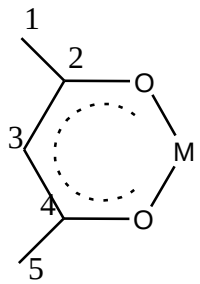

Much exploratory work has been carried out with acetylacetonates; the $PhCOCH_2COMe$ and $PhCOCH_2COPh$ analogues which, in general react more sluggishly, an effect attributed to steric hindrance.[45]

Hydrolysis of metal β-diketone complexes is usually just the reverse of the preparative reaction but detailed study of such processes provides considerable insight into the mechanisms of inorganic substitution reactions.[45]

2.3 Rhodium complexes

2.3.1 Introduction

Rhodium chemistry was opened up by the discovery of the remarkable catalytic properties of $[RhCl(PPh_3)_3]$. The facile changes of oxidation state exhibited by rhodium complex catalysts pointed the way to the employment of rhodium complexes in the photochemical decomposition of water. Apart from catalytic reactions in organic and industrial chemistry there are few practical applications of rhodium complexes. Some interest has been shown in the use of rhodium(II) carboxylates in chemotherapy.[56]

A new field of potential application of both β-diketone complexes of rhodium(I) and derivatives of ferrocene, *e.g.* [Rh(acac)(cod)] (acac = acetylacetone, cod = 1,5-cyclooctadiene) has evolved in recent years with reports that some of these compounds show appreciable antineoplastic activity.[56]

2.3.2 Square-planar rhodium complexes

A variety of neutral, air stable, crystalline dicarbonyl complexes containing the anion of a β-diketone have been prepared by treatment of $[\{RhCl(CO)_2\}_2]$ with the β-diketone in the presence of a base such as $BaCO_3$, as shown in **Scheme 2.13.** Alternatively these dicarbonyl complexes can be synthesized directly by heating $[RhCl_3]$ and a β-diketone in DMF.[57]

These dicarbonyls are usually dichroic, with colours varying with the β-diketone substituents. These compounds react rapidly with PPh_3 or $AsPh_3$ with displacement of one CO ligand to afford the monocarbonyls.[57,58,59,60]

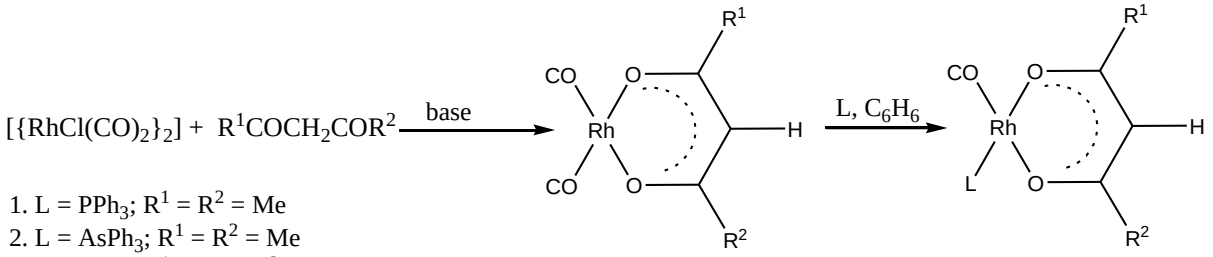

1. L = PPh_3; $R^1 = R^2$ = Me
2. L = $AsPh_3$; $R^1 = R^2$ = Me
3. L = PPh_3; $R^1 = CF_3$; R^2 = 2-thienyl

Scheme 2.13: Synthesis of dicarbonyl complexes and the displacement of one CO ligand to afford monocarbonyls.

The X-ray crystal structures of compounds **1**[61], and **3**[59] show them to be square planar complexes. Electron impact spectral studies of the above dicarbonyls have demonstrated an increase in ionization potential on changing the Me to CF_3 or Ph groups on the β-diketonate ligand.[62]

Long-chain β-diketones can be widely used as organic ligands in mesogenic (properties of liquid crystals) coordination complexes of most transition metal ions.[62] Since the metal ion of the β-diketone complexes is mostly situated at the center of the molecules, such molecules always have central symmetry. Terminal metal ions have good conjugation structures, and great dipole moments, both factors beneficial to the improvement of the mesogenic properties. An example of a series of Y-substituted β-diketonato dicarbonylrhodium (I) complexes with mesomorphic properties is given in **Scheme 2.14.**[63]

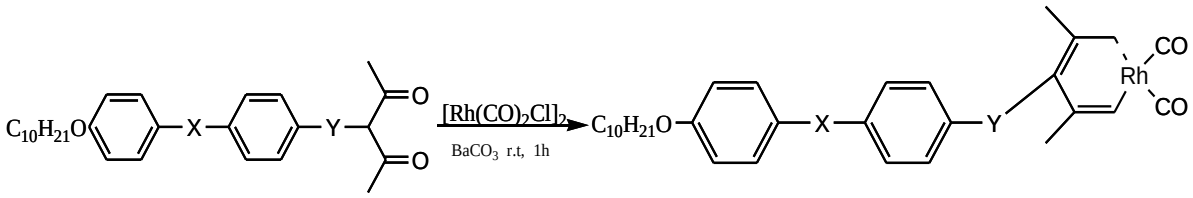

1. X = -CH=CHCOO- and Y = -COO-
2. X = -CH=CHCOO and Y = -CH=CHCOO
3. X = -COO- and Y = -CH=CHCOO
4. X = -CH_2O- and Y = -COO-
5 X = -N=N- and Y = -COO-

Scheme 2.14: Synthesis of β-diketonato dicarbonylrhodium (I) complexes with mesomorphic properties.

Two factors may be attributed to this mesomorphic (intermediate state between liquid and crystal) behaviour: (i) the chelating ring of the β-diketone complexes is not only a six-membered conjugation structure but also planar because of its aromaticity, which may enhance the rigidity and extend the conjugated system of the complexes; and (ii) the terminal carbon monoxides in the complexes are strong ligands which can be easily coordinated with the metal rhodium(I) by the d-π and π- π^* interaction.[63]

β-diketone complexes of Rh(I) of the type [Rh(β-diketone)$(CO)_2$] undergo substitution reactions with a large variety of ligands. To examine these reactions, knowledge of the relative thermodynamic *trans*-influence of the different ligands is necessary.[64] The *trans*-influence of a ligand is the influence on the metal-ligand bond strength and thus also on the bond lengths trans to it.[61] Consequently the group trans to the ligand with the largest trans influence, will be substituted.

In Rh(I) complexes of the type [Rh(bidentate ligand)$(CO)_2$], the most electronegative atom of the chelate ring has the smallest *trans* influence. In the case of two identical atoms (like the oxygen atoms of β-diketones) the atom nearest to the strongest electron attracting group has the smallest *trans* influence. These results are in agreement with the polarization theory and the σ-*trans* effect since the most electronegative atom (or in the case of β-diketones the oxygen atom nearest to the most electronegative group) will be the least polarizable and also a weaker σ-donor.[65]

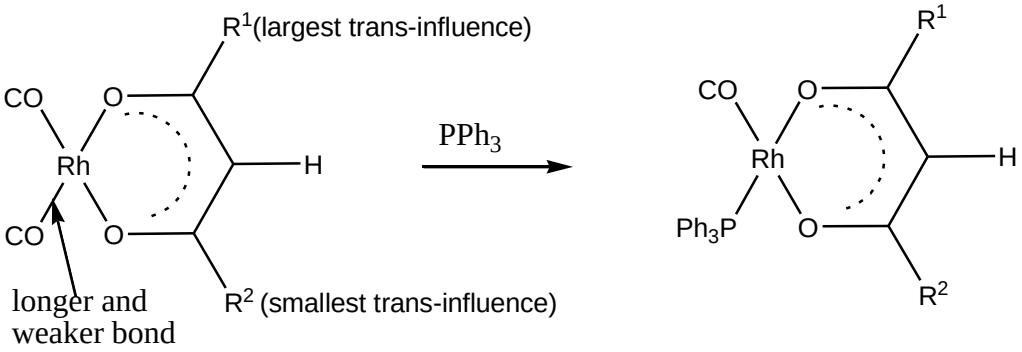

R^2 more electronegative than R^1

The crystal structure determination of [Rh(TTA)(CO)(PPh_3)], prepared by the reaction between [Rh(TTA)$(CO)_2$] and triphenylphosphine, PPh_3,[57] showed that the carbonyl group *trans* to the oxygen atom nearest to the thenoyl group has been displaced, (TTA = thenoyltrifluoroacetone).[59]

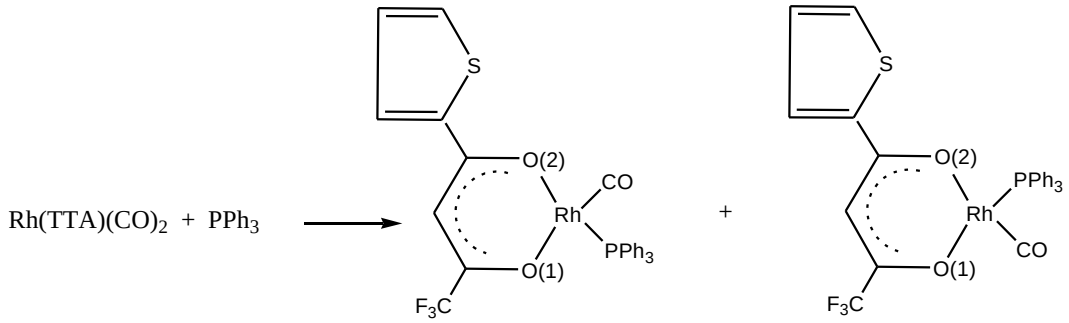

Scheme 2.15: Synthesis of [Rh(TTA)(CO)(PPh$_3$)]

According to this result O(2), (**Scheme 2.15**) has a larger *trans* influence than O(1). This is in agreement with the polarization theory since the oxygen atom nearest to the CF_3-group will be least polarizable as a result of the electron-attracting power of the CF_3-group.[60]

X-ray structural analysis of the monocarbonyl complexes obtained in the solid state and studied by a number of researchers[66,60 ,67 ,68] showed that if monocharged bidentate ligands contains donor atoms O,N or O,S, the phosphine replaces the carbonyl *trans* to either the nitrogen or sulphur atom respectively.[67] These results can be explained in terms of the stronger *trans* influence of the N and S atoms compared to that of the O atom.

Another obvious way to distinguish between the thermodynamic *trans* influence of two bonded atoms is to determine the bond distance of the atoms *trans* to these atoms. When the chelating ligand such as β-diketone is symmetrical like acetylacetone (acac), the bonds *trans* to the chelating ligand group should be chemically equivalent as was confirmed by the structure determination of [Rh(acac)(CO)$_2$] where the two Rh-O and the two Rh-C bond lengths were the same, within experimental error: 2.044(4) and 2.040(4) respectively. If one of the CO groups is substituted by PPh_3 as in Rh(acac)(CO)(PPh_3), the Rh-O bond *trans* PPh_3 lengthens to 2.087(4)Å while the bond length *trans* to the CO group shortens to 2.029(5) Å. This result indicates that PPh_3 has a larger *trans* influence than CO.[69]

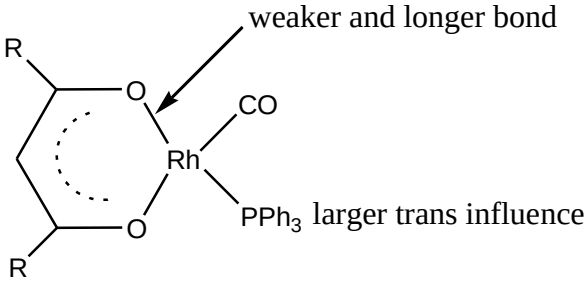

In summary the trans influence in complexes of the type [Rh(R^1COCHCOR)(CO)(PPh_3)] is a function of:

i) The relative influence of PPh_3 and CO on (R^1COCHCOR) and

ii) the relative influence of R and R^1 on the Rh-P bond length.

In cases where there is a relatively small difference in the bonding capability of the two donor atoms, the electronic effect giving rise to the trans influence, may be dominated by steric interactions, *i.e.* large substituents on the bidentate ligand backbone.[60,67,68] ^{31}P and ^{13}C NMR studies showed that the reaction between the β-aminvinylketonatodicarbonylrhodium (I) complexes, [Rh(AVK)$(CO)_2$], and triphenylphosphine in benzene and chloroform yields in the solution two [Rh(AVK)(PPh_3)(CO)] isomers in a ~10:1 ratio for P-*trans*-N and P-*trans*-O respectively.[66] The crystal-structure of [Rh(ba)(PPh_3)(CO)] showed that both the trans and cis isomers crystallised in the same unit cell.

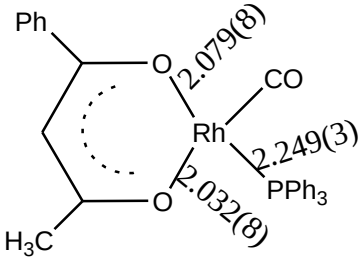

cis

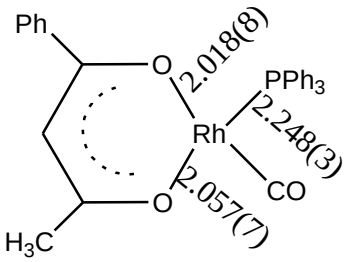

trans

IR studies show that replacement of one or more CO's of a transition metal carbonyl with a triply connected phosphorus ligand causes the CO stretching frequencies of the remaining carbonyls to fall, by an amount depending on the number and nature of the phosphorus ligands. The electron donor-acceptor properties of the ligands in the complexes would influence their catalytic behavior. It is expected that reactions in a catalytic sequence in which the formal oxidation state of the transition metal changes will be particularly influenced by changes in the electronic nature of the ligand.[70]

2.4 Crystal structure determination

2.4.1 β-diketones

X-ray analysis of acetylacetone was carried out at 110 K, and it was found that acetylacetone exists as a dynamic or static mixture of the two nondistinguishable *cis*-enol isomers with the enolic hydrogen atom equally distributed over two positions close to the oxygen atoms.[71]

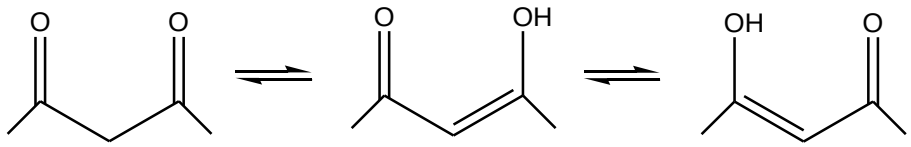

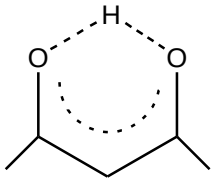

A

The lengths of the C-O and the central C-C bond in **A** were observed to be 1.291 and 1.402 Å, respectively. (Typical C-C single bond = 1.55 Å, C=C double bond = 1.34 Å, C-O bond = 1.43 Å and C=O bond = 1.22 Å)

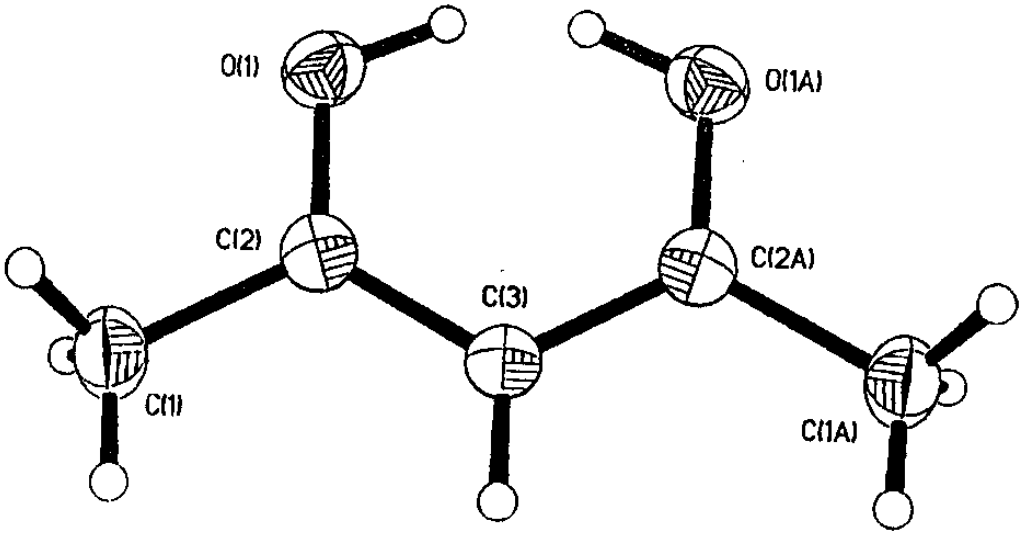

Figure 2.2: General view of the crystalline acetylacetone molecule at 110K.

Table 2.5: Molecular geometry of acetylacetone (Bond lengths in Å and bond angles in °)

O(1)-C(2)	1.291(2)	C(1)-C(2)-C(3)	121.2(1)
C(1)-C(2)	1.497(3)	C(1)-C(2)-O(1)	117.0(1)
C(2)-C(3)	1.402(2)	O(1)-C(2)-C(3)	121.8(1)
O(1)-O(1a)	2.547(2)	C(2)-C(3)-C(2a)	121.0(1)
O(1)-H(1)	0.89(5)	C(2)-O(1)-H(1)	113(2)
H(1)-H(1a)	0.94(11)	O(1)-H(1)-O(1a)	155(2)
H(1)-O(1a)	1.78(5)		

A certain degree of aromaticity of the double bond system causes the C=O and C=C bonds to be lenghtened slightly and the C-O and C-C bonds to be shortened slightly when there is a mixture 1:1 isomers in comparison to the corresponding isolated bonds.[72]

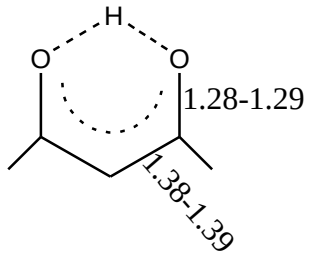

It has been found that the enol form of acetylacetone has been selectively included into several host-guest systems. The relatively strong, resonance assisted intramolecular hydrogen bond present in acetylacetone lowers the barrier for proton transfer between the two oxygen atoms. As a result average C-O and C-C bond lengths are detected, giving rise to the assumption that the enol forms are both present on the X-ray experiment time scale.[72]

2.4.2 Rh(I) complexes of the type [Rh(β-diketone)$(CO)_2$]

The structure of the complex [Rh(acac)$(CO)_2$] has been determined[73] and crystallised from acetone as orange-green pleochroic needles (a property of exhibiting different colours, possessed by some crystals, especially three different colours, when viewed along different axes). The crystals were found to be unstable under X-rays in air, but when covered with a thin coat of picture varnish no decomposition occurred during data collection.

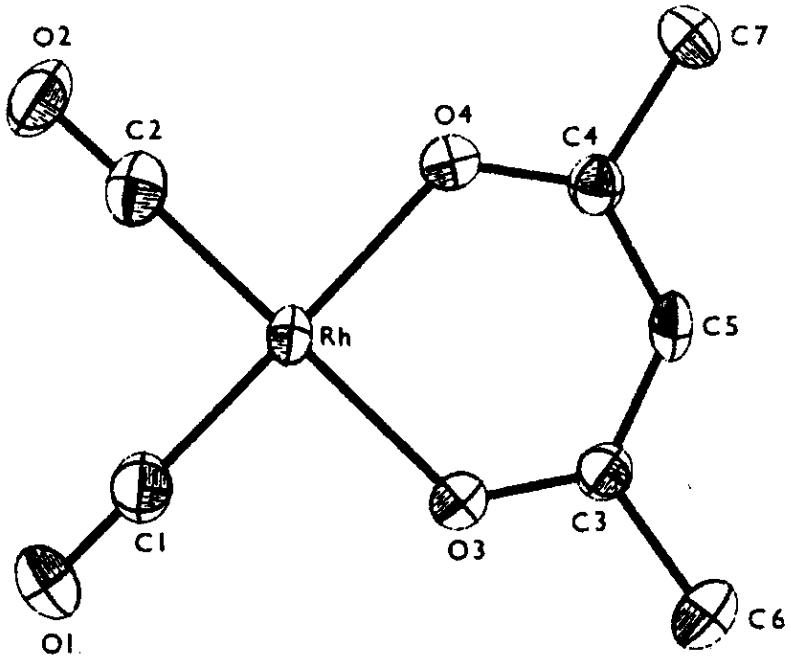

Figure 2.3: Molecular structure of [Rh(acac)(CO)$_2$][73]

Huq *et.al.*[73] found that the rhodium atom has a square-planar coordination with two Rh-O(acac) distances of 2.040 and 2.044 Å, and two Rh-C(carbonyl) distances both equal to 1.831 Å, with O-Rh-O and C-Rh-C angles of 90.8 and 88.9^o respectively. A spectroscopic view of the packing of molecules is shown in **Figure 2.4**

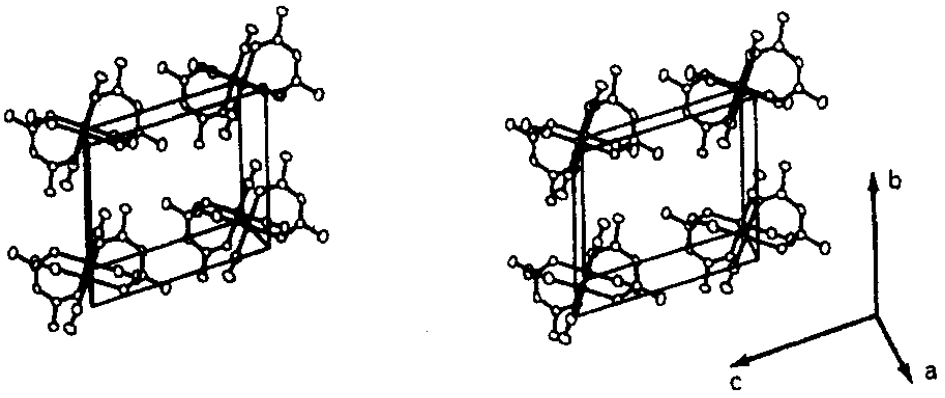

Figure 2.4: Stereoscopic view of the packing of Rh(acac)(CO)$_2$ molecules.[73]

Molecules which are related to each other by centres of symmetry stack in the *a*-axis direction in such a way that the rhodium atoms of neighbouring molecules occupy the two remaining pseudo-octahedral positions, with Rh….Rh distances of 3.253 and 3.271 Å. E. A. Shor *et.al.*[74] determined the structure of compounds shown in **Figure 2.5**

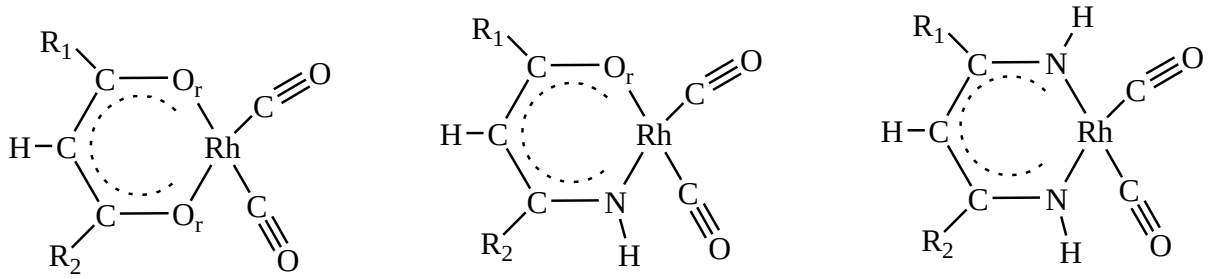

Figure 2.5: Schematic diagram of rhodium(I)dicarbonyl complexes with chelate ligands like: I-β-diketonate; II-immoketonate; III-β-diiminate (R_1, R_2 = a-H, H; b-CH_3, H; c-CH_3, CH_3; d-CF_3, CH_3; e-CF_3, CF_3).

Ligand surroundings of rhodium centre in all chelate complexes conform well to a square-planar configuration. In all complexes, the angle C-Rh-C lie in the range of 92-93^o up to 89^o and 91^o. **Table 2.6** show calculated bond lengths and bond angles for the complexes [Rh (R_1COCHCO)R_2(CO)$_2$].

Table 2.6: Calculated bond lengths (Å) and bond angles (deg) for the complexes [Rh (R_1COCHCOR_2)(CO)$_2$].[74]

R_1, R_2	H, H	CH_3, H	CH_3, CH_3
	Ia	Ib	Ic
Rh-C	1.883	1.882	1.882
		1.881	
Rh-O_r	2.074	2.065	2.061
		2.064	
C-O	1.148	1.148	1.149
		1.148	
C-C	1.397	1.394	1.403
		1.406	
C-Rh-C	92.2	91.6	92.3
C-Rh-O_r	88.5	88.8	89.0
		89.2	
Rh-C-O	177.8	178.9	177.6
		178.2	
O_r-Rh-O_r	90.8	90.3	89.9
Rh-O_r-C	123.8	126.2	125.8
		123.5	
O_r-C-C	128.5	125.7	126.4
		129.2	
C-C-C	124.6	125.1	125.7

2.4.3 Rh(I) complexes of the type [Rh(β-diketone)(CO)(PPh_3)]

In the structural determination of [Rh(acac)(CO)(PPh_3)][61] the following Rh-O bond distances were found: Rh-O(2) = 2.087(4) Å and Rh-O(1) = 2.029(5) Å. The effect of the PPh_3 group is also observed in comparing the Rh-O bond distances in [Rh(acac)(CO)(PPh_3)] and in [Rh(acac)$(CO)_2$].

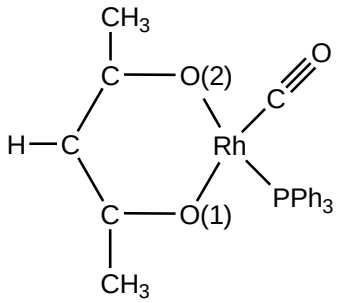

The significant difference in the two Rh-O bond distances in [Rh(acac)(CO)(PPh_3)] indicates that the PPh_3-group has a larger *trans* effect than the CO-group in these type of compounds.[61]

A. Roodt *et.al*. prepared [Rh(bzaa)(CO)(PPh_3)] from mixing equimolar amounts of PPh_3 with [Rh(bzaa)$(CO)_2$] (bzaa = 3-benzylacetylacetonato anion) in acetone. Slow evaporation of acetone at 295 K yielded yellow needle–like crystals suitable for crystal structure determination.[75]

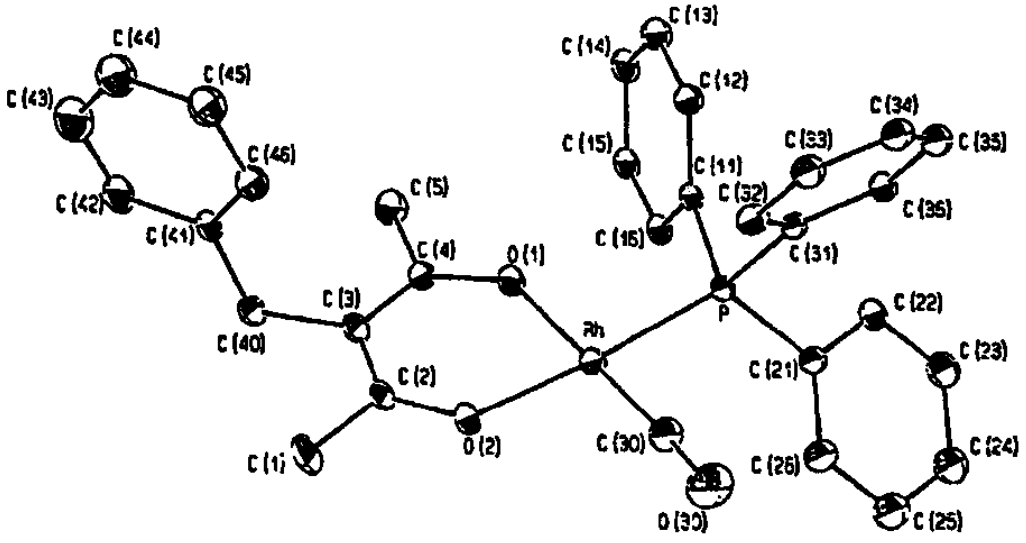

Figure 2.6: Perspective view and atom labelling of the molecule [Rh(bzaa)(CO)(PPh_3)] (H atoms omitted for clarity).[75]

No observed influence by the benzyl substituent in the third position could be detected structurally, thereby indicating that the reactivity of the β-diketone complex would most probably not be altered significantly by a benzyl substituent in the 3-position of the β-diketone.[75]

To minimize the effect of different groups on the monocharged β-dikenate ligand Lamprecht *et.al.*[76] chose symmetrical β-diketonato ligand 1,3-diphenyl-1,3-propandinato (dbm).

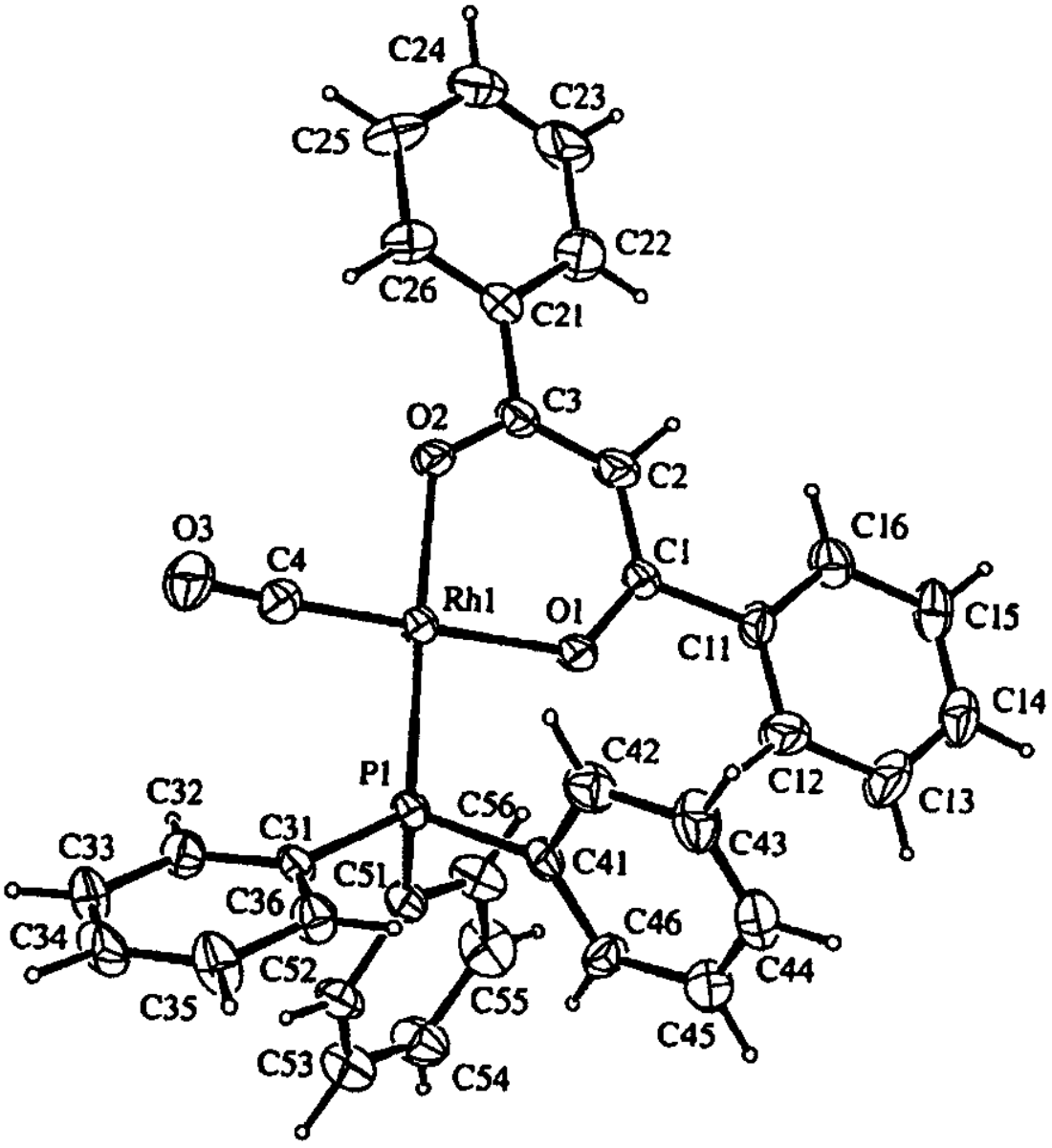

Figure 2.7: The structure of one of the two independent molecules of [Rh(dbm)(CO)(PPh_3)] with the atomic numbering scheme.[76]

The asymmetric unit consist of two crystallographically independent molecules of [Rh(dbm)(CO)PPh_3)] and they form a very closely centrosymmetric pair. The square-planar coordination of the Rh atom is clear from the bond angles in **Table 2.7**

Table 2.7: Selected geometric parameters (Å, °) for [Rh(dbm)(CO)(PPh_3)].[76]

Rh1-P1	2.237(7)	P1-Rh-O1	87.07(3)
Rh1-O1	2.038(10)	P1-Rh1-O2	175.2(4)
Rh1-O2	2.081(9)	P1-Rh1-C4	91.1(5)
Rh1-C4	1.812(13)	O1-Rh1-O2	88.5(5)
		O1-Rh1-C4	175.3(6)
		O2-Rh1-C4	92.9(5)

The distances Rh-O2 = 2.081(9)Å and Rh-O1 = 2.038(10)Å illustrate clearly the larger *trans* influence of triphenylphosphine compared with a carbonyl group. Some authors[61,77,78] claimed that the Rh-P distance could be used to estimate the relative *trans* influence of different donor atoms in the chelate rings.

2.5 Oxidative addition

2.5.1 Introduction

Oxidative addition is a fundamental reaction and often serves as the critical activation step in many homogeneous catalytic processes.[79] Oxidative addition reactions have been used in preparing supramolecular and polymeric materials[80] and reactions involving the addition of alkyl halides are shown to proceed normally by the classical S_N2 mechanism, although in some relatively rare cases, the reaction proceed by a radical mechanism.[81] The two step S_N2 mechanism is supported by the observation of second-order kinetics with large negative activation entropies indicating a highly ordered transition state.[82]

In oxidative-addition, both the oxidation state and coordination number of the metal increases. Examples of two-electon, oxidative-additions are known for virtually all even d^n configurations (n = 2, 4, 6, 8, 10), but these reactions are far better studied for the d^8 and d^{10} compounds found toward the right of the transition series (especially Group VIII). Both

coordinatively saturated and unsaturated complexes undergo oxidative-addition reactions, the latter being more reactive. The general cases for d^8 compounds are illustrated below.

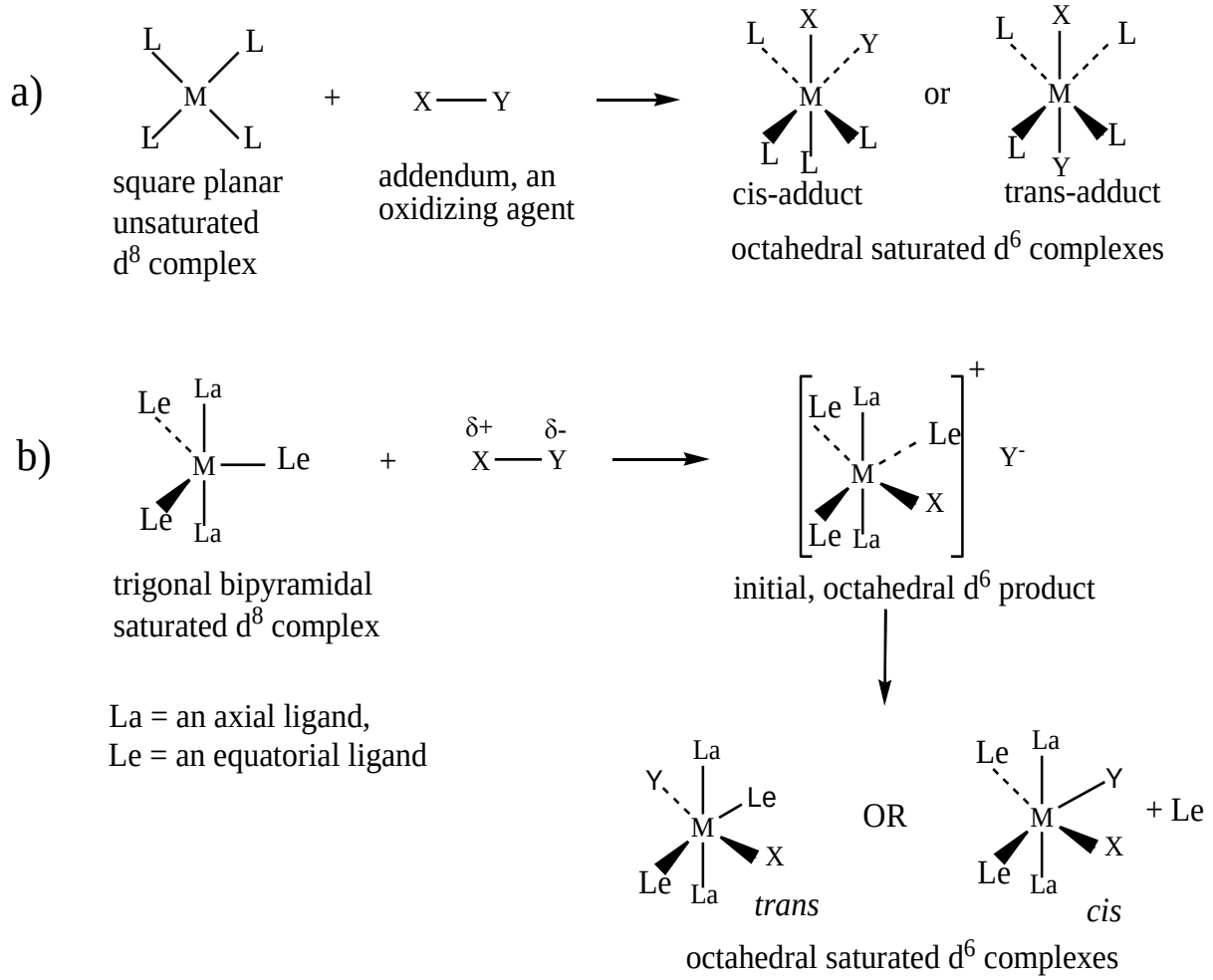

Scheme 2.16[83]: Oxidative addition of the neutral molecule XY to transition metal complexes ML_n (n = number of ligands bonded to the metal M): a) unsaturated square planar d^8 ML_4 complex and b) saturated trigonal bipiramidal d^8 ML_5 complex

In certain cases, the oxidative addition reaction to a saturated d^8 complex has been shown to proceed in a stepwise manner, with the initial attack by X^+ forming a coordinatively saturated complex which may subsequently incorporate Y^- by replacement of the ligand Le. The final product can be that of over-all cis-addition, or trans-addition, depending on the mechanism of the ligand displacement step. The reactivity of the saturated complex seems to depend on its formal charge; anionic compounds, being electron-rich, are more reactive. In certain cases a saturated d^8 complex may lose a ligand prior to oxidative addition.[83]

Square planar Rh(I) complexes, being coordinatively unsaturated, undergo oxidative addition reactions with various organic and inorganic molecules.[84] The impetus for these

investigations has been the desire to gain a better understanding of the electronic and steric factors influencing the oxidative addition reactions, which are vital steps in the functioning of many of these compounds as homogeneous catalysts.[85] The electronic effect can however be dominated by steric hindrance and can therefore be important in controlling the rate of oxidative addition reactions. The relation between electrochemical oxidation (oxidation potential determination by means of cyclic voltammetry) and the pK_a values of the various β-diketones co-ordinated onto the rhodium is expected to be independent of steric parameters. Electrochemical investigations can therefore offer numerous new ways to explore the steric hindrance effect on rhodium complexes.[84]

Kinetic studies of [Rh(β-diketonato)($P(OPPh)_3)_2$] complexes (β-diketonato = trifluoroacetylacetone(tfaa)),[86] revealed that the electronic effect of the substituents on the β-diketones decrease the reaction rate of oxidative addition with the lowering of the pK_a-values of the free β-diketones. The effect of more electronegative substituents on the reactivity of the Rh(I) centre is explained by the fact that electron density is removed from the rhodium metal, making the complex a stronger Lewis acid and less reactive towards oxidative addition. The rhodium atom thus becomes a weaker nucleophile.[87]

2.5.2 Addition of iodomethane to rhodium(I) complexes

2.5.2.1 Introduction

The original rhodium/iodide process was initiated in 1966 at the Monsato laboratories.[88, 85] The harsh conditions of the Monsato process have driven the researchers to the synthesis of new rhodium complexes bearing electron-donating ligands,[89] as these might facilitate the oxidative addition of methyl iodide. The catalytic performance of rhodium complexes containing monophosphines (PEt_3),[90] diphosphines (PPh_2-CH_2CH_2-PPh_2)[91] and mixed bidentate ligands (PPh_2-CH_2-$P(O)Ph_2$,[92] PPh_2-$(CH_2)_2$-$P(O)Ph_2$,[93] PPh_2-CH_2-$P(S)Ph_2$,[94, 95] S,P-$SC_2B_{10}H_{10}PPh_2$[96] and PPh_2-CH_2-$P(NPh)Ph_2$)[97] was similar or better than the Monsanto process. Electronically unsymmetrical diphosphine complexes are also active and selective catalysts in industrially significant conditions.[98] Most of these ligands except for PPh_2-CH_2-$P(S)Ph_2$ enhanced oxidative addition but as a consequence they usually retard the subsequent CO migratory insertion because the increased electron density at the metal also leads to a

stronger Rh-CO bond.[99] The strong donor property of the mixed P,S ligand, PPh_2-CH_2-$P(S)Ph_2$, accelerates the rate determining oxidative addition of methyl iodide to Rh(I) as expected, while the steric requirements of the PPh_2-CH_2-$P(S)Ph_2$ ligand destabilised the octahedral oxidative addition intermediate (which would undergo migratory insertion to release such steric pressure), accelerating the subsequent CO insertion.[95]

In the field of olefin polymerization, metal complexes with a coordinatively unsaturated Lewis acidic metal centre are generally required[100], whereas for transformations such as the carbonylation of methanol, electron-rich metal centres are necessary to oxidative addition of MeI to Rh(I).[101,95,102,103] In the carbonylation of methanol to acetic acid an important reaction is that of *cis* –$[Rh(CO)_2I_2]^-$ with methyl iodide which is the rate determining step.[104,105]

2.5.2.2 Mechanism of the oxidative addition of iodomethane to rhodium complexes

The three main mechanisms govern oxidative addition reactions to square planar d^8 metal complexes[106] are

(i) the one step concerted three centre mechanism,

(ii) the two step S_N2 mechanism,

(iii) radical mechanism.

It is widely accepted that oxidative addition of MeI occurs via a two step mechanism involving (i) nucleophilic attack by the metal on the methyl carbon to displace iodide and form a metal-carbon bond and (ii) coordination of iodide to the five-coordinate intermediate. Depending upon the stereochemical rigidity of the intermediate complex, the methyl and iodide ligands can be placed mutually trans or cis in the octahedral product.[82]

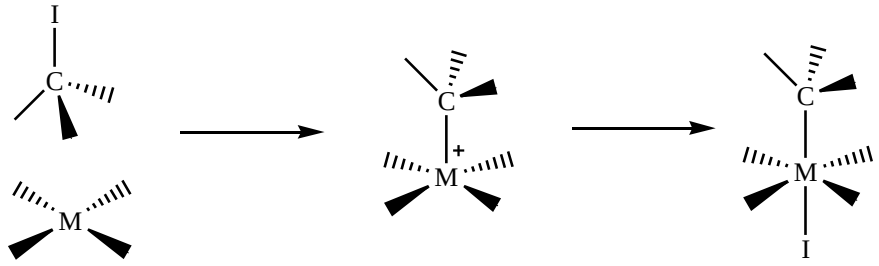

Scheme2: 17: S_N2 Mechanism for oxidative addition of MeI to a square planar complex.

The two-step S_N2 mechanism is supported by the observation of second-order kinetics with large negative activation entropies indicating a highly ordered transition state.[107] Information has been obtained on the nature of the transition state in terms of **I** (for a concerted three-

centered mechanism) or **II** (for a S_N2 mechanism) through solvent and pressure effects studies.[108]

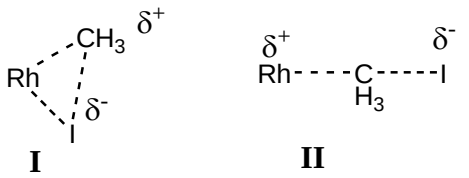

I **II**

The oxidative addition of iodomethane (and the subsequent carbonyl insection reaction) to four selected classes of rhodium(I) complexes will be discussed in the next paragraphs.

2.5.2.3 Oxidative addition of iodomethane to [Rh(tridentate ligand)(CO)]

Bassetti *et.al*[109] revealed from IR, ^1H and ^{13}C NMR studies that oxidative addition of methyl iodide to the cationic rhodium(I) carbonyl center *mer*-$[Rh(L)(CO)]^+$ with L = 2,6-bis(benylthiomethyl)pyridine occurs via an observable methyl-rhodium(III) intermediate (alkyl species) followed by methyl migration to give the acyl derivative.

When the reaction is performed in neat MeI at 31°C and monitored in situ by FT-IR (**Fig. 2.8**), the disappearance of the carbonyl band of **1** at 2015 cm^{-1} is accompanied by formation and then the consumption of a new species (2099 cm^{-1}) and by a slow appearance of the acetyl band of **2** at 1731 cm^{-1}.[109] This implies that oxidative addition of MeI and CO migratory insertion occurred sequentially at the metal centre.[101, 110]

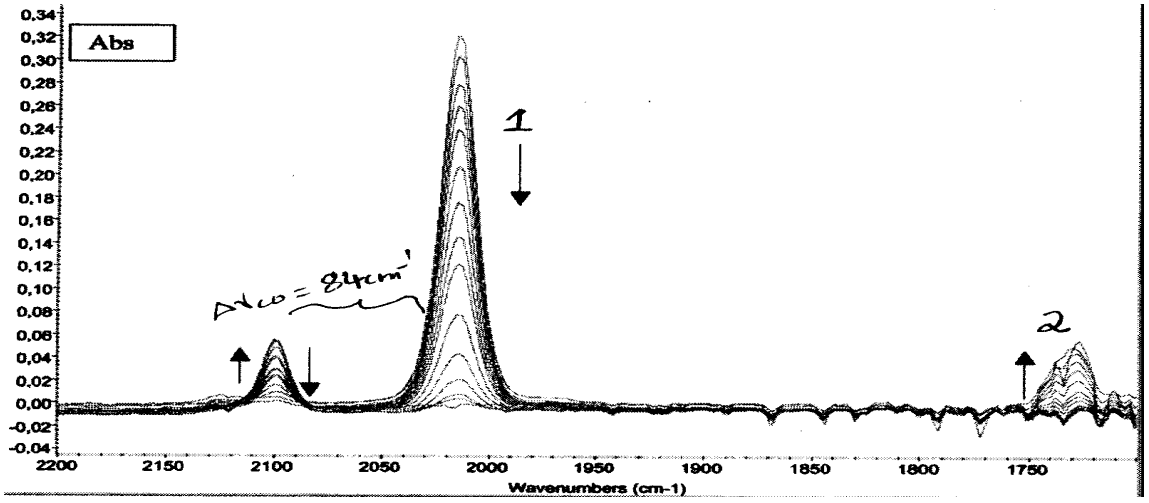

Figure2.8: Series of FT-IR spectra for the reaction of $[Rh(L)(CO)]PF_6$ with MeI (in neat MeI, 31°C). The arrows indicate the evolution of each band during the progress of the reaction.[109]

The frequency shift of the intermediate with respect to rhodium(I) (Δ_{VCO} = 84 cm^{-1}) suggests that the new species is the product of oxidative addition of MeI, $[Rh(L)(Me)I(CO)]^{+}$.[109] The reaction scheme for the above mentioned spectra is as follows:

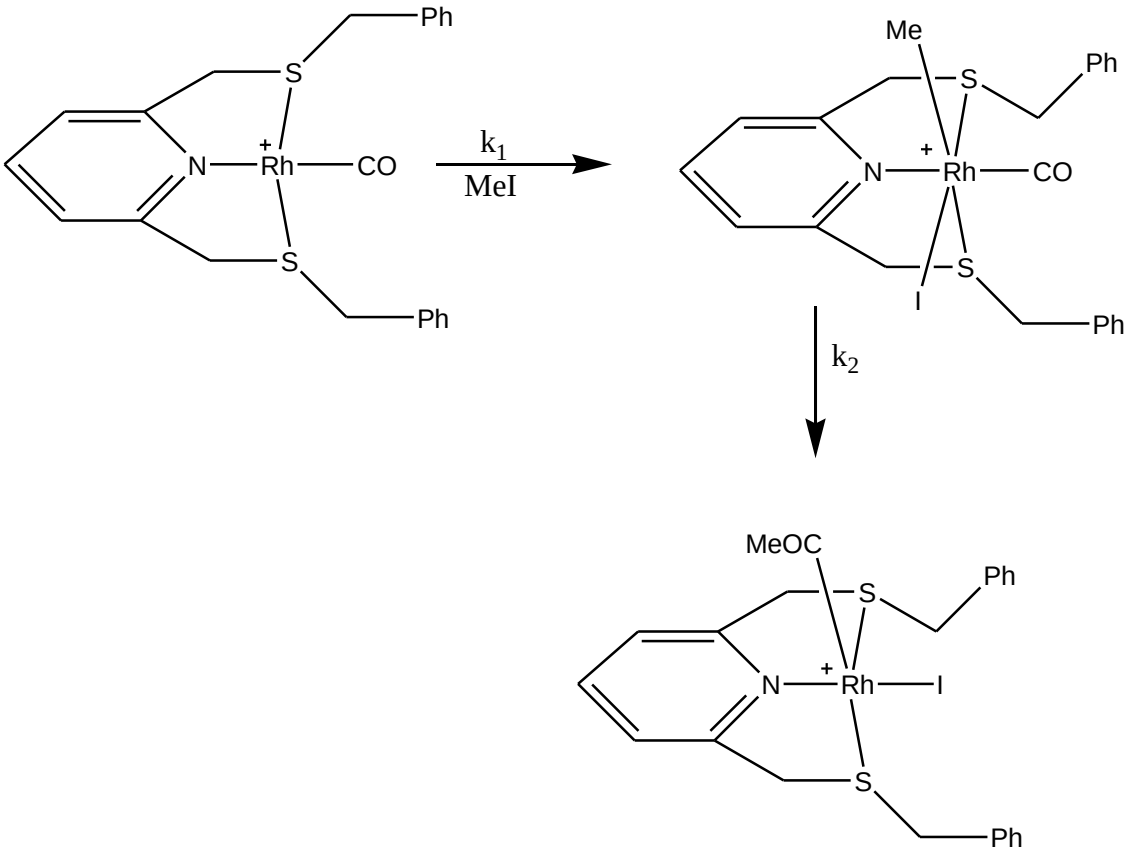

Scheme 2.18: Reactivity of $[Rh(L)(CO)]PF_6$ with MeI.[109]

Pelabatti *et.al*[111] studied the reactivity of MeI towards the three coordinated carbonyl Rh(I) complex Rh(L)(CO) (complex **1** in **Scheme 2.19** below) where HL = the tridentate ligand 2-(diphenylphosphino)benzaldehyde benzoylhydrazone (ligand 1 in **Scheme 2.19** below).

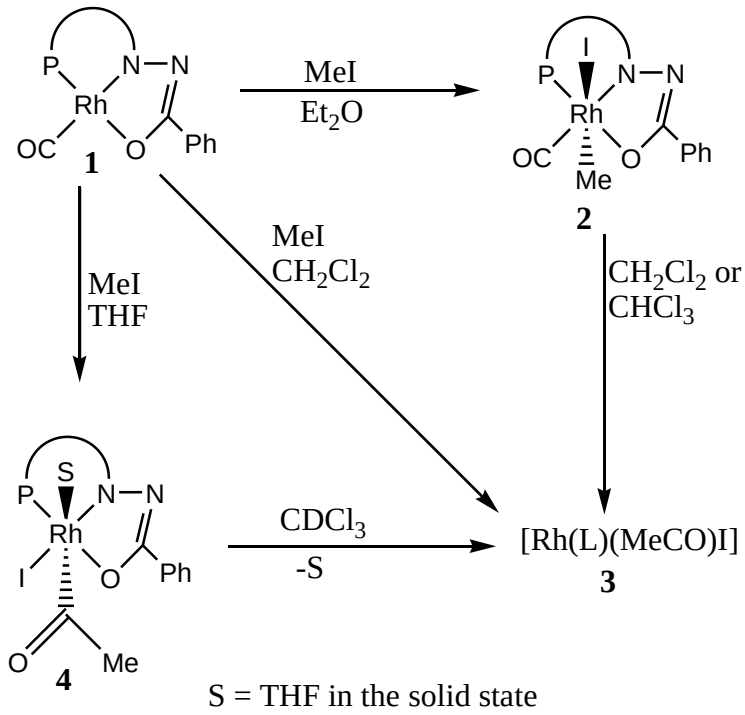

Scheme 2.19: The tridentate 2-(diphenylphosphino)benzaldehyde benzoylhydrazone ligand L and the corresponding rhodium(I) complex Rh(L)(CO) studied by Pelabatti *et.al*.[111]

Different solvents (dichloromethane, THF, diethyl ether and deuterated chloroform) used for the reaction of MeI with complex **1** afforded products (**Scheme 2.19: 2, 3, and 4**).[111] When dichloromethane was used as a solvent, the MeCO moiety originates a singlet at 2.95 ppm in the ^{1}H NMR spectrum and a strong IR stretching band at 1727 cm^{-1} (both in KBr and in CH_2Cl_2). In the ^{31}P NMR spectrum a doublet centered at 49.4 ppm was observed with a $J_{Rh\text{-}P}$ = 144 Hz. When the reaction was done in THF the spectroscopic patterns of the product (**4**) were similar to those of **3** where dichloromethane was used as the solvent, but the acetyl stretching band was centered at 1690 cm^{-1} (1727 cm^{-1} in CH_2Cl_2). The two characteristic multiples of an uncoordinated THF molecule were observed on the ^{1}H NMR spectrum recorded in $CDCl_3$. The structure showed an octahedral coordination, where the three donors of the anionic ligand and an iodine atom completed the square plane, while a THF molecule and an acetyl group occupied the apical positions. The reaction was repeated in diethyl ether and in its IR spectrum the presence of the C≡O ligand was pointed out by an intense band at 2075 cm^{-1}, while the remaining part of the spectrum was identical to that of **1**. In deuterated chloroform the methyl group attached to the rhodium was observed as a triplet at 0.99 ppm with a $J_{Rh\text{-}P} = J_{P\text{-}H}$ = 2.2 Hz. All the data found agree with the role of intermediate species **2** in the formation of **4** (**Scheme 2.19**)[111]

J.A.Gaunt *et.al*[112] studied the oxidative addition of iodomethane to the rhodium(I) complex, $LRh^{I}(CO)$, containing the tridentate ligand L = [bis(imino)carbazolide] (see **Scheme 2.20**).[113114115] The product of oxidative addition $LRh^{III}I(CO)Me$ was characterised by ^{1}H NMR, ^{13}C NMR, IR, and FAB-mass spectroscopy. No evidence for a migratory CO insertion into the Rh-Me bond to give a Rh-acyl complex (which is common with related Rh(III) complexes containing {NNN} ligands), was found. By contrast, products resulting from MeI addition to Rh(I) carbonyl complexes containing some tridentate [PNO], [NON], or [SNS] ligands are known to undergo spontaneous migratory CO insertion.[111, 116,109] The CO stretching frequency of $LRh^{III}I(CO)Me$ was observed at 2083 cm^{-1}, which is a considerable shift from the value of 1980 cm^{-1} to higher wavenumber for the complex before MeI addition. A shift to higher wavenumber for ν(CO) by 80-100 cm^{-1} is characteristic of the transformation from a square-planar $LRh^{I}(CO)$ complex to an octahedral $LRh^{III}I(CO)Me$ species and is the result of weaker back-donation in Rh(III) complexes compared to those bearing Rh(I) centers. It was not possible to establish whether the CO or the iodide ligand is *trans* to the Rh-Me group. An Eyring plot of variable-temperature data (15-35°C) gave activation parameters $\Delta H^{\#}$ 19(±1) $kJmol^{-1}$ and $\Delta S^{\#}$ - 179 (±4) $Jmol^{-1}K^{-1}$. The large negative value of $\Delta S^{\#}$ is consistant with a highly ordered S_N2 transition state for attack by Rh(I) on MeI.[112]

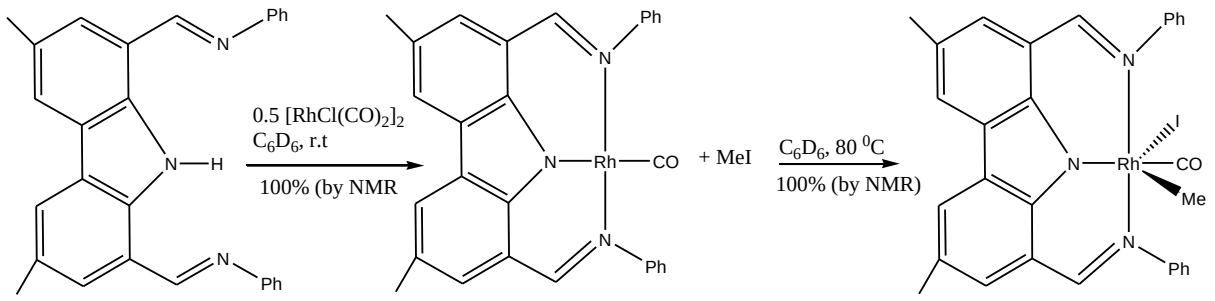

Scheme 2.20: The bis(imino)carbazolide ligand L and the corresponding rhodium(I) complex $LRh^{I}(CO)$ and rhodium(III) complex $LRh^{III}I(CO)Me$ studied by Gaunt *et.al*.[112]

Bassetti *et.al.*[117] extended their work from the initial kinetic study carried out in neat methyl iodide and in acetonitrile to the solvents acetone, dichloromethane, and methanol and reported on the results regarding the oxidative addition step. The reaction proceeds in all solvents, with quantitative disapearance of complex [Rh(L)(CO)]-PF_6 (L = 2,6-bis(benzylthiomethyl)pyridine), as observed from FT-IR spectra at the end of the kinetic run. An NMR analysis of this reaction revealed the formation of two isomers of the intermediate rhodium(III) alkyl complex. A plot of pseudo-first-order rate constant obtained from the

disappearance of rhodium(I) complex, k_{obs}, vs the concentration of methyl iodide for all the solvents used showed a linear dependence with a non-zero intercept on the concentration of methyl iodide in acetonitrile, acetone and dichloremethane. In methanol, saturation kinetics was observed.

Table2.8[112]: Values of kinetic constants for the reaction of $[Rh(L)(CO)]PF_6$ with MeI in various solvents, at 31°C

[MeI] M	k_{obs} s^{-1} in **CH_2Cl_2**	k_1 s^{-1}	k_2 $M^{-1}s^{-1}$
0.76	1.6 x 10^{-5}	1.1(±0.1)] x10^{-5}	6.4(±0.6)] x 10^{-6}
1.46	2.1 x 10^{-5}		
2.09	2.3 x 10^{-5}		
3.20	3.2 x 10^{-5}		
	k_{obs} s^{-1} in **Me_2CO**	6.7(±1)] x10^{-6}	5.9(±0.1)] x10^{-5}
0.392	2.99 x 10^{-5}		
0.618	4.35 x 10^{-5}		
0.944	6.15 x 10^{-5}		
1.120	7.35 x 10^{-5}		
	k_{obs} s^{-1} in **MeOH**	1.7(±0.1)] x10^{-4}	
0.16	6.5 x 10^{-5}		
0.50	3.6 x 10^{-5}		
1.05	6.3 x 10^{-5}		
1.53	7.8 x 10^{-5}		
2.09	8.7 x 10^{-5}		

The change of k_2 with solvent (acetonitrile > acetone > neat methyl iodide ≈ dichloromethane) indicates that increased solvent polarity assists the oxidative addition reaction, presumably characterized by the development of charge in the rate determining step. V. Chauby *et.al*[82] agrees that for neutral reactant complexes, polar solvents promote the reaction rate due to their ability to solvate and therefore stabilize the intermediate ion pair. Bassetti[109] found that with regard to the CO migratory insertion step, which leads from the rhodium(III) methyl species to the isolable acyl complex $[Rh(L)(COMe)]PF_6$ (L = 2,6-bis(benzylthiomethyl)pyridine), the reaction is independent of methyl iodide concentration, as expected for an intramolecular step. A mechanistic description which accounts for the kinetic patterns observed in acetonitrile, acetone, and dichloromethane is shown in **Scheme 2.21**.[117]

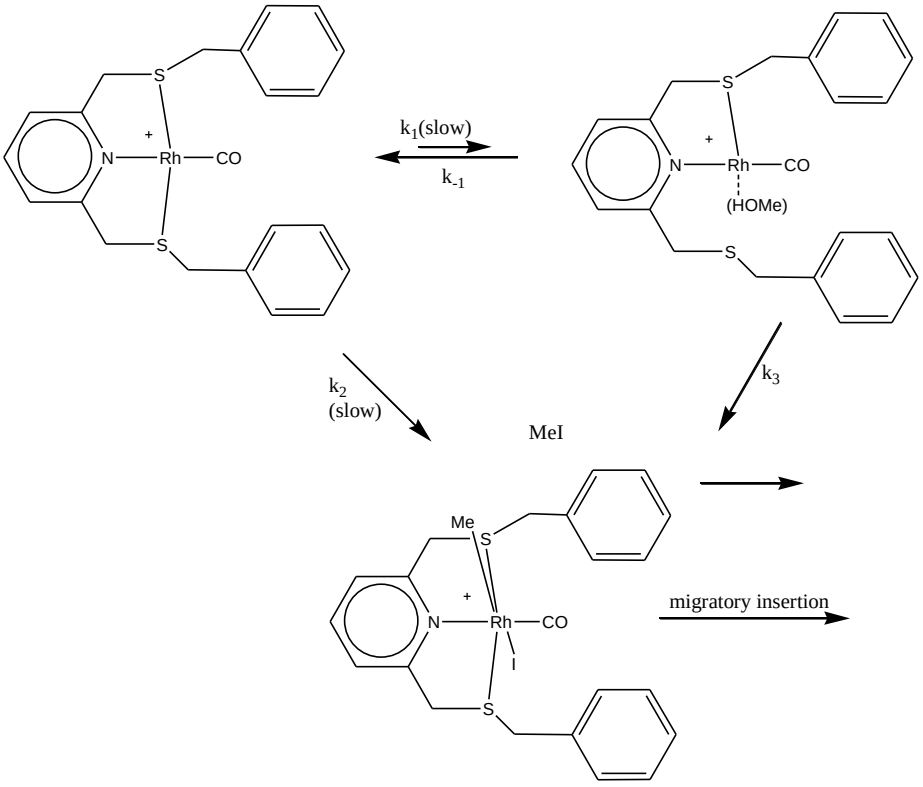

Scheme 2.21: Mechanism of the reaction of [Rh(L)(COMe)]PF_6

2.5.2.4 Oxidative addition of iodomethane to [Rh(β-diketonato)$(P(OPh)_3)_2$]

The reaction between [Rh(β-diketonato)$(P(OPh)_3)_2$] and CH_3I could only be studied in a limited range of solvents due to the insolubility of the Rh(I) complexes in many solvents. It was found that the reaction rate is enhanced by more polar solvents.[118,119,120,121] Similar solvent effects were also found for various other oxidative addition reactions. The significant solvent effect is indicative of a mechanism in which a polar transition state is stabilized by more polar solvents. It can be taken as evidence that the function of the solvent is to ease the charge separation during the rearrangement and formation of a 5-coordinate intermediate.[122]

TABLE2.9:.Second order rate constants at various temperatures of the reaction of [Rh(β-diketonato)$(P(OPh)_3)_2$] with CH_3I in acetone medium. The pK_a values corresponding to the β-diketone wavelengths where the reaction was followed and activation parameters are also listed.[122]

β-diketone	Substituents on β-diketone		pK_a	λ nm	T °C	k $mol^{-1}dm^3s^{-1}$	$\Delta H^{\#}$ $kJmol^{-1}$	$\Delta S^{\#}$ $Jmol^{-1}K^{-1}$
	R_1	R_2						
acac	CH_3	CH_3	8.94	340	30.4	$1.26(3)x10^{-1}$	40(3)	-128(9)
BA	CH_3	C_6H_5	8.70	388	33.7	$4.5(2)x10^{-2}$	30(6)	-172(20)
DBM	C_6H_5	C_6H_5	9.35	373	29.8	$2.12(7)x10^{-2}$	49(2)	-115(7)

The $\Delta H^{\#}$ values are relatively small, compensated by highly negative $\Delta S^{\#}$ values, both of which may be considered as characteristic of an associative mechanism. The large negative $\Delta S^{\#}$ values indicate an increase in the coordination number during the formation of the transition state. With the structures of the reactant and final product known from ^{1}H NMR and the structure determination of a similar rhodium(III) complex, the kinetic data (the effect of the substituents of the β-diketone and solvent on the reaction rate as well as the $\Delta S^{\#}$ and $\Delta V^{\#}$ values) suggests the reaction mechanism in **Scheme 2.22**.[122]

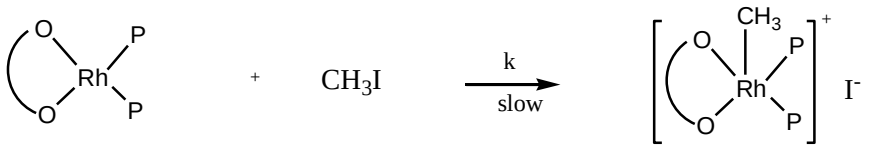

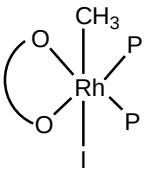

The proposed first step may be represented as

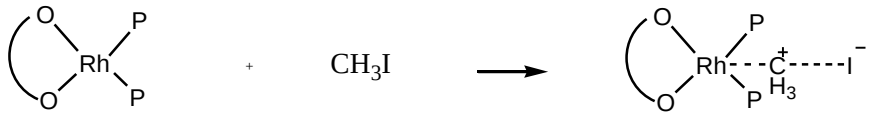

i.e. a linear transition state.

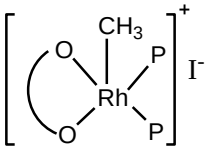

Scheme 2.22[122]: Reaction mechanism for the oxidative addition of iodomethane to Rh(I)

Oxidative addition reactions can proceed by different reaction pathways[123] and one of the factors influencing the preferred choice is the nucleophilicity of the metal in the complex. Apart from the general increasing Lewis basicity on descending in a periodic group for a given type of complex it is also the σ- and π-bonding framework of metal-ligand interactions which play a major role.[119]

2.5.2.5 Oxidative addition of iodomethane to [Rh(β-diketonato)(CO)(PPh_3)]

Replacement of one CO in [Rh^I(β-diketonato)$(CO)_2$] by a less capable π-acid such as triphenylphosphine (PPh_3) could enhance the rate of oxidative addition still further. With this in mind the kinetics and mechanism of the following reaction was studied.[119]

[Rh(β-diketonato)(CO)(PPh_3)] + CH_3I ⟶ [Rh(β-diketonato)(CH_3)(I)(CO)(PPh_3)]

β-diketonato = acac, thdmaa (1,1,1-trifluoro-5-methyl-2,4-hexanedione), tfaa and hfaa.

Repeated time scanning on the IR of 1,2-dichloroethane solutions of the rhodium(I) complex **I** containing excess CH_3I showed an immediate intensity decrease in its CO peak corresponding to an acyl species **II** and an alkyl species **III** respectively.

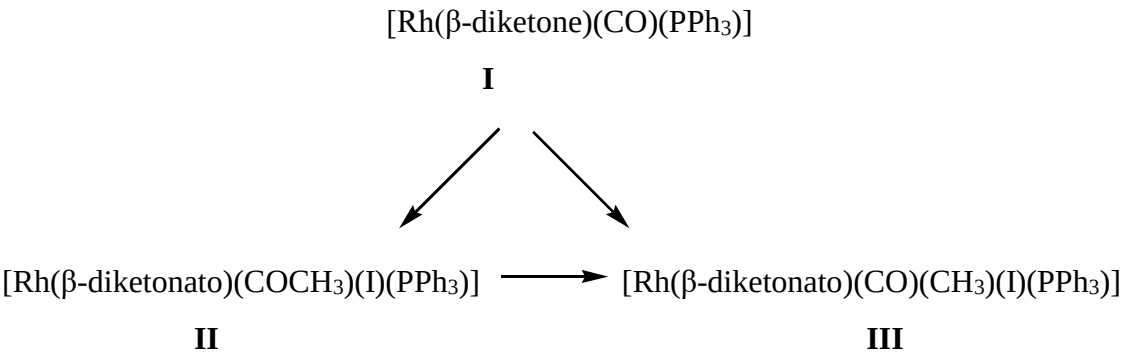

The peak of **III** developed at a faster rate compared to that of **II.**[119] The IR spectra showed that one final product **III** was formed at infinite time. The much slower **II** to **III** conversion was confirmed by successive IR spectra of a solution of [Rh(acac)(CO)(PPh_3)] containing less than the stoichiometric amount of CH_3I. These spectra clearly showed that after the initial **I** to **II** to **III** conversions, the peak of unreacted **I** remained constant and that of **III** increased further at the cost of **II**. The reactions followed pseudo-first-order kinetics with

$$k_{obs} = \frac{k_2 K_1 [CH_3]}{1 + K_1 [CH_3 I]}$$

where the constants are interpreted in terms of **Scheme 2.23**

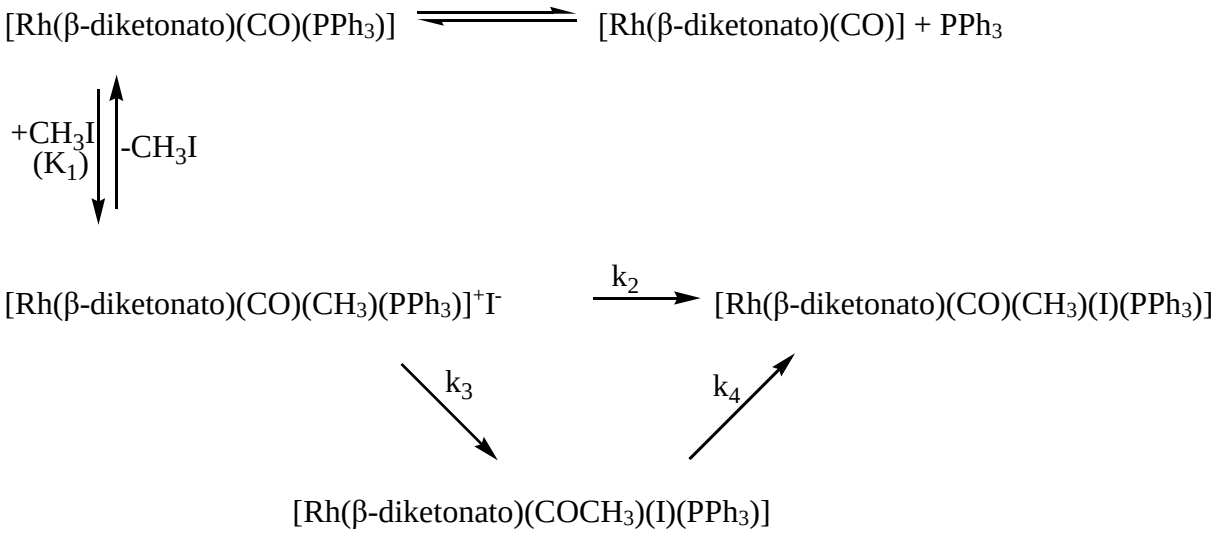

Scheme2.23[119]: Reaction mechanism for [Rh(β-diketonato)(CO)(PPh3)] with MeI

The proposed mechanism shows the reacting complex, [Rh(β-diketonato)(CO)(PPh_3)], to be partly dissociated to a coordinatively unsaturated compound. The vacated site on the rhodium may now be occupied by a solvent molecule or it may even dimerize to [Rh(β-diketonato)(CO)]$_2$, similar to the case of CH_3I addition to Wilkinson's complex, [RhCl(PPh_3)$_3$].[119]

2.5.2.6 Oxidative addition of iodomethane to [Rh(LL^1-BID)(CO)(PPh_3)]

The general route for the oxidative addition of iodomethane to [Rh^I(LL^1-BID)(CO)(PPh_3)]-complexes can be presented[124,125] by steps A and B (**Scheme 2.24**).

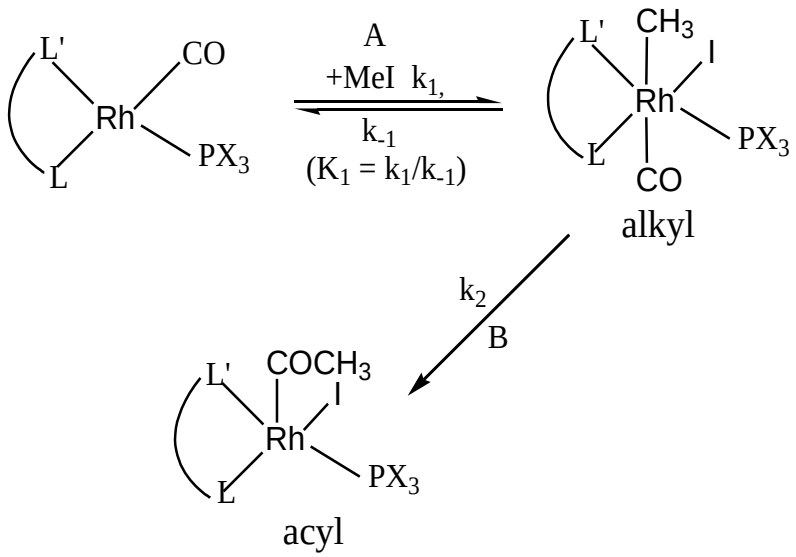

Scheme 2.24[126] The general route for the oxidative addition of iodomethane to Rh(I).

In this reaction steps A and B are characterized firstly by the formation of an Rh(III) alkyl as intermediate, followed by the disappearance thereof, coupled to the simultaneous formation of the Rh(III) acyl species. The pseudo first-order rate constant for the formation of the intermediate alkyl species was shown to be: $k_{alkyl} = k_1[MeI] + k_{-1}$. Similarly, the pseudo first-order rate constant for the formation of the acyl species is given by: $k_{acyl} = k_2K_1[MeI] / (1 + K_1[MeI])$.[126] G.J.J. Steyn *et.al.*[124] compared the kinetic data of various monocarbonylphosphine complexes containing monocharged bidentate ligands with O:O, O:N, and N:S donor atoms. Results obtained showed a dramatic increase in the oxidative addition rate for the N:S type ligands when compared to the O:O donor system. This increased reactivity is explained by the fact that these N:S ligands are capable of strongly donating electron density to the metal centre. The more favourable thermodynamic equilibrium for the first step **(Scheme 2.24)** is due to the fact that the formation of the acyl species in the second step is much less dependent on the type of bidentate ligand. This can be indicative for the acyl formation or methyl migration to be concerted (combined) process dependent on both the Rh(III)-Me bond and the strength of the Rh(III)-CO bond.

S.S. Basson *et. al.*[119,127,128] reported on the oxidative addition of iodomethane to [Rh(LL')(CO)(PX_3)] complexes (LL'=β-diketones or cupferron, X=Ph, *p*-PhCl or *p*-PhOMe) for which the results were strongly in favour of an ionic S_N2 two-step mechanism. The electronic effect[128,118] of the substituent on the β-diketonato ligand on the rate of the oxidative addition of CH_3I to metal complexes is clearly illustrated by the reactivity of the complexes [Rh(β-diketone)(CO)(PPh_3)] towards the oxidative addition of CH_3I that increased for

example 50 fold from β-diketone = hexafluoroacetylacetone to acectylacetone (the group electronegativity of CH_3 and CF_3 are 2.3 and 3.35 respectively). The inhibiting effect of the strong electronegative CF_3 groups on the reactivity of the metal complex is explained by the fact that electron density is removed from the metal, making the complex a stronger Lewis acid and thus less reactive in an associative mechanism.[119]

Roodt *et.al.*[129] studied the oxidative addition of iodomethane in complexes of the form [Rh(N,S-BID)(CO)(PPh_3)] (N,S-BID= monoanionic bidentate ligand containing an N,S donor set) which proceeds via an alkyl intermediate to form the corresponding acyl complexes as final products. The mechanism as presented in **Scheme 2.25** was confirmed to consist of a rapid first oxidative addition equilibrium step followed by the slower acyl formation. The solvent pathway did not observably contribute to the reaction. The rate expression for the oxidation addition step and the CO insertion step is given by

k_{obs}(oxidative addition). = k_1[MeI] + k_{-1}.

$$k_{obs}(\text{CO insertion}). = \frac{k_2 K_1 [MeI]}{1 + K_1 [MeI]} + k_{-2}$$

with $K_1 = \frac{k_1}{k_{-1}}$ the equilibrium constant for the formation of the alkyl complex.

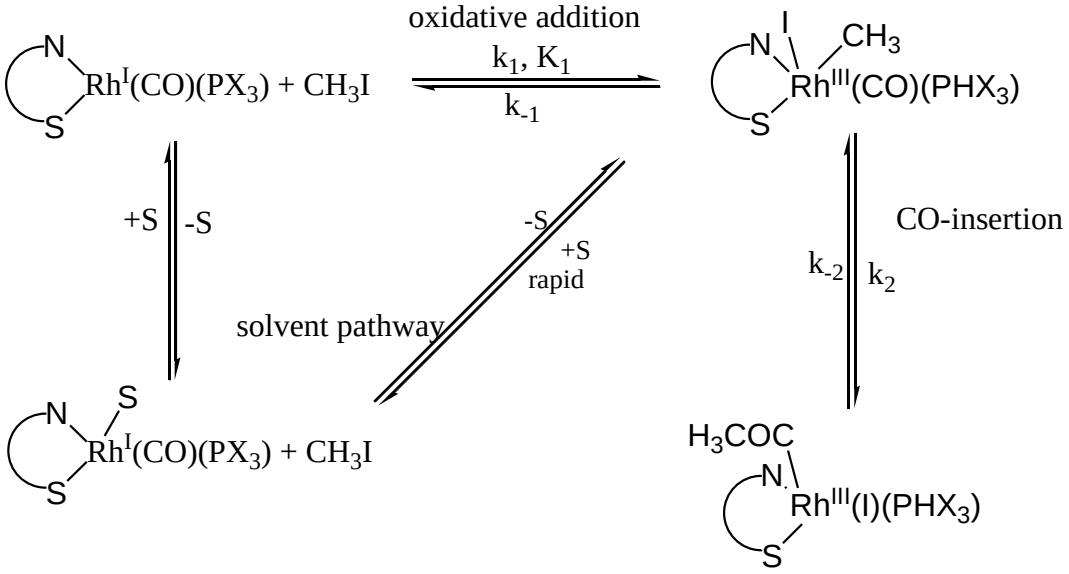

Scheme 2.25: Proposed reaction scheme for the oxidation addition of iodomethane to [Rh(N,S-BID)(CO)(PPh_3)] complexes (S denotes Solvent)

The proposed mechanism is illustrated by considering the formation of the intermediate alkyl complex from the IR data (**Fig 2.9**) for the [Rh(cacsm)(CO)(PPh_3)] complex, cacsm = methyl(2-cyclohexylamino-1-cyclopentene-1-dithiocarboxylate).

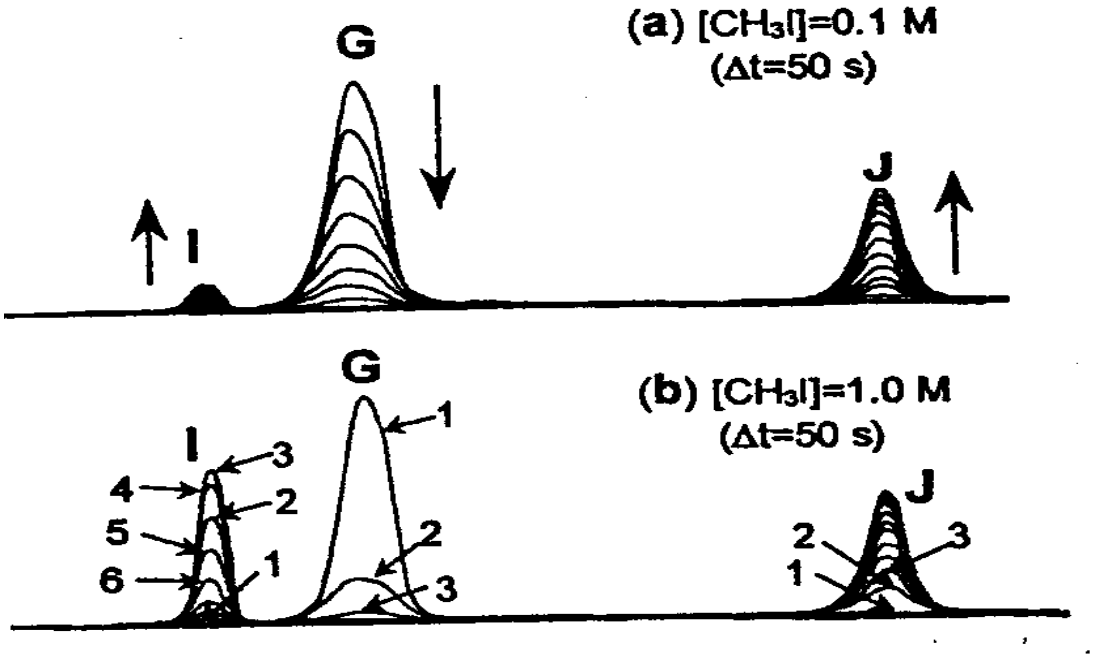

Figure 2.9: Repetitive IR scans in $CHCl_3$ for the [Rh(cacsm)(CO)(PPh_3)] complex at 25°C. G = Rh(I)-reactant, I = Rh(III)-alkyl, J = Rh(III)-acyl.[129]

At low [CH_3I] (**Fig.2.9** top), only a relative small amount of the alkyl intermediate **I** is formed from the Rh(I) reactant **G**. However, when a large concentration of CH_3I is introduced, a significantly larger amount of the alkyl intermediate is formed and much more rapid. In both cases the alkyl intermediate is converted to the acyl species **J**. Infrared, UV/V, and NMR spectroscopy were used to monitor the disappearance of the Rh(I)-CO peak and the formation of the Rh(III)-alkyl-CO peak and within experimental error gave identical observed rate constants.

References

[1] A. Nagpal, R. Unny, Y. C. Joshi, *Heterocycl. Commun.*, **32**, 1585, (2001)

[2] M. Rowley, H. B. Broughton, I. Collins, R. Baker, F. Emms, R. Marwood, S. Patel, C. I. Ragan, S. B. Freedman, P. D. Leeson, *J. Med.Chem.*, **39**, 1943, (1996).

[3] V. V. Alekseev, K. N. Zelenin, S. I. Yakimovich, *Russ. J. Org. Chem.* **31**, 868, (1995).

[4] S. Kawaguchi, *Coord. Chem. Rev.*, **70**, 51, (1986)

[5] M. T. Huang, Y. R. Lou, J. G. Xie, W. Ma, Y.P. Lu, P. Yen, B. T. Zhu, H. Newmark, C. T. Ho, *Carcinogenesis*, **19**, 1697-1700 (1998)

[6] K. M. Jackson, M. DeLeon, C. R Verret, W. B. Harris, *Cancer Letters*, **178**, 161-165 (2002)

[7] M. G., Wirthensohn, *Scientia Horticulturae.*, **82**, 279-288 (1999)

[8] J. A. Kenar, *J. Am. Oil Chem. Soc.*, **80**, 1027-1032 (2003)

[9] M. C. Etter, D. A. Jahn, Z. Yrbanczyk-Lipkowska, *Acta Cryststallogr.,Sect. C:Cryst. Struct. Commun.*, **260**, 43 (1987)

[10] C. R. Hauser, F. W. Swamer, and J. T. Adams, *Organic Reactions*, John Wiley and Sons, New York, **8**, chapter 3, 59 (1954)

[11] J. T. Adams., and C. R. Hauser., *J. Am. Soc.*,***66***, 1220 (1944)

[12] A. Sprague, B. Beckham, C. Adkins, *J. Am. Chem. Soc.*, **56**, 2665 (1934)

[13] H. G. Walker Jr., J. J. Sanderson., and C. R. Hauser, *J. Am. Chem. Soc.*, **75**, 4109 (1953)

[14] A. L. Marzinzik, E. R. Felder., *Tetrahedron Lett.*, **37**, 1003, (1996)

[15] Kyung-Ho Park and L. J. Cox., *Tetrahedron Lett*., **44**, 1067-1069 (2003)

[16] R. C. Mehrotra, R. Bohra, D. P. Gaur, *Metal β-Diketonato and Allied Derivatives.*, Academic Press, New York (1978)

[17] M. R. Jaffe., D. P. Fay., M. Scefola., N. Sutin., *J. Am. Chem. Soc.*, **93**, 2878 (1971)

[18] J. Bordner, P.D. Hammen, E.B. Wipple, *J. Am. Chem. Soc.* **111**, 6572 (1989)

[19] J. L. Burdett, M. T. Rogers, *J. Am. Chem. Soc.*, 2105 (1964)

[20] J. L. Burdett, M. T. Rogers, *J.Phys. Chem.*,**70**(3), 939-941 (1966)

[21] S. Yambe, N. Tsuchida, K. Miyajima, *J. Phys. Chem.*, **108**, 2750-2757 (2004)

[22] Du Plessis, W.C., Vosloo, T.G. and Swarts, J.C., *J. Chem. Soc., Dalton Trans.*, 2507 (1998).

[23] Park, J.D., Brown, H.A. and Lachen, J.R., *J. Am. Chem. Soc.*, **75,** 4753 (1953).

[24] Klose, G., Thomas, P., Uhlemann, E. and Marki, J., *Tetrahedron*, **22,** 2695 (1966).

[25] S. Yambe, N. Tsuchida, *J. Compt. Chem.*, **24**, 939 (2003)

[26] S. G. Mills, P. J. Beak, *Org. Chem*. **50**, 1216 (1985)

[27] E. Iglesians, *J. Org. Chem.*, **68**, 2680-2688 (2003)

[28] S. Bolving, P.E. Hansen, *Mag. Res. Chem*. **34**, 467-478 (1996)

[29] T. J. Wenzel, E. J. Williams, C. Haltiwanger, R. E. Seivers, *Polyhedron*, 3, 4, 369 (1985)

[30] W. Bell, J. A. Crayston, C. Glidewell, M. A. Maxzid, and M. B. Hursthouse, *J. Organomet. Chem.,* **115**, 434 (1992)

[31] A. Yoger, and Y. Mazur, *J. Org.Chem.,* **32**, 2162 (1967)

[32] R. G. Wilkins, *The study of kinetics and mechanism of reactions of transition metal complexes*, Allyn and Bacon, Boston, 44-45 (1974)

[33] C. Coty, *Drug Discovery Dev.*, **6,** 55-60 (2003)

[34] A Avdeef, K.J.Box, J.E.A. Comer, M. Gilges, M. Hadley, C. Hibbert, W. Patterson, K.Y. Tam, *J. Pharm. Biomed. Anal.* **20**, 631-641 (1999)

[35] P. Wiczling, P. Kawczak, A. Nasal, R. Kaliszan, *Anal. Chem.*,**78**, 239-249 (2006)

[36] D.A. Skoog, D.M. West, F. J. Holler, *Fundamentals of Analytical Chemistry*, 6th ed. 146 (1992)

[37] Stary, J., *The Solvent Extraction of Metal Chelates*, Pergamon Press LTD Oxford, England, p 196, 1964.

[38] Ellinger, M., Duschner, H. and Starke, K., *J. Inorg. Nucl. Chem.,* **40**, 1063 (1978).

[39] (a) M. J. Hynes, *Rev.Inorg.Chem.* **11**, 121 (1990); (b) J. P. Fackler,Jr., *Prog. Inorg.Chem.,* **8**, 361 (1966)

[40] T. J. Wenzel, E. J. Williams, C. Haltiwanger, R. E. Seivers, *Polyhedron*, 3, 4, 369 (1985)

[41] K. E. Laintz, E. Tachikava, *Anal.Chem.,* **66**, 2190 (1994)

[42] T. A. Heiner, S. T. D'Arcangelis, F. Farzad, J. M. Stipkala, G. J. Meyer, *Inorg.Chem.,* **35**, 5319 (1996)

[43] W. R. Cullen, E. B. Wickenheiser, *J. Organomet.Chem.* **370**, 141 (1989)

[44] J. Yu, H. Zhang, *Inorg. Chem. Commun.,* **6**(7), 852-854 (2003)

[45] R. G. Wilkinson., *Comprehensive Coordination Chemistry.*, **2**, Pergamon Press, Oxford, 365-9 (1989)

[46] (a) C. J. Pedersen, N. J. Salem, V. Weinmayr, *US Pat.*, **2**, 875, 223 (1959); (b) V. Weinmayr, *Naturwissenschaften*, **45**, 311 (1958)

[47] (a) J. G. Leipolt, S. S. Basson, G. J. van Zyl, G. J. J. Steyn, *J. Organomet. Chem.*, **418**, 241 (1999); (b) J. G. Leipolt, E.C. Grobler, *Transition Met. Chem. (Weinheim, Ger.),* **11**,110

(1986); (c) J. G. Leipolt, G.J. Lamprecht, E. C. Steynberg, *J. Organomet. Chem.*, **402**, 259 (1991)

[48] (a) A. Roodt, J.G. Leipolt, J. C. Swarts, G. J. J. Steyn, *Acta Crystallogr.,Sect. C: Cryst. Struct. Commun.*, **48**, 547 (1992); (b) J. C. Swarts, T.G. Vosloo, J. G. Leipolt, G. J. Lamprecht, *Acta Crystallogr., Sect. C: Cryst. Struct. Commun*, **49**, 82 (1993); (d) C. Glidewell, C. M. Zakaria, *Acta Crystallogr., Sect. C: Cryst. Struct. Commun* , **50**, 1673 (1994); (e) A. Haaland, J. Nilsson, *Chem. Commun.* **88**, (1968); (f) A. Yogev, Y. Mazur, *J. Org. Chem.*, **32**, 2162 (1967)

[49] (a) W. R. Cullen, S. J. Rettig, E. B. Wickenheiser, *J. Mol. Catal.*, **66**, 251 (1991) (b)) W. R. Cullen, E. B. Wickenheiser, *J. Organomet. Chem.*, **370**, 141 (1989)

[50] R. C. Mehrotra, R. Bohra, D. P. Gaur, *Metal β-Diketones and Allied Derivatives*, Academic Press, London, 268-277 (1978)

[51] D. Gibson, *Coord. Chem. Rev.*, **4**, 225 (1969)

[52] S. Peter,*U.S Patent*, **4**, 892, 718 (9 Jan. 1990)

[53] (a) M. B. Ros, J. L. Serrano, *Metallomesogens. Synthesis, Properties and Applications*, Ed, VCH: Weinheim, Germany, Chapter 11 (1996); (b) D. W. Bruce, *J. Chem. Soc. Dalton Trans.*, 2984 (1993); (c) P. Espinet, M. A. Esteruelas, L. A. Oro, J. L. Serrano, E. Sola, *Coord. Chem. Rev.*, **117**, 215 (1992)

[54] W. C. Fernelius., *Inorg. Synth.*, **5**, 188 (1957)

[55] R. G. Wilkinson., *Comprehensive Organometallic Chemistry.*, **3**, Pergamon Press, Oxford, 365-380 (1982)

[56] S. T. Trzaska, H. Zheng., T. M. Swager, *Chem. Mater.* **11**, 130 (1999)

[57] Y. S. Varshavskii, T. G. Cherkasova, *Russ. J. Inorg. Chem.(Engl. Transl.)*, **12**, 899 (1967)

[58] F. Bonati., and G. Wilkinson.,*J. Chem. Soc.*, 3156 (1964)

[59] J. G. Leipolt, L. D. C. Bok, J. S. Van Vollenhoven, A. I. Pieterse, *J. Inorg. Nucl. Chem,*, **40**, 61 (1978)

[60] J. G. Leipolt, L. D. C. Bok, S. S. Basson, T. I. A. Gerber, *Inorg. Chim. Acta*, **34**, L293 (1979)

[61] J. G. Leipoldt., L. D. C. Bok., S. S. Basson and T. I. A. Gerber., *Inorg. Chim. Acta.*, **26**, L35 (1978)

[62] F. Bonati, G. Distefano, G. Minghetti, S. Pignataro, *Z. Anorg. Allg. Chem.*, **386**, 107 (1971)

[63] J. Han., L. F. Zhang., W. Wan., *J. Organomet. Chem.* **672**, 86-93 (2003)

[64] J. G. Leipoldt., S. S. Basson., G. J. Lamprecht.,L. D. C. Bok., and J. J. J. Schlebusch., *Inorg. Chim. Acta.*, **40**, 43-46 (1980)

[65] C. H. Langford and H. B. Gray., *Ligand Substitution Processes*., Benjamin, New York (1966)

[66] L. J. Damoense, W. Purcell, A. Roodt, J. G. Leipolt, *Rhodium Express*, **5**, 10-13 (1995)

[67] J. G. Leipoldt., S. S. Basson., and J. T. Nel., *Inorg. Chim. Acta.,* **74**, 85 (1983)

[68] E. C. Steynberg., G. J. Lamprecht., and J. G. Leipoldt., *Inorg. Chim. Acta.*, **33**, 133 (1987)

[69] F. Huq and A. C. Skapski., *J. Cryst. Mol. Struct.*, **4**, 411 (1974)

[70] C. A. Tolman., *Electron Donor-Acceptor Properties of Phosphorus Ligands.*, No. 1577 from the Central Research Department, Experimental station., E.I. du Pont de Nemours and Company, Welmington, Delaware. (1969)

[71] R. Boese, M. Y. Antipin, D. Blaser, K. A. Lyssenko, *J. Phys. Chem.*, B, **102**, 8654-8660 (1998)

[72] Z. Urbarnczyk-Lipokowska, K. Yoshizawa, S. Toyota, F. Toda, *Cryst. Eng. Comm.*, **5**, 22, 114-116 (2003)

[73] F Huq, A. C. Skapski, *J. Cryst. Struct.* **4**, 411-418 (1974)

[74] E. A. Shor, A.M. Shor, V. A. Nasluzov, A. I. Rubaylo, *J. Struct. Chem.*, **46**, 2, 220-229 (2005)

[75] A. Roodt, J.G. Leipolt, J. C. Swarts, G. J. J. Steyn, *Acta Crystallogr., Sect. C: Cryst. Struct. Commun* , **48**, 547 (1992)

[76] D. Lamprecht, D. J. Lamprecht, J. M. Botha, K. Umakoshi, Y. Sasaki, *Acta Cryst. Sect. C: Cryst. Struct. Commun* **, 53**. 1403-1405 (1997)

[77] J. G. Leipoldt, L. D. C. Bok, S. S. Basson, H. Meyer, *Inorg. Chim. Acta*, **42**, 105-108 (1980)

[78] D. E. Graham, G. J. Lamprecht, I. M. Potgieter, A. Roodt, J. G. Leipoldt, *Trans.Met. Chem.*, **16**,193-195 (1991)

[79] (a) J. P. Collman, L. S. Hegedus, J. R. Norton, R. J. Fink, *Principles and Applications of Organotransition Metal Chemistry*, University Science Books: Mill Valley, CA, (1987) (b) R. H. Crabtree, *Organometallic Chemistry of Transition Metals*, 3rd ed. ,John Wiley & Sons, New York, (2001) (c) J. D. Atwood, *Inorganic and Organometallic Reaction Mechanism*, 2nd ed. Wiley-VCH, New York, (1997)

[80] (a) J. Mana, C. J. Kuehl, J. A. Whiteford, P. J. Stang, *Organomet. Chem.*, **16,** 1897 (1997); (b) C. S. A. Fraser, D. J. Eigler, M. C. Jennings, R. J. Puddephatt, *J. Chem. Soc. Chem.*

Commun., 1224 (2002); (c) C. S. A. Fraser, M. C. Jennings, R. J. Puddephatt, *J. Chem. Soc. Chem. Commun.*, 1310 (2001);(d) S. Achar, R. J. Puddephatt, *J. Chem. Soc. Chem. Commun.*, 1895 (1994)

[81] R. H. Hill, R. J. Puddephatt, *J. Am. Chem. Soc.*, **107,** 1218 (1985)

[82] V. Chauby, J. Daran, C. S. Berre, F. Malbase, P. Kalck, O. D. Ganzalez, C. E. Haslam, and A. Haynes. *Inorg. Chem.*, **41**, 3280-3290 (2002)

[83] J. P. Collman and L. S. Hegedus., *Principles and Applications of Organotransition Metal Chemistry*., 989 (1987)

[84] J. P. Collman, *Acc. Chem. Res*. **1**, 136 (1968)

[85] D. Foster., *Adv. Organomet. Chem.*, **17**, 255, (1979)

[86] G. J. van Zyl., G. J. Lamprecht., J. G. Leipoldt., *Inorg. Chim. Acta*., **75**, 122 (1986)

[87] D. Lamprecht., G. J. Lamprecht., *Inorg. Chim. Acta.*, **309**, 72-76 (2000)

[88] D. Forster, *J. Am. Chem. Soc.*, **98**, 846 (1976)

[89] C. M. Thomas, G. Suss-Fink, *Coord. Chem. Rev.*, **243**, 125 (2003)

[90] (a) J. Rankin, A. D. Poole, A. C. Benyei, D. J Cole-Hamilton, *Chem. Commun.*, 1835 (1997); (b) J. Rankin, A. D. Poole, A. C. Benyei, D. J Cole-Hamilton, *J. Chem. Soc., Dalton Trans.*, 3771 (1999)

[91] K. G. Moloy, R. W. Wegman, *Organomet.* **8**, 2889 (1989)

[92] R. W. Wegman, *Chem. Abstr*. **105**, 78526g (1986)

[93] R. W. Wegman, A. G. Abutjoglou, A. M. Harrison, *J. Chem. Soc., Chem. Commun.*, 1891 (1987)

[94] M. J. Baker, M. G. Giles, A. G. Orpen, M. J. Taylor, R. J. Watt, *J. Chem. Soc., Chem. Commun.*, 197 (1995)

[95] L. Gonsalvi, H. Adams, G.J. Sunley, E. Ditzel, A. Haynes, *J. Am. Chem. Soc.*, **121**, 11233 (1999)

[96] H. S. Lee, J. Y. Bae, D. H. Kim, H. S. Kim, S. J. Kim, S. Cho, J. Ko, S. O. Kang, *Organomet.*, **21**, 210-219 (2002)

[97] K. V. Katti, B. D. Santarsiero, A. A. Pinkerton, R. G. Cavell, *J. Inorg. Chem.* **32**, 5919 (1993)

[98] C. A. Carraz, E. J. Ditzel, A. G. Orpen, D. D. Ellis, P. G. Pringle, G. Sunley, *J. Chem. Commun.*, 1277-1278 (2000)

[99] L. Cavallo, and M. Sola, *J. Am. Chem. Soc*., **123**, 12294-12302 (2001)

[100] G. J. P. Britovsek, V. C. Gibson, D. F. Wass, *Angew. Chem., Int. ed.*, **38**, 429 (1999)

[101] P. M. Maitlis, A. Haynes, G. J. Sunley, M. J. Howard, *j. Chem. Soc., Dalton Trans.*, 2187 (1996)

[102] L. Gonsalvi, H. Adams, G.J. Sunley, E. Ditzel, A. Haynes, *J. Am. Chem. Soc.*, **124**, 13597 (2002)

[103] J. Rankin, A. D. Poole, A. C. Benyei, D. J. Cole-Hamilton, *J. Chem. Soc., Dalton Trans.*, 3771 (1999)

[104] (a) D. Forster, *Adv. Organomet.Chem.*, **17**, 255 (1979) (b) T. W. Dekleva, D. Forster, *Adv. Catal.*, **34**, 81 (1986) (c) M. J. Howard, M. D. Jones, M. S. Roberts, M. S. Taylar, *Catal. Today*, **18**, 325 (1993)

[105] A. Haynes, B. E. Mann, G. E. Morris, P. M. Maitlis, *J. Am. Chem. Soc.*, **115**, 4093 (1993)

[106] Pearson, R.G., *Symmetry rules for Chemical reactions*, Wiley Interscience, New York, (1976) p.280 -353, 405 – 413.

[107] P. B. Chock, J. Halpern, *J. Am. Chem. Soc.*, **88**, 3511 (1966)

[108] (a)J. G. Leipoldt., S. S. Basson., L. Botha., *J. Inorg. Chim. Acta.*, **168**, 215 (1990); (b) J. G. Leipoldt, E. C. Steynberg, R. van Eldik, *Inorg. Chem.*, **26**, 3068 (1987); (c) G. J. Van Zyl, G. J. Lamprecht, J. G. Leipolt, T. W. Swaddle, *Inorg. Chem. Acta*, **143**, 223 (1988)

[109] M. Bassetti, A. Capone, L. Mastrofrancesco, and M. Salamone., *Organomet.*, **22**, 2535-2538 (2003)

[110] L. Cavallo, M. Sola, *J. Am. Chem. Soc.*, **123**, 12294-12302 (2001)

[111] P. Pelagatti, A. Bacchi, C. Bobbio, M. Carcelli, M. Costa, C. Pelizzi, and C. Vivorio., *Organomet.*, **19,** 5440-5446 (2000)

[112] J. A. Gaunt, V. C Gibson, A. Haynes, S. K. Spitzmesser, A. J. P. White, and D. J. Williams., *Organomet.*, **23**, 1015-1023 (2004)

[113] W. O. Siegl, *J. Organomet. Chem.* **107**, C27 (1976)

[114] M. D. Fryzuk, P. A. macneil, S. Rettig, *J. Organomet.*, **5,** 2469 (1986)

[115] D. Cuervo, J. Diez, M. P. Gamasa, S. Garcia-Granda, J. Gimeno, *Inorg. Chem.*, **41**, 4999 (2002)

[116] D. A. Cooper, S. J. Rettig, A. Storr, *Can. J. Chem.*, **64**, 566 (1986)

[117] M. Bassetti, A. Capone, M. Salamone., *Organomet.*, **23**, 247-253 (2004)

[118] A. J. Hart-Davies and W. A. G. Graham., *Inorg. Chem.*, **9**, 2658 (1970)

[119] S. S. Basson., J. G. Leipoldt., and J. T. Nel. *Inorg. Chim. Acta.*, **84**, 167 (1984)

[120] M. Kubota, G. W. Kiefer, R. M. Ishikawa, K. E. Bencala, *Inorg. Chim. Acta*, **7**, 195 (1973).

[121] R. Ugo., A. Pasini., A. Fusi., and S. Cerini., *J. Am. Chem. Soc.*, **94**, 7364 (1972)

[122] G. J. van Zyl., G. J. Lamprecht., J. G. Leipoldt., *Inorg. Chim. Acta*., **143**, 223 -227 (1988)

[123] J. K. Stille, S. Y. Lau, *Acc. Chem. Res.*, **10**, 434 (1977)

[124] G. J. J. Steyn, A. Roodt., J. G. Leipoldt., *Inorg. Chem*., **31**, 3477 (1992)

[125] J. A. Venter., J. G. Leipoldt., R. van Eldik., *Inorg. Chem*., **30**, 2207 (1991)

[126] J. J. Gideon., A. Roodt., and J. G. Leipoldt., *Rhodium Express.*, **1**, 25-29 (1992)

[127] S. S. Basson., J. G. Leipoldt., A. Roodt., and J. A. Venter., *Inorg. Chim. Acta.*, **119**, 35, (1986)

[128] S. S. Basson., J. G. Leipoldt., A. Roodt., and J. A. Venter., and T.J. van der Walt., *Inorg. Chim. Acta.*, **119**, L9 (1986)

[129] A. Roodt, and G. J. J. Steyn., *Recent Res. Devel. Inorganic Chem.*, **2**, 1-23 (2000)

3 Results and discussion.

3.1 Introduction.

In this study the synthesis, oxidative addition kinetics, thermodynamic properties and crystal structure of a series of new complexes of the type [Rh(β-diketonato)(CO)(PPh_3)] are described. Four β-diketones, Hba (1-phenyl-1,3-butanedione, benzoylacetone, $C_6H_5COCHCOCH_3$); Hbap (1-phenylpentane-1,3-dione, propanylacetophenone, $C_6H_5COCHCOCH_2CH_3$); Hbab (1-phenylhexane-1,3-dione, buterylacetophenone, $C_6H_5COCHCOCH_2CH_2CH_3$); Hbav (1-phenylheptane-1,3-dione, valerylacetophenone, $C_6H_5COCHCOCH_2CH_2CH_2CH_3$), were synthesized and characterized for this purpose.

Spectroscopic characterisation of the complexes include techniques such as infra-red (IR), ultra violet (UV/VIS), X-ray crystallography, nuclear magnetic resonance (^1H ^{13}C and ^{31}P NMR) spectroscopy and the determination of the pK_a values for the β-diketones synthesized.

3.2 Synthesis and identification of β-diketones

3.2.1 Synthesis of β-diketones

Four phenyl-containing β-diketones {Hba (1-phenyl-1,3-butanedione, benzoylacetone); Hbap (1-phenylpentane-1,3-dione, propanylacetophenone); Hbab (1-phenylhexane-1,3-dione, buterylacetophenone) and Hvab (1-phenylheptane-1,3-dione, valerylacetophenone)} were prepared by Claisen condensation of acetophenone and the appropriate ester (ethylacetate, propanylacetate, buterylacetate, and valerylacetate respectively). Lithium diisopropylamide (LDA) or sodium ethoxide was used as a basic initiator for the synthesis. Synthetic routes of these β-diketones are shown in **Scheme 3.1.**

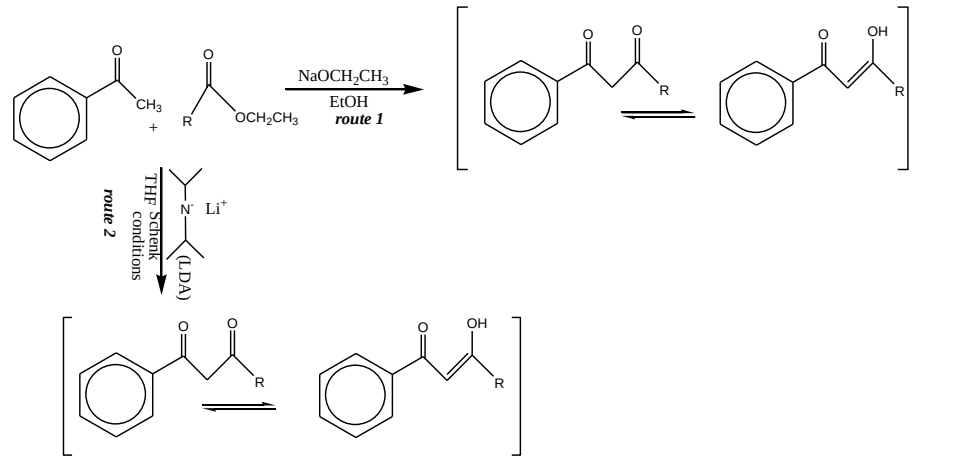

Scheme 3.1: **Synthetic routes utilized during the synthesis of β-diketones by Claisen condensation of acetophenone and an appropriate ester in the presence of a base.**

Pure products are mostly found when route 2 is followed with yields ranging from 24-65 %. Route 1 was followed by introducing the appropriate ester (pure and dry) into sodium ethoxide on ice and after stirring acetophenone was added dropwise, ethanol being the solvent used. The reaction mixture was left to stand in ice overnight giving the product. Route 2 on the other hand, was followed under Schlenk conditions where acetophenone was dissolved in tetrahydrofuran (THF) and after some stirring a slight excess amount of lithium diisopropylamide (LDA) was added followed by an appropriate ester giving the product. During the addition of a base LDA which is a brown-red liquid the colour disappears. The discolouring of LDA implies that it has reacted with the ketone and when the reaction mixture changes to orange colour it signifies an excess of LDA. The slow addition of LDA is important to avoid hot spots leading to decomposition. Flash column chromatography was used to separate the β-diketones from the starting material and other side products.

Low yields and impure tar like products were obtained when route 1 was followed for the synthesis of Hbap; Hbab and Hbav. This is attributed to the fact that the longer the alkyl chain of the β-diketone, the less soluble it becomes in the polar solvent ethanol, which then allows the occurrence of other undesired side reactions.

Synthesis of Hba 70%, Hbap 55%, Hbab 42% and Hbav 40% was done by R. Levine *et.al*[1] utilising sodium amide as a base and got better yields.

A proposed mechanism for both routes is shown in the following **Scheme 3.2** below.

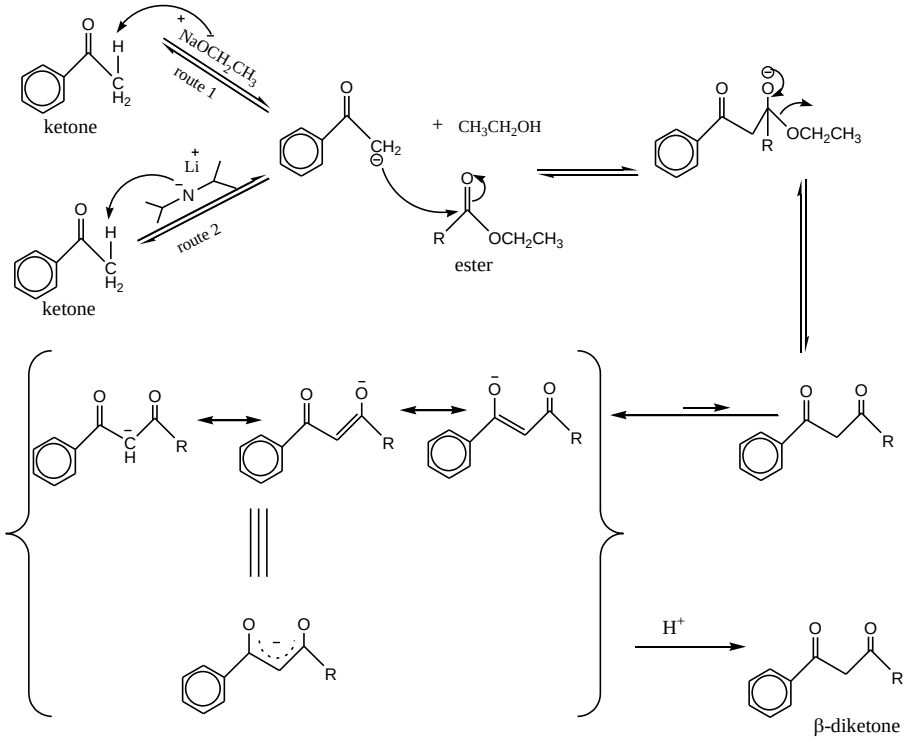

Scheme 3.2: Proposed mechanism for the synthesis of β-diketones

β-diketones exist in solution and in vapour phase as mixtures of keto and enol tautomers. In the solid state, the enol form is often the form mostly observed.[2] In this study, a comparision of the relative intensities of the CH_2 (keto) and CH (enol) signals in solution was done, where the enol form dominates. The ^1H NMR spectra of all the β-diketones synthesised clearly distinguish between the two tautomers. The difference between the two tautomers manifested in especially in the large difference in the position, δ_H in ppm, of the signal of the methine proton. The ^1H NMR of Hbap is provided in **Figure 3.1** as an example.

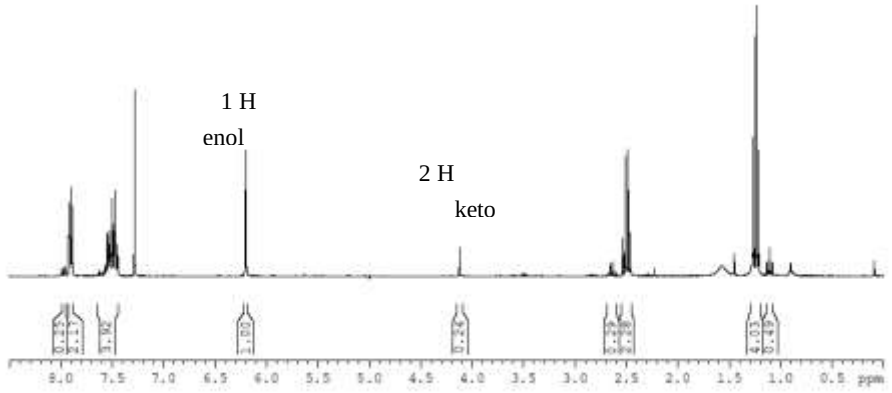

Figure 3.1: **^{1}H NMR spectrum in $CDCl_3$ indicating the two tautomers for the β-diketone Hbap (1-phenylpentane-1,3-dione, $C_6H_5COCH_2COCH_2CH_3$). δ_H(300 MHz, $CDCl_3$) ENOL:1.25 (3H, t, CH_3), 2.45 (2H, q, CH_2), 6.21 (1H, s, CH), 7.44-7.58 (3H, m, aromatic), 7.88-7.99 (2H,m, aromatic).**
δ_H(300 MHz, $CDCl_3$) KETO: 1.15 (3H, t, CH_3),.2.65 (2H, q, CH_2), 4.12 (2H, s, CH_2), 7.44-7.58 (3H, m, aromatic), 7.88-7.99 (2H,m, aromatic).

The equilibrium constant K_c = [keto]/[enol] = 0.122/1.00 of the Hbap toutomers, is calculated from the integrals of the methine proton of the enol toutomer. The K_c value for other β-diketone toutomers (Hbab, Hbav) were 0.087/1.00 and 0.086/1.00 respectively.

3.2.2 Determination of group electronegativities

Accurate apparent electronegativities (χ_R) of R groups for esters can be obtained from a linear fit between χ_R and the carbonyl IR stretching frequencies (ν_{CO}).[4] The group electronegativities of the R groups = CH_2CH_3, $CH_2CH_2CH_3$ and $CH_2CH_2CH_2CH_3$ were determined in this study using the ν_{CO} of their appropriate esters. **Figure 3.2** shows a calibration curve of some known group electronegativities where a linear fit gave the relationship $\nu_{CO} = 74.53\ \chi_R + 1561$.

Table 3.1: **IR stretching frequencies of esters of the type $RCOOCH_3$ and group electronegativities of each R group.**[4]

R	ν_{CO}	χ_R
CF_3	1785	3.01
Cl	1780	2.97
CCl_3	1768	2.76
$CHCl_2$	1755	2.62
CH_2Cl	1748	2.48
CH_2Br	1740	2.44
CH_3	1738	2.34
Ph	1725	2.21
H	1717	2.13
Fc	1700	1.87
CH_2CH_3 (This study)	1733	2.31
$CH_2CH_2CH_3$ (This study)	1740	2.41
$CH_2CH_2CH_2CH_3$ (This study)	1726	2.22

The experimentally determined ν_{CO} for R = CH_2CH_3, $CH_2CH_2CH_3$ and $CH_2CH_2CH_2CH_3$ were then fitted to the calibration curve (see **Figure 3.2**).

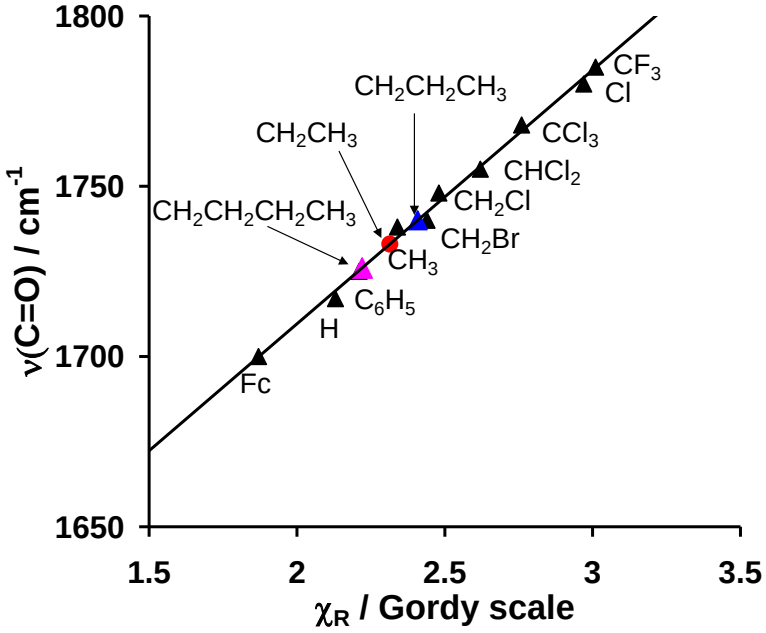

Figure 3.2: Linear relationship observed between the carbonyl stretching frequencies (ν_{CO}) and group electronegativities (χ_R) of esters of the type $RCOOCH_3$.

The proportion of the enol tautomers generally increases when an electron withdrawing group is substituted at an ∝-position relative to a carbonyl group in β-diketones or when the ligands contain an aromatic ring.[3] In this study, β-diketones synthesised contain an aromatic ring as such enol tautomers were dominant.

In order to explain the dominance of the observed enol isomer in each case, two different driving forces controlling the conversion from β-diketone to an enolic isomer must be considered. The first is an electronic driving force in which the formation of the preferred enol isomer is controlled by the electronegativity of phenyl substituent and the R group. When the electronegativity of the R group is greater than that of the phenyl group the carbon atom of the carbonyl adjacent to the phenyl group will be less positive in character than the carbon atom of the other carbonyl group. Consequently, from an electronic point of view, the dominant isomer should be RCOCH=C(OH)Ph. Another driving force that determines the preferred enol isomer configuration in β-diketones where aromatic side groups are present, is the resonance driving force. The resonance driving force implies that the formation of different canonical forms of a specific isomer of PhCOCH=C(OH)R will lower the energy of this specific isomer enough to allow it to dominate over the existence of other isomers.[4]

Inspection of the ^1H NMR of the β-diketones $C_6H_5COCHCOR$ with R = $(CH_2(CH_2)_nCH_3)$, n = 0 - 2 indicate that the enol isomer RCOCH=C(OH)Ph is formed in each case. The CH_2 signal of the R group ($\underline{CH_2}(CH_2)_nCH_3$) near 2.6 ppm (**Figure 3.1**), which is relatively deshielded, is typical of an α methylene group to the C=O. This is due to the deshielding effect of the electron withdrawing C=O. If the enolization was on the side of the R group, then the CH_2 signal would be less deshielded at approximately 2.2 ppm due to the less effected electron withdrawing effect of the conjugated enol system. Thus the ^1H NMR implies that the enolization is on the side of the Ph group.

Thus the electronic driving forces carry priority over resonance driving forces for Hbap, Hbab and Hbav, contrary with what was proposed by Plessis *et. al.*[29] that for β-diketone possessing aromatic side groups resonance driving forces carry priority over electronic driving forces.

3.2.3. pK_a determination.

The pK_a values of the β-diketones Hacac, Hba, Hbap, Hbab and Hbav were obtained by measuring the UV absorbance/pH data during an acid-base titration in 10% water-acetonitrile mixture, μ = 0.100 mol dm^{-3} (sodium perchlorate monohydrate, $NaClO_4$) at 25(1)˚C. A least squares fit of absorbance/pH data with β-diketone concentration ± 0.04 mmol dm^{-3} using the following equation was obtained:

$$A_T = \frac{A_{HA}10^{-pH} + A_A 10^{-pK_a}}{10^{-pH} + 10^{-pK_a}}$$

A_T = total absorbance, A_{HA} = the absorbance of the β-diketone in the protonated (acidic) form and A_A = the absorbance of the β-diketone in deprotonated (basic) form. Apparent pK_a values, pK'_a were determined in this study, since no attempt was made to distinguish the experimentally obtained pK'_a value to separate pK_a values for the enol and keto tautomers.

The UV/visible spectra of the protonated (acidic) and deprotonated (basic) forms of β-diketones Hacac, Hba, Hpab, Hbab, and Hbav with their basic and acidic titration curves are shown in **Figure 3.3** to **Figure 3.7** with the peak absorption coefficients in **Table 3.2**. Values obtained from titration from low to high pH or from high to low pH, yield pK'_a values within 0.1 units from each other.

Table 3.2: pK_a values of β-diketones at 360 nm in 10% acetonitrile/water mixture.

β-diketone	Concentration m mol. dm^{-3}	pK_a at 360nm (acidic)	pK_a at 360nm (basic)	Published value
Hacac	**0.34**	**9.32(2)**	**8.99(1)**	**8.9[4]**
Hba	**0.308**	**8.81(8)**	**8.90(1)**	**8.7[5]**
Hbap	**0.183**	**9.38(1)**	**9.28(3)**	
Hbab	**0.147**	**9.28(1)**	**9.17(5)**	
Hbav	**0.172**	**9.40(6)**	**9.25(5)**	

Table 3.3: pK_a[1] values of various phenyl containing β-diketone.

$C_6H_5COCH_2COR$	R	pK_a
Hba	**CH_3**	**8.7**
Hdbm	**C_6H_5**	**9.35**
Hbfcm	**Fc**	**10.41**
Hbtfa	**CF_3**	**6.3**
Hbap	**CH_2CH_3**	**9.33**

Hbab	**$CH_2CH_2CH_3$**	**9.23**
Hbav	**$CH_2CH_2CH_2CH_3$**	**9.33**

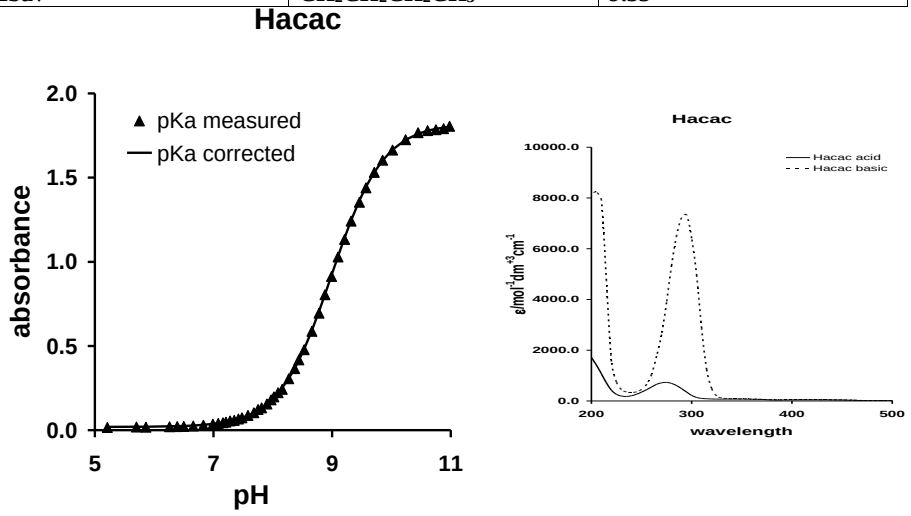

Figure 3.3: **UV/visible spectra of the protonated (acidic) and deprotonated (basic) forms of 0.34mmoldm^{-3} of Hacac in 10% acetonitrile/water mixture, μ = 0.100 moldm^{-3} ($NaClO_4$) at 25.0(1)^{0}C (right) with graphs showing an effect of pH on absorbance at 360 nm (left).**

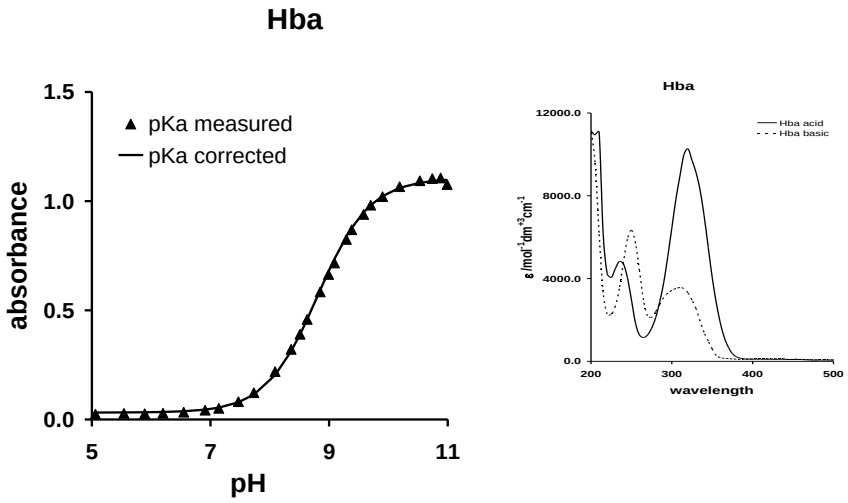

Figure 3.4: **UV/visible spectra of the protonated (acidic) and deprotonated (basic) forms of 0.308mmoldm^{-3} of Hba in 10% acetonitrile/water mixture, μ = 0.100 moldm^{-3} ($NaClO_4$) at 25.0(1)^{0}C (right) with graphs showing an effect of pH on absorbance at 360 nm (left).**

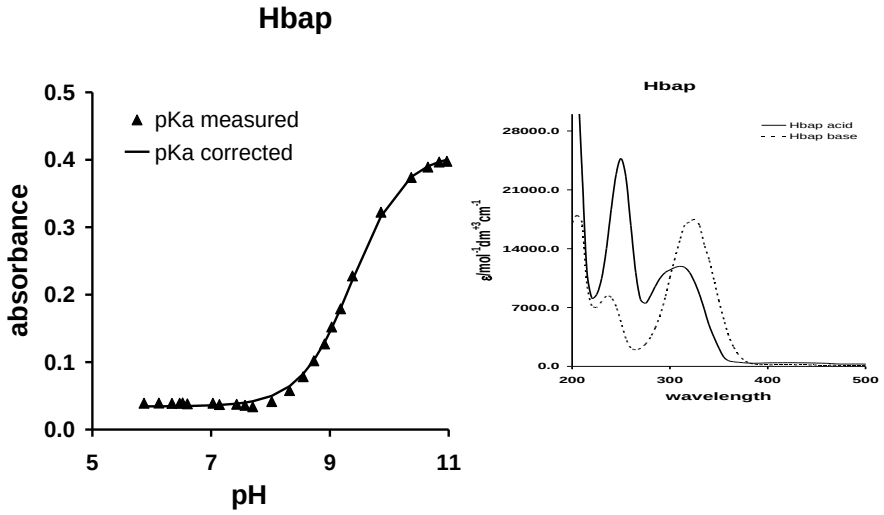

Figure 3.5: **UV/visible spectra of the protonated (acidic) and deprotonated (basic) forms of 0.183mmoldm^{-3} of Hbap in 10% acetonitrile/water mixture, μ = 0.100 moldm^{-3} ($NaClO_4$) at 25.0(1)^{0}C (right) with graphs showing an effect of pH on absorbance at 360 nm (left).**

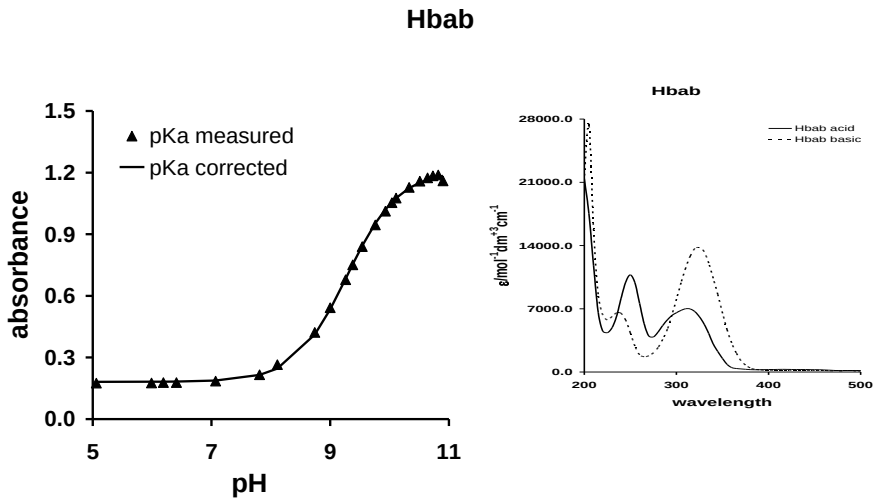

Figure 3.6: **UV/visible spectra of the protonated (acidic) and deprotonated (basic) forms of 0.147mmoldm^{-3} of Hbab in 10% acetonitrile/water mixture, μ = 0.100 moldm^{-3} ($NaClO_4$) at 25.0(1)^{0}C (right) with graphs showing an effect of pH on absorbance at 360 nm (left).**

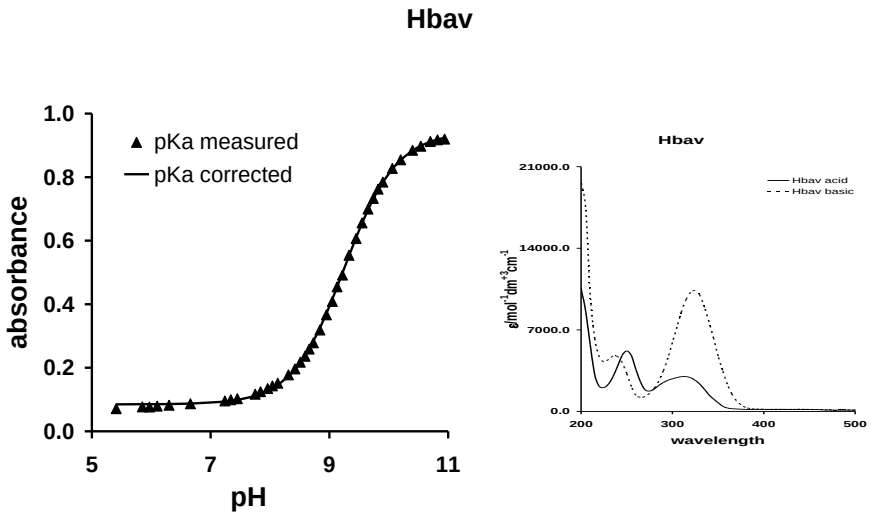

Figure 3.7: **UV/visible spectra of the protonated (acidic) and deprotonated (basic) forms of 0.172mmoldm^{-3} of Hbav in 10% acetonitrile/water mixture, μ = 0.100 moldm^{-3} ($NaClO_4$) at 25.0(1)^{0}C (right) with graphs showing an effect of pH on absorbance at 360 nm (left).**

The pK'_a value obtained for Hacac in a 10% CH_3CN/water mixture in this study is with in 99% of the last published value of the pK'_a (Hacac) obtained in water titrated with sodium hydroxide.[4] 10% CH_3CN/water mixture was used in this study, since the β-diketones Hba, Hbap, Hbab and Hbav were not soluble in pure water. The pK'_a value obtained for Hba in this study is within 98% of the last published value.[5] To the knowledge of the author, no pK'_a values for the β-diketones Hbap, Hbab and Hbav are available. The pK'_a values of $C_6H_5COCH_2CO(CH_2)_nCH_3$ for n = 1-3 are, within the experimental error, the same, though 0.4 pH units higher than Hba (n = 0). The pK'_a values of a series of phenyl containing β-diketones are given in

Table 3.3.

An increase in the chain length of the R group seem not to have any impact or influence on the pK_a[1] values of the β-diketones synthesized.

3.3 Synthesis and identification of Rh(I)-complexes

3.3.1 Synthesis of [Rh(β-diketonato)$(CO)_2$]

The yellow-orange complexes of [Rh(β-diketonato)$(CO)_2$] with β-diketonato = ba (95% yield), pab (new compound, 27% yield), bab (new compound, 17% yield), and bav (new compound, 18%) were synthesized by a reaction pathway shown in **Scheme 3.3.**

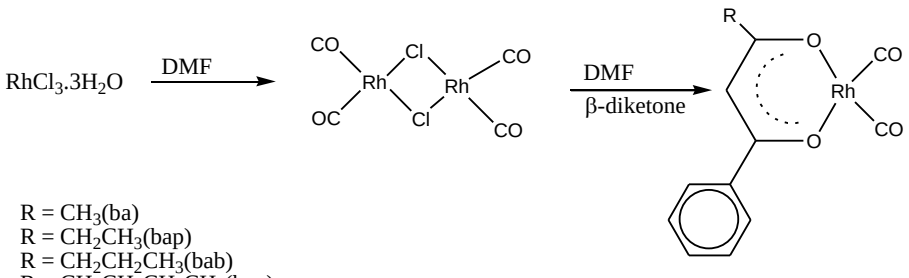

Scheme 3.3: Synthetic route for the synthesis of the [Rh(β-diketonato)$(CO)_2$] complexes.

The dimer [$Rh_2Cl_2(CO)_4$] used was a convenient starting material for the synthesis of all the [Rh(β-diketonato)$(CO)_2$] complexes. [$Rh_2Cl_2(CO)_4$] was obtained *in situ* by refluxing $RhCl_3.3H_2O$ in DMF for *ca*. 30 minutes until a light yellow refluxing mixture was obtained. An equivalent amount of β-diketone added into the reaction mixture while stirring yielded the desired products. The obtained products were precipitated by ice water. Crystallographic quality products were obtained by recrystallization from hot hexane. The longer the chain on the R-group the more difficult it is to crystallise the product. Silica gel column chromatography was employed to clean the products which were analysed by NMR. **Figure 3.8** shows the ^1H NMR spectrum of a complexe of the type [Rh(β-diketone)$(CO)_2$].

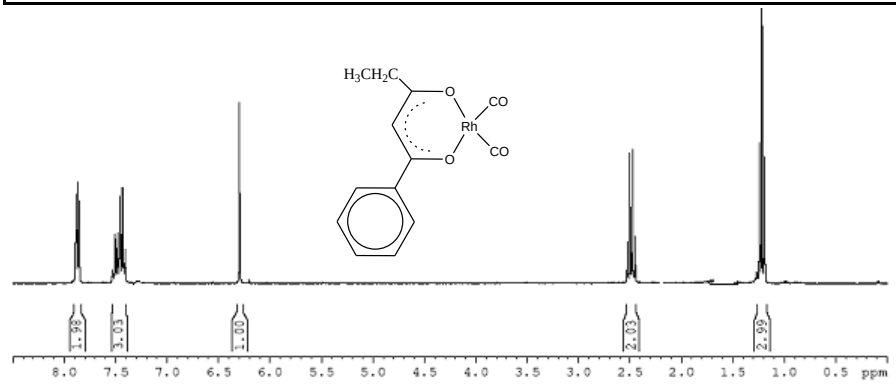

Figure 3.8: ^{1}H NMR of [Rh(bap)(CO)$_2$] δ_H(300 MHz, $CDCl_3$) [Rh(bap)(CO)$_2$]: 1.21 (3H, t, CH_3), 2.49 (2H, q, CH_2), 6.31 (H, s, CH), 7.39-7.54 (3H, m, aromatic), 7.84-7.90 (2H, m, aromatic).

3.3.2 Synthesis of [Rh(β-diketonato)(CO)(PPh_3)].

The light yellow [Rh(β-diketonato)(CO)(PPh_3)] complexes with β-diketonato = bap (new compound 16% yield), bab (new compound, 13% yield) and bav (new compound, 14% yield) were obtained by adding an equivalent amount of PPh_3 dissolved in hot hexane, to a hot [Rh(β-diketonato)(CO)$_2$] *n*-hexane orange solution. The reaction is immediate with displacement of one CO ligand and the precipitation of the monocarbonyl product [Rh(β-diketonato)(CO)(PPh_3)].

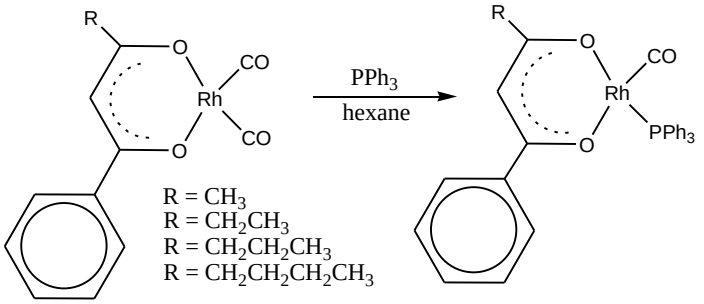

Scheme 3.4: Synthesis of [Rh(β-diketonato)(CO)(PPh_3)] complexes from the corresponding [Rh(β-diketonato)(CO)$_2$] complexes.

Spectra by ^{1}H NMR showed that for each of the [Rh(β-diketonato)(CO)(PPh_3)] complexes synthesised, two isomers exist in solution.

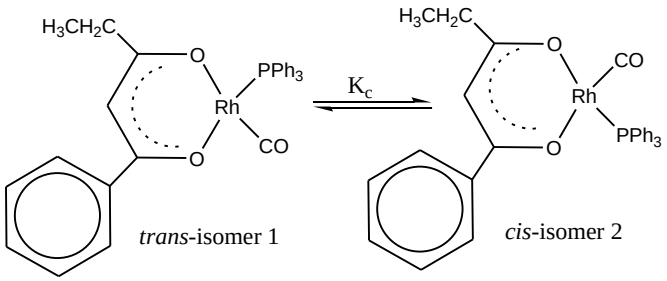

Scheme 3.5: The equilibrium between the two isomers of the complex [Rh(bap)(CO)(PPh$_3$)]. Theory[678910] confirms that isomer 1 should be dominant.

$$K_c = \frac{[isomer\,2]}{[isomer\,1]}$$

The difference between the two isomers is manifested especially in the large difference in the position, δ_H in ppm, of the signals of the protons of the alkyl group of the β-diketonato ligand, see **Figure 3.9** for [Rh(bap)(CO)(PPh$_3$)].

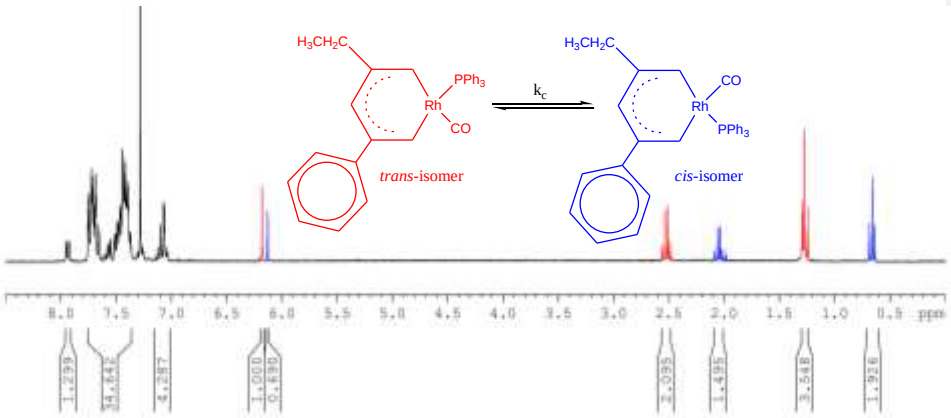

Figure 3.9: ^{1}H NMR of isomer mixture of [Rh(bap)(CO)(PPh$_3$)]. δ_H (300 MHz, $CDCl_3$) ISOMER 1 (red): 1.27 (3H, t, CH_3), 2.52 (2H, q, CH_2), 6.21 (1H, s, CH), 7.02-7.99 (20H, m, aromatic).
δ_H (300 MHz, $CDCl_3$) ISOMER 2 (blue): 0.66 (3H, t, CH_3), 2.01 (2H, q, CH_2), 6.10 (1H, s, CH), 7.02-7.99 (20H, m, aromatic).

The equilibrium constant K_c = [isomer 2]/[isomer 1] = 0.69/1.00 of [Rh(bap)(CO)(PPh$_3$)] isomers, is calculated from the peak integrals of the methine proton of the β-diketonato ligand

bap. The two isomers are the isomer with PPh_3 *trans* to the oxygen nearest to the more electron donating phenyl group of the chelate ring., the expected isomer labelled as isomer 1 (red), and the isomer with PPh_3 *cis* to the oxygen nearest to the phenyl group as defined in **Scheme 3.1** is labelled isomer 2 (blue). Isomer 1 is the predominant isomer due to the *trans*-influence where PPh_3 is *trans* to the oxygen near an electron donating group (phenyl) which has a larger *trans*-influence compared to an alkyl group and will be referred to as the *trans* isomer. This is in agreement with the polarization theory since the oxygen atom nearest to an alkyl group will be least polarisable since the alkyl group is electron attracting.

Table 3.4: ^{1}H NMR spectral parameters and the ratio of the isomers (as illustrated in Scheme 3.5) in solution of $CDCl_3$ [Rh(β-diketonato)(CO)(PPh_3)] complexes.

β-diketonato	Concentration dm^3mol^{-1}	Isomer no.	δ ^{1}H/ppm	Ratio isomers	K_c
bap	**0.01483**	**1**	**6.21, 2.52, 1.27**	**41%**	**0.69**
		2	**6.10, 2.01, 0.66**	**59%**	
bab	**0.01367**	**1**	**6.21, 2.47, 1.78, 1.01**	**44%**	**0.78**
		2	**6.09, 1.99, 1.13, 0.68**	**56%**	
bav	**0.02867**	**1**	**6.21, 2.49, 1.74, 1.44, 0.97.**	**44%**	**0.78**
		2	**6.09, 2.02, 1.07, 0.74**	**56%**	

The K_c values of synthesised [Rh(β-diketonato)(CO)(PPh_3)] complexes varied with temperature. These values could be quantified by the following equation:

$$\ln K_{c2} = \ln K_{c1} - \frac{\Delta H}{R}\left(\frac{1}{T_2} - \frac{1}{T_1}\right)$$

where K_{c2} and K_{c1} are equilibrium constants at temperatures T_2 and T_1, R = 8.314$JK^{-1}mol^{-1}$ and ΔH the reaction enthalpy. From this equation then a linear relationship of $\ln K_c$ *vs* 1/T is expected with a slope of -ΔH/R. **Figure 3.10** shown the expected linearity of the synthesised complexes in this study, [Rh(bap)(CO)(PPh_3)], [Rh(bab)(CO)(PPh_3)] and [Rh(bav)(CO)(PPh_3)].

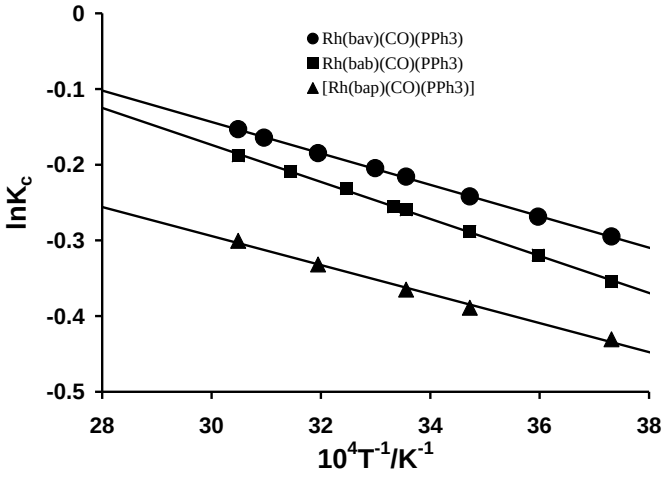

Figure 3.10: Temperature dependence of K_c for the equilibrium position between the *trans* and *cis* isomers of [Rh(bap)(CO)(PPh_3)], [Rh(bab)(CO)(PPh_3)] and [Rh(bav)(CO)(PPh_3)].
The thermodynamic quantities ΔG and ΔS may be calculated from the equation $\Delta G = RTInK_c$ and $\Delta G = \Delta H - T\Delta S$. An increase in temperature increases the K_c value. Results at 298K are summerized in Table 3.5

Table 3.5: The equilibrium constant K_c at 298.15K and the thermodynamic data at 298.15K relevant for [Rh(bap)(CO)(PPh_3), [Rh(bab)(CO)(PPh_3) and [Rh(bav)(CO)(PPh_3).

Complex	K_c (298.15K)	ΔH ($kJmol^{-1}$)	ΔG ($kJmol^{-1}$)	ΔS ($Jmol^{-1}K^{-1}$)
[Rh(bap)(CO)(PPh_3)	0.72	2.2	0.8	4.6
[Rh(bab)(CO)(PPh_3)	0.77	2.0	0.6	4.7
[Rh(bav)(CO)(PPh_3)	0.80	1.7	0.5	4.0

3.3.3 Infrared spectra of mono and di-carbonyl rhodium complexes.

The mono and di-carbonyl products formed during the synthesis give different stretching frequencies for the CO moieties. For example, the spectrum of [Rh(bab)$(CO)_2$] gives two distinctive separate peaks at 2084 and 2014 cm^{-1}.

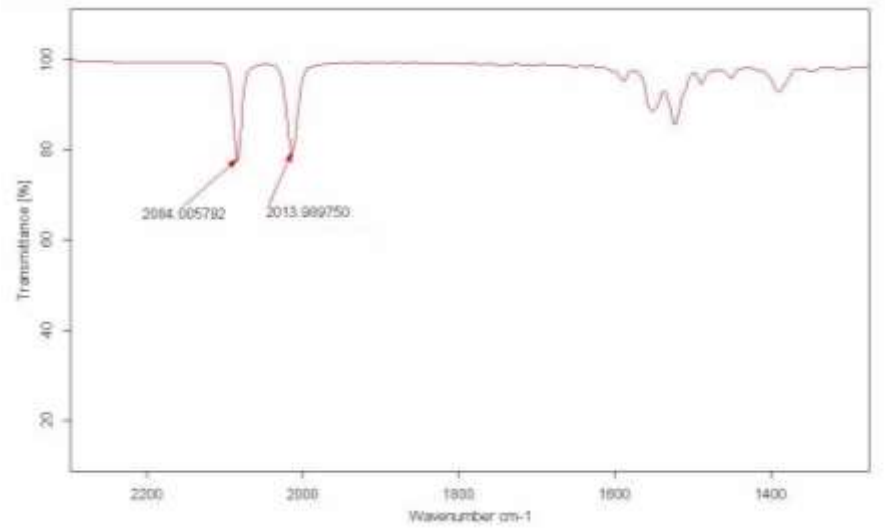

Figure 3.11: Infrared spectrum for [Rh(bab)(CO)$_2$]

Upon substitution of one of the carbonyl ligands with a tertiary phosphine PPh_3, monocarbonyl(phosphine) rhodium(I) compounds are obtained. These compounds show only one carbonyl peak.

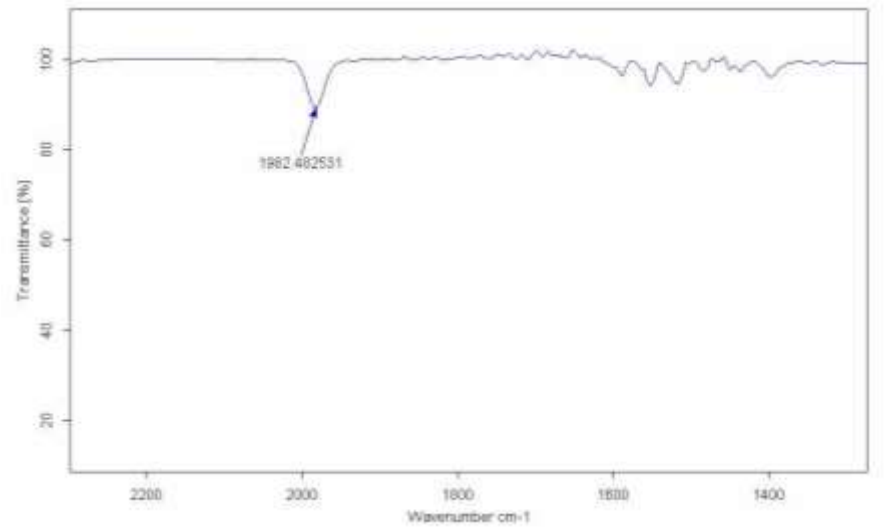

Figure 3.12: Infrared spectrum for [Rh(bap)(CO)(PPh$_3$)]

The lower CO wavenumber observed for monocarbonyl(phosphine) rhodium(I) compounds is in agreement with the higher electron density on the rhodium centre due to the fact that PPh_3 is electron donating to the rhodium nucleus through the σ bond.

The reaction of monocarbonyl(phosphine) rhodium(I) compounds with methyl iodide yield to the formation of Rh(III) complexes.

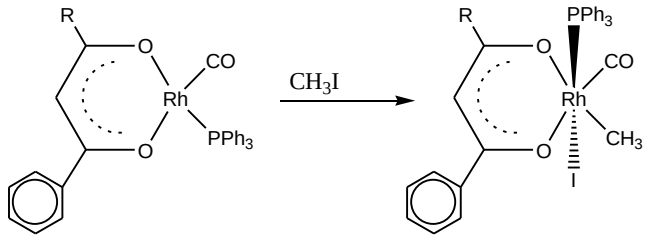

Scheme 3.6: Oxidative addition of MeI to [Rh(β-diketonato)(CO)(PPh_3)] leads to the rhodium(III) complex [Rh(β-diketonato)(CO)(PPh_3)(CH_3)(I)].

For example the IR CO stretching CO wavenumber for [Rh(bab)(CO)(PPh_3)(CH_3)(I)] is 2064 cm^{-1}. This is because rhodium(III) nucleus is more electron deficient than the rhodium(I) nucleus and this then manifests in a single peak observed at a higher wavenumber than that observed for monocarbonyl(phosphine) rhodium(I) complex.

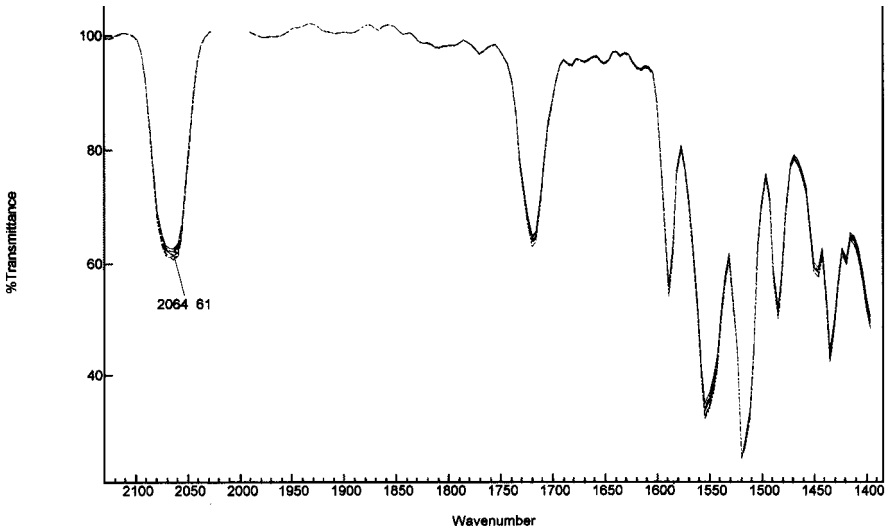

Figure 3.13: Infrared spectrum for [Rh(bab)(CO)(CH_3)(I)(PPh_3)].

From the de Broglie equation, $\Delta E = hc/\lambda$, it is noted that shorter wavelengths (longer wavenumber in cm^{-1}) represent stronger C-O bond energies in CO and therefore weaker Rh-C bonds. This then implies that the Rh(III)-C bond (ν = 2064 cm^{-1} in [Rh(bab)(CO)(CH_3)(I)(PPh_3)]) is weaker than Rh(I)-C bonds (ν = 1982 cm^{-1} in [Rh(bap)(CO)(PPh_3)]. Observed long wavenumbers for CO signals in [Rh(β-diketonato)$(CO)_2$] complexes imply that the rhodium(I) nucleus in the dicarbonylrhodium(I) complexes should be oxidized with more difficulty than the rhodium(I) nucleus in monocarbonyl(phosphine) rhodium(I) complexes.

Table 3.6: Carbonyl stretching frequencies of synthesized rhodium(I) complexes.

β-diketonato ligand	**ν (CO)/cm^{-1}**	
	[Rh(β-diketonato)$(CO)_2$]	**[Rh(β-diketonato)(CO)(PPh_3)]**
ba	2087, 2016	1980
bap	2065, 2008	1982
bab	2084, 2014	1981
bav	-	1983

Formatted: Not Highlight

3.4 Structure Determinations

To further the characterisation of the [Rh(β-diketonato)$(CO)_2$] and [Rh(β-diketonato)$(CO)(PPh_3)$] complexes, the results of a single crystal structure determination for dicarbonyl(1-phenyl-1,3-pentanedionato-κ^2*O,O*')rhodium(1), ([Rh(bap)$(CO)_2$]), dicarbonyl(1-phenyl-1,3-hexanedionato-κ^2*O,O*')rhodium(1), ([Rh(bab)$(CO)_2$]), carbonyl(1-phenyl-1,3-pentanedionato-κ^2*O,O*')triphenylphosphine-rhodium(1), ([Rh(bap)$(CO)(PPh_3)$]), carbonyl(1-phenyl-1,3-hexanedionato-κ^2*O,O*')triphenylphosphine-rhodium(1), ([Rh(bab)$(CO)(PPh_3)$]) and carbonyl(1-phenyl-1,3-octanedionato-κ^2*O,O*')triphenylphosphine-rhodium(1), ([Rh(bav)$(CO)(PPh_3)$]) is presented. The author acknowledges Dr. A. J. (Fanie) Muller of the Department of Chemistry, University of the Free State, for the data collection, refinement and useful discussions of the crystal structures.

3.4.1 Crystal structures of [Rh(β-diketonato)$(CO)_2$] complexes.

A molecular diagram of [Rh(bap)$(CO)_2$], and [Rh(bab)$(CO)_2$], showing atom labeling is presented in **Figure 3.14**. Crystal data and details of data collection and refinement are given in **Table 3.7**. The complete table of bond lengths and angles is given in Appendix B.

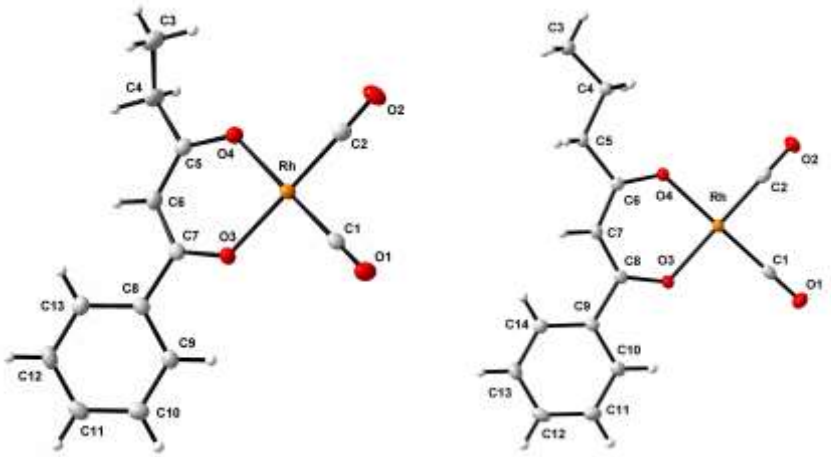

Figure 3.14: A molecular diagram of [Rh(bap)$(CO)_2$] (left) and [Rh(bab)$(CO)_2$] (right) showing atom labelling and displacement ellipsoids of 50% probability.

Table 3.7: Crystal data and structure refinement for [Rh(bap)(CO)$_2$] and [Rh(bab)(CO)$_2$]

	[Rh(bap)(CO)$_2$]	**[Rh(bab)(CO)$_2$]**
Empirical formula	$C_{13}H_{11}O_4Rh$	$C_{14}H_{13}O_4Rh$
Formula weight	334.13	348.15
Temperature	293(2) K	100(2) K
Wavelength	0.71073 Å	0.71073 Å
Crystal system	monoclinic	triclinic
Space group	$P2_1/n$	$P\bar{1}$
Unit cell dimensions	a = 10.4080(4) Å	a = 7.9342(3) Å
	b = 7.8360(3) Å	b = 8.6907(4) Å
	c = 15.9878(6) Å	c = 11.0334(5) Å
	α= 90°	α= 111.416(2)°
	β= 103.2130(10)°	β= 95.249(2)°
	γ = 90°	γ = 106.031(2)°
Volume	1269.40(8) Å^3	664.81(5) Å^3
Z	4	2
Density (calculated)	1.748 Mg/m^3	1.739 Mg/m^3
Absorption coefficient	1.348 mm^{-1}	1.290 mm^{-1}
F(000)	664	348
Crystal size	0.25 x 0.21 x 0.12 mm^3	0.27 x 0.26 x 0.12 mm^3
Theta range for data collection	2.13 to 28.30°	2.61 to 28.36°.
Index ranges	-13<=h<=13, -10<=k<=10, -21<=l<=21	-10<=h<=7, -11<=k<=11, -13<=l<=14
Reflections collected	14494	8867
Independent reflections	3154 [R(int) = 0.0342]	3299 [R(int) = 0.0251]
Completeness to theta = 28.35°	100.0 %	99.0 %
Max. and min. transmission	0.8550 and 0.7293	0.8605 and 0.7220
Refinement method	Full-matrix least-squares on F^2	Full-matrix least-squares on F^2
Data / restraints / parameters	3154 / 0 / 164	3299 / 0 / 173
Goodness-of-fit on F^2	1.105	1.062
Final R indices [I>2sigma(I)]	R1 = 0.0219, wR2 = 0.0543	R1 = 0.0211, wR2 = 0.0462
R indices (all data)	R1 = 0.0273, wR2 = 0.0572	R1 = 0.0244, wR2 = 0.0478
Largest diff. peak and hole	0.531 and -0.598 e.Å^{-3}	0.629 and -0.544 e.Å^{-3}

3.4.2 Comparison of crystal structures of [Rh(β-diketonato)(CO)$_2$] complexes.

3.4.2.1 Introduction.

The structures obtained from single crystal studies of complexes of the type [Rh(β-diketonato)(CO)$_2$] are discussed below. To the knowledge of the author[14], only three other single crystal structures are known from literature on complexes of the type [Rh(β-diketonato)(CO)$_2$]. These are [Rh(acetylacetonato)(CO)$_2$],[9] [11] [Rh(benzoyltrifluoroacetonato)(CO)$_2$][12] and [Rh(FcCOCHCOCF$_3$)(CO)$_2$] complex (Fc = ferrocenyl).[13] Selected comparisons of [Rh(β-diketonato)(CO)$_2$] complexes from this study and analogous complexes from literature are presented in **Table 3.9**.

3.4.2.2 Geometrical aspects

Selected bond lengths and angles for the [Rh(bap)$(CO)_2$] and [Rh(bab)$(CO)_2$] molecules are listed in **Table 3.8**. [Rh(bap)$(CO)_2$] and [Rh(bab)$(CO)_2$] packs in the $P2_1/n$ and $P\bar{1}$ space groups with Z= 4 and 2 respectively, resulting in molecules lying on general positions in their unit cells. All bond lengths and angles are in the typical range for these type of compounds[14, 15] and will be discussed in more detail later in the chapter.

Table 3.8: Selected bond lengths (Å) and angles (°) for [Rh(bap)$(CO)_2$]

[Rh(bap)$(CO)_2$]		[Rh(bab)$(CO)_2$]	
Atoms	**Bond**	**Atoms**	**Angle**
Rh-C1	1.849(2)	Rh-C1	1.851(2)
Rh-C2	1.852(2)	Rh-C2	1.8446(19)
Rh-O3	2.0288(13)	Rh-O3	2.0300(12)
Rh-O4	2.0285(14)	Rh-O4	2.0295(13)
O1-C1	1.135(2)	O1-C1	1.132(2)
O2-C2	1.137(2)	O2-C2	1.138(2)
C1-Rh-C2	89.14(9)	C1-Rh-C2	89.14(8)
C2-Rh-O4	89.87(7)	C2-Rh-O4	90.04(7)
C1-Rh-O3	90.53(7)	C1-Rh-O3	90.06(6)
O3-Rh-O4	90.36(6)	O3-Rh-O4	90.72(5)
C5-C6-C7	126.3(2)	C6-C7-C8	126.8(2)

The phenyl rings of [Rh(bap)$(CO)_2$] and [Rh(bab)$(CO)_2$] forms a dihedral angle of 20.6° and 16.4° respectively with the pseudo aromatic core of the β-diketonato ligand, see **Figure 3.15.**

Figure 3.15 also shows the square planar structures of [Rh(bap)$(CO)_2$] and [Rh(bab)$(CO)_2$] where there is an even distribution of electrons in the β-diketonato skeleton. Both rhodium centers have square planar environments (see table 3.8), showing slight distortion from the ideal 90° geometry expected for dsp^2 hybridization. The metal atoms are displaced by 0.039 and 0.030 Å from this coordination plane for [Rh(bap)$(CO)_2$] and [Rh(bab)$(CO)_2$] respectively.

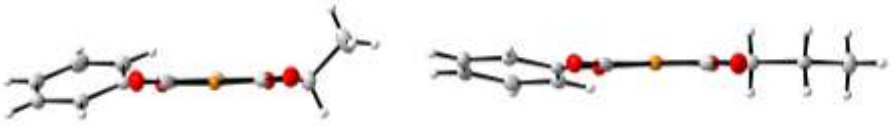

a) [Rh(bap)$(CO)_2$] **b) [Rh(bab)$(CO)_2$]**

Figure 3.15: View of the plane of [Rh(bap)$(CO)_2$] and [Rh(bab)$(CO)_2$]

Table 3.9: **Selected geometrical and crystallographic data for [Rh(β-diketonato)$(CO)_2$] complexes**

Complex	Angle (C-Rh-C') /degree	Rh-O distance /(Å)	Rh-O' distance /(Å)	Rh-C distance /(Å)	Rh-C' distance /(Å)	Space group
[Rh(acac)$(CO)_2$][11]	85	2.06	2.05	1.75	1.76	$P\bar{1}$
[Rh(acac)$(CO)_2$][9]	88.9(3)	2.044(4)	2.040(4)	1.831(7)	1.831(7)	$P\bar{1}$
[Rh(tfba)$(CO)_2$][12]	87(1)	2.02(2)	2.02(2)	1.79(3)	1.82(3)	*Pbac*
[Rh(fctfa)$(CO)_2$][13]	89.1(6)	2.054(8)	2.022(8)	1.84(1)	1.83(2)	*C*2/*c*
[Rh(bap)$(CO)_2$]	89.14(9)	2.0288(13)	2.0285(14)	1.852(2)	1.849(2)	
[Rh(bab)$(CO)_2$]	89.14(8)	2.0300(12)	2.0295(13)	1.8446(19)	1.851(2)	$P\bar{1}$

O' is the β-diketonato oxygen atom nearest to the most electronegative group on the β-diketonato ligand. C' is the carbon atom of the carbonyl group *trans* to O'.

There is a 5-7° deviation from the expected 120° found in the sp^2 hybridized C atoms of the β-diketonato skeleton. The observed bond angles are 126.3(2)° for [Rh(bap)$(CO)_2$] and 126.8(2)° for [Rh(bab)$(CO)_2$]. The Rh-O distances for both [Rh(bap)$(CO)_2$] and [Rh(bab)$(CO)_2$] are similar (*ca*. 2.03 Á), slightly shorter than in the [Rh(acac)$(CO)_2$] complex (2.055 Á). They are considered similar due to the standard deviation on bap and bab complexes. This might be due to the similar electron donating properties of the CH_3, Ph, CH_2CH_3 and $CH_2CH_2CH_3$ groups (χ_{Ph} = 2.21, χ_{CH3} = 2.34, χ_{CH2CH3} = 2.31, $\chi_{CH2CH2CH3}$ = 2.41 and $\chi_{CH2CH2CH2CH3}$ = 2.22 on the Gordy scale, see paragraph 3.2.2.). In the [Rh($FcCOCHCOCF_3$)$(CO)_2$][13] complex (see **Table 3.9**), however, the Rh-O bonds differ slightly with *c.a.* 0.03 Å, probably because of the stronger electron donating properties of the ferrocenyl and Fc groups (χ_{Fc} = 1.87) compared to that of the CF_3 group (χ_{CF3} = 3.01) on the β-diketonato ligand $FcCOCHCOCF_3^-$. Also the Rh-C1 and Rh-C2 bonds of [Rh(bap)$(CO)_2$] and [Rh(bab)$(CO)_2$] did not show a clear electronic *trans* influence of the different groups on the β-diketonato ligands bap and bab with Rh-C bonds of *ca*. 1.85 Å for both complexes. On the grounds of the similar Rh-C bond lengths in [Rh(bap)$(CO)_2$] and [Rh(bab)$(CO)_2$], it is not possible to predict which carbonyl group will be replaced by PPh_3 in the substitution reaction:

$$[Rh(\beta\text{-diketonato})(CO)_2] + PPh_3 \rightarrow [Rh(\beta\text{-diketonato})(CO)(PPh_3)] + CO$$

3.4.2.3 Crystallographic aspects

The [Rh(bap)$(CO)_2$] and [Rh(bab)$(CO)_2$] molecules packs in pairs with Rh....Rh distances of 3.175 and 3.179 Å respectively. See for a view of the packing of the [Rh(β-diketonato)$(CO)_2$] molecules**.** Both [Rh(bap)$(CO)_2$] and [Rh(bab)$(CO)_2$] packs in pairs orientated with an angle of 180° between them due to an inversion symmetry operation. The [Rh(bap)$(CO)_2$] pairs stack around each corner (and the center) of the unit cell along the a-axis. The [Rh(bab)$(CO)_2$] pairs stack halfway on the cell edges along the b-axis. This same packing pattern was observed for [Rh(acac)$(CO)_2$] where a pair of molecules were orientated with an angle of 180° between them due to an inversion symmetry operation. The [Rh(acac)$(CO)_2$] pairs, however, stack as an infinite chain around the corners of the unit cell along the b-axis. The distance between the [Rh(acac)$(CO)_2$] pairs is 3.302(4) Å and the Rh....Rh distance between the molecules 3.253 Å. The packing of the dicarbonyl complexes with an unsymmetrical betadiketonato ligand, fctfa[21] and tfba[20] are illustrated in **Figure 3.17**. The [Rh(tfba)$(CO)_2$] molecules stacks in infinite arrays along the c-axis. The [Rh(fctfa)$(CO)_2$] molecules stacks in pairs with a Rh....Rh distances of 3.346. The packing of [Rh(fctfa)$(CO)_2$] further revealed that one molecule of such a pair was flipped and then rotated by an angle of *ca*. 96°.

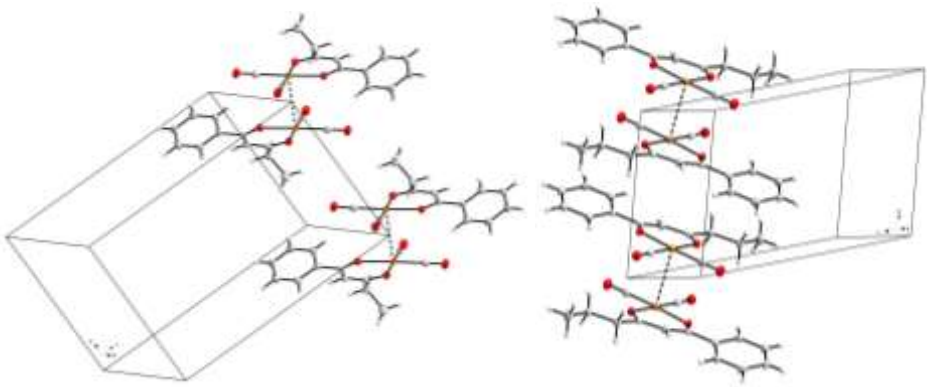

a) [Rh(bap)$(CO)_2$] **b) [Rh(bab)$(CO)_2$]**

Figure 3.16: View of the packing of [Rh(bap)$(CO)_2$] and [Rh(bab)$(CO)_2$]

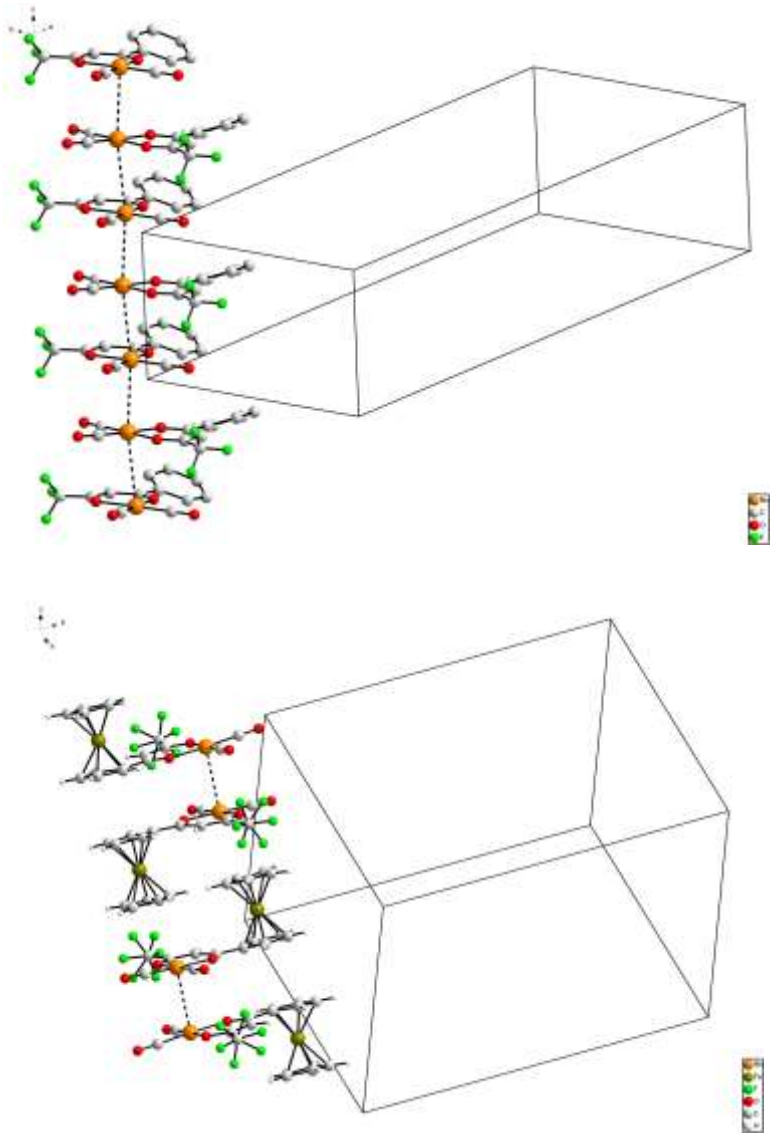

Figure 3.17: Packing diagrams of $[Rh(tfba)(CO)_2]$ molecules (top) and $[Rh(fctfa)(CO)_2]$ (bottom). The $[Rh(tfba)(CO)_2]$ molecules stacks in infinite arrays along the c-axis. The $[Rh(fctfa)(CO)_2]$ molecules stacks in pairs.

3.4.3 The crystal structure data of [Rh(β-diketonato))(CO)(PPh_3)] complexes.

A molecular diagram of [Rh(bap)(CO)(PPh_3)], [Rh(bab)(CO)(PPh_3)] and [Rh(bav)(CO)(PPh_3)] showing atom labeling is presented in **Figure 3.18**. Crystal data and details of data collection and refinement are given in **Table 3.10**. The complete table of bond lengths and angles is given in Appendix B.

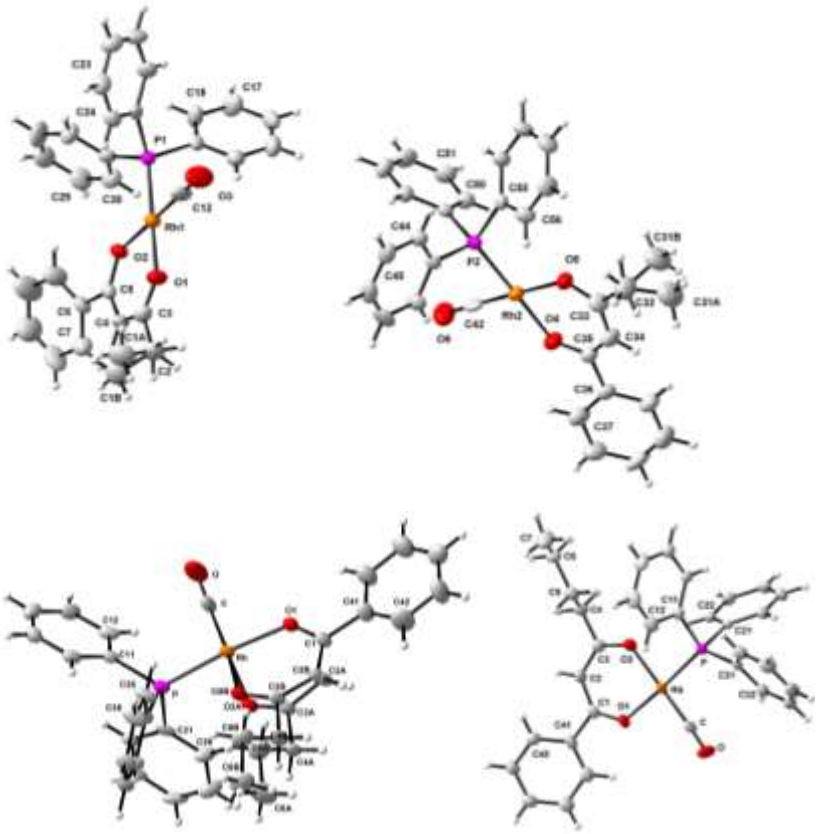

Figure 3.18: A molecular diagram of [Rh(bap)(CO)(PPh_3)] (top), [Rh(bab)(CO)(PPh_3)] (bottom left) and [Rh(bav)(CO)(PPh_3)] (bottom right) showing atom labelling and displacement ellipsoids of 50% probability.

Table 3.10: Crystal data and structure refinement for [Rh(bap)(CO)(PPh$_3$)], [Rh(bab)(CO)(PPh$_3$)] and [Rh(bav)(CO)(PPh$_3$)].

	[Rh(bap)(CO)(PPh$_3$)]	[Rh(bab)(CO)(PPh$_3$)]	[Rh(bav)(CO)(PPh$_3$)]
Empirical formula	$C_{30}H_{26}O_3PRh$	$C_{31}H_{28}O_3P$ Rh	$C_{32}H_{30}O_3PRh$
Formula weight	568.39	582.41	596.44
Temperature	100(2) K	100(2) K	100(2) K
Wavelength	0.71073 Å	0.71069 Å	0.71069 Å
Crystal system	triclinic	monoclinic	monoclinic
Space group	*P*$\bar{1}$	$P2_1/n$	$P2_1/n$
Unit cell dimensions	a = 8.9967(3) Å	a = 10.034(5) Å	a = 10.261(5) Å
	b = 15.7725(5) Å	b = 26.771(5) Å	b = 25.393(5) Å
	c = 19.3044(7) Å	c = 9.918(5) Å	c = 10.793(5) Å
	α= 90.051(2)°	α= 90°	α= 90°
	β= 94.536(2)°	β= 101.746(5)°	β= 102.444(5)°
	γ = 104.963(2)°	γ = 90°	γ = 90°
Volume	2637.48(15) Å^3	2608.4(19) Å^3	2746.1(19) Å^3
Z	4	4	4
Density (calculated)	1.431 Mg/m^3	1.483 Mg/m^3	1.443 Mg/m^3
Absorption coefficient	0.737 mm^{-1}	0.747 mm^{-1}	0.711 mm^{-1}
F(000)	1160	1192	1224
Crystal size	0.23 x 0.12 x 0.05 mm^3	0.17 x 0.10 x 0.02 mm^3	0.33 x 0.28 x 0.28 mm^3
Theta range for data collection	1.06 to 28.37°	1.52 to 26.25°	1.60 to 28.37°
Index ranges	-12<=h<=12, -21<=k<=21, -25<=l<=25	-9<=h<=12, -33<=k<=33, -12<=l<=12	-9<=h<=13, -33<=k<=33, -14<=l<=14
Reflections collected	64974	20242	27483
Independent reflections	13157 [R(int) = 0.0408]	5273 [R(int) = 0.0994]	6865 [R(int) = 0.0316]
Completeness to theta = 28.35°	99.8 %	99.9 %	99.8 %
Max. and min. transmission	0.9641 and 0.8488	0.9852 and 0.8835	0.8257 and 0.7991
Refinement method	Full-matrix least-squares on F^2	Full-matrix least-squares on F^2	Full-matrix least-squares on F^2
Data / restraints / parameters	13157 / 79 / 651	5273 / 201 / 380	6865 / 0 / 335
Goodness-of-fit on F^2	1.060	1.105	1.207
Final R indices [I>2sigma(I)]	R1 = 0.0436, wR2 = 0.1055	R1 = 0.0709, wR2 = 0.1283	R1 = 0.0613, wR2 = 0.1246
R indices (all data)	R1 = 0.0676, wR2 = 0.1192	R1 = 0.1124, wR2 = 0.1441	R1 = 0.0671, wR2 = 0.1279
Largest diff. peak and hole	1.880 and -0.788 e.Å^{-3}	1.273 and -0.802 e.Å^{-3}	2.836 and -1.940 e.Å^{-3}

3.4.4 Comparison of the crystal structures of [Rh(β-diketonato))(CO)(PPh_3)] complexes.

3.4.3.1 Geometrical aspects of [Rh(bap)(CO)(PPh_3)], [Rh(bab)(CO)(PPh_3)] and [Rh(bav)(CO)(PPh_3)]

Selected bond lengths and angles for [Rh(bap)(CO)(PPh_3)], [Rh(bab)(CO)(PPh_3)] and [Rh(bav)(CO)(PPh_3)] are listed in **Table 3.11**, **Table 3.12** and **Table 3.13** respectively. The [Rh(bap)(CO)(PPh_3)] structure crystallizes in the monoclinic system, space group $P\bar{1}$ with a = 10.034(5), b= 26.771(5), c= 9.918(5) A, α= 90.000(5)°, β= 101.746(5)°, γ= 90.000(5)°and Z=4. The [Rh(bab)(CO)(PPh_3)] structure crystallizes in the monoclinic system, space group $P2_1/n$ with a = 10.034(5) Å, b = 26.771(5) Å, c = 9.918(5) Å, α = 90.000(5)°, β = 101.746(5)°, γ = 90.000(5)°. and Z = 4. The [Rh(bav)(CO)(PPh_3)] structure crystallizes in the monoclinic system, space group $P2_1/n$ with a = 10.261(5) Å, b = 25.393(5) Å, c = 10.793(5) Å, α = 90.000(5)°, β = 102.444(5)°, γ = 90.000(5)°. and Z = 4. All bond lengths and angles are in the typical range for these type of compounds[14, 15] and will be discussed in more detail later in the chapter.

Table 3.11: **Selected bond-lengths (Å) and angles (°) for the two isomers in [Rh(bap)(CO)(PPh_3)].**

Bond in Isomer I	Isomer I	Bond in Isomer II	Isomer II
Rh1-C12	1.793(9)	Rh2-C42	1.788(5)
Rh1-P1	2.2403(18)	Rh2-P2	2.2387(9)
Rh1-O1	2.050(4)	Rh2-O5	2.032(3)
Rh1-O2	2.036(4)	Rh2-O4	2.067(3)
C5-O2	1.289(4)	C35-O4	1.285(4)
C3-O1	1.263(5)	C33-O5	1.282(5)
C5-C4	1.382(6)	C35-C34	1.376(6)
C3-C4	1.390(6)	C33-C34	1.380(6)
C12-Rh1-O1	179.08(17)	C42-Rh2-O5	178.59(17)
O1-Rh1-O2	89.39(10)	O5-Rh2-O4	87.84(11)
O2-Rh1-P1	91.62(7)	O5-Rh2-P2	92.99(8)
P1-Rh1-C12	88.15(14)	P2-Rh2-C42	87.47(12)
C5-C4-C3	127.0(4)	C35-C34-C33	127.2(4)

Table 3.12: **Selected bond-lengths (Å) and angles (°) for [Rh(bab)(CO)(PPh_3)].**

Atoms	Bond	Atoms	Angle
Rh-C	1.790(7)	C3A-O2A	1.281(9)
Rh-O2B	1.94(3)	C-Rh-O2B	163.2(12)
Rh-O1	2.062(4)	C-Rh-O1	91.1(2)
Rh-O2A	2.063(8)	O2B-Rh-O1	91.5(9)
Rh-P	2.2408(19)	C-Rh-O2A	178.5(3)
P-C31	1.824(6)	O2B-Rh-O2A	15.9(10)
P-C11	1.827(7)	O1-Rh-O2A	88.0(2)
P-C21	1.828(7)	C-Rh-P	92.4(2)
O1-C1	1.277(8)	O2B-Rh-P	86.4(8)
C-O	1.150(8)	O1-Rh-P	174.52(13)
C1-C2B	1.398(17)	O2A-Rh-P	88.6(2)
C1-C2A	1.401(10)	C3A-C2A-C1	123.7(8)
C2A-C3A	1.391(10)	C3B-C2B-C1	128(2)

Table 3.13: **Selected bond-lengths (Å) and angles (°) for [Rh(bav)(CO)(PPh_3)].**

Atoms	Bond	Atoms	Angle
O1-C1	1.274(5)	C1-C2-C3	125.6(4)
O2-C3	1.291(5)	O2-C3-C2	126.7(4)
C1-C2	1.391(6)	O2-C3-C4	114.6(4)
C2-C3	1.391(6)	C-Rh-O2	177.98(19)
C3-C4	1.508(6)	C-Rh-O1	91.99(16)
C4-C5	1.510(7)	O2-Rh-O1	88.68(13)
Rh-C	1.805(5)	C-Rh-P	92.13(13)
Rh-O2	2.027(3)	O2-Rh-P	87.30(10)
Rh-O1	2.074(3)	O1-Rh-P	174.93(9)
Rh-P	2.2429(13)		

A special feature of the crystal structure of [Rh(bap)(CO)(PPh_3)] is that two isomers, one with PPh_3 *cis* to the oxygen atom nearest to the phenyl group and the second isomer with PPh_3 *trans* to the oxygen nearest to the phenyl group, co-crystallize in the same unit cell. ^{1}H NMR spectra in $CDCl_3$ also clearly showed the existence of both isomers in solution, see paragraph 3.3.2.

The fact that both isomers are found in the same crystal lattice, in contrast to what has been observed for other β-diketone complexes, is rare.[14] The only other [Rh(β-diketonato)(CO)(PPh_3)] complex for which both isomers were isolated, is the [Rh(ba)(CO)(PPh_3)] complex.[19] Factors like thermodynamic control, ligand basicity, metal type and especially solvent polarities can play a role in which isomer in a mixture of isomers is most likely to crystallize. The size and shape of the molecule will also determine if the two isomers are compatible to pack together in the crystalline state. A compilation of crystal structures for [Rh(LL')(CO)(PPh_3)] complexes[16] has shown that the reaction of equimolar or excess PPh_3 on the precursor [Rh(LL')($CO)_2$)] complexes (LL' = unsymmetrical β-diketones) gave substitution

of only one CO group and that the preferred solid state isomer had a *cis*-like arrangement, that is, with PPh_3 *cis* to the more electronegative substituent of the β-diketone ring. Although the NMR data show a 0.69:1 isomer ratio in $CDCl_3$ for [Rh(bap)(CO)(PPh_3)], the crystallization in the non-polar hexane solvent could have changed the isomer composition ratio towards a 1:1 ratio. Such a change is, however, no pre-requisite towards co-crystallization of these isomers since only one form usually dominates the solid state geometry.

Another equalizing factor between the *cis*- and *trans*-like forms could be the comparable group electronegativities of 2.21 and 2.34 for the ethyl and phenyl substituents, respectively. As a result of this there is within experimental error no meaningful difference between Rh-O, Rh-P and Rh-C bond distances (**Figure 3.18**) for the two isomers. Given these similarities, a fine balance of thermodynamic control over enthalpy and entropy related factors together with minimization of crystallization energy and associate packing effects are responsible for this unusual crystal composition.

The Rh-P and Rh-CO bond distances in both the isomers of [Rh(bap)(CO)(PPh_3)] are in agreement with those found in [Rh(acac)(CO)(PPh_3)] and [Rh(ba)(CO)(PPh_3)] (**Table 3.14)** . The Rh-P bond distances in the two isomers are the same within experimental error, 2.2376(9) and 2.2387(9) Å for isomers I and II, respectively. The complex has a square-planar geometry with Rh displaced slightly by 0.018 and 0.007 Å from the plane formed by P, the carbonyl carbon and the two β-diketonato oxygen atoms for the two molecules.

The average C-C bond distance (1.389, 1.385 and 1.3897 Å) of the phenyl rings of PPh_3 in for [Rh(bap)(CO)(PPh_3)], [Rh(bab)(CO)(PPh_3)] and [Rh(bav)(CO)(PPh_3)] and the average C-C bond distance (1.385, 1.364 and 1.385 Å respectively) of the phenyl ring of the β-diketonato ligand in [Rh(bap)(CO)(PPh_3)], [Rh(bab)(CO)(PPh_3)] and [Rh(bav)(CO)(PPh_3)] are in agreement with the normal value (1.394 Å) for the aromatic C-C bond.[17] All the bond angles of the phenyl rings are equal to 120° within the experimental error, *e.g.* for the [Rh(bap)(CO)(PPh_3)] complex C16-C15-C14 = 120.5(5) and C44-C45-C46 = 120.8(4). The phosphorus atom displays a distorted tetrahedral geometry and is surrounded by the rhodium atom and three carbon atoms of the phenyl rings bound to it. The bond angles around P differ at most 11° (for the [Rh(bap)(CO)(PPh_3)] complex) from 109°28', which is the angle for a regular tetrahedron. The O-C-Rh chain is approximately linear with an angle of 177.9(8)° 174.8(7) and 177.2(4)° and the C-O bond distance is 1.149(8), 1.150(8) and 1.143(6) Å for [Rh(bap)(CO)(PPh_3)], [Rh(bab)(CO)(PPh_3)] and [Rh(bav)(CO)(PPh_3)] respectively. The Rh-P bond distance,

2.2403(18), 2.2408(19) and 2.2429(13) Å respectively, is in the same order as found for [Rh(β-diketonato)(CO)(PPh_3)] complexes with β-diketonato = acac, ba and dbm as summarized in **Table 3.14**.

3.4.3.2 Crystallographic aspects

The refinements of [Rh(bab)(CO)(PPh_3)] and [Rh(bab)(CO)(PPh_3)] showed large thermal vibrations on some parts of the periphery of the molecules. These were treated by disordered refinement techniques to obtain more satisfactory refinement parameters. In both cases refinement was kept stable with additional geometric and anisotropic restraints.

The methyl carbon in the ethyl groups of both isomers of [Rh(bap)(CO)(PPh_3)] are refined as disordered. Site occupancies for both disordered methyl groups were left to refine freely but restricted to add up to one for each methyl. These refined to ratios of 0.737:0.263 for C1A and C1B, and 0.664:0.336 for C31A and C31B.

The structure of [Rh(bab)(CO)(PPh_3)] showed a more severe disorder with part of the 2,4-propanedione also refined as disordered. This resulted in half of the β-diketonato backbone as well as the butane moiety being refined as disorderd. Site occupancies was treated similarly as in the case of [Rh(bap)(CO)(PPh_3)] which refined to a ratio of 0.7876:0.2124 for disordered parts A and B respectively.

Figure 3.19 show the packing diagrams of [Rh(bap)(CO)(PPh_3)], [Rh(bab)(CO)(PPh_3)] and [Rh(bav)(CO)(PPh_3) of the packing in the unit cell. No obvious or significant packing effects or interactions are noted.

The plane of the phenyl ring on the β-diketonato ligand makes an angle of 28.61, 4.8 and 20.7° with the plane of the enol ring of the β-diketonato skeleton for [Rh(bap)(CO)(PPh_3)], [Rh(bab)(CO)(PPh_3)] and [Rh(bav)(CO)(PPh_3)] respectively. **Figure 3.20** illustrates how the plane of the phenyl ring on the β-diketonato ligand deviate from a plane through the β-diketonato skeleton.

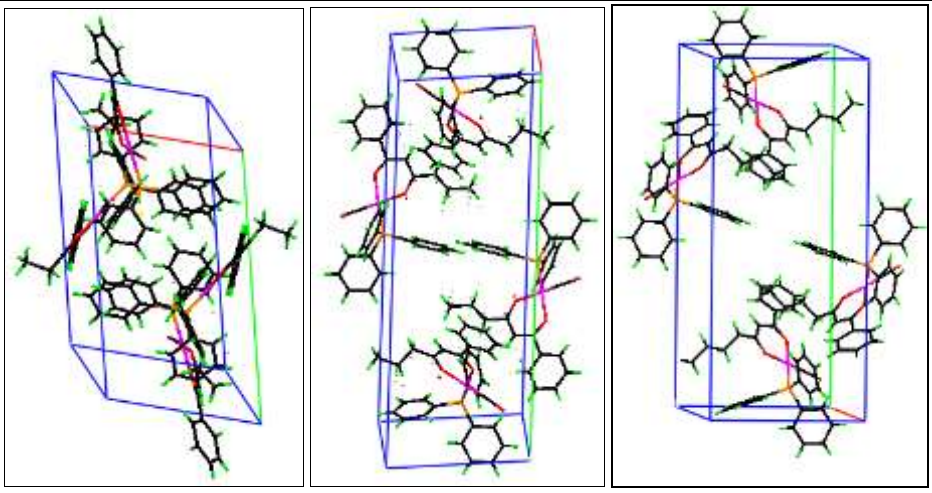

[Rh(bap)(CO)(PPh$_3$)] **[Rh(bab)(CO)(PPh$_3$)]** **[Rh(bav)(CO)(PPh$_3$)]]**

Figure 3.19: Packing diagram of [Rh(bav)(CO)(PPh$_3$)] showing the packing in the unit cell.

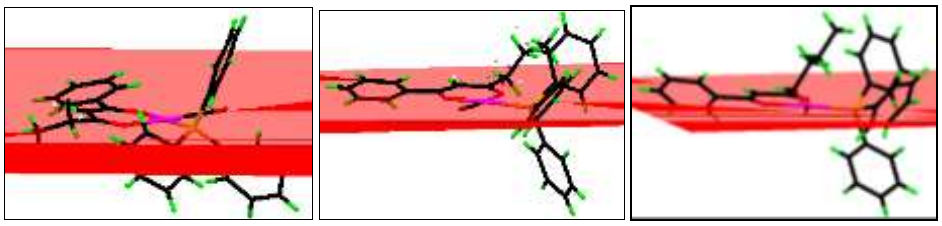

[Rh(bap)(CO)(PPh$_3$)] **[Rh(bab)(CO)(PPh$_3$)]** **[Rh(bav)(CO)(PPh$_3$)]]**

Figure 3.20: View of the plane of the enol ring of the β-diketonato skeleton for [Rh(bap)(CO)(PPh$_3$)], [Rh(bab)(CO)(PPh$_3$)] and [Rh(bav)(CO)(PPh$_3$)]]

3.4.3.3 Comparison of crystal structure of [Rh(β-diketonato)(CO)(PPh$_3$)] complexes.

In this paragraph, the structures of this study will be compared with selected similar crystal structures from literature. **Table 3.14** and **Table 3.15** give comparative result of selected bond-lengths and selected bond angles respectively for [Rh(acac)(CO)(PPh$_3$)],[18] [Rh(ba)(CO)(PPh$_3$)],[19] [Rh(dbm)(CO)(PPh$_3$)],[20] [Rh(bap)(CO)(PPh$_3$)], [Rh(bab)(CO)(PPh$_3$)] and [Rh(bav)(CO)(PPh$_3$)].

There is a significant decrease in the Rh-C bond of the Rh-triphenylphosphine complexes [Rh(bap)(CO)(PPh$_3$)], [Rh(bab)(CO)(PPh$_3$)] and [Rh(bav)(CO)(PPh$_3$)] compared to that of the dicarbonyl complexes [Rh(bap)(CO)$_2$] and [Rh(bab)(CO)$_2$] (see **Table 3.9** and **Table 3.14**).

This implies that there is high degree of back donation exerted by the metal on the CO molecule, strengthening the Rh-C bond and weakening the C=O bond, which manifests in the single, lower ν(CO) stretching wave number that was observed for the monocarbonyl(phosphine)rhodium(I) complexes (see **Table 3.6**). The significant difference in the two Rh-O1 and Rh-O2 bond lengths in all the complexes shown in **Table 3.14** indicates that the PPh_3-group has a larger *trans*-effect than the CO-group in this type of compounds.

Table 3.14: Selected bond-lengths for [Rh(acac)(CO)(PPh_3)], [Rh(ba)(CO)(PPh_3)], [Rh(dbm)(CO)(PPh_3)], [Rh(bap)(CO)(PPh_3)], [Rh(bab)(CO)(PPh_3)] and [Rh(bav)(CO)(PPh_3)].

Bond	acac[18]	ba[19]	dbm[20]	bap	bab	bav
Rh-C	1.801(8)	1.739	1.812(13)	1.793(9)	1.790(7)	1.805(5)
Rh-O1	2.087(4)	2.078	2.081(9)	2.050(4)	2.062(4)	2.074(3)
Rh-O2	2.029(5)	2.032	2.038(10)	2.036(4)	1.94(3)	2.027(3)
Rh-P	2.244(4)	2.249	2.237(7)	2.2403(18)	2.2408(19)	2.2429(13)

Table 3.15: Selected bond-angles for [Rh(acac)(CO)(PPh_3)], [Rh(ba)(CO)(PPh_3)], [Rh(dbm)(CO)(PPh_3)], [Rh(bap)(CO)(PPh_3)], [Rh(bab)(CO)(PPh_3)] and [Rh(bav)(CO)(PPh_3)].

Angles	acac[18]	ba[19]	dbm[20]	bap	bab	bav
C-Rh-P	88.92	88.92	91.1(5)	88.3(2)	92.4(2)	92.13(13)
C-Rh-O1	94.61	90.30	92.9(5)	90.7(3)	91.1(2)	91.99(16)
O1-Rh-O2	87.50	88.13	88.5(5)	89.41(18)	88.0(2)	88.68(13)
O2-Rh-P	88.95	92.63	87.7(3)	91.64(13)	88.6(2)	87.30(10)

The ligand-rhodium-ligand bond angles of [Rh(bap)(CO)(PPh_3)], [Rh(bab)(CO)(PPh_3)] and [Rh(bav)(CO)(PPh_3)] deviate by *ca*. 2° from the expected 90° for a dsp^2 hybridization, see **Table 3.15**. *Cis* Ligand-rhodium-ligand bond angles close to 90° is not found in all [Rh(β-diketonato)(CO)(PPh_3)] complexes, for example in [Rh(acac)(CO)(PPh_3)] and [Rh(fctfa)(CO)(PPh_3)][21] a deviation of more than 4° was reported.

3.4.3.3 [Rh(β-diketonato)(CO)(PPh_3)] complexes and the *trans* influence.

The crystal structures of [Rh(bab)(CO)(PPh_3)] and [Rh(bav)(CO)(PPh_3)] showed that the carbonyl atom *trans* to the less electronegative Ph-group was substituted with PPh_3. These results indicate that the oxygen atom nearest to an electron attracting group of the chelate ring, such as $(CH_2)_2CH_3$, has the smallest *trans* influence. This is in agreement with the polarisation theory[22] and the σ-*trans* effect[23], since the oxygen nearest to the $(CH_2)_2CH_3$ group will be the least polarizable and a weaker σ-donor as a result of the electron attraction by the $(CH_2)_nCH_3$ group.

3.5 Oxidative addition.

3.5.1 Introduction

In this study the oxidative addition of iodomethane to complexes of the type [Rh(β-diketonato)(CO)(PPh_3)] with β-diketonato ligands bap, bab, and bav is described. For all three complexes a similar reaction sequence was observed. The full reaction scheme[24] can be divided into three sets of reactions as follows:

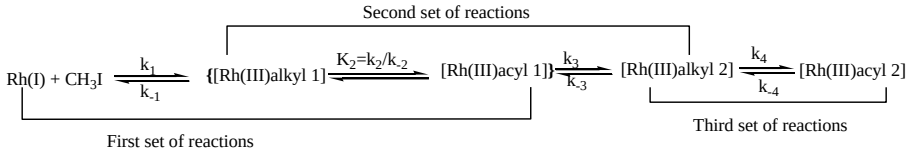

Scheme 3.7.

The initial oxidative addition is followed by CO insertion. NMR measurements showed that each of the general species Rh(I), Rh(III)alkyl 1, Rh(III)alkyl 2, Rh(III)acyl 1 and Rh(III)acyl 2 complexes is a mixture of isomers originating from both unsymmetric β-diketonato ligands and from the stereochemistry originating from methyl iodide addition.

3.5.2 The infrared monitored reaction between CH_3I and [Rh(β-diketonato)(CO)(PPh_3)].

The kinetic rate constants for the oxidative addition reaction between methyl iodide and [Rh(β-diketonato)(CO)(PPh_3)] complexes were determined by IR, UV/visible, and NMR spectroscopy under pseudo first-order conditions. Rate constants were obtained and calculated utilizing a suitable fitting program fitting the kinetic data to the first order equation:

$\ln(A_t - A_\infty) = -k_{obs}t + \ln(A_0 - A_\infty)$.

3.5.2.1 The reaction between iodomethane and [Rh(bap)(CO)(PPh$_3$).

The first step for the reaction between methyl iodide and [Rh(bap)(CO)(PPh$_3$)] complex in chloroform as observed on IR in the range 1650-2150 cm^{-1} at 25^{o}C is illustrated in **Figure 3.21.** This shows that the disappearance of the Rh(I)-carbonyl complex (signal at 1982 cm^{-1}, k_{obs} = 0.0071(4) s^{-1}) leads to the immediate formation of the Rh(III)-alkyl 1 species (signal at 2075 cm^{-1}, too fast) and the subsequent formation of the Rh(III)-acyl 1 species (signal at 1720 cm^{-1}, k_{obs} = 0.0049(1) s^{-1}) as a result of CO insertion. The half-life of this reaction, under the indicated MeI concentration and temperature is 116 s. Comparative results for the oxidative addition and subsequent CO insertion reactions of MeI to [Rh(bap)(CO)(PPh$_3$)], [Rh(bab)(CO)(PPh$_3$)] and [Rh(bav)(CO)(PPh$_3$)] are tabulated in **Table 3.16**. The faster oxidative addition observed for Rh(I)-carbonyl complex is attributed to the anionic character of the ligands, which makes rhodium more nucleophilic.[25]

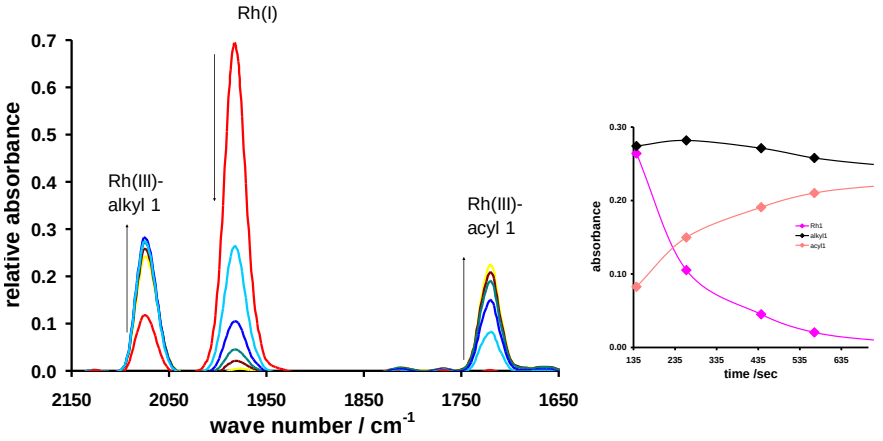

Figure 3.21: The first set of reactions indicating disappearance of Rh(I) at 1982 cm^{-1} and the simultaneous appearance of Rh(III)-alkyl 1 at 2075 cm^{-1} and Rh(III)-acyl 1 at 1720 cm^{-1}.

The frequency shift of the product at 2070 cm^{-1} with respect to Rh(I)-carbonyl complex ($\Delta\nu_{CO}$ = 93 cm^{-1}) suggests that the new species is the product of oxidative addition of MeI to Rh(I) This shift to higher wavenumber is also a characteristic of the transformation of a square-planar Rh(I)-carbonyl complex to an octahedral Rh(III)-alkyl species and is the result of weaker back-donation in Rh(III) complexes compared to those bearing Rh(I) centers.[26] The exponential decay of Rh(I)-carbonyl showed the reaction to be in first order. The intermediate Rh(III)-alkyl species

then converts to an acyl species according to the mechanism proposed in **Scheme 3.8**. The σ-donating properties of the coordinated phosphines fulfil the role of nucleophilic enhancement of CH_3 migration and as such the formation of an Rh(III) acyl species. The appearance and the disappearance of these peaks do not only demonstrate the presence but also give an indication of the relative concentration and the rate of appearance of the different species. This process has been labelled the first set of reactions in **Scheme 3.8** where $K_2 = k_2/k_{-2}$ represents the equilibrium constant between the Rh(III)-alkyl 1 and Rh(III)-acyl 1 species. The first reaction set (**Scheme 3.8**) is driven to the right due to the excess of MeI.

$$[\text{Rh}(\beta\text{-diketonato})(\text{CO})(\text{PPh}_3)] + \text{MeI} \underset{k_{-1}}{\overset{\text{oxidative addition } k_1}{\rightleftharpoons}} \{\text{Rh(III)-alkyl 1} \underset{k_{-2}}{\overset{\text{CO insertion } k_2}{\rightleftharpoons}} \text{Rh(III)-acyl 1}\}$$

Scheme 3.8: First set of reactions.

The second reaction set for the reaction between methyl iodide and [Rh(bap)(CO)(PPh_3)] in chloroform as observed in IR in the range 1650-2150 cm^{-1} at 25°C is illustrated in **Figure 3.22.** This is a slower set of reaction than the first set with a half life of ≈ 31 minutes ($t_{1/2}$ = 1860 s) where the Rh(III)-acyl 1 species at 1720 cm^{-1} (k_{obs} = 0.00037(7) s^{-1}) and the Rh(III)-alkyl 1 species at 2075 cm^{-1} (k_{obs} = 0.00033(3) s^{-1}) disappears as the formation of the Rh(III)-alkyl 2 species at 2056 cm^{-1} (k_{obs} = 0.00041(9) s^{-1}) occurs.

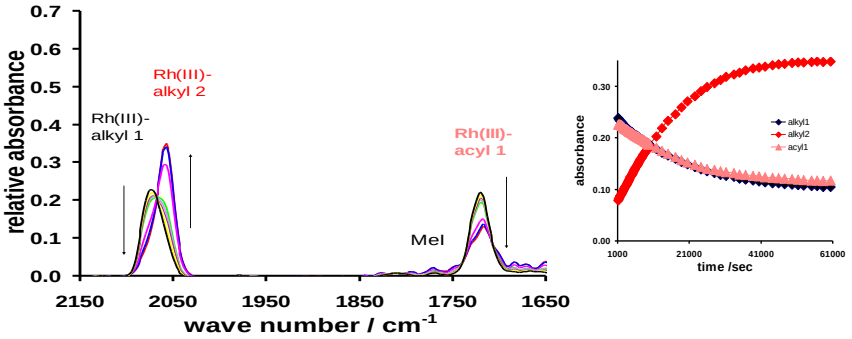

Figure 3.22: The second set of reactions illustrating the simultaneous disappearance of Rh(III)-alkyl 1 at 2075 cm^{-1} and Rh(III)-acyl 1 at 1720 cm^{-1} and the formation of a Rh(III)-alkyl 2 species at 2056 cm^{-1}.

Comparing the half-lives of first with the second set of reactions, it shows that the second set of reaction set is 16 times slower than the first. The disappearance of Rh(III)-alkyl 1 at 2075 cm^{-1} species and Rh(III)-acyl 1 species at 1720 cm^{-1} at the same rate is evidence that there exists a fast

equilibrium between Rh(III)-alkyl-1 species and the Rh(III)-acyl 1 species. This second set of reactions is independent of the methyl iodide concentration.

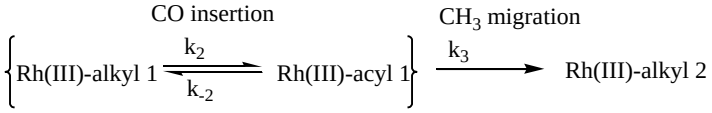

Scheme 3.9: Second set of reactions.

The third reaction set for the reaction between methyl iodide and [Rh(bap)(CO)(PPh_3)] complex in chloroform as observed on the IR in the range 1650-2150 cm^{-1} at 25°C is illustrated in **Figure 3.23.** This process includes a slow first-order disappearance of the Rh(III)-alkyl 2 species at 2059 cm^{-1} (k_{obs} = 0.00013(2) s^{-1}) and the appearance at the same rate of a new Rh(III)-acyl 2 species at 1716 cm^{-1} (k_{0bs} = 0.00015(2) s^{-1}). This set of reaction is independent of methyl iodide concentration.

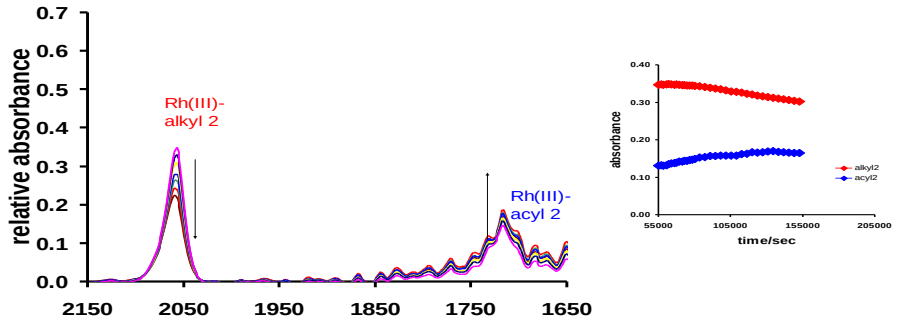

Figure 3.23: The third set of reactions illustrating the simultaneous disappearance of Rh(III)-alkyl 2 at 2059 cm^{-1} and the formation of new Rh(III)-acyl 2 at 1716 cm^{-1}.

This is a slower reaction compared with the first and the second set of reactions with a half-life of 83 minutes (4980 s)

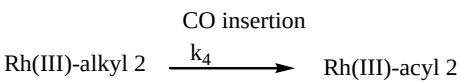

Scheme 3.10: Third set of reactions.

The overall mechanism for all the three sets from **Scheme 3.8** to **Scheme 3.10** is given **Scheme 3.7**. The reaction rates for the infrared monitoring of the oxidative addition reaction between

CH_3I and all the synthesised complexes in this study in chloroform at 25°C, are summarized in **Table 3.16**.

3.5.2.2 The reaction between iodomethane and [Rh(bab)(CO)(PPh_3)].

The reaction sequence of the reaction between [Rh(bab)(CO)(PPh_3)] and iodomethane, with chloroform as reaction medium, in the range 1900 cm^{-1} – 2150 cm^{-1} was monitored by infrared spectroscopy at 25°C.

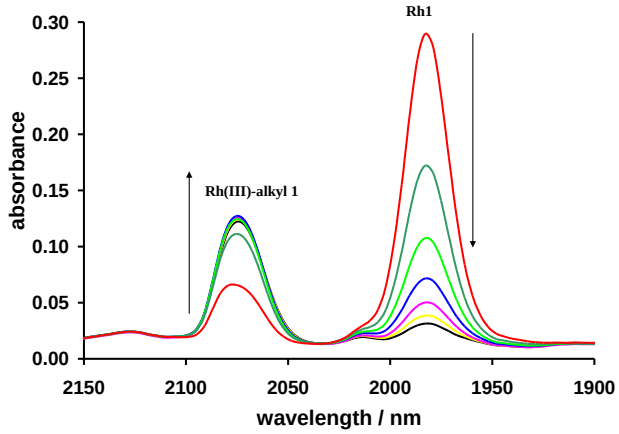

Figure 3.24: The first set of reactions indicating disappearance of Rh(I) at 1982 cm^{-1} and the simultaneous appearance of Rh(III)-alkyl 1 at 2075 cm^{-1}

The reaction shows the disappearance of Rh(I)-carbonyl complex at 1982 cm^{-1} (k_{obs} = 0.0071(2) s^{-1}) with the simultaneous formation of the Rh(III)-alkyl 1 species at 2075 cm^{-1} (k_{obs} = 0.0152(1) s^{-1}) followed by the slow formation of the Rh(III)-acyl 1 species at 1720 cm^{-1} (k_{obs} = 0.0042(3) s^{-1}). The observed slow rate of Rh(III)-acyl appearance imply that there is a slow equilibrium between Rh(III)-alkyl 1 species and Rh(III)-acyl 1 species. Rh(III)-alkyl 1 formation is four times faster than the Rh(III)-acyl 1 formation. A second, much slower, set of reactions was observed on IR.

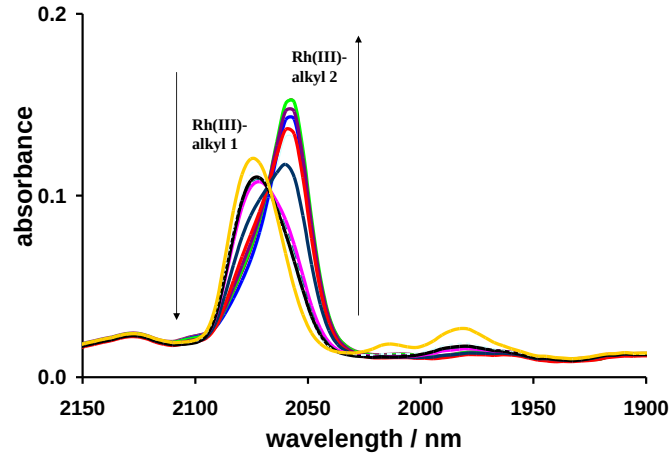

Figure 3.25: The second set of reactions illustrating the simultaneous disappearance of Rh(III)-alkyl 1 at 2075 cm^{-1} and the formation of a Rh(III)-alkyl 2 species at 2056 cm^{-1}.

Rh(III)-alkyl 1 species at 2075 cm^{-1} (k_{obs} = 0.00106(1) s^{-1}) and Rh(III)-acyl 1 species at 1720 cm^{-1} (k_{obs} = 0.00089(2) s^{-1}) disappearing approximately at the same rate was followed by the simultaneous formation of the Rh(III)-alkyl 2 species at 2056 cm^{-1} (k_{obs} = 0.00113(1) s^{-1}) also approximately at the same rate. This observation that the Rh(III)-alkyl 1 species disappears at the same rate as Rh(III)-acyl 1 species is the evidence that there exists an equilibrium between these species.

The third set of reactions for this complex could was not observed within the experimental time give to the reaction.

3.5.2.3 The reaction between iodomethane and [Rh(bav)(CO)(PPh_3)].

Three sets of reactions in the infrared monitored reaction between CH_3I and [Rh(bav)(CO)(PPh_3)] in chloroform at 25°C were also observed. It is clear from the first set of reactions (**Figure 3.26a**) that the pseudo-first –order rate constant for disappearance of the Rh(I)-carbonyl complex at 1982 cm^{-1} (k_{obs} = 0.0066(2) s^{-1}) basically corresponds to the simultaneous formation of the Rh(III)-alkyl 1 species at 2075 cm^{-1} (k_{obs} = 0.037(1) s^{-1}) followed by the slower formation of the Rh(III)-acyl 1 species at 1720 cm^{-1} (k_{obs} = 0.0033(2) s^{-1}).

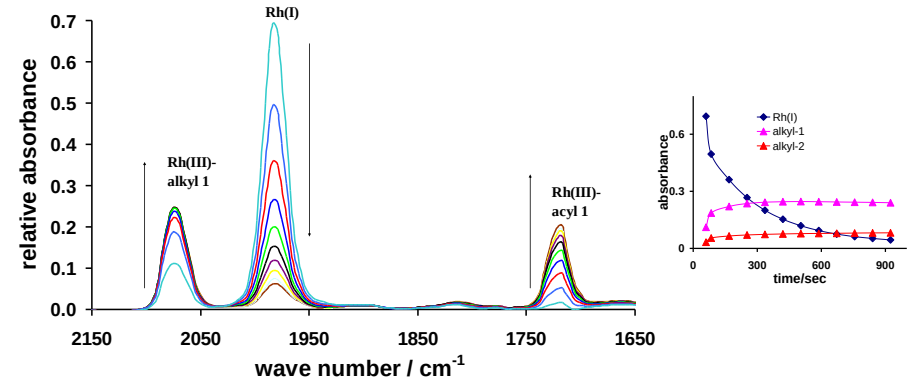

(a) First set of reactions

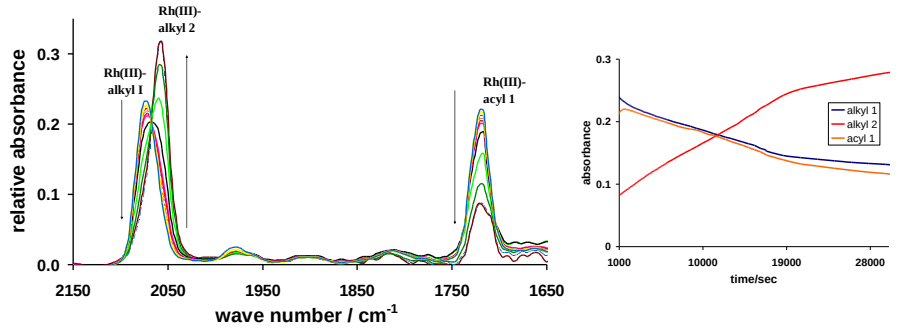

(b) Second set of reactions

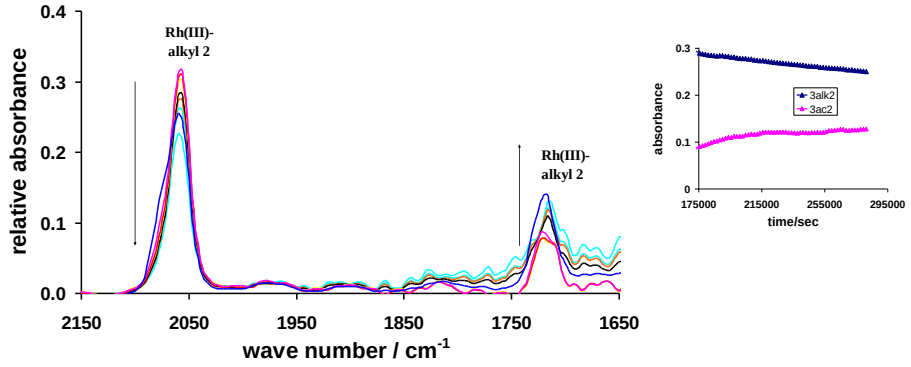

(c) Third set of reactions

Figure 3.26: Infrared monitoring of the oxidative addition reaction between CH_3I and [Rh(bav)(CO)(PPh_3)] in chloroform, [MeI] = 0.2143 mol dm^{-3}.

IR data of the three rhodium complexes synthesised in this study shows that the values of the rate constant for the disappearance of Rh(I)-carconyl and the formation of Rh(III)-alkyl 1 are in agreement with each other. A slow equilibrium between Rh(III)-alkyl 1 species and Rh(III)-acyl 1 species during the disappearance of Rh(I)-carbonyl species can be attributed to the fact that Rh(III)-alkyl 1 species is first formed during oxidative addition of MeI to Rh(I)-carbonyl species and after its formation, it rearranges by carbonyl insertion at a lower rate to form aRh(III)-acyl 1 species.

3.5.2.4 Summary

The influence of the different substituents R bonded to the phenyl-containing β-diketones $PhCOCH_2COR$ coordinated to the [Rh(β-diketonato)(PPh_3)(CO)] complexes, on the rate of oxidative addition, is illustrated in **Table 3.16**. It is obvious that the reaction rate of the oxidative addition step in chloroform (first reaction set) was not influenced by the increasing alkyl chain length of the β-diketonato ligand: k_1 = 0.0341 ([Rh(bap)(CO)(PPh_3)]), 0.047 ([Rh(bab)(CO)(PPh_3)]) and 0.0.31 $dm^3\ mol^{-1}s^{-1}$ ([Rh(bav)(CO)(PPh_3)]) respectively.

Table 3.16: Kinetic rate constants for the oxidative addition of MeI to [Rh(β-diketonato)(CO)(PPh_3)] in chloroform at 25ºC.

Complexes with MeI	[MeI] / mol dm^{-3}	IR: First reactions			
		Rh(1) disappearance (1982 cm^{-1})		Rh(III)-alkyl1 Formation (2075 cm^{-1})	Rh(III)-acyl1 Formation (1720 cm^{-1})
		k_{obs} / s^{-1}	k_1 / $dm^3\ mol^{-1}\ s^{-1}$	k_{obs} / s^{-1}	k_{obs} / s^{-1}
[Rh(bap)(CO)(PPh_3)]	0.2085	0.0071(4)	0.0341(4)	Too fast	0.0049(1)
[Rh(bab)(CO)(PPh_3)]	0.1500	0.0071(2)	0.047(2)	0.0152(1)	0.0042(3)
[Rh(bav)(CO)(PPh_3)]	0.2143	0.0066(2)	0.031(2)	0.037(1)	0.0033(2)

IR: Second set of reactions			
	Rh(III)-alkyl1 disappearance (2075 cm^{-1})	Rh(III)-acyl1 disappearance (1720 cm^{-1})	Rh(III)-alkyl2 Formation (2056 cm^{-1})
	k_{obs} / s^{-1}	k_{obs} / s^{-1}	k_{obs} / s^{-1}
[Rh(bap)(CO)(PPh_3)]	0.00033(3)	0.00037(7)	0.00041(9)
[Rh(bab)(CO)(PPh_3)]	0.00106(1)	0.00089(2)	0.00113(1)
[Rh(bav)(CO)(PPh_3)]	$6.2(1)\times10^{-5}$	$4.1(2)\times10^{-5}$	$5.3(1)\times10^{-5}$

IR: Third set of reactions		
	Rh(III)-acyl2 Formation (1716 cm^{-1}), k_{obs} / s^{-1}	Rh(III)-alkyl2 disappearance (2059 cm^{-1}) k_{obs} / s^{-1}
[Rh(bap)(CO)(PPh_3)]	0.00015(2)	0.00013(2)
[Rh(bab)(CO)(PPh_3)]	-	-
[Rh(bav)(CO)(PPh3)]	$4.25(3)\times10^{-5}$	$2.76(5)\times10^{-6}$

3.5.5 The UV/visible monitored reaction between CH_3I and [Rh(β-diketonato)(CO)(PPh_3).

The reaction between CH_3I and [Rh(β-diketonato)(CO)(PPh_3)] with β-diketonato = bap, bab and bav was also monitored on an UV/visible spectrophotometer. Only the first reaction set was observed on the UV/visible spectrophotometer as illustrated in **Figure 3.27** to **Figure 3.29** using chloroform as solvent at 25ºC.

Figure 3.27: **Left: UV spectra during the oxidative addition reaction [Rh(bap)(CO)(PPh_3)] + MeI. Right The absorbance-time data at 340 nm.**

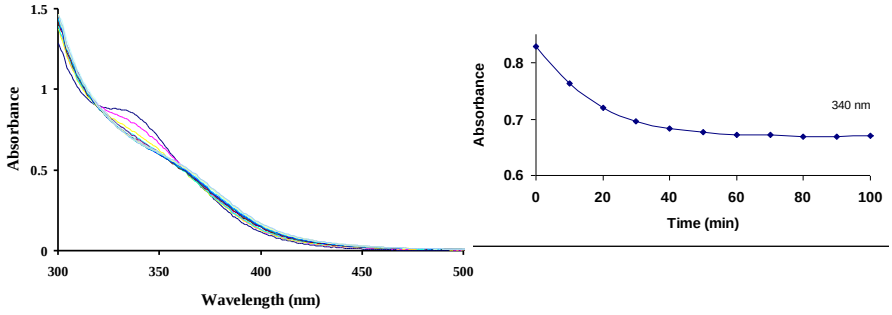

Figure 3.28: **Left: UV spectra during the oxidative addition reaction [Rh(bab)(CO)(PPh$_3$)] + MeI. Right The absorbance-time data at 340 nm.**

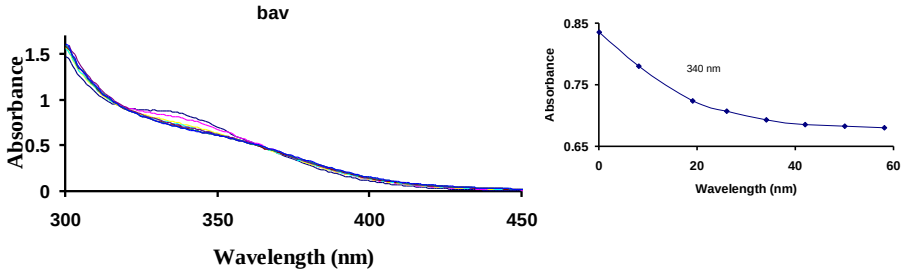

Figure 3.29: **Left: UV spectra during the oxidative addition reaction [Rh(bav)(CO)(PPh$_3$)] + MeI. Right The absorbance-time data at 340 nm.**

The reaction rate constant observed for the first set of reactions corresponded to the rate constant for the disappearance of the Rh(I) monocarbonyl species as observed by IR(see **Table 3.16**).

The temperature and MeI concentration dependence of the oxidative addition reaction (first reaction)

$$\left\{ \text{Rh(I)} + \text{MeI} \rightleftharpoons \text{[Rh(III)-alkyl 1} \rightleftharpoons \text{Rh(III)-acyl 1]} \right\}$$

between CH_3I and [Rh(β-diketonato)(CO)(PPh_3)] as monitored on the UV/visible spectrophotometer is given in **Figure 3.30** for β-diketonato = bap, **Figure 3.31** for β-diketonato = bab and **Figure 3.32** for β-diketonato = bav.

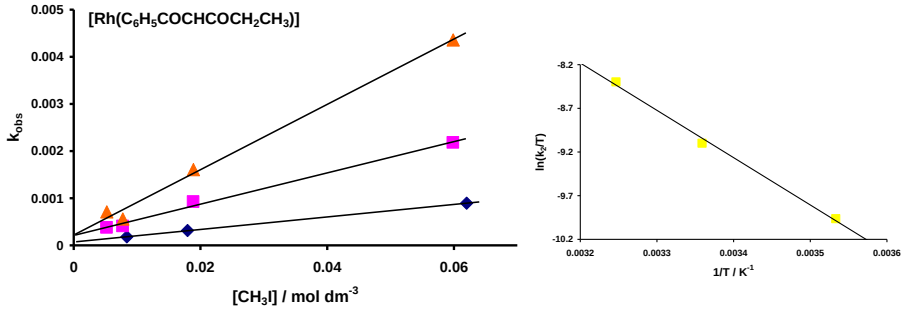

Figure 3.30: **Temperature and MeI concentration dependence for the oxidative addition of MeI to [Rh(bap)(CO)(PPh$_3$) as monitored on the UV/visible spectrophotometer in chloroform at 340 nm for the first reaction (Oxidative addition step).**

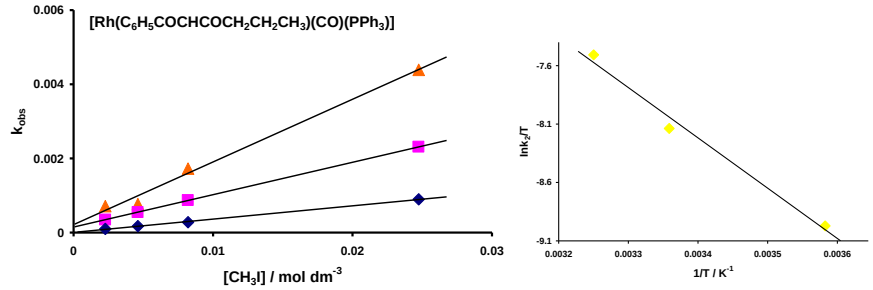

Figure 3.31: Temperature and MeI concentration dependence for the oxidative addition of MeI to [Rh(bab)(CO)(PPh$_3$) as monitored on the UV/visible spectrophotometer in chloroform at 340 nm for the first reaction (Oxidative addition step).

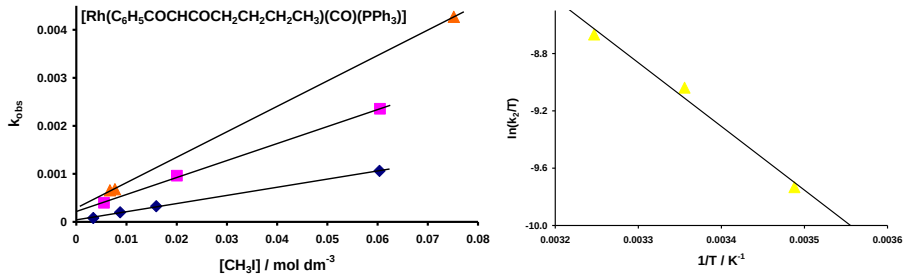

Figure 3.32: Temperature and MeI concentration dependence for the oxidative addition of MeI to [Rh(bav)(CO)(PPh$_3$) as monitored on the UV/visible spectrophotometer in chloroform at 340 nm for the first reaction (Oxidative addition step).

Plots of k_{obs} *vs* [MeI] are linear with non zero intercepts (**Figure 3.30** to **Figure 3.32**), indicating the oxidative addition reactions to be first order in MeI and hence second order overall. This linear dependence on concentration of MeI is characteristic of oxidative addition to d^8 transition-metal complexes.[27] This reaction can be expressed by the following equation.

$$k_{obs} = k_1[MeI] + k_{-1}$$

The disappearance of the Rh(III)-alkyl peak corresponds within experimental error to the formation of the Rh(III)-acyl species.

The standard enthalpy and entropy of activation, ΔH^* and ΔS^*, for the different reaction steps were determined from least-squares fit of the reaction rate constants *vs* temperature data according to the Eyring relationship **Equation 3.1**.

$$\ln k_2 = (\frac{-\Delta H^*}{R})(\frac{1}{T}) + (\frac{\Delta S^*}{R} + \ln \frac{R}{Nh})$$

Equation 3.1

The free energy of activation ΔG^* was determined from $\Delta G^* = \Delta H^* - T\Delta S^*$.

The rate constants and the activation parameters obtained from the UV/visible spectrophotometer monitoring the oxidative addition reaction between [Rh(β-diketonato)(CO)(PPh_3)] and MeI for β-diketonato = bap, bab and bav is summarised in **Table 3.17**. The large negative values obtained for the first step for ΔS^* are in agreement with associative step, in line with the S_N2 pathway proposed.

Table 3.17: Temperature dependant kinetic rate constants and activation parameters for the oxidative addition of MeI to [Rh(β-diketonato)(CO)(PPh_3)] complexes.

β-di-keto-nato	10°		25°		35^0		ΔH*	ΔS*	ΔG*
	k_1 / $dm^3\ mol^{-1}\ s^{-1}$	k_{-1} / s^{-1}	k_1 / $dm^3\ mol^{-1}\ s^{-1}$	k_{-1} / s^{-1}	k_1 / $dm^3\ mol^{-1}\ s^{-1}$	k_{-1} / s^{-1}	kJ mol^{-1}	J K^{-1} mol^{-1}	kJ mol^{-1}
bap	0.0133	7×10^{-5}	0.0332	0.0002	0.0693	0.0002	45(6)	-121(19)	81(11)
bab	0.0358	4×10^{-6}	0.0437	0.0001	0.1691	0.0002	39(7)	-131(18)	78(12)
bav	0.017	4×10^{-5}	0.0354	0.0002	0.053	0.003	37(8)	-150(25)	81(15)

The activation parameters ΔH^* and ΔS^* (see **Table 3.17**) show no worked variation with the character of the β-diketone.

The formation of the acyl species is much less dependent on the type of bidentate ligand. This indicates that the acyl formation (methyl migration) is a concerted process dependent on both the Rh(III)-CH_3 bond and the electron density of the CO carbon atom (the strength of the Rh(III)-CO bond).

3.5.6 The ^{1}H monitored reaction between CH_3I and [Rh(bap)(CO)(PPh_3)].

The reaction between CH_3I and [Rh(bap)(CO)(PPh_3)] was monitored by ^{1}H NMR in order to identify the reaction products. No rate constants were determined. Selected fragments of ^{1}H

NMR spectra recorded during the oxidative addition of CH_3I to [Rh(bap)(CO)(PPh_3)] in $CDCl_3$ is given in **Figure 3.33**. The same reaction sequence as observed on the IR was observed.

During the first reaction step, the two major Rh(I) isomers {referred to as Rh(I)A and Rh(I)B, the choice of the labels are arbitrary and has no significance, see **Figure 3.33 (a)**} reacted with CH_3I to form at least two isomers of the Rh(III)-alkyl1 product {referred to as Rh(III)-alkyl 1A and Rh(III)-alkyl 1B} which underwent a CO insertion reaction to form at least two isomers of the Rh(III)-acyl1 product {referred to as Rh(III)-acyl 1A and Rh(III)-acyl 1B} (the first set of reactions – see reaction scheme below). The alkyl1 and acyl1 reaction products was identified by the two overlapping alkyl CH_3 signals at 1.45 ppm and the two distinct singlet resonances of the acyl CH_3 group at 1.45 and 2.98 and 3.02 ppm respectively (**Figure 3.33 (c)** and **(e)**).

During the second reaction step, the acyl ligand of the two isomers of the Rh(III)-acyl1 product underwent decarbonylation to form two isomers of the Rh(III)-alkyl2 complex {referred to as Rh(III)-alkyl 2A and Rh(III)-alkyl 2B, see **Figure 3.33 (d)**}. The Rh(III)-alkyl1 and Rh(III)-acyl1 disappeared at the same rate, indicating that these two products are in equilibrium with each other.

Due to the long reaction time of the third reaction set (half life = 4980s), the third reaction set could not be followed completely. The appearance of two Rh(III)-acyl2 isomers {referred to as Rh(III)-acyl 2A and Rh(III)-acyl 2B} was observed at 2.9 - 3.0 ppm (**Figure 3.33 (c)**).

The reaction sequence observed by NMR was therefore completely consistent with that implicated by IR and UV studies. The new feature introduced by the NMR study, however, is the existence of at least two main isomers for each intermediate. Taking into account that there exist two main isomers of each reactant and reaction product, the complete reaction sequence for the oxidative addition of CH_3I to [Rh(bap)(CO)(PPh_3)] is therefore:

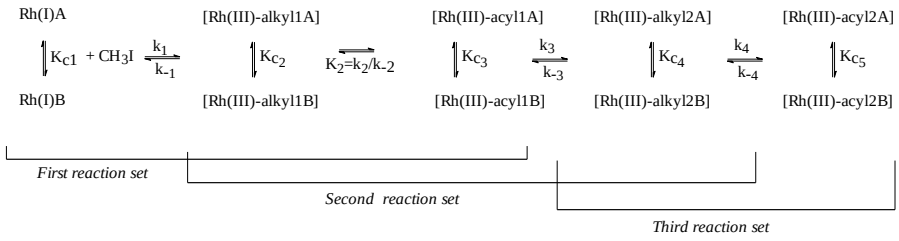

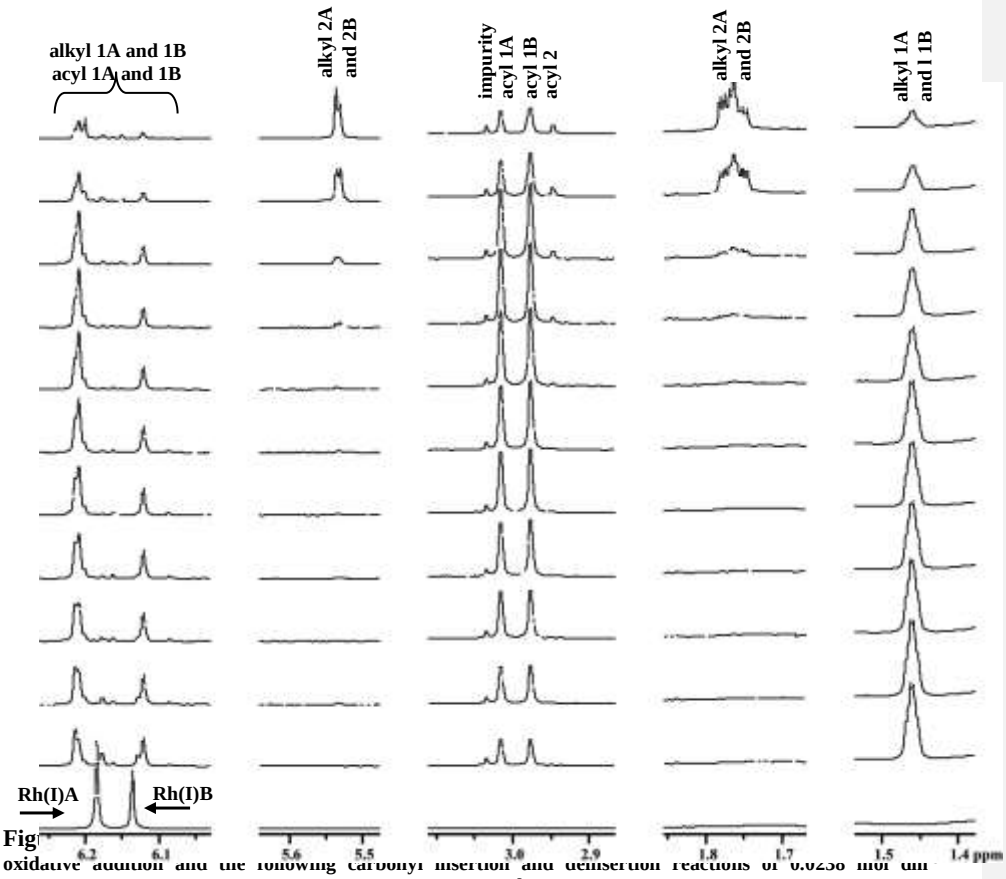

Fig

oxidative addition and the following carbonyl insertion and deinsertion reactions of 0.0238 mol dm^{-3} [Rh(bap)(CO)(PPh$_3$)] reacting with 0.1799 mol dm^{-3} CH_3I in $CDCl_3$ (T = 25°C) at time (i) t = 54 s, 160 s, 479 s, 1486 s, 4768 s.

(a) The spectra illustrate the decrease in the signal of the methine proton of the β-diketone ligand of the Rh(I)A and Rh(I)B isomers at 6.1 - 6.2 ppm with the simultaneous formation and decrease of the signals of the methine proton of the β-diketone ligand of the alkyl 1A and 1B, as well as the acyl 1A and 1B isomers at 6.1 – 6.3 ppm.
(b) The spectra illustrate the increase in the signals of the methine proton of the β-diketone ligand of the alkyl 2A and 2B at 5.7 ppm.
(c) The reaction sequence is also illustrated by the increase and decrease of the CH_3-group of the acyl 1A and 1B isomers at ca 3ppm, followed by the increase of the CH_3-group of the acyl 2A and 2B isomers.
(d) The increase in the signals of the CH_3-group of the alkyl 1A and 2B isomer at 1.75 ppm
(e) The formation and depletion of the CH_3 group of alkyl 1A and 1B isomers at ca 1.45 ppm.
Note the multiplet of the CH_3 group of the Rh(III)-alkyl1 and Rh(III)-alkyl2 isomers is due to coupling with Rh (spin ½).

3.5.7 The ^{31}P NMR monitored reaction between CH_3I and [Rh(β-diketonato)(CO)(PPh_3)].

The oxidative addition of MeI to [Rh(bap) (CO)(PPh_3)] and to [Rh(bav)(CO)(PPh_3)] was monitored on ^{31}P NMR in $CDCl_3$ at T = 25°C. The main aim of this experiment was to identify the reaction products and not to do an accurate kinetic run, therefore only a few spectra were taken during the reaction period. **Figure 3.34** illustrates the integration units *vs.* time data for the specified signals of the oxidative addition reaction of MeI (0.0267 mol dm^{-3}) to [Rh(bav)(CO)(PPh_3)] for the first 10000 s. The reaction rate for the signals as summarized in **Table 3.18** could be determined. It was not practical to follow the reaction longer since the signals of the different products became very small. Selected ^{31}P NMR spectra, illustrating the reaction sequence for oxidative addition of MeI (0.0267 mol dm^{-3}) to [Rh(bap)(PPh_3)(CO)] (0.0139 mol dm^{-3}), are given in **Figure 3.35**.

Table 3.18: **Kinetic rate constants of the oxidative addition of 0.0267 mol dm^{-3} MeI to 0.0139 mol dm^{-3} [Rh(bav)(PPh_3)(CO)], as monitored on ^{31}P NMR in $CDCl_3$ at T = 25°C.**

reaction	signal	δ^{31}P / ppm	k_{obs} / s^{-1}
first	Rh(III)-acyl 1A appearance	37.85	0.00176(6)
	Rh(III)-acyl 1B appearance	37.61	0.0018(1)
second	Rh(III)-alkyl 1A disappearance	33.60	0.0006(3)

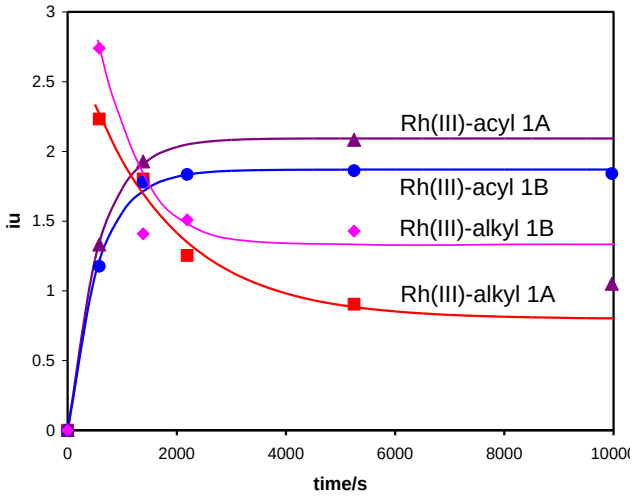

Figure 3.34: **Integration units (iu) *vs.* time data for the specified signals of the oxidative addition of 0.0267 mol dm^{-3} MeI to 0.0139 mol dm^{-3} [Rh(bav)(PPh_3)(CO)] as monitored on ^{31}P NMR in $CDCl_3$ at T = 25°C.**

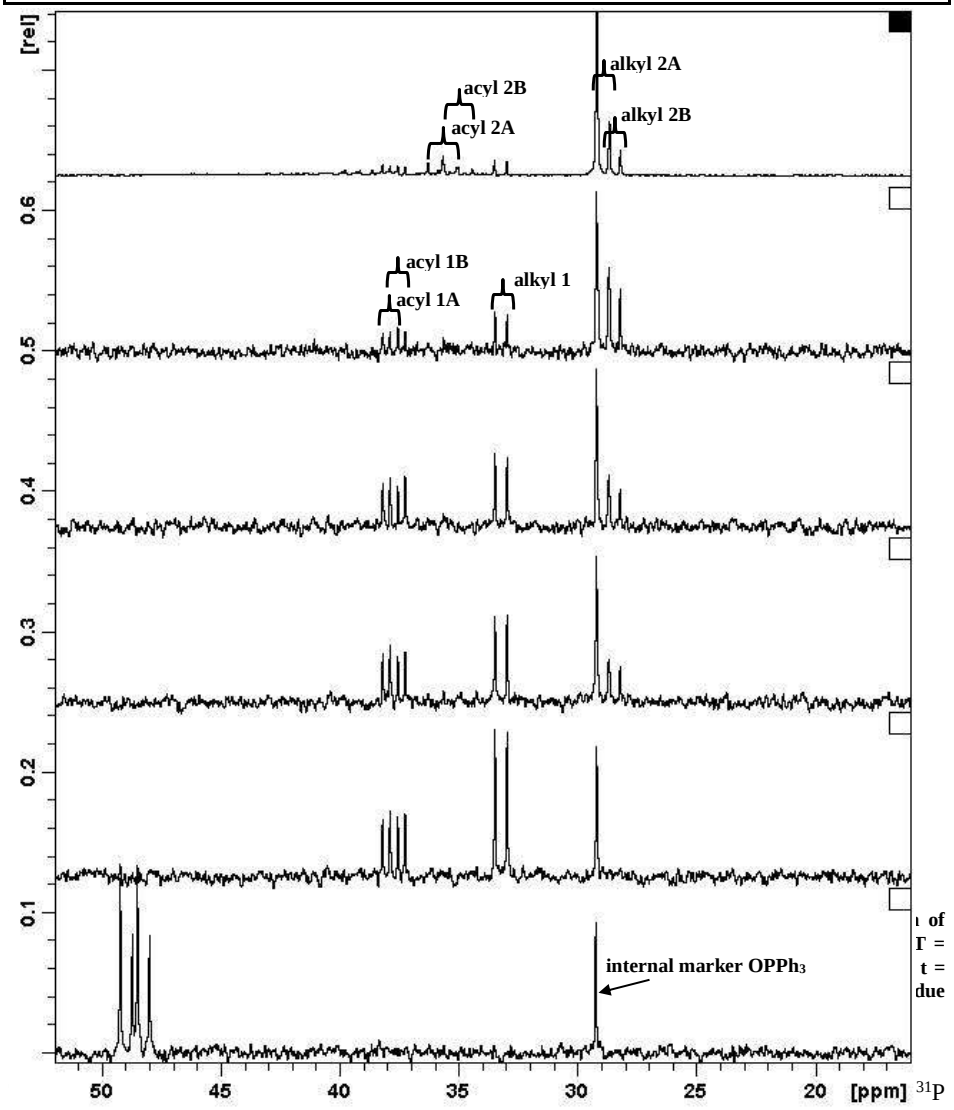

NMR. Rate constants that was obtained for the acyl 1 formation and the alkyl 1 disappearance were consistent with the rate constants determined by IR and UV/vis spectroscopy. As in ^{1}H NMR, two isomers of each reaction product were observed. The ^{31}P NMR spectral parameters of the ^{31}P NMR monitored oxidative addition reaction of [Rh(β-diketonato)(CO)(PPh_3)] with CH_3I in $CDCl_3$ are given in **Table 3.19**.

Table 3.19: ^{31}P NMR spectral parameters of the different isomeric forms of [Rh(β-diketonato)(CO)(PPh$_3$)] and the Rh(III) complexes formed during the oxidative addition reaction of MeI to [Rh(β-diketonato)(CO)(PPh$_3$)].

compound	δ^{31}P /ppm	^{1}J(^{31}P-^{103}Rh) /Hz	δ^{31}P /ppm	^{1}J(^{31}P-^{103}Rh) /Hz	δ^{31}P /ppm	^{1}J(^{31}P-^{103}Rh) /Hz
	[Rh(bap)(CO)(PPh$_3$)]		[Rh(bab)(CO)(PPh$_3$)]		[Rh(bav)(CO)(PPh$_3$)]	
Rh(I)A	48.88	176	48.80	175	48.84	176
Rh(I)B	48.36	177	48.56	175	48.53	175
Rh(III)-alkyl 1A	33.22	125	*	*	33.40	124
Rh(III)-alkyl 1B			*	*	32.88	127
Rh(III)-acyl 1A	37.89	153	*	*	37.92	151
Rh(III)-acyl 1B	37.57	153	*	*	37.29	151
Rh(III)-alkyl 2A	28.91	117	*	*	28.81	*
Rh(III)-alkyl 2B	28.45	117	*	*	28.22	119
Rh(III)-acyl 2A	35.97	155	*	*	*	*
Rh(III)-acyl 2B	34.75	155	*	*	*	*

* Peaks could not uniquely be identified.

3.6 Relationships.

For all the complexes of the type [Rh(R_1COCHCOR_2)(CO)(PPh$_3$it is clear that the group electronegativity of the R groups on the β-diketonato ligand directly influences the electron density on the metal centre. Since the change in electron density on the metal is reflected by parameters such as the kinetic rate constants, carbonyl stretching frequencies and pK_a, a relationship between these parameters and group electronegativities of R_1 and R_2 should exist. **Table 3.20** gives a summary of the parameters that will be used to determine these relationships.

Table 3.20: Kinetic rate constants and carbonyl stretching frequencies of [Rh(R_1COCHCOR_2)(CO)(PPh$_3$)], as well as pK_a and group electronegativities of the R substituents of the free uncoordinated the β-diketone.

β-diketonato ligand (R_1COCHCOR_2)$^-$					[Rh(R_1COCHCOR_2)(CO)(PPh$_3$)] [(a)]	
abreviation	R_1	R_2	(χ_{R1} + χ_{R2})/ (Gordy scale) [(b)]	pK_a[(c)]	v(C=O)/ cm^{-1}	k_1/ mol^{-1}dm^{3}s^{-1}
dfcm	Fc	Fc	3.74	13.1	1977	0.155 [(e)]

bfcm	Fc	C_6H_5	4.08	10.41	1977	0.077 [e]
fca	Fc	CH_3	4.21	10.01	1980	0.065 [e]
dbm	C_6H_5	C_6H_5	4.42	9.35	1979	0.00961[f]
acac	CH_3	CH_3	4.68	8.95	1978	0.024 [g]
fctfa	Fc	CF_3	4.88	6.56	1986	0.00611 [e]
tfba	C_6H_5	CF_3	5.22	6.30	1983	0.00112 [f]
tfaa	CF_3	CH_3	5.35	6.30	1983	0.00146 [f]
ba	C_6H_5	CH_3	4.55	8.70	1980	0.00930 [f]
bap	C_6H_5	CH_2CH_3	4.52	9.33	1982	0.0337 [e]
bab	C_6H_5	$CH_2CH_2CH_3$	4.62	9.23	1981	0.0454.[e]
bav	C_6H_5	$CH_2CH_2CH_2CH_3$	4.43	9.33	1983	0.0332 [e]

(a) ν(C=O) this study **Table 3.6** and ref [28]
(b) group electronegativities of this study **Table 3.1** and ref [29].
(c) pK_a of this study

Table 3.3 and from ref. [30].
(e) value in chloroform
(f) value in acetone
(f) value in 1,2-dichloroethane

3.6.1 Group electronegativities and rate constants.

Figure 3.36 illustrates that the sum of the group electronegativities of R_1 and R_2 of the β-diketonato ligand $(R_1COCHCOR_2)^-$ coordinated to [Rh(β-diketonato)(CO)(PPh_3)] and [Rh(β-diketonato)($POPh_3$)$_2$] is linearly dependant on logk_1. k_1 is the rate constant for the oxidative addition of iodomethane to these rhodium complexes. This result is expected since the metal atom Rh acts as a nucleophile when it undergoes oxidative addition. The nucleophilicity (or basicity) of the metal, will influence the rate of oxidative addition reactions. Any influence of a ligand bonded to the metal, that will increase the electron density on the metal centre, will thus lead to an increased rate of oxidative addition, assuming all other influences, factors and parameters remain constant. From the linear relationship in **Figure 3.36** it follows that the sum of the group electronegativities R_1 and R_2 of the β-diketonato ligand $(R_1COCHCOR_2)^-$ coordinated to [Rh(β-diketonato)(CO)(PPh_3)] gives a good indication of the electron density (nucleophilicity) of rhodium in each complex.

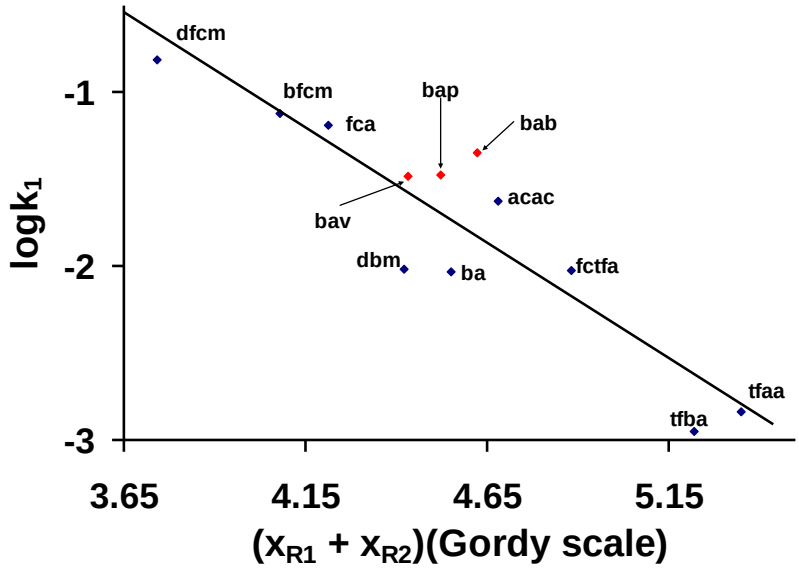

Figure 3.36: **Relationship between $logk_1$, the second-order rate constant for the first step of oxidative addition of iodomethane to [Rh($R_1COCHCOR_2$)(CO)(PPh_3)] and the sum of the group electronegativities of R_1 and R_2, ($\chi_{R1} + \chi_{R2}$), of the β-diketonato ligand ($R_1COCHCOR_2$)$^-$ coordinated to the rhodium complexes. The β-diketonato ligands are as indicated.**

3.6.2 Group electronegativities and carbonyl stretching frequencies.

Figure 3.37 illustrates that the sum of the group electronegativities of R_1 and R_2 of the β-diketonato ligand ($R_1COCHCOR_2$)$^-$ coordinated to [Rh(β-diketonato)(CO)(PPh_3)] and [Rh(β-diketonato)($POPh_3$)$_2$] is linearly dependant on CO stretching frequency ν_{CO}. Therefore in complexes of the type [Rh(β-diketonato)(CO)(PPh_3)] th infrared CO stretching frequency increases as R_1 and R_2 of the β-diketonato ligand are replaced by more electron withdrawing groups, *i.e.* groups with high electronegativity. This also give a clear indication of the nucleophilicity of the rhodium metal.

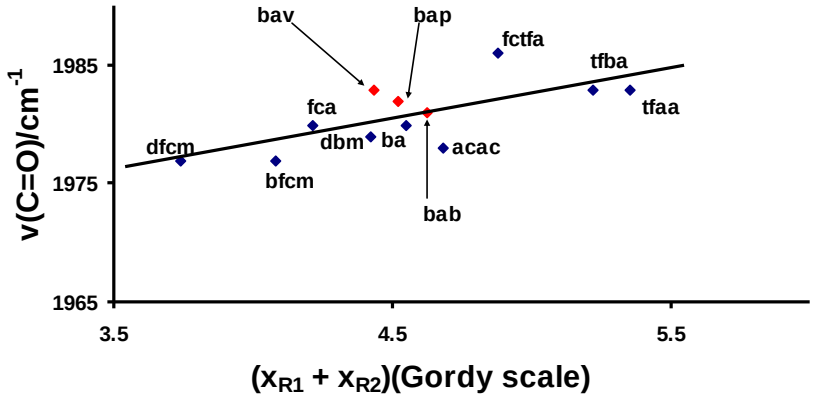

Figure 3.37: **Relationship between the carbonyl stretching frequency ν(C=O) of [Rh(R_1COCHCOR_2)(CO)(PPh_3)] and the sum of the group electronegativities of R_1 and R_2 ($\chi_{R1} + \chi_{R2}$) of the β-diketonato ligand ($R_1COCHCOR_2$)$^-$ coordinated to [Rh(R_1COCHCOR_2)(CO)(PPh_3)]. The β-diketonato ligands are as indicated.**

3.6.3 Group electronegativities and pK_a of the β-diketones.

Figure 3.38 illustrates the relationship between the sum of the group electronegativities of R_1 and R_2 of the β-diketonato ligand ($R_1COCHCOR_2$)$^-$ coordinated to [Rh(β-diketonato)(CO)(PPh_3)] and [Rh(β-diketonato)($POPh_3$)$_2$] and the pK_a of the β-diketones. High electronegative groups on the β-diketonato ligand result in a decrease in pK_a of the β-diketone making it more acidic.

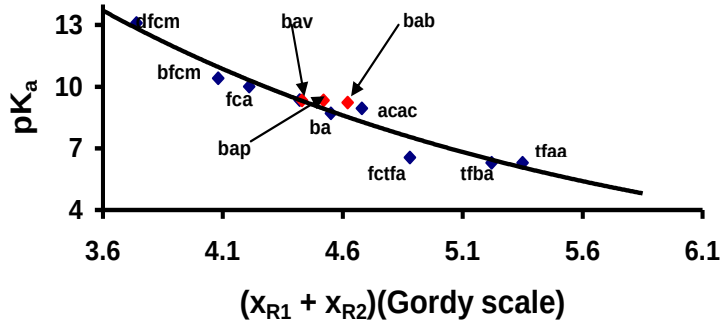

Figure 3.38: **Relationship between the pK_a and the sum of the group electronegativities ($\chi_{R1} + \chi_{R2}$) of the groups R_1 and R_2 on the β-diketone [$R_1COCH_2COR_2$]. The β-diketones are as indicated.**

3.6.4 Rh-P bond lengths and coupling constants.

^{13}C and ^{31}P NMR studies[31, 32] of [Rh(RCOCHCNR')(CO)(PPh_3)] complexes, R, R' = CH_3, C_6H_5, CF_3 and $C(CH_3)_3$, showed that the values of $^1J(^{13}C\text{-}^{103}Rh)$ and $^1J(^{31}P\text{-}^{103}Rh)$, are larger when the CO group (for ^{13}C spectra) or the PPh_3 ligand (for ^{31}P spectra) is *trans* to the weakly donating O-atom, and they are smaller when the ligands are in the *trans*-position to the stronger donor N-atom,

$$^1J(^{31}P\text{-}^{103}Rh)\ (P\text{-}trans\text{-}O) > {}^1J(^{31}P\text{-}^{103}Rh)\ (P\text{-}trans\text{-}N)$$

$$^1J(^{13}C\text{-}^{103}Rh)\ (CO\text{-}trans\text{-}O) > {}^1J(^{13}C\text{-}^{103}Rh)\ (CO\text{-}trans\text{-}N).$$

For example, for the two isomers of [Rh(dmavk)(CO)(PPh_3)] it was found that $^1J(^{31}P\text{-}^{103}Rh)$ = 149.7 Hz (P *trans* to N) is smaller than the $^1J(^{31}P\text{-}^{103}Rh)$ value of 172.0 Hz (P *trans* to O).

Table 3.21: ^{31}P NMR parameters and Rh-P bond lengths for square planar complexes [Rh(L,L'-BID)(CO)(PPh_3)] and related rhodium(III) complexes. L,L'-BID = six-membered chelate ring containing donor atoms L and L'.

no.	L,L'-BID	Rh-P bond *trans*	Rh-P distance/(Å)	$\delta^{31}P$/ppm	$^1J(^{31}P\text{-}^{103}Rh)$/Hz
1	**fctfa**	O, O	2.232(1),[28] -	48.04, 48.04	176.4, 176.4
2	**dbm**	O	2.237(7)[33]	49.56	177.9
3	**tftma**	O, O	2.238(3),[34] -	47.85, 47.85	172.9, 172.9
4	**tfdma**	O, O	2.239(2),[35]	48.72, 47.75	175.7, 178.0
5	**bzaa**	O	2.243(1)[36]	49.44	175.0
6	**acac**	O	2.244(2)[18]	48.84	175.7
7	**tta**	O, O	2.245(3),[37]-	47.84, 47.78	177.7, 176.7
8	**ba**	O, O	2.248(3), 2.249(3)[38]	49.28, 49.37	175.8, 174.8
9	**tfhd**	O, O	2.252(3),[39] -	49.14, 47.86	177.2, 174.8
10	**dmavk (acyl)**	-	2.260(4)[40]	-	153
11	**cacsm**	N	2.268(1)[41]	45.2	144.6
12	**dmavk**	N, O	2.275(1),[42] -	41.45, 54.91	149.7, 172.0
13	**hacsm**	S	2.283(1)[43]	42.70	148.9
14	**sacac**	S	2.300(2)[44]	35.36	144.5
15	**fctfa (alkyl)**	-	2.319(3)[33]	28.34	116
16	**dmavk (alkyl)**	-	2.356(3)[45]	-	107
17	**bap***	O, O	2.240(2), 2.239 (2)	48.88, 48.36	176, 177
18	**bab***	O, O	2.241(2)	48.80, 48.56	175, 175
19	**bav***	O, O	2.243(1)	48.84, 48.53	176, 175

^{31}P NMR parameters from 33, except for L,L'-BID = acac, tta, cacsm, dmavk, hacsm and sacac which is from reference 43, dmavk (alkyl and acyl) from reference 45. * This study.

The rhodium-bond lengths 2.240(2) and 2.239 (2) of the two isomers of the complex [Rh(bap)(CO)(PPh_3)], characterized in this study, were very similar, probably since in both crystals the rhodium-bond was *trans* to an oxygen. The same was found for the two isomers of the complex [Rh(ba)(CO)(PPh_3)].

The data of **Table 3.21** clearly indicate that longer Rh-P bonds result in smaller $^{1}J(^{31}P\text{-}^{103}Rh)$ values. **Figure 3.39** illustrates the linear relationship between $^{1}J(^{31}P\text{-}^{103}Rh)$ and Rh-P bond distances for six-membered chelate rings. The linear relationship between $\delta^{31}P$, in ppm, and Rh-P bond lengths is also illustrated. The graphs imply that approximate Rh-P bond lengths can be calculated utilizing the equations

$$\mathbf{d(Rh\text{-}P) = -0.0014(1) \times {}^{1}J(^{31}P\text{-}^{103}Rh) + 2.49(2) = -0.0039(4) \times \delta^{31}P + 2.44(2).}$$

These two equations are applicable for Rh-P bond lengths, d(Rh-P), between 2.23 Å and 2.36 Å.

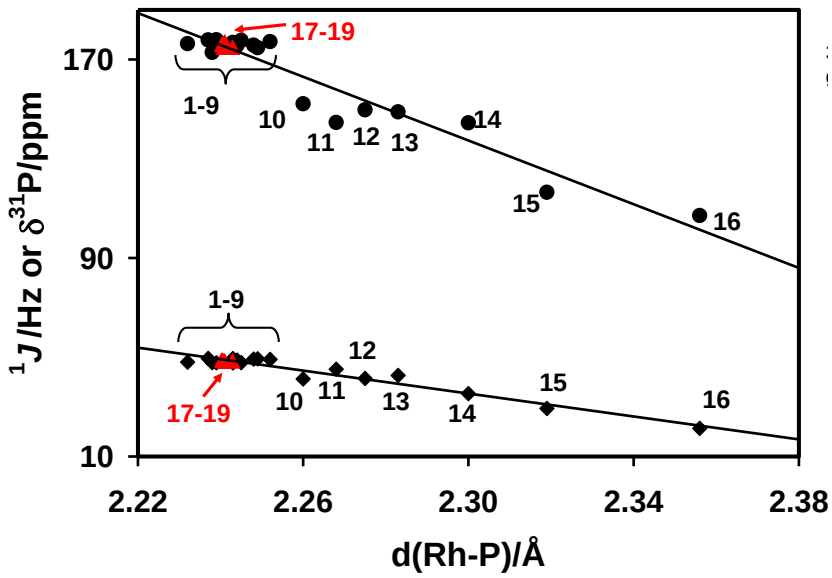

Figure 3.39: **Linear relationship between the coupling constant, $^{1}J(^{31}P\text{-}^{103}Rh)$, or the chemical shift, $\delta^{31}P$, *and* the Rh-P bond distance in various [Rh(L,L'-BID)(CO)(PR_3)] complexes. L,L'-BID = six-membered chelate ring with donor atoms L and L'. The numbering of complexes corresponds to that given in Table 3.21. The red dots corresponds to the complexes synthesized and characterized in this study: [Rh(bap)(CO)(PPh_3)], Rh(bab)(CO)(PPh_3)] and Rh(bav)(CO)(PPh_3)].**

3.7 References

[1] R. Levine, J.A. Conroy, J. T. Adams and C. R. Hauser. *J. Am. Chem. Soc.*, **67**, 1510 (1945).

[2] M. C. Etter, D. A. Jahn, Z. Yrbanczyk-Lipkowska, *Acta Cryststallogr.,Sect. C:Cryst. Struct. Commun.*, **260**, 43 (1987)

[3] J. D. Park, H. A. Brown, and J. R. Lachen, *J. Am. Chem. Soc.*, **75,** 4753 (1953).

[4] Du Plessis, W.C., Vosloo, T.G. and Swarts, J.C., *J. Chem. Soc., Dalton Trans.,* 2507 (1998).

[5] J. G. Leipoldt, and E. C. Grobler, *Trans. Met. Chem. (weinheim, Ger.)*, **11**, 110 (1986).

[6] J. G. Leipolt, L. D. C. Bok, J. S. Van Vollenhoven, A. I. Pieterse, *J. Inorg. Nucl. Chem,*, **40**, 61 (1978)

[7] J. G. Leipolt, L. D. C. Bok, S. S. Basson, T. I. A. Gerber, *Inorg. Chim. Acta*, **34**, L293 (1979)

[8] C. H. Langford and H. B. Gray., *Ligand Substitution Processes*., Benjamin, New York (1966)

[9] F. Huq and A. C. Skapski., *J. Cryst. Mol. Struct.*, **4**, 411 (1974)

[10] C. A. Tolman., *Electron Donor-Acceptor Properties of Phosphorus Ligands.*, No. 1577 from the Central Research Department, Experimental station., E.I. du Pont de Nemours and Company, Welmington, Delaware. (1969)

[11] N. A. Bailey, E. Coates, G. B. Robertson, F. Bonati, R. Ugo, *J. Chem. Soc., Chem. Commun.*, 1041 (1967).

[12] J. G. Leipoldt, L. D. C. Bok, S. S. Basson, J. S. Van Vollenhoven, T. I. A. Gerber, *Inorg. Chim. Acta*, **25**, L63-L64 (1977).

[13] J. Conradie, T. S. Cameron, M. A. S. Aquino, G. J. Lamprecht and J. C. Swarts, *Inorg. Chim. Acta.*, **358**, 2530-2542 (2005).

14 Cambridge Structural Database (CSD), Version 5.27, August 2006 update

15 Allen, F. H. (2002). Acta Cryst. B58, 380–388.

[16] D.E. Graham, G.J. Lamprecht, I.M. Potgieter, A. Roodt and J.G. Leipoldt, *Transition Met. Chem.*, **193**. (1991).

[17] L. E. Sutin, *Tables of Interatomic Distances and configuration in Molecules and Ions, Supplement 1956 – 1959*, The Chemical Society, London, p. S16s

[18] J. G. Leipoldt, S. S. Basson, L. D. C. Bok, and T. I. A. Gerber, *Inorg. Chim. Acta.*, **26**, L35 (1978).

[19] W. Purcell, S. S. Basson, J. G. Leipoldt, A. Roodt, H. Preston, Inorg.Chim.Acta, **234**, 153, (1995).

[20] D. Lamprecht, G. J. Lamprecht, J. M. Botha, K. Umakoshi, Y. Sasaki, *Acta Crystallogr., Sect.C:Cryst.Struct.Commun*. **53**, 1403, (1997).

[21] G. J. Lamprecht, J. C. Swarts, J. Conradie and J. G. Leipoldt, *Acta Cryst.* **C49**, 82-84 (1993).

[22] A. A. Grinberg. *Acta Physiochim,* USSR, **3**, 573 (1935).

[23] C. H. Langford and H. B. Gray, *Ligand Substitution Processes,* W.A. Benjamin Inc., New York (1965).

[24] J. Conradie, *Chemical kinetics, electrochemistry and structural aspects of ferrocene-containing β-diketonato complexes of rhodium(I) and iridium(I),* Ph. D. Thesis, University of the Free State, 2000.

[25] P. Pelagatti, A. Bacchi, C. Bobbio, M. Carcelli, M. Costa, C. Pelizzi, and C. Vivorio., *Organomet.,* **19,** 5440-5446 (2000).

[26] J. A. Gaunt, V. C Gibson, A. Haynes, S. K. Spitzmesser, A. J. P. White, and D. J. Williams., *Organomet.,* **23**, 1015-1023 (2004).

[27] A. J. Hart-Davis, W. A. G. Graham.,*Inorg. Chem.*, **9**, 2658-2663 (1970).

[28] J. Conradie, G.J. Lamprecht, S. Otto and J.C. Swarts, *Inorg. Chim. Acta.,* **328**, 191-203 (2002).

[29] W.C. du Plessis, J.C. Erasmus, G.J. Lamprecht, J. Conradie, T.S. Cameron, M.A.S. Aquino, and J.C. Swarts, *Can. J. Chem.*, **77**, 378 - 386 (1999).

[30] W. C. (Ina) du Plessis, T. G. Vosloo and J. C. Swarts, *J. Chem. Soc., Dalton Trans*., 2507–2514, (1998).

[31] T. G. Cherkasova, L. V. Osetrova, and Yu. S. Varshavsky, *Rhodium Ex.*, **1**, 8 (1993).

[32] M. R. Galding, T. G. Cherkasova, L. V. Osetrova, and Yu. S. Varshavsky, *Rhodium Ex.*, **1**, 14 (1993).

[33] D. Lamprecht, G. J. Lamprecht, J. M. Botha, K. Umakoshi, and Y. Sasaki, *Acta Cryst.*, **C53**, 1403 (1997).

[34] E. C. Steynberg, G. J. Lamprecht, and J. G. Leipoldt, J.G., *Inorg. Chim. Acta*, **133**, 33 (1987).

[35] J. G. Leipoldt, S. S. Basson, and J. T. Nel, *Inorg. Chim. Acta*, **74**, 85 (1983).

[36] A. Roodt, J. G. Leipoldt, J. C. Swarts, and G. J. J. Steyn, *Acta Cryst.,* **C48**, 547 (1992).

[37] J. G. Leipoldt, L. D. C. Bok, J. S. van Vollenhoven, and A. I. Pieterse, *J. Inorg. Nucl. Chem.*, **40**, 61 (1978).

[38] W. Purcell, S. S. Basson, J. G. Leipoldt, A. Roodt, and H. Preston, *Inorg. Chim. Acta*, **234**, 153 (1995).

[39] J. G. Leipoldt, S. S. Basson, and J. H. Potgieter, *Inorg. Chim. Acta*, **117**, L3 (1986).

[40] L. J. Damoense, W. Purcell, and A. Roodt, *Rhodium Ex.,* **14**, 4 (1995).

[41] G. J. J. Steyn, "*Mechanistic study of Nitrogen/Sulphur Donor Atom Bidentate Ligand Influence on the Iodomethane Oxidative Addition to Carbonylphosphinerhodium(I) Complexes"*, *Ph.D. Thesis*, University of the Orange Free State, R.S.A., (1994).

[42] L. J. Damoense, W. Purcell, A. Roodt, and J. G. Leipoldt, *Rhodium Ex.*, **5**, 10 (1994).

[43] G. J. J. Steyn, A. Roodt, I. Poletaeva, and Y. S. Varshavsky, *J. Organomet. Chem.*, **536**, 197 (1997).

[44] L. J. Botha, S. S. Basson, and J. G. Leipoldt, *Inorg. Chim. Acta*, **126**, 25 (1987).

[45] L. J. Damoense, A. Roodt, W. Purcell, M. R. Galding, and Y. S. Varshavsky, *Manuscript in preparation.*

4 Experimental.

4.1 Materials.

Solid and liquid materials (Merck, Aldrich) were used without further purification. Solvents were distilled before use and water was double distilled. Flash chromatography was performed on Silica gel 60 (Merck, grain size 0.040 – 0.063 mm, eluent ether-hexane 1:4 by volume) utilizing an overpressure that never exceeded 100 Torr (1 Torr = 1 mmHg = 133.32 Pa).

4.2 Syntesis and identification of compounds.

4.2.1 Syntesis of β-diketones.

4.2.1.1 Synthesis of 1-phenyl-1,3-butanedione ($C_6H_5COCH_2COCH_3$, benzoylacetone, Hba)

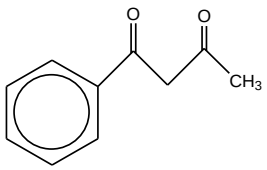

Sodium ethoxide was prepared by adding freshly pressed sodium wire to diethyl ether (± 200 ml) with the aid of sodium press as described elsewhere.[1] The ether-sodium mixture was transferred to a 3-necked flask. The flask was equipped with a dropping funnel, reflux condenser and a drying tube containing $CaCl_2$. The mixture was slowly heated on an oil bath in such a way that the temperature could not exceed 43°C. Ethanol (60.0 ml) was slowly added by means of a dropping funnel into ether-sodium mixture while stirring. The reaction mixture was refluxed overnight, afterwhich thewhite snow crystals were filtered on a sinted glass funnel and dried in a dessicator in the dark cupboard. Ethyl acetate (0.413 mol, 40 ml) was introduced into sodium ethoxide (6.905 g, 0.1 mol). The solution was stirred and acetophenone (12 ml, 0.103 mol) was slowly added from a dropping funnel. The reaction commenced with the separation of the sodium salt of benzoylacetone. The stirring was continued for two hours and the reaction was

allowed to stand in an ice bath overnight. The crude product was dissolved in cold water and acidified by few drops of acetic acid. The dark solid cleared after filtration, washing with ether to pale yellow crystals and were dried in the dessicator overnight. Purification was done under reduced pressure. The product benzoylacetone was collected at 125° – 130°C and solidified on cooling to white crystalline solid. Yield: (50.023 g, 65%).

4.2.1.2 Synthesis of 1-phenylpentane-1,3-dione ($C_6H_5COCH_2COCH_2CH_3$, propanylacetophonone, Hbap)

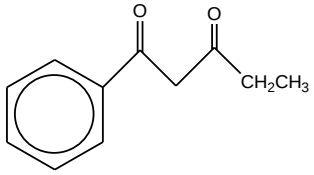

A Schlenk setup was used. In a 3-necked round bottomed flask with a magnetic stirrer bar acetophenone (1.2015 g, 10 ml) was added in dried, freshly distilled and degassed THF (1.0 ml). The flask was attached to a gas flow adapter and N_2 bubbler. The solution was degassed while stirring for 30 minutes. Lithium diisopropylamide (LDA) (6.0 ml of 1.8 M, 10.8 mmol) was added to the solution at 0°C with a syringe, under nitrogen, a colour change to clear orange showed that a slight excess of LDA was added. The solution was allowed to stir for 10 minutes before ethylpropanoate (1.0230 g, 10 mmol) was slowly added into the solution at 0°C while stirring. The reaction mixture was stirred overnight under N_2 atmosphere. Ether (30 ml) was added into the reaction mixture and stirred for 20 minutes. The resulting precipitate was filtered and washed with ether (2 x 30 ml). Ether (20 ml) was added to the precipitate with 0.3 M HCl (20 ml) while stirring till a pH lower than 4 was reached. The product was extracted with ether (2x50 ml). The combined ether extracts were dried with anhydrous $MgSO_4$ and ether was evaporated. Silica gel column chromatography was used to separate the product. Yield: (0.2894 g, 36%). δ_H (300 MHz, $CDCl_3$)/ppm:1.1 (3H, t, keto CH_3), 1.2 (3H, t, enol CH_3), 2.5 (2H, q, enol CH_2), 2.6 (2H, q, keto CH_2), 4.1 (2H, s, keto CH_2), 6.2 (1H, s, enol CH), 7.4-7.9 (5H, m, 2xC_6H_5); R_f = 0.39 (ether : hexane = 1: 4).

4.2.1.3 Synthesis of 1-phenylhexane-1,3-dione ($C_6H_5COCH_2COCH_2CH_2CH_3$, butyrylacetophenone, Hbab).

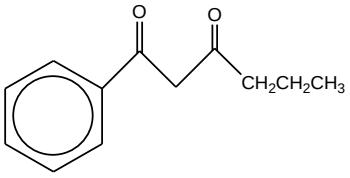

Hbab was prepared using lithium diisopropylamide under Schlenk conditions as described for Hbap by replacing ethylpropanoate with ethylbutyrate (1.1602 g, 10.0 mmol). Yield: (0.3339 g, 25%). δ_H (300 MHz, $CDCl_3$)/ppm: 0.9 (3H, t, keto CH_3), 1.0 (3H, t, enol CH_3), 1.6 (2H, q, keto CH_2), 1.7 (2H, q, enol CH_2), 2.4 (2H, t, enol CH_2), 2.6 (2H, t, keto CH_2), 4.1 (2H, s, keto CH_2), 6.2 (1H, s, enol CH), 7.5-8.0 (5H, m, 2xC_6H_5); R_f = 0.34 (ether : hexane = 1 : 4).

4.2.1.4 Synthesis of 1-phenylheptane-1,3-dione ($C_6H_5COCH_2COCH_2CH_2CH_2CH_3$, valerylacetophenone, Hbav).

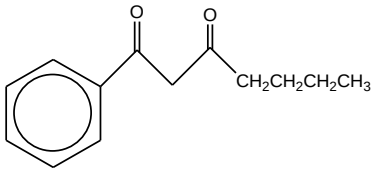

Hbav was prepared using lithium diisopropylamide under Schlenk conditions as described for Hbap by replacing ethylpropanoate with ethylvalerate (1.3013 g, 10.0 mmol). Silica gel column chromatography was used to separate the product. A better yield (0.731 g, 22%) was obtained due to freshly used lithium diisopropylamide. δ_H (300 MHz, $CDCl_3$)/ppm: 0.9 (3H, t, keto CH_3), 1.0 (3H, t, enol CH_3), 1.3 (2H, m, keto CH_2), 1.4 (2H, m, enol CH_2), 1.6 (2H, m, keto CH_2), 1.7 (2H, m enol CH_2), 2.4 (2H, t, enol CH_2), 2.6 (2H, t, keto CH_2), 4.1 (2H, s, keto CH_2), 6.2 (1H, s, enol CH), 7.5-8.0 (5H, m, 2 x C_6H_5); R_f = 0.58 (ether : hexane = 1 : 4).

4.2.2 Dicarbonyl(β-diketone)rhodium(1) [$Rh((\beta\text{-dik})(CO)_2$]

4.2.2.1 Dicarbonyl(1-phenyl-1,3-butanedionato-κ^2*O,O*')rhodium(1)

[Rh($C_6H_5COCH_2COCH_3$)($CO)_2$]

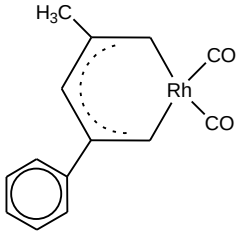

$[Rh_2Cl_2(CO)_4]$ was prepared *in situ* by refluxing $RhCl_3.3H_2O$ (0.1001 g, 0.38 mmol) in DMF (4.00 ml) for 20 minutes. The solution was allowed to cool in ice. An equivalent amount of ethylacetophenone (0.1009 g, 0.57 mmol) was slowly added to a stirred solution. After 30 minutes of stirring the crude product of $[Rh(ba)(CO)_2]$ was precipitated with an excess of water, filtered, washed with cold water and put in a dessicator overnight. The product was cleaned by flash column chromatography. Yield: (0.0959 g, 95%). δ_H (300 MHz, $CDCl_3$)/ppm: 2.3 (3H, s, CH_3), 6.3 (1H, s, CH) 7.4-7.9 (5H, m, C_2H_5). R_f = 74 (ether : hexane = 1 : 4). M.p. = 103-105^{o}C.

4.2.2.2 Dicarbonyl(1-phenyl-1,3-pentanedionato-κ^2*O,O*')rhodium(1)

.[Rh($C_6H_5COCH_2COCH_2CH_3$)($CO)_2$]

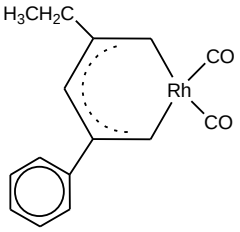

$[Rh(Hbap)(CO)_2]$ was prepared as described for $[Rh(Hba)(CO)_2]$ by replacing ethylacetophenone with propanylacetophenone (0.1022 g, 0.54 mmol). The crude product was precipitated with an excess of water and extracted with ether (3x30 ml). The combined ether extracts were washed with water, dried with ($MgSO_4$) and the solvent removed under reduced pressure. The product was dissolved in hot hexane, put in the refrigerator overnight. Yield: (0.0899 g, 27%) of light yellow crystals. δ_H (300 MHz, $CDCl_3$)/ppm: 1.2 (3H, t, CH_3), 2.4 (2H, q, CH_2), 6.2 (1H, s, CH) 7.4-7.9 (5H, m, C_2H_5); Rf = 0.67 (ether : hexane = 1 : 4). M.p. = 79-81^{o}C.

4.2.2.3 Dicarbonyl(1-phenyl-1,3-hexanedionato-κ^2*O,O*')rhodium(1)

[Rh($C_6H_5COCH_2COCH_2CH_2CH_3$)($CO)_2$]

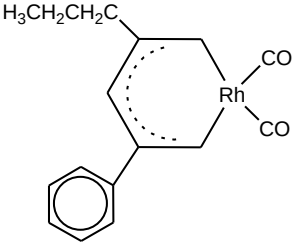

[Rh(bab)$(CO)_2$] was prepared as described for [Rh(bap)$(CO)_2$] by replacing propanylacetophenone with butyrylacetophenone (0.0718 g, 0.2063 mmol). The dark red oily product was recrystalised with hot hexane and allowed to cool overnight in the refrigerator. Silica gel column chromatography was used to purify the product. Yield: (0.0615g, 17%). δ_H (300 MHz, $CDCl_3$)/ppm: 1.0 (3H, t, CH_3), 1.7 (2H, m, CH_2), 2.4 (2H, t, CH_2), 6.3 (1H, s, CH), 7.4-7.9 (5H, m, C_2H_5); Rf 0.69 (ether : hexane = 1 : 4). M.p. = 53-55 °C

4.2.2.4 Dicarbonyl(1-phenyl-1,3-octanedionato-κ^2*O,O'*)rhodium(1) [Rh($C_6H_5COCH_2COCH_2CH_2CH_2CH_3$)$(CO)_2$]

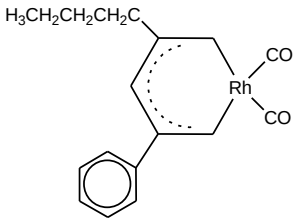

[Rh(Hbav)$(CO)_2$] was prepared as described for [Rh(Hbab)$(CO)_2$] by replacing butyrylacetophenone with valerylacetophenone (0.1069 g, 0.2953 mmol). The dark red oily product was recrystalised with hot hexane and allowed to cool overnight in the refrigerator. Silica gel column chromatography was also used to purify the product. Yield: (0.0657 g, 18%). δ_H (300 MHz, $CDCl_3$)/ppm: 0.9 (3H, t, CH_3), 1.4 (2H, m, CH_2), 1.7 (2H, m, CH_2), 2.4 (2H, t, CH_2), 6.3 (1H, s, CH), 7.4-7.9 (5H, m, C_2H_5); Rf = 0.83 (ether : hexane = 1 : 4). M.p. = 45-50 °C

4.2.3 [Rh(β-diketone)(CO)(PPh_3)] complexes

4.2.3.1 Carbonyl(1-phenyl-1,3-butanedionato-κ^2*O,O*')triphenylphosphine-rhodium(1) [Rh($C_6H_5COCH_2COCH_3$)(CO)(PPh_3)]

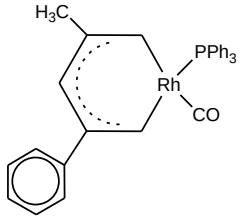

[Rh(ba)$(CO)_2$] (0.0599 g, 0.157 mmol) was dissolved in hot hexane (20.0 ml). To the hot solution PPh_3 (0.0417 g, 0.157 mmol) was added which resulted in bubbling off of CO gas. The resulting reaction mixture was stirred over boiling water until no more CO gas was released and was then filtered. Crystals were obtained by slowly cooling the reaction mixture overnight. Yield = 0.1755 g. δ_H (300 MHz, $CDCl_3$)/ppm: isomer 1: 2.3 (3H, s, CH_3), 6.2 (1H, s, CH), 6.9-7.9 (20H, m, aromatic); δ_H (300 MHz, $CDCl_3$)/ppm: isomer 2: 1.7 (3H, s, CH_3), 6.0 (1H, s, CH), 6.9-7.9 (20H, m, aromatic); ratio isomer 1 : isomer 2 = 1.00 : 0.46.

4.2.3.2 Carbonyl(1-phenyl-1,3-pentanedionato-κ^2*O,O*')triphenylphosphine-rhodium(1) [Rh($C_6H_5COCH_2COCH_2CH_3$)(CO)(PPh_3)]

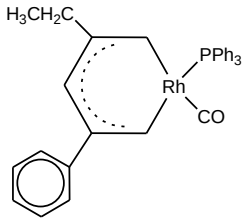

[Rh(bap)$(CO)_2$] (0.0899 g, 0.269 mmol) was dissolved in hot hexane (20.0 ml). To the hot solution PPh_3 (0.0707 g, 0.269 mmol) was added which resulted in bubbling off of CO gas. The resulting reaction mixture was stirred over boiling water until no more CO gas was released and was then filtered. Crystals were obtained by slowly cooling the reaction mixture overnight. Yield = 0.0955 g. δ_H (300 MHz, $CDCl_3$)/ppm: isomer 1: 1.2 (3H, t, CH_3), 2.5 (2H, q, CH_2), 6.2 (1H, s, CH), 7.0-8.0 (20H, m, aromatic); δ_H (300 MHz, $CDCl_3$)/ppm: isomer 2: 0.6 (3H, t, CH_3), 2.0(2H, q, CH_2), 6.1 (1H, s, CH), 7.0-8.0 (20H, m, aromatic); ratio isomer 1 : isomer 2 = 1.00 : 0.69. M.p. = 139-144^{o}C.

4.2.3.3 Carbonyl(1-phenyl-1,3-hexanedionato-κ²*O,O'*)triphenylphosphine-rhodium(1)[Rh($C_6H_5COCH_2COCH_2CH_2CH_3$)(CO)($PPh_3$)]

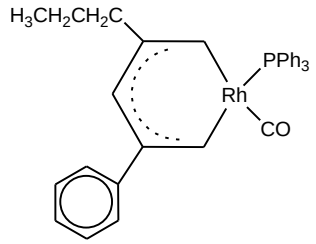

[Rh(bab)$(CO)_2$] (0.0690 g, 0.198 mmol) was dissolved in hot hexane (20.0 ml). To the hot solution PPh_3 (0.0520 g, 0.198 mmol) was added which resulted in bubbling off of CO gas. The resulting reaction mixtue was stirred over boiling water until no more CO gas was released and was filtered. Silica gel column chromatography was used to separate the product. Yield = 0.0732 g. δ_H (300 MHz, $CDCl_3$)/ppm: isomer 1: 0.6 (3H, t, CH_3), 1.2 (2H, m, CH_2), 2.0 (2H, t, CH_2), 6.1 (1H, s, CH), 7.0-8.0 (20H, m, aromatic), δ_H (300 MHz, $CDCl_3$)/ppm: isomer 2:1.0 (3H, t, CH_3), 1.8 (2H, m, CH_2), 2.5 (2H, t, CH_2), 6.2 (1H, s, CH), 7.0-8.0 (20H, m, aromatic); ratio isomer 1 : isomer 2 = 1.00 : 0.78. M.p. = 135-138°C.

4.2.3.4 Carbonyl(1-phenyl-1,3-octanedionato-κ²*O,O'*)triphenylphosphine-rhodium(1) [Rh($C_6H_5COCH_2COCH_2CH_2CH_2CH_3$)(CO)($PPh_3$)]

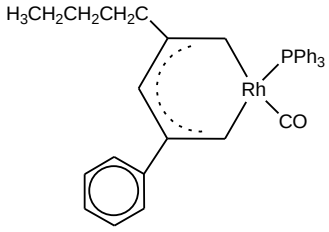

[Rh(bav)(CO)(PPh_3)] (0.0657 g, 0.1815 mmol) was dissolved in hot hexane (20.0 ml). To the hot solution PPh_3 (0.0476 g, 0.1815 mmol) was added which resulted in bubbling off of CO gas. The resulting reaction mixtue was stirred over boiling water until no more CO gas was released and was filtered. Silica gel column chromatography was used to purify the product. Yield = 0.0805 g. δ_H (300 MHz, $CDCl_3$)/ppm: isomer 1: 0.7 (3H, t, CH_3), 1.2 (4H, m, 2xCH_2), 2.0 (2H, t, CH_2), 6.1 (1H, s, CH), 7.0-8.0 (20H, m, aromatic), δ_H (300 MHz, $CDCl_3$)/ppm: isomer 2:1.0 (3H, t, CH_3), 1.4 (2H, m, CH_2), 1.7 (2H, m, CH_2), 2.5 (2H, t, CH_2), 6.2 (1H, s, CH), 7.0-8.0 (20H, m, aromatic); ratio isomer 1 : isomer 2 = 1.00 : 0.78. M.p. = 139-145°C.

4.3 Spectroscopic, kinetic and pK_a measurements.

A Bruker Advance DPX 300 NMR spectrometer was used to record NMR measurements [^1H (300 MHz)]. The chemical shifts are reported relative to $SiMe_4$ (0 ppm) for the ^1H spectra.

IR spectra were recorded from neat samples on a Digilab FTS 2000 Fourier transform spectrometer utilizing a He-Ne laser at 632.6 nm.

Acid dissociation was monitored on a Cary 50 Probe UV/Visible spectrophotometer. pH-measurements were done on a Hanna instruments model HI 9321, fitted with a glass electrode. The pH-meter was calibrated with buffers at a pH of 4.01, 7.01 and 10.01 respectively.

Melting points were determined with a Reichert Thermopan microscope with a Kofler hot-stage and are reported uncorrected.

The following spectrometers were used to monitor kinetic measurements: a Digilab FTS 2000 Fourier transform infrared spectrometer, a Cary 50 Probe UV/visible spectrophotometer and a Bruker Advance DPX 300 NMR spectrometer (for ^{1}H NMR) and Bruker Advance II 600 NMR spectrometer for ^{31}P NMR.

4.3.1 Oxidative addition reactions.

Formation and disappearance of the carbonyl peaks was monitored on the IR spectrometer, change in absorbance at the specified wavelength was monitored on the UV/visible spectrometer and change in integration units of the specified signals was monitored on the NMR spectrometer. Pseudo-first-order conditions were used to monitor all kinetic measurements with methyl iodide concentration of 10 to 400 times the concentration of the [Rh(β-diketone)(CO)(PPh_3)] complex. [Rh(β-diketone)(CO)(PPh_3)] concentrations used for these measurements were ≈ 0.0003 mol dm^{-3} for UV/visible and ≈ 0.03 mol dm^{-3} for IR and NMR. The first-order rate constants were obtained from least square fits of absorbance *vs* time data.

The least-square fits of the second order reaction rate constants *vs*. temperature data was used for the determination of the activation parameters ΔH^* (activation enthalphy) and ΔS^* (activation entropy) for the oxidative addition reactions according to the Arrehenius equation:

$$k = \frac{RT}{Nh} e^{\frac{-\Delta H^*}{RT}} e^{\frac{\Delta S^*}{R}} \quad \text{which can be written in a linear form:} \quad \frac{k}{T} = \frac{-\Delta H^*}{RT} + \frac{\Delta S}{R} + \ln\frac{R}{Nh}$$

where h = Planck constant = 6.625 x 10^{-34} J s, N = Avogadro's constant = 6.023 x 10^{23} mol^{-1}, R

= Gas constant = 8.314 J $mol^{-1}K^{-1}$. The activation free energy was calculated from: $\Delta G^* = \Delta H^* - T\Delta S^*$.

4.3.2 Acid dissociation contant determination.

Acid-base titrations were used to determine the pK_a values by measuring the absorbance at different pH. Titrations were done in acetonitrile-water mixtures, 1:9 by volume and an ionic strength of 0.10 mol dm^{-3} $NaClO_4.H_2O$. UV-spectra of β-diketones (0.00007-0.00034 mol dm^{-3}) in acidic and basic mediums were obtained. The spectra was used to determine the wavelength where the change in absorbance between the protonated and deprotonated forms is the greatest. Commercial buffers (Sigma) were used to ensure a linear response by the pH meter, fitted with a glass electrode. Calibrations were done at pH = 4.00, 7.00 and 12.00. A titration of acetylacetone with sodium hydroxide which was done and used as a test to determine pK_a, resulted in a pK_a of 8.99(1). The pK_a obtained was, within experimental error, the same as the best available published pK_a for acetylacetone (Hacac) in water (8.878(5) when μ = 1 mol dm^{-3} and 8.98 when μ = 0.0172 mol dm^{-3}).[2] It was therefore concluded that the electrode was calibrated to measure hydrogen ion activity under the conditions used. It is not expected that the electrode would behave differently for any of the other pK_a determinations because only pK_a values of a series of β-diketones were determined. Titrations of 50.0 ml β-diketone-solution were done with 0.1 mol dm^{-3} - 1.0 mol dm^{-3} NaOH or with $HClO_4$ depending on whether a bacic or acidic titration was performed. The pK_a values were determined by measuring the UV absorbance/pH data with titration from low to high pH and titration from high to low pH, followed by a least squares fit of the absorbance/pH data using $A_T = \frac{A_{HA}10^{-pH} + A_A 10^{-pK_a}}{10^{-pH} + 10^{-pK_a}}$, with A_T = total absorbance, A_{HA} = the absorbance of the β-diketone in the protonated (acidic) form and A_A = the absorbance of the β-diketone in the deprotonated (basic) form.

4.4 Crystallography.

The author acknowledges Dr. A.J. (Fanie) Muller of the Department of Chemistry, University of the Free State, for the data collection and refinement of the crystal structures.

4.4.1 Crystal structure determination of [Rh(PhCOCHCOCH$_2$CH$_3$)(CO)$_2$]

The crystal was mounted on a glass fiber and used for the X-ray crystallographic analysis. The X-ray intensity data was measured on a Bruker X8 Apex II 4K Kappa CCD diffractometer area detector system equipped with a graphite monochromator and Mo K_α fine-focus sealed tube (λ= 0.71073 Å) operated at 1.5 KW power (50 KV, 30 mA). The detector was placed at a distance of 3.75 cm from the crystal. Crystal temperature during the data collection was kept constant at 100(2) K using an Oxford 700 series cryostream cooler.

The initial unit cell and data collection was achieved by the Apex2 software[3] utilizing COSMO[4] for optimum collection of more than a hemisphere of reciprocal space. A total of 1127 frames were collected with a scan width in φ and an exposure time of 10 s frame^{-1}. The frames were integrated using a narrow-frame integration algorithm and reduced with the Bruker SAINT-Plus[5] and XPREP[5] software packages respectively. The integration of the data using a monoclinic cell yielded a total of 14494 reflections to a maximum θ angle of 28.30°, of which 3154 were independent with a R_{int} = 0.0342. Analysis of the data showed no significant decay during the data collection. Data was corrected for absorption effects using the multi-scan technique SADABS[6]) with minimum and maximum transmission coefficients of 0.7293 and 0.8550 respectively.

The structure was solved by the direct method package SIR97[7] and refined using the WinGX software package[8] incorporating SHELXL.[9] The final anisotropic full-matrix least-squares refinement on F^2 with 164 variables converged at R1 = 0.0273 for the observed data and wR2 = 0.0572 for all data. The GOF was 1.105. The largest peak on the final difference electron density synthesis was 0.53 e.Å^{-3} at 0.88 Å from Rh and the deepest hole -0.60 e.Å^{-3} at 0.91 Å from Rh.

The aromatic, methylene and methyl H atoms were placed in geometrically idealized positions (C–H = 0.93 – 0.98 Å) and constrained to ride on their parent atoms with U_{iso}(H) = 1.2U_{eq}(C) for aromatic, methylene and U_{iso}(H) = 1.5U_{eq}(C) for methyl. The methyl H's were located from a

Fourier difference map and refined as a rigid rotor. Non-hydrogen atoms were refined with anisotropic displacement parameters. Atomic scattering factors were taken from the International Tables for Crystallography Volume C.[10] The molecular plot was drawn using the DIAMOND program[11] with a 50% thermal envelope probability for non-hydrogen atoms. Hydrogen atoms were drawn as arbitrary sized spheres with radius of 0.135 Å.

4.4.2 Crystal structure determination of [Rh(PhCOCHCO(CH$_2$)$_2$CH$_3$)(CO)$_2$]

The crystal was mounted on a glass fiber and used for the X-ray crystallographic analysis. The X-ray intensity data was measured on a Bruker X8 Apex II 4K Kappa CCD diffractometer area detector system equipped with a graphite monochromator and Mo K_α fine-focus sealed tube (λ= 0.71073 Å) operated at 1.5 KW power (50 KV, 30 mA). The detector was placed at a distance of 3.75 cm from the crystal. Crystal temperature during the data collection was kept constant at 100(2) K using an Oxford 700 series cryostream cooler.

The initial unit cell and data collection was achieved by the Apex2 software[3] utilizing COSMO[4] for optimum collection of more than a hemisphere of reciprocal space. A total of 1124 frames were collected with a scan width ω in φ and an exposure time of 1 s frame^{-1}. The frames were integrated using a narrow-frame integration algorithm and reduced with the Bruker SAINT-Plus[5] and XPREP[5] software packages respectively. The integration of the data using a monoclinic cell yielded a total of 8867 reflections to a maximum θ angle of 28.36°, of which 3299 were independent with a R_{int} = 0.0251. Analysis of the data showed no significant decay during the data collection. Data was corrected for absorption effects using the multi-scan technique SADABS[6]) with minimum and maximum transmission coefficients of 0.7220 and 0.8605 respectively.

The structure was solved by the direct method package SIR97[7] and refined using the WinGX software package[8] incorporating SHELXL.[9] The final anisotropic full-matrix least-squares refinement on F^2 with 173 variables converged at R1 = 0.0244 for the observed data and wR2 =

0.0478 for all data. The GOF was 1.062. The largest peak on the final difference electron density synthesis was 0.63 e.Å^{-3} at 1.56 Å from H14 and the deepest hole -0.54 e.Å^{-3} at 0.87 Å from Rh

The aromatic, methylene and methyl H atoms were placed in geometrically idealized positions (C–H = 0.93 – 0.98 Å) and constrained to ride on their parent atoms with $U_{iso}(H) = 1.2U_{eq}(C)$ for aromatic, methylene and $U_{iso}(H) = 1.5U_{eq}(C)$ for methyl. The methyl H's were located from a Fourier difference map and refined as a rigid rotor. Non-hydrogen atoms were refined with anisotropic displacement parameters. Atomic scattering factors were taken from the International Tables for Crystallography Volume C.[10] The molecular plot was drawn using the DIAMOND program[11] with a 50% thermal envelope probability for non-hydrogen atoms. Hydrogen atoms were drawn as arbitrary sized spheres with radius of 0.135 Å.

4.4.3 Crystal structure determination of [Rh(PhCOCHCOCH$_2$CH$_3$)(CO)(PPh$_3$)]

The crystal was mounted on a glass fiber and used for the X-ray crystallographic analysis. The X-ray intensity data was measured on a Bruker X8 Apex II 4K Kappa CCD diffractometer area detector system equipped with a graphite monochromator and Mo K_α fine-focus sealed tube (λ= 0.71073 Å) operated at 1.5 KW power (50 KV, 30 mA). The detector was placed at a distance of 3.75 cm from the crystal. Crystal temperature during the data collection was kept constant at 293(2) K using an Oxford 700 series cryostream cooler.

The initial unit cell and data collection was achieved by the Apex2 software[3] utilizing COSMO[4] for optimum collection of more than a hemisphere of reciprocal space. A total of 2473 frames were collected with a scan width of ω in φ and an exposure time of 20 s frame^{-1}. The frames were integrated using a narrow-frame integration algorithm and reduced with the Bruker SAINT-Plus[5] and XPREP[5] software packages respectively. The integration of the data using a monoclinic cell yielded a total of 64974 reflections to a maximum θ angle of 28.37°, of which 13157 were independent with a R_{int} = 0.0408. Analysis of the data showed no significant decay during the data collection. Data was corrected for absorption effects using the multi-scan

technique SADABS[6]) with minimum and maximum transmission coefficients of 0.8488 and 0.9641 respectively.

The structure was solved by the direct method package SIR97[7] and refined using the WinGX software package[8] incorporating SHELXL.[9] The final anisotropic full-matrix least-squares refinement on F^2 with 380 variables converged at R1 = 0.1297 for the observed data and wR2 = 0.1290 for all data. The GOF was 0.948. The largest peak on the final difference electron density synthesis was 1.88 e.Å^{-3} at 0.86 Å from Rh2 and the deepest hole -0.79 e.Å^{-3} at 0.60 Å from Rh2.

The aromatic, methylene and methyl H atoms were placed in geometrically idealized positions (C–H = 0.93 – 0.98 Å) and constrained to ride on their parent atoms with $U_{iso}(H) = 1.2U_{eq}(C)$ for aromatic, methylene and $U_{iso}(H) = 1.5U_{eq}(C)$ for methyl. The methyl H's were located from a Fourier difference map and refined as a rigid rotor. Non-hydrogen atoms were refined with anisotropic displacement parameters. Atomic scattering factors were taken from the International Tables for Crystallography Volume C.[10] The molecular plot was drawn using the DIAMOND program[11] with a 50% thermal envelope probability for non-hydrogen atoms. Hydrogen atoms were drawn as arbitrary sized spheres with radius of 0.135 Å.

4.4.4 Crystal structure determination of [Rh(PhCOCHCO(CH$_2$)$_2$CH$_3$)(CO)(PPh$_3$)]

The crystal was mounted on a glass fiber and used for the X-ray crystallographic analysis. The X-ray intensity data was measured on a Bruker X8 Apex II 4K Kappa CCD diffractometer area detector system equipped with a graphite monochromator and Mo K_α fine-focus sealed tube (λ= 0.71073 Å) operated at 1.5 KW power (50 KV, 30 mA). The detector was placed at a distance of 3.8 cm from the crystal. Crystal temperature during the data collection was kept constant at 100(2) K using an Oxford 700 series cryostream cooler.

The initial unit cell and data collection was achieved by the Apex2 software[3] utilizing COSMO[4] for optimum collection of more than a hemisphere of reciprocal space. A total of 918 frames

were collected with a scan width in φ and an exposure time of 60 s frame^{-1}. The frames were integrated using a narrow-frame integration algorithm and reduced with the Bruker SAINT-Plus[5] and XPREP[5] software packages respectively. The integration of the data using a monoclinic cell yielded a total of 20242 reflections to a maximum θ angle of 26.25°, of which 5273 were independent with a R_{int} = 0.0994. Analysis of the data showed no significant decay during the data collection. Data was corrected for absorption effects using the multi-scan technique SADABS[6]) with minimum and maximum transmission coefficients of 0.8835 and 0.9852 respectively.

The structure was solved by the direct method package SIR97[7] and refined using the WinGX software package[8] incorporating SHELXL.[9] The final anisotropic full-matrix least-squares refinement on F^2 with 380 variables converged at R1 = 0.1124 for the observed data and wR2 = 0.1441 for all data. The GOF was 1.105. The largest peak on the final difference electron density synthesis was 1.27 e.Å^{-3} at 0.91 Å from H6A2 and the deepest hole -0.80 e.Å^{-3} at 1.03 Å from H14.

The aromatic, methylene and methyl H atoms were placed in geometrically idealized positions (C–H = 0.93 – 0.98 Å) and constrained to ride on their parent atoms with $U_{iso}(H) = 1.2U_{eq}(C)$ for aromatic, methylene and $U_{iso}(H) = 1.5U_{eq}(C)$ for methyl. The methyl H's were located from a Fourier difference map and refined as a rigid rotor. Non-hydrogen atoms were refined with anisotropic displacement parameters. Atomic scattering factors were taken from the International Tables for Crystallography Volume C.[10] The molecular plot was drawn using the DIAMOND program[11] with a 50% thermal envelope probability for non-hydrogen atoms. Hydrogen atoms were drawn as arbitrary sized spheres with radius of 0.135 Å.

4.4.5 Crystal structure determination of [Rh(PhCOCHCO(CH$_2$)$_3$CH$_3$)(CO)(PPh$_3$)]

The crystal was mounted on a glass fiber and used for the X-ray crystallographic analysis. The X-ray intensity data was measured on a Bruker X8 Apex II 4K Kappa CCD diffractometer area detector system equipped with a graphite monochromator and Mo K_α fine-focus sealed tube (λ= 0.71073 Å) operated at 1.5 KW power (50 KV, 30 mA). The detector was placed at a distance

of 4.7 cm from the crystal. Crystal temperature during the data collection was kept constant at 100(2) K using an Oxford 700 series cryostream cooler.

The initial unit cell and data collection was achieved by the Apex2 software[3] utilizing COSMO[4] for optimum collection of more than a hemisphere of reciprocal space. A total of 1125 frames were collected with a scan width ω in φ and an exposure time of 10 s frame^{-1}. The frames were integrated using a narrow-frame integration algorithm and reduced with the Bruker SAINT-Plus[5] and XPREP[5] software packages respectively. The integration of the data using a monoclinic cell yielded a total of 27483 reflections to a maximum θ angle of 28.37°, of which 6865 were independent with a R_{int} = 0.0316. Analysis of the data showed no significant decay during the data collection. Data was corrected for absorption effects using the multi-scan technique SADABS[6]) with minimum and maximum transmission coefficients of 0.7991 and 0.8257 respectively.

The structure was solved by the direct method package SIR97[7] and refined using the WinGX software package[8] incorporating SHELXL.[9] The final anisotropic full-matrix least-squares refinement on F^2 with 335 variables converged at R1 = 0.0671 for the observed data and wR2 = 0.1279 for all data. The GOF was 1.207. The largest peak on the final difference electron density synthesis was 2.84 e.Å^{-3} at 0.73 Å from Rh and the deepest hole -1.94 e.Å^{-3} at 0.69 Å from Rh.

The aromatic, methylene and methyl H atoms were placed in geometrically idealized positions (C–H = 0.93 – 0.98 Å) and constrained to ride on their parent atoms with $U_{iso}(H) = 1.2U_{eq}(C)$ for aromatic, methylene and $U_{iso}(H) = 1.5U_{eq}(C)$ for methyl. The methyl H's were located from a Fourier difference map and refined as a rigid rotor. Non-hydrogen atoms were refined with anisotropic displacement parameters. Atomic scattering factors were taken from the International Tables for Crystallography Volume C.[10] The molecular plot was drawn using the DIAMOND program[11] with a 50% thermal envelope probability for non-hydrogen atoms. Hydrogen atoms were drawn as arbitrary sized spheres with radius of 0.135 Å.

4.5 References

[1] A. I. Vogel. *Vogel's Textbook of Practical Organic Chemistry*. Longmans, UK (1956).

[2] J. Starý, *The Solvent Extraction of Metal Chelates*, MacMillan Company, New York, 1964, Appendix.

[3]. *Apex2*. (Version 1.0-27), Bruker AXS Inc., Madison, Wisconsin, USA, 2005.

[4]. *COSMO*. Version 1.48, Bruker AXS Inc., Madison, Wisconsin, USA, 2003.

[5]. *SAINT-Plus*. Version 7.12 (including XPREP), Bruker AXS Inc., Madison, Wisconsin, USA, 2004.

[6]. *SADABS*. Version 2004/1, Bruker AXS Inc., Madison, Wisconsin, USA, 1998.

[7]. A. Altomare.; M. C. Burla.; M. Camalli.; G. L Cascarano.; C Giacovazzo.; A Guagliardi.; A. G. G. Moliterni.; G. Polidori.; R Spagna,. *J. Appl. Cryst*. **1999**, *32*, 115.

[8]. L. J. Farrugia, WinGX Version 1.70.01, *J. Appl. Cryst*. **1999**, *32*, 837.

[9]. G. M. Sheldrick. *SHELXL97 Program for crystal structure refinement*. University of Göttingen, Germany, 1997.

[10]. *International Tables for Crystallography*, Kluwer Academic Publishers, Dordrecht, The Netherlands, 1002, Vol C.

[11]. K. Brandenburg ; H Putz, *DIAMOND*, Release 3.1a. Crystal Impact GbR, Bonn, Germany 2005.

5 Summary.

Synthetic routes to prepare β-diketonatones and new β-diketonato rhodium(I) complexes of the type [Rh(PhCOCHCOR)$(CO)_2$] and [Rh(PhCOCHCOR)(CO)(PPh_3)] with Ph = C_6H_5 and R = CH_2CH_3, $CH_2CH_2CH_3$ and $CH_2CH_2CH_2CH_3$ have been developed and optimized.

Two synthetic routes were used for the synthesis of β-diketones of the type $C_6H_5COCH_2COR$, R = CH_3 (Hba), CH_2CH_3 (Hbap), $CH_2CH_2CH_3$ (Hbab) and $CH_2CH_2CH_2CH_3$ (Hbav), by Claisen condensation of acetophenone and the appropriate ester. The first route is where sodium ethoxide in ethanol was used as the base during the synthesis and the second route is where lithiumdiisopropylamide in THF was used as a base. The first route failed when the alkyl chain $(CH_2)_nCH_3$, n = 1 – 3, of the β-diketone was increased Percentage yields of these β-diketones decreased with an increase in the alkyl chain-length of the β-diketone. The p$K_a^{/}$ values of the β-diketones and group electronegativities of the R substituents were found to be (R, p$K_a^{/}$, χ_R) = (CH_3, 8.81, 2.21), (CH_2CH_3, 9.28, 2.31), ($CH_2CH_2CH_3$, 9.17, 2.41) and ($CH_2CH_2CH_2CH_3$, 9.25, 2.22). ^{1}H NMR studies indicated that in $CDCl_3$ solution these β-diketones exist as mixtures of keto and enol tautomers with enolization dominant in a direction away from the R group. The equilibrium constant K_c = [keto]/[enol] = 0.084 (Hba), 0.122 (Hbap), 0.087 (Hbab) and 0.086 (Hbav) respectively.

The synthesised β-diketones were complexed to rhodium to form new rhodium-dicarbonyl complexes of the type [Rh(β-diketonato)$(CO)_2$] which were thereafter reacted with triphenylphosphine ligand to yield new rhodium complexes of the type [Rh(β-diketonato)(CO)(PPh_3)]. At least two isomers were observed for each of the later complexes - *cis* and *trans* isomers in equilibrium with each other. The dominant isomer in solution was found to be the isomer where PPh_3 is *trans* to the oxygen near an electron donating group (phenyl) in accordance to the theory of trans-influence.[1] The equilibrium constant, K_c, between these isomers in $CDCl_3$ solution increased with increasing alkyl chain length of the β-diketonato ligand, K_c = 0.47 (ba), 0.69 (bap), 0.77 (bab) and 0.80 (bav) respectively. A crystal structure determination showed that both the *cis* and *trans* isomers of [Rh(bap)(CO)(PPh_3)] crystallized in the same unit cell. In agreement with the polarisation theory[2] and the σ-*trans* effect[3], the crystal structures of [Rh(bab)(CO)(PPh_3)] and [Rh(bav)(CO)(PPh_3)] showed that the

carbonyl atom *trans* to the less electronegative Ph-group was substituted with PPh_3. [Rh(β-diketonato)$(CO)_2$] crystal structures are virtually unavailable,[4] only three structures has been reported previously. This study provides the crystal structure of two new rhodium(I)-dicarbonyl complexes [Rh(bap)$(CO)_2$] and [Rh(bab)$(CO)_2$].

The chemical kinetics of oxidative addition of CH_3I to [Rh($C_6H_5COCHCOR$)$(CO)(PPh_3)$] in chloroform has been studied in detail utilising IR, UV/visible, ^1H and ^{31}P NMR techniques. Three definite reaction sets involving at least two Rh(III)-alkyl and two Rh(III)-acyl species were observed:

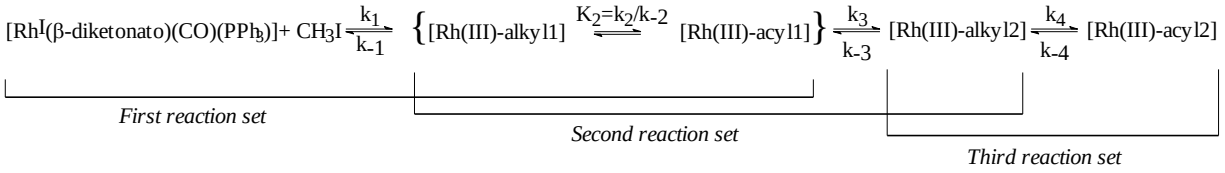

The first reaction set is the fastest of the three as it is 100 (for [Rh(bap)$(CO)(PPh_3)$]), 40 (for [Rh(bab)$(CO)(PPh_3)$]) and 600 (for [Rh(bav)$(CO)(PPh_3)$]) times faster than the second set of reactions for [MeI] = 1 mol dm^{-3}. The rate of the oxidative addition step in chloroform (first reaction set) was not influences by the increasing alkyl chain length of theβ-diketonato ligand: k_1 = 0.0341 ([Rh(bap)$(CO)(PPh_3)$]), 0.047 ([Rh(bab)$(CO)(PPh_3)$]) and 0.0.31 dm^3 $mol^{-1}s^{-1}$ ([Rh(bav)$(CO)(PPh_3)$]) respectively. Thermodynamic properties for the first oxidative addition step determined for all the synthesised complexes showed small positive ΔH^* and large negative value for ΔS^*, consistent with an associative mechanism.[5]

The ^{31}P NMR study on different six-membered chelate complexes, [Rh(L,L'-BID)$(CO)(PPh_3)$] and related Rh(III) complexes, indicated a general decrease in the coupling constant $^1J(^{31}P$-$^{103}Rh)$ (in Hz), as the Rh-P bond length (in Å), determined by X-ray crystallography, increases. L,L'-BID is a bidentate ligand with donor atoms L and L', such as the β-diketonatos bav, bap, bav, tfhd, tftma, sacac *etc.* Utilizing the results of this study as well as previously published results this relationship was quantified as

$$d(\text{Rh-P}) = -0.0014(1) \times {}^1J(^{31}\text{P-}^{103}\text{Rh}) + 2.49(2) = -0.0039(4) \times \delta^{31}\text{P} + 2.44(2).$$

with the Rh-P bond lengths, d(Rh-P), varying between 2.23 Å and 2.36 Å.

References

[1] A. Roodt and G. J. J. Steyn, *Inorg. Chem.*, **2**, 1-23 (2000).

[2] A. A. Grinberg. *Acta Physiochim,* USSR, **3**, 573 (1935).

[3] C. H. Langford and H. B. Gray, *Ligand Substitution Processes,* W.A. Benjamin Inc., New York (1965).

[4] The Cambridge Crystallographic Data Centre (CCDC), ConQuest Version 1.8, Copyright © (2005).

[5] V. Chauby, J. Daran, C. S. Berre, F. Malbosc, P. Kalck, O. D. Gonzalez, C. E. Haslam and A Haynes. *Inorg.Chem.* **21**, 3280-3290 (2002).

Acknowledgements

The author wishes to thank everyone that was so graciously helpful. Special acknowledgement goes to my promoter, Dr. Jeanet Conradie, for her assistance, skilful guidance and special effort during the course of this study and the writing of this thesis.

My thanks go to all my colleagues of the Department of Chemistry, both in Bloemfontein and in Qwaqwa, who somehow or other contributed to the success of this study. In this regard I would like to make special mention of Dr. A. J. (Fanie) Muller for the data collection, refinement and useful discussions of the crystal structures, Ernie Langner who read this thesis for grammatical corrections, Prof. Jannie Swarts and Prof. Riaan Luyt.

Many thanks to my family and friends who were somehow inconvenienced by my absence at home, their motivation, sacrifice and support during the years of study. Special thanks to my cousins Pumza and Molefi Mahanke for hosting me in their house when I had to be in Bloemfontein during this study.

Thank you

A ^{1}H and ^{31}P NMR

Spectrum 1: 1-phenylpentane-1,3-dione, Hpab

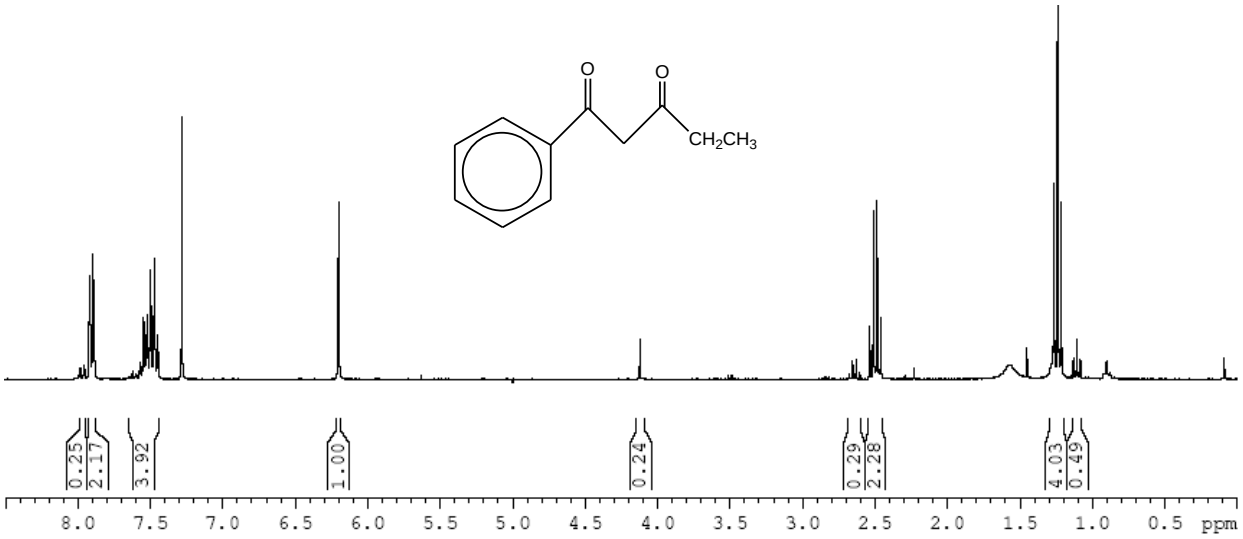

Spectrum 2: 1-phenylhexane-1,3-dione, Hbab

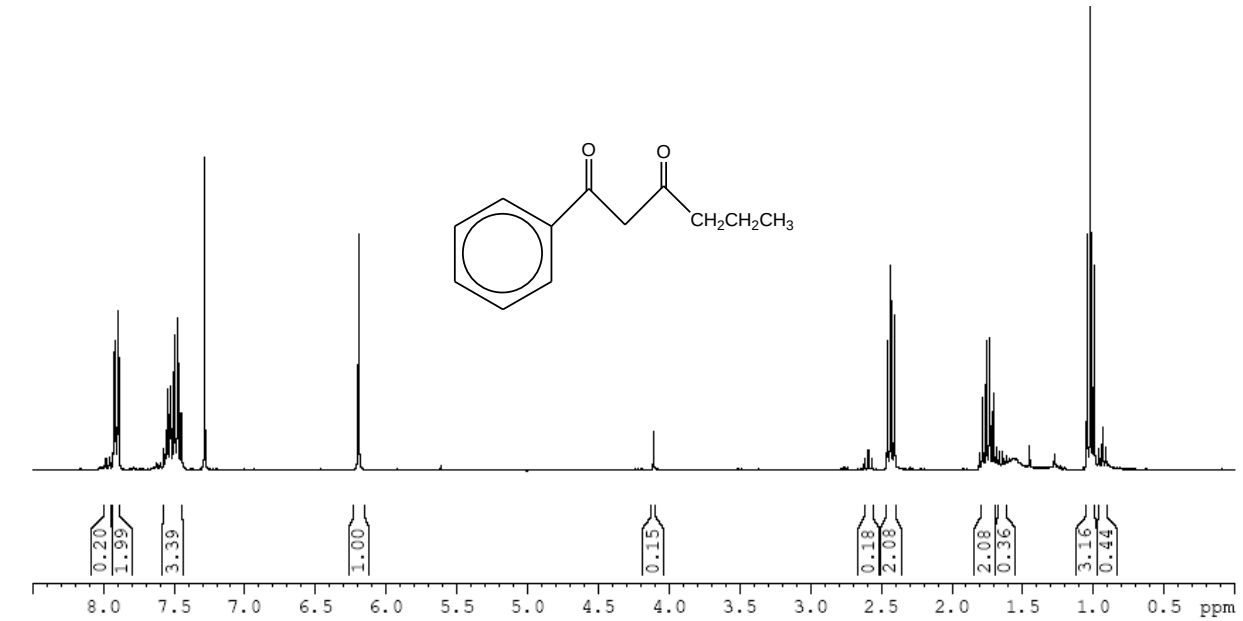

Spectrum 3: 1-phenylheptane-1,3-dione, Hbav

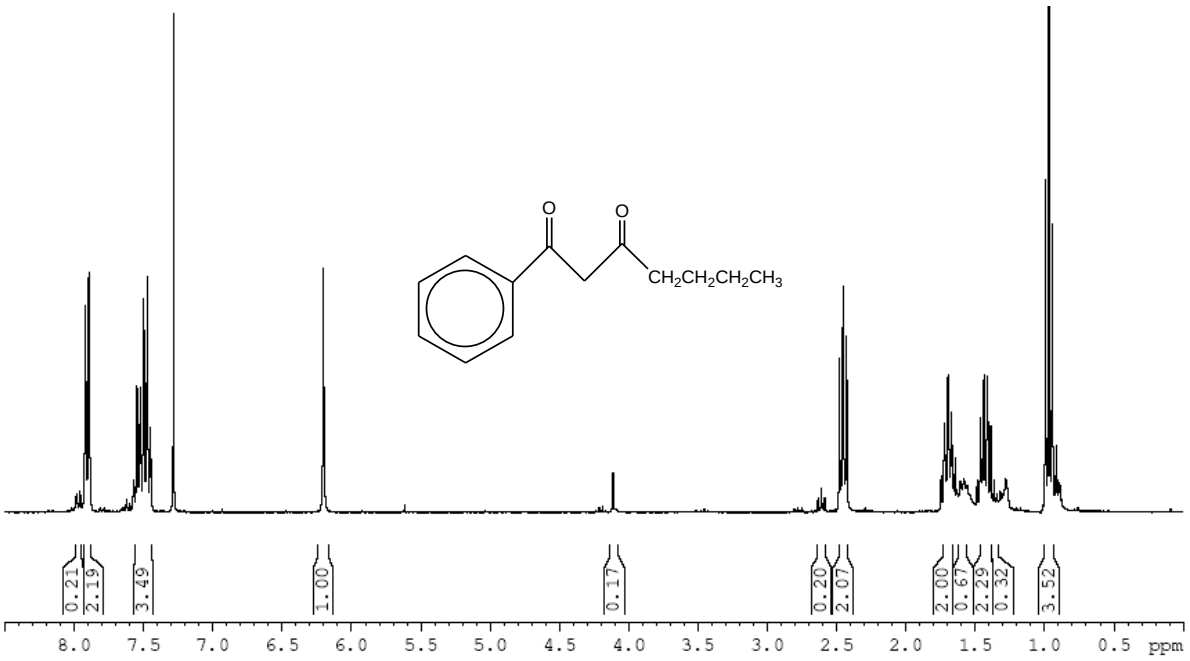

Spectrum 4: Dicarbonyl(1-phenyl-1,3-pentanedionato-κ^{2}*O,O*')rhodium(1), [Rh(Hbap)(CO)$_2$]

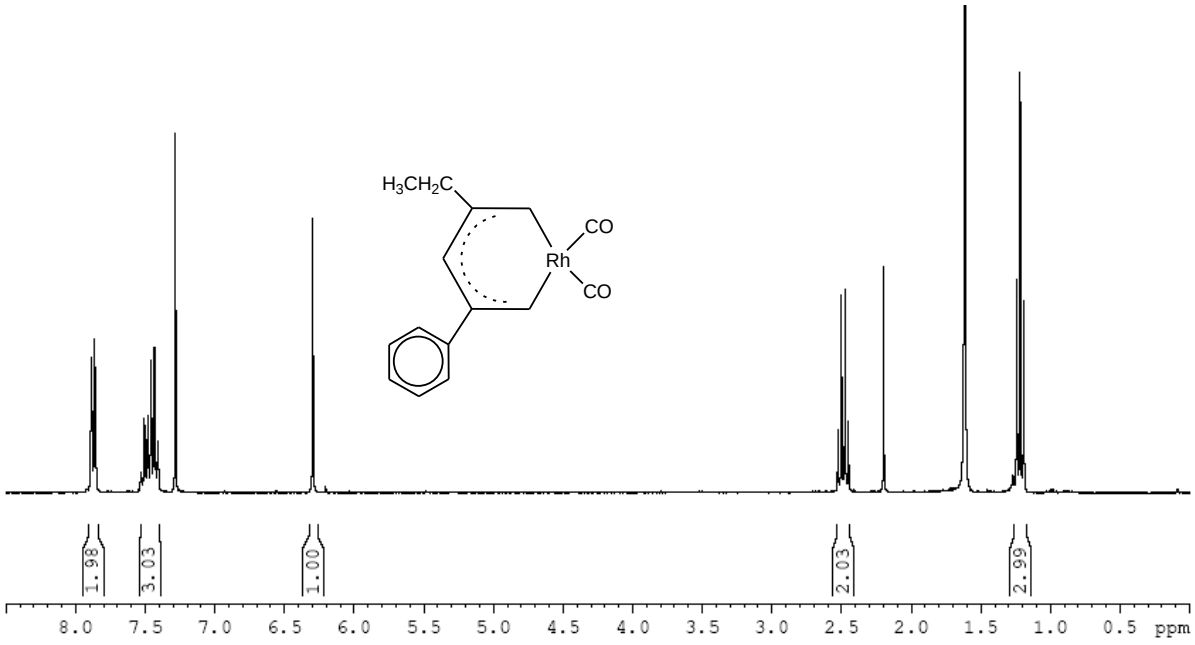

Spectrum 5: Spectrum Dicarbonyl(1-phenyl-1,3-hexanedionato-κ^2*O,O*')rhodium(1), [Rh(Hbab)(CO)$_2$]

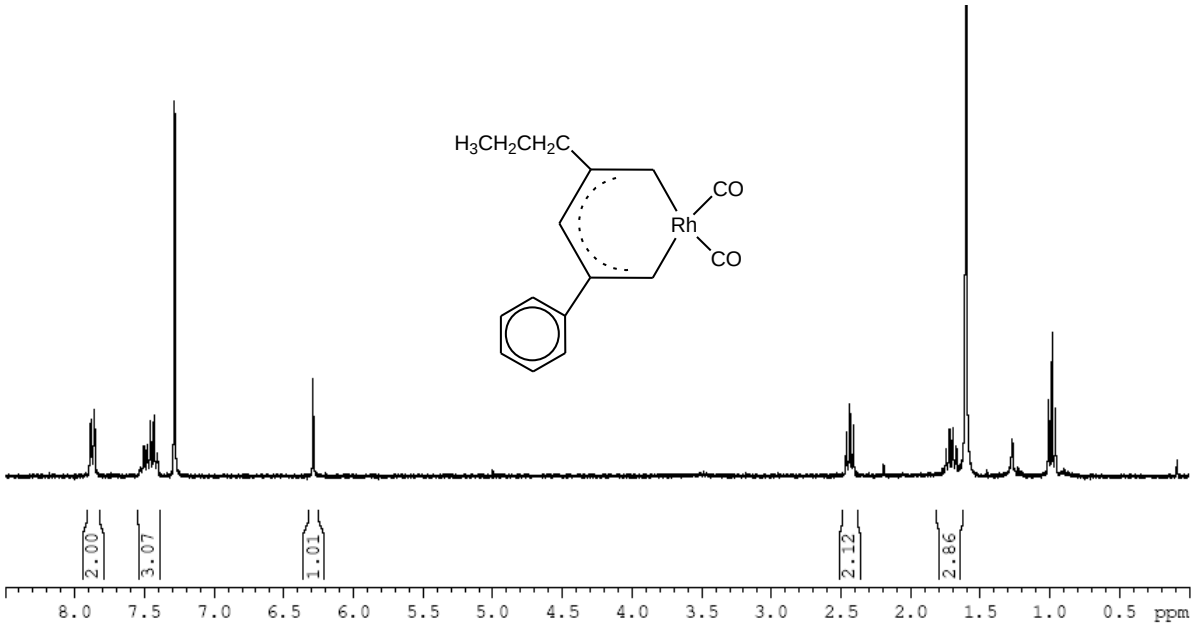

Spectrum 6: Dicarbonyl(1-phenyl-1,3-octanedionato-κ^2*O,O*')rhodium(1), [Rh(Hbav)(CO)$_2$]

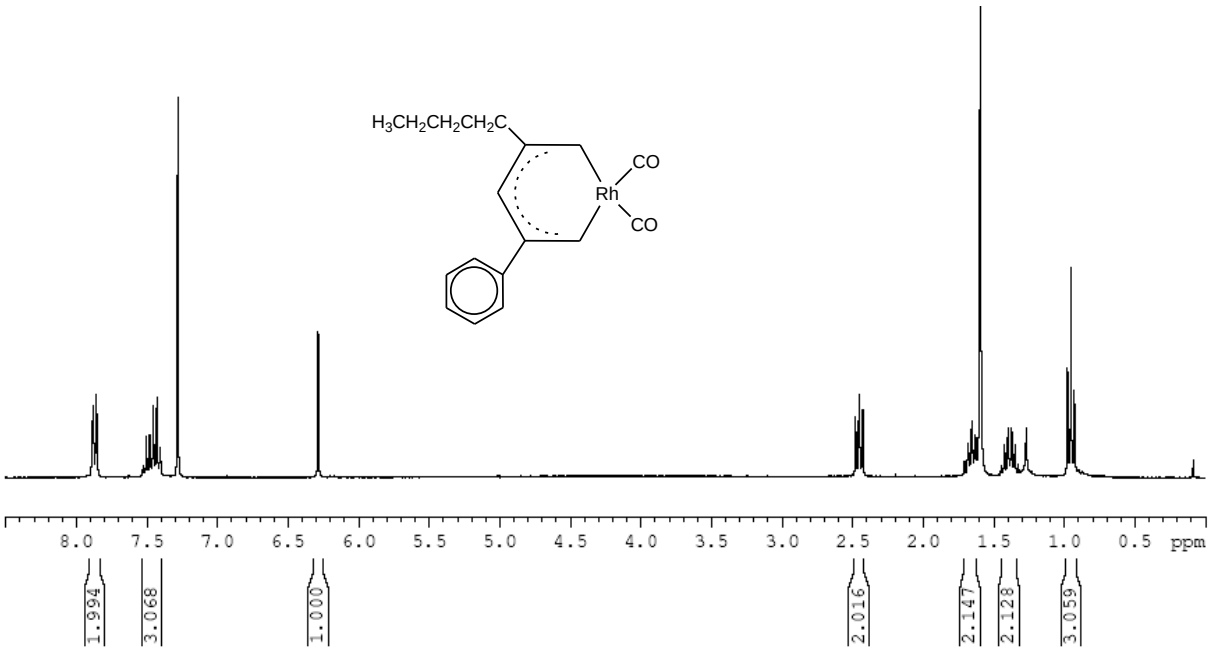

Spectrum 7: Carbonyl(1-phenyl-1,3-pentanedionato-κ^{2}*O*,*O*')triphenylphosphine-rhodium(1), [Rh(Hbap)(CO)(PPh$_3$)]

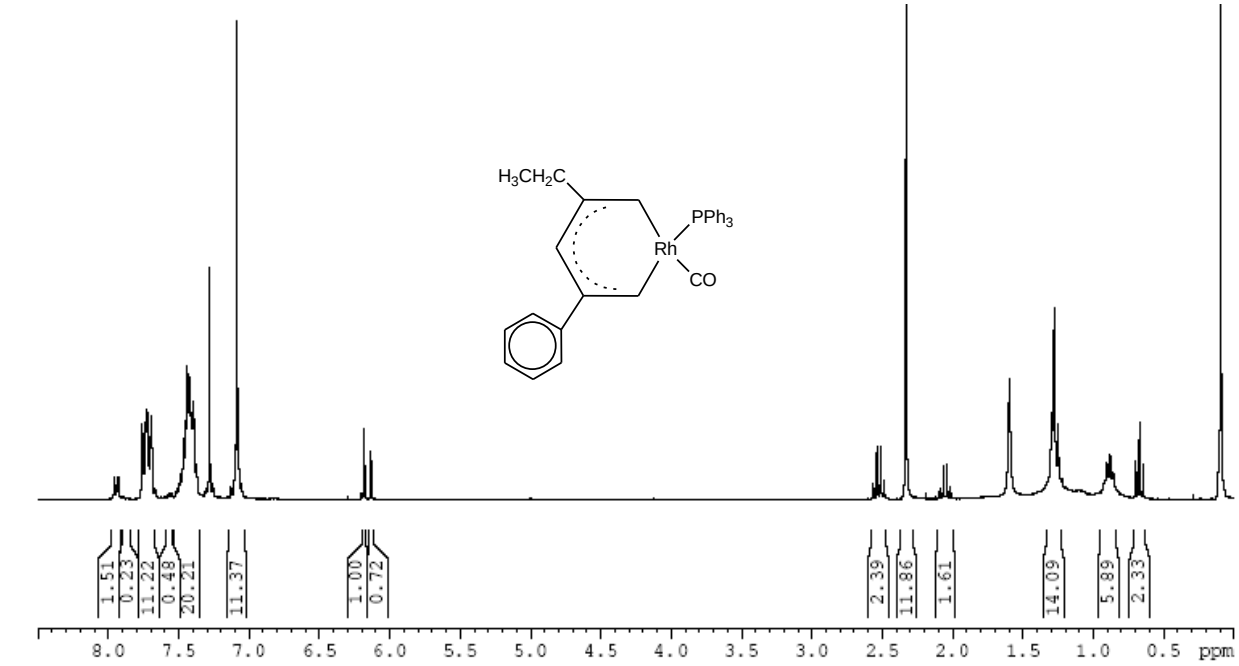

Spectrum 8: **Carbonyl(1-phenyl-1,3-hexanedionato-κ^{2}*O*,*O*')triphenylphosphine-rhodium(1), [Rh(Hbab)(CO)(PPh$_3$)]**

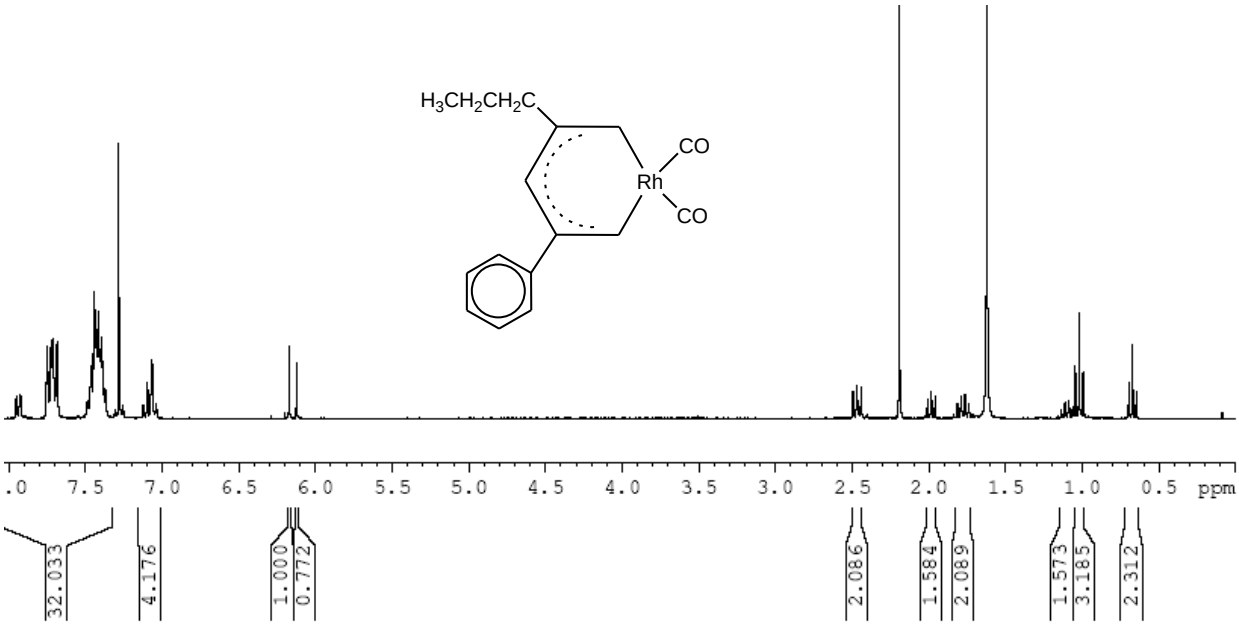

Spectrum 9: Carbonyl(1-phenyl-1,3-octanedionato-κ^2*O,O'*)triphenylphosphine-rhodium(1), [Rh(Hbav)(CO)(PPh$_3$)]

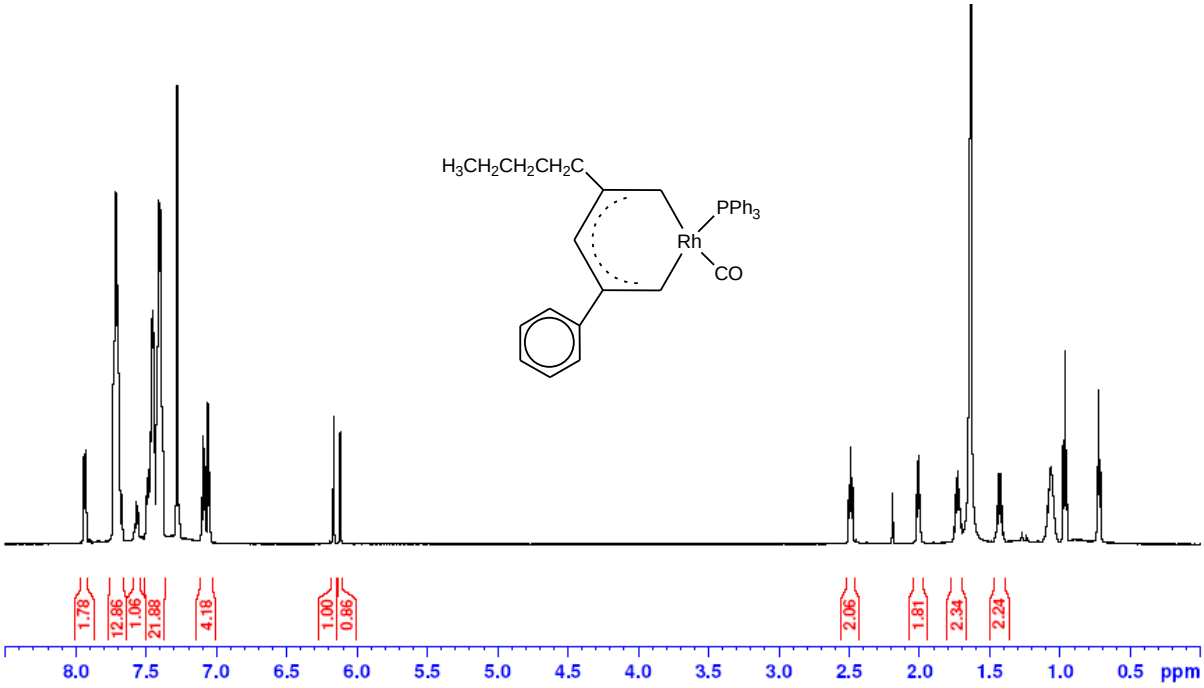

Spectrum 10: [Rh(Hbap)(CO)(PPh$_3$)]

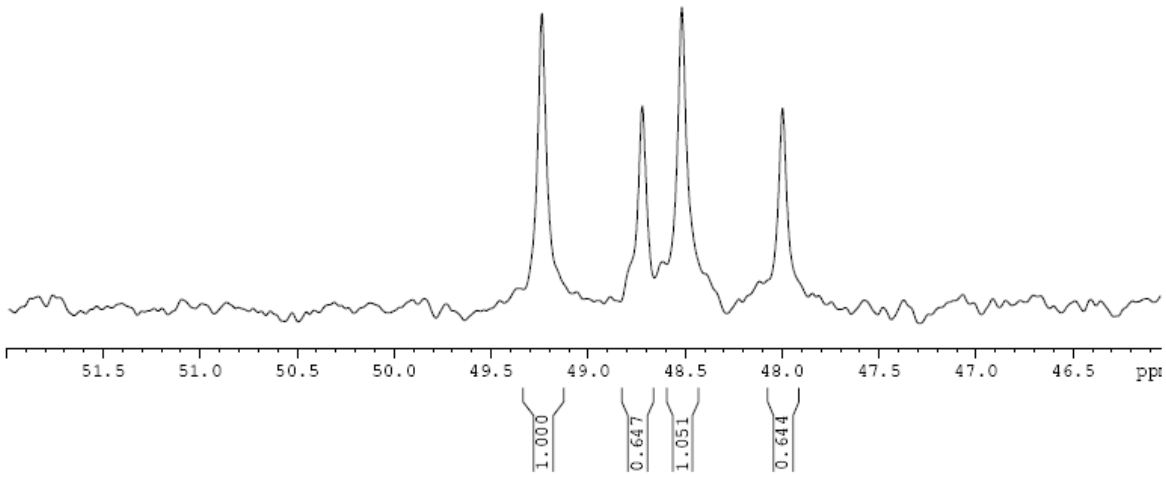

Spectrum 11: [Rh(Hbab)(CO)(PPh$_3$)]

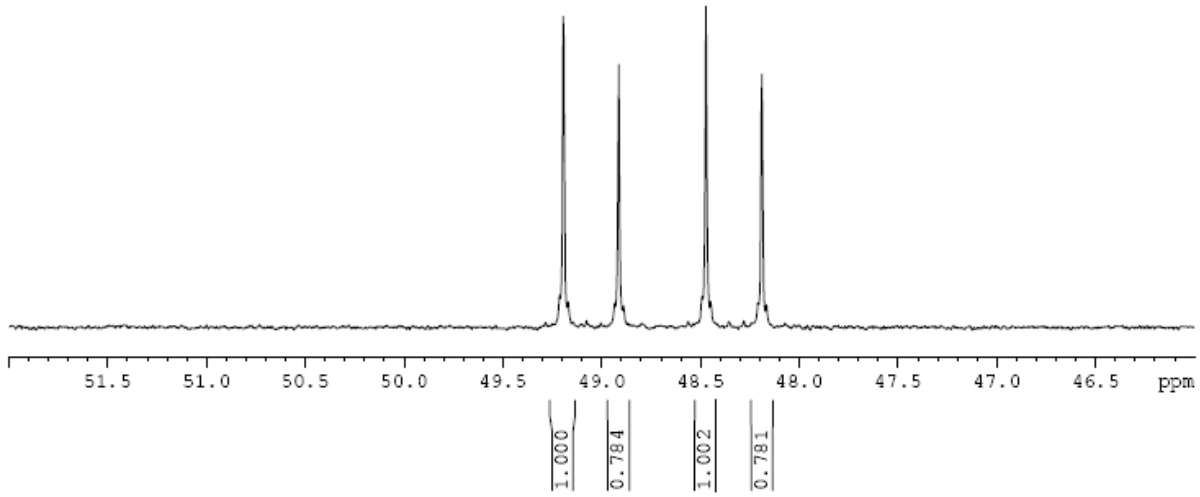

Spectrum 12: [Rh(Hbav)(CO)(PPh$_3$)]

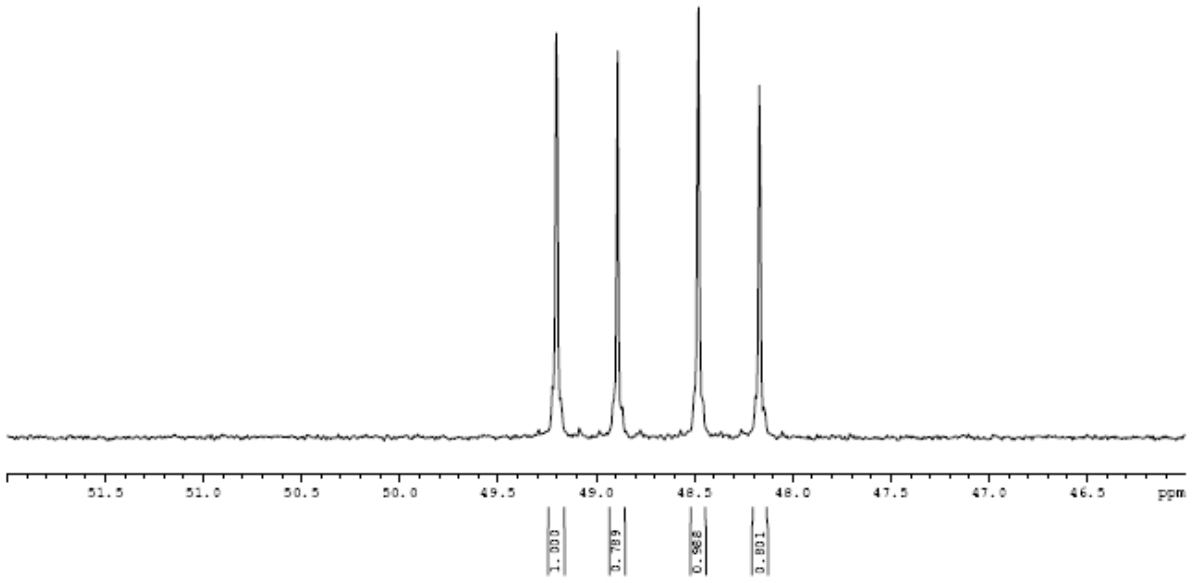

B Listed atomic coordinates and anisotropic displacement parameters.

B.1 Rh(bap)(CO)$_2$]

Table 1. Crystal data and structure refinement for 6fms3_0m.

Identification code	6fms3_0m	
Empirical formula	C13 H11 O4 Rh	
Formula weight	334.13	
Temperature	293(2) K	
Wavelength	0.71073 Å	
Crystal system	Monoclinic	
Space group	P 21/n	
Unit cell dimensions	a = 10.4080(4) Å	α= 90°.
	b = 7.8360(3) Å	β= 103.2130(10)°.
	c = 15.9878(6) Å	γ = 90°.
Volume	1269.40(8) Å^3	
Z	4	
Density (calculated)	1.748 Mg/m^3	
Absorption coefficient	1.348 mm^{-1}	
F(000)	664	
Crystal size	0.25 x 0.21 x 0.12 mm^3	
Theta range for data collection	2.13 to 28.30°.	
Index ranges	-13<=h<=13, -10<=k<=10, -21<=l<=21	
Reflections collected	14494	
Independent reflections	3154 [R(int) = 0.0342]	
Completeness to theta = 28.30°	100.0 %	
Absorption correction	Semi-empirical from equivalents	
Max. and min. transmission	0.8550 and 0.7293	
Refinement method	Full-matrix least-squares on F^2	
Data / restraints / parameters	3154 / 0 / 164	
Goodness-of-fit on F^2	1.105	
Final R indices [I>2sigma(I)]	R1 = 0.0219, wR2 = 0.0543	
R indices (all data)	R1 = 0.0273, wR2 = 0.0572	
Largest diff. peak and hole	0.531 and -0.598 e.Å^{-3}	

Table 2. Atomic coordinates (x 10^4) and equivalent isotropic displacement parameters ($Å^2$x 10^3) for 6fms3_0m. U(eq) is defined as one third of the trace of the orthogonalized U^{ij} tensor.

	x	y	z	U(eq)
Rh	3873(1)	4144(1)	4285(1)	14(1)
C(1)	4845(2)	2172(3)	4276(1)	18(1)
O(1)	5438(2)	960(2)	4263(1)	26(1)
C(2)	3022(2)	3111(3)	5049(1)	18(1)
O(2)	2481(2)	2486(2)	5512(1)	27(1)
O(3)	4761(1)	5230(2)	3412(1)	17(1)
O(4)	2728(2)	6245(2)	4264(1)	18(1)
C(3)	424(2)	8396(3)	3875(2)	35(1)
C(4)	1834(2)	8990(3)	3948(2)	24(1)
C(5)	2751(2)	7584(3)	3805(1)	17(1)
C(6)	3544(2)	7831(3)	3223(1)	19(1)
C(7)	4491(2)	6699(3)	3055(1)	16(1)
C(8)	5300(2)	7158(2)	2428(1)	16(1)
C(9)	6495(2)	6323(3)	2479(1)	19(1)
C(10)	7252(2)	6660(3)	1885(1)	22(1)
C(11)	6813(2)	7828(3)	1235(1)	23(1)
C(12)	5630(2)	8665(3)	1183(1)	26(1)
C(13)	4877(2)	8348(3)	1775(1)	22(1)

Table 3. Bond lengths [Å] and angles [°] for 6fms3_0m.

Rh-C(1)	1.849(2)
Rh-C(2)	1.852(2)
Rh-O(4)	2.0285(14)
Rh-O(3)	2.0288(13)
Rh-Rh#1	3.1752(3)
C(1)-O(1)	1.135(2)
C(2)-O(2)	1.137(2)
O(3)-C(7)	1.287(2)
O(4)-C(5)	1.283(2)
C(3)-C(4)	1.518(3)
C(3)-H(3A)	0.9600
C(3)-H(3B)	0.9600
C(3)-H(3C)	0.9600
C(4)-C(5)	1.509(3)
C(4)-H(4A)	0.9700
C(4)-H(4B)	0.9700
C(5)-C(6)	1.390(3)
C(6)-C(7)	1.398(3)
C(6)-H(6)	0.9300
C(7)-C(8)	1.492(3)
C(8)-C(9)	1.391(3)
C(8)-C(13)	1.394(3)
C(9)-C(10)	1.390(3)
C(9)-H(9)	0.9300
C(10)-C(11)	1.382(3)
C(10)-H(10)	0.9300
C(11)-C(12)	1.381(3)
C(11)-H(11)	0.9300
C(12)-C(13)	1.383(3)
C(12)-H(12)	0.9300
C(13)-H(13)	0.9300
C(1)-Rh-C(2)	89.14(9)
C(1)-Rh-O(4)	177.22(8)
C(2)-Rh-O(4)	89.87(7)
C(1)-Rh-O(3)	90.53(7)
C(2)-Rh-O(3)	177.92(8)
O(4)-Rh-O(3)	90.36(6)

C(1)-Rh-Rh#1	92.49(7)
C(2)-Rh-Rh#1	95.47(7)
O(4)-Rh-Rh#1	90.19(4)
O(3)-Rh-Rh#1	86.60(4)
O(1)-C(1)-Rh	179.4(2)
O(2)-C(2)-Rh	178.9(2)
C(7)-O(3)-Rh	126.34(13)
C(5)-O(4)-Rh	125.82(13)
C(4)-C(3)-H(3A)	109.5
C(4)-C(3)-H(3B)	109.5
H(3A)-C(3)-H(3B)	109.5
C(4)-C(3)-H(3C)	109.5
H(3A)-C(3)-H(3C)	109.5
H(3B)-C(3)-H(3C)	109.5
C(5)-C(4)-C(3)	113.48(19)
C(5)-C(4)-H(4A)	108.9
C(3)-C(4)-H(4A)	108.9
C(5)-C(4)-H(4B)	108.9
C(3)-C(4)-H(4B)	108.9
H(4A)-C(4)-H(4B)	107.7
O(4)-C(5)-C(6)	126.02(19)
O(4)-C(5)-C(4)	114.49(17)
C(6)-C(5)-C(4)	119.49(19)
C(5)-C(6)-C(7)	126.34(19)
C(5)-C(6)-H(6)	116.8
C(7)-C(6)-H(6)	116.8
O(3)-C(7)-C(6)	125.08(18)
O(3)-C(7)-C(8)	114.44(17)
C(6)-C(7)-C(8)	120.48(18)
C(9)-C(8)-C(13)	118.88(19)
C(9)-C(8)-C(7)	118.78(18)
C(13)-C(8)-C(7)	122.30(19)
C(10)-C(9)-C(8)	120.7(2)
C(10)-C(9)-H(9)	119.7
C(8)-C(9)-H(9)	119.7
C(11)-C(10)-C(9)	119.8(2)
C(11)-C(10)-H(10)	120.1
C(9)-C(10)-H(10)	120.1
C(12)-C(11)-C(10)	119.8(2)
C(12)-C(11)-H(11)	120.1

C(10)-C(11)-H(11)	120.1
C(11)-C(12)-C(13)	120.7(2)
C(11)-C(12)-H(12)	119.7
C(13)-C(12)-H(12)	119.7
C(12)-C(13)-C(8)	120.1(2)
C(12)-C(13)-H(13)	119.9
C(8)-C(13)-H(13)	119.9

Symmetry transformations used to generate equivalent atoms:

#1 -x+1,-y+1,-z+1

Table 4. Anisotropic displacement parameters ($Å^2$x 10^3)for 6fms3_0m. The anisotropic displacement factor exponent takes the form: $-2\pi^2[h^2a^{*2}U^{11} + ... + 2 h k a^* b^* U^{12}]$

	U^{11} U^{22}	U^{33}	U^{23}	U^{13}	U^{12}
Rh	15(1) 12(1)	16(1)	1(1)	5(1)	-1(1)
C(1)	18(1) 19(1)	19(1)	2(1)	6(1)	-4(1)
O(1)	26(1) 19(1)	35(1)	2(1)	13(1)	3(1)
C(2)	18(1) 15(1)	22(1)	-2(1)	4(1)	0(1)
O(2)	30(1) 25(1)	28(1)	0(1)	15(1)	-6(1)
O(3)	20(1) 16(1)	18(1)	3(1)	7(1)	2(1)
O(4)	19(1) 16(1)	22(1)	2(1)	7(1)	2(1)
C(3)	23(1) 34(1)	51(2)	14(1)	13(1)	9(1)
C(4)	24(1) 18(1)	31(1)	3(1)	10(1)	6(1)
C(5)	16(1) 16(1)	19(1)	-1(1)	2(1)	0(1)
C(6)	21(1) 15(1)	21(1)	4(1)	4(1)	2(1)
C(7)	15(1) 16(1)	15(1)	1(1)	2(1)	-4(1)
C(8)	18(1) 16(1)	15(1)	-1(1)	4(1)	-4(1)
C(9)	21(1) 20(1)	18(1)	2(1)	5(1)	0(1)
C(10)	19(1) 25(1)	23(1)	-2(1)	7(1)	-1(1)
C(11)	25(1) 24(1)	21(1)	-1(1)	10(1)	-7(1)
C(12)	34(1) 26(1)	17(1)	7(1)	5(1)	0(1)
C(13)	21(1) 25(1)	19(1)	3(1)	2(1)	3(1)

Table 5. Hydrogen coordinates (x 10^4) and isotropic displacement parameters (Å^{2}x 10^3) for 6fms3_0m.

	x	y	z	U(eq)
H(3A)	60	8008	3300	53
H(3B)	-95	9327	4008	53
H(3C)	416	7477	4271	53
H(4A)	1836	9887	3530	29
H(4B)	2166	9472	4515	29
H(6)	3432	8850	2916	23
H(9)	6790	5531	2914	23
H(10)	8053	6101	1926	26
H(11)	7313	8049	834	27
H(12)	5336	9450	745	31
H(13)	4088	8930	1738	26

Table 6. Torsion angles [°] for 6fms3_0m.

C(2)-Rh-C(1)-O(1)	126(19)
O(4)-Rh-C(1)-O(1)	57(19)
O(3)-Rh-C(1)-O(1)	-52(19)
Rh#1-Rh-C(1)-O(1)	-138(19)
C(1)-Rh-C(2)-O(2)	-135(10)
O(4)-Rh-C(2)-O(2)	43(10)
O(3)-Rh-C(2)-O(2)	-54(11)
Rh#1-Rh-C(2)-O(2)	133(10)
C(1)-Rh-O(3)-C(7)	175.64(17)
C(2)-Rh-O(3)-C(7)	95(2)
O(4)-Rh-O(3)-C(7)	-1.73(17)
Rh#1-Rh-O(3)-C(7)	-91.90(16)
C(1)-Rh-O(4)-C(5)	-108.3(14)
C(2)-Rh-O(4)-C(5)	-177.57(18)
O(3)-Rh-O(4)-C(5)	0.37(17)
Rh#1-Rh-O(4)-C(5)	86.97(16)
Rh-O(4)-C(5)-C(6)	1.5(3)
Rh-O(4)-C(5)-C(4)	-177.31(14)
C(3)-C(4)-C(5)-O(4)	-51.8(3)
C(3)-C(4)-C(5)-C(6)	129.3(2)
O(4)-C(5)-C(6)-C(7)	-2.5(4)
C(4)-C(5)-C(6)-C(7)	176.2(2)
Rh-O(3)-C(7)-C(6)	1.4(3)
Rh-O(3)-C(7)-C(8)	-179.39(12)
C(5)-C(6)-C(7)-O(3)	0.9(4)
C(5)-C(6)-C(7)-C(8)	-178.3(2)
O(3)-C(7)-C(8)-C(9)	-20.5(3)
C(6)-C(7)-C(8)-C(9)	158.7(2)
O(3)-C(7)-C(8)-C(13)	157.1(2)
C(6)-C(7)-C(8)-C(13)	-23.6(3)
C(13)-C(8)-C(9)-C(10)	-0.4(3)
C(7)-C(8)-C(9)-C(10)	177.32(19)
C(8)-C(9)-C(10)-C(11)	-0.4(3)
C(9)-C(10)-C(11)-C(12)	0.6(3)
C(10)-C(11)-C(12)-C(13)	0.0(3)
C(11)-C(12)-C(13)-C(8)	-0.8(4)
C(9)-C(8)-C(13)-C(12)	1.0(3)
C(7)-C(8)-C(13)-C(12)	-176.6(2)

Symmetry transformations used to generate equivalent atoms:

#1 -x+1,-y+1,-z+1

B.2 [Rh(bab)(CO)$_2$]

Table 1. Crystal data and structure refinement for 5fjc2_0m.

Identification code	5fjc2_0m	
Empirical formula	C14 H13 O4 Rh	
Formula weight	348.15	
Temperature	273(2) K	
Wavelength	0.71073 Å	
Crystal system	Triclinic	
Space group	P -1	
Unit cell dimensions	a = 7.9342(3) Å	α= 111.416(2)°.
	b = 8.6907(4) Å	β= 95.249(2)°.
	c = 11.0334(5) Å	γ = 106.031(2)°.
Volume	664.81(5) Å^3	
Z	2	
Density (calculated)	1.739 Mg/m^3	
Absorption coefficient	1.290 mm^{-1}	
F(000)	348	
Crystal size	0.27 x 0.26 x 0.12 mm^3	
Theta range for data collection	2.61 to 28.36°.	
Index ranges	-10<=h<=7, -11<=k<=11, -13<=l<=14	
Reflections collected	8867	
Independent reflections	3299 [R(int) = 0.0251]	
Completeness to theta = 28.36°	99.0 %	
Absorption correction	Semi-empirical from equivalents	
Max. and min. transmission	0.8605 and 0.7220	
Refinement method	Full-matrix least-squares on F^2	
Data / restraints / parameters	3299 / 0 / 173	
Goodness-of-fit on F^2	1.062	
Final R indices [I>2sigma(I)]	R1 = 0.0211, wR2 = 0.0462	
R indices (all data)	R1 = 0.0244, wR2 = 0.0478	
Largest diff. peak and hole	0.629 and -0.544 e.Å^{-3}	

Table 2. Atomic coordinates (x 10^4) and equivalent isotropic displacement parameters ($Å^2$x 10^3) for 5fjc2_0m. U(eq) is defined as one third of the trace of the orthogonalized U^{ij} tensor.

	x	y	z	U(eq)
Rh	3487(1)	8210(1)	-257(1)	13(1)
C(1)	2158(2)	8094(2)	-1776(2)	16(1)
O(1)	1377(2)	8053(2)	-2705(1)	22(1)
C(2)	2078(2)	9305(2)	735(2)	17(1)
O(2)	1201(2)	9964(2)	1349(1)	24(1)
O(3)	4930(2)	6888(2)	-1383(1)	15(1)
O(4)	4901(2)	8325(2)	1421(1)	15(1)
C(3)	7251(3)	9003(3)	5291(2)	23(1)
C(4)	6309(3)	8910(3)	3995(2)	16(1)
C(5)	7096(2)	8011(2)	2836(2)	16(1)
C(6)	6220(2)	7775(2)	1477(2)	13(1)
C(7)	6926(2)	6970(2)	391(2)	16(1)
C(8)	6261(2)	6532(2)	-939(2)	14(1)
C(9)	7123(2)	5582(2)	-1983(2)	14(1)
C(10)	6774(3)	5560(2)	-3254(2)	18(1)
C(11)	7547(3)	4682(3)	-4247(2)	20(1)
C(12)	8668(3)	3812(3)	-3986(2)	21(1)
C(13)	8996(3)	3812(3)	-2736(2)	21(1)
C(14)	8237(2)	4694(2)	-1736(2)	17(1)

Table 3. Bond lengths [Å] and angles [°] for 5fjc2_0m.

Rh-C(2)	1.8446(19)
Rh-C(1)	1.851(2)
Rh-O(4)	2.0295(13)
Rh-O(3)	2.0300(12)
Rh-Rh#1	3.1786(3)
C(1)-O(1)	1.132(2)
C(2)-O(2)	1.138(2)
O(3)-C(8)	1.284(2)
O(4)-C(6)	1.270(2)
C(3)-C(4)	1.516(3)
C(3)-H(3A)	0.9600
C(3)-H(3B)	0.9600
C(3)-H(3C)	0.9600
C(4)-C(5)	1.524(2)
C(4)-H(4A)	0.9700
C(4)-H(4B)	0.9700
C(5)-C(6)	1.509(2)
C(5)-H(5A)	0.9700
C(5)-H(5B)	0.9700
C(6)-C(7)	1.402(2)
C(7)-C(8)	1.384(3)
C(7)-H(7)	0.9300
C(8)-C(9)	1.496(2)
C(9)-C(14)	1.392(3)
C(9)-C(10)	1.397(3)
C(10)-C(11)	1.389(3)
C(10)-H(10)	0.9300
C(11)-C(12)	1.388(3)
C(11)-H(11)	0.9300
C(12)-C(13)	1.380(3)
C(12)-H(12)	0.9300
C(13)-C(14)	1.388(3)
C(13)-H(13)	0.9300
C(14)-H(14)	0.9300

C(2)-Rh-C(1)	89.14(8)
C(2)-Rh-O(4)	90.04(7)
C(1)-Rh-O(4)	178.91(6)

C(2)-Rh-O(3)	177.05(7)
C(1)-Rh-O(3)	90.06(6)
O(4)-Rh-O(3)	90.72(5)
C(2)-Rh-Rh#1	93.88(6)
C(1)-Rh-Rh#1	94.62(5)
O(4)-Rh-Rh#1	86.16(4)
O(3)-Rh-Rh#1	89.02(4)
O(1)-C(1)-Rh	178.44(16)
O(2)-C(2)-Rh	179.28(17)
C(8)-O(3)-Rh	125.73(11)
C(6)-O(4)-Rh	125.50(11)
C(4)-C(3)-H(3A)	109.5
C(4)-C(3)-H(3B)	109.5
H(3A)-C(3)-H(3B)	109.5
C(4)-C(3)-H(3C)	109.5
H(3A)-C(3)-H(3C)	109.5
H(3B)-C(3)-H(3C)	109.5
C(3)-C(4)-C(5)	110.98(15)
C(3)-C(4)-H(4A)	109.4
C(5)-C(4)-H(4A)	109.4
C(3)-C(4)-H(4B)	109.4
C(5)-C(4)-H(4B)	109.4
H(4A)-C(4)-H(4B)	108.0
C(6)-C(5)-C(4)	116.05(15)
C(6)-C(5)-H(5A)	108.3
C(4)-C(5)-H(5A)	108.3
C(6)-C(5)-H(5B)	108.3
C(4)-C(5)-H(5B)	108.3
H(5A)-C(5)-H(5B)	107.4
O(4)-C(6)-C(7)	125.76(17)
O(4)-C(6)-C(5)	116.78(15)
C(7)-C(6)-C(5)	117.46(16)
C(8)-C(7)-C(6)	126.80(18)
C(8)-C(7)-H(7)	116.6
C(6)-C(7)-H(7)	116.6
O(3)-C(8)-C(7)	125.22(16)
O(3)-C(8)-C(9)	114.95(16)
C(7)-C(8)-C(9)	119.82(16)
C(14)-C(9)-C(10)	118.92(17)
C(14)-C(9)-C(8)	122.17(17)

C(10)-C(9)-C(8)	118.91(17)
C(11)-C(10)-C(9)	120.26(18)
C(11)-C(10)-H(10)	119.9
C(9)-C(10)-H(10)	119.9
C(12)-C(11)-C(10)	120.31(18)
C(12)-C(11)-H(11)	119.8
C(10)-C(11)-H(11)	119.8
C(13)-C(12)-C(11)	119.55(17)
C(13)-C(12)-H(12)	120.2
C(11)-C(12)-H(12)	120.2
C(12)-C(13)-C(14)	120.53(19)
C(12)-C(13)-H(13)	119.7
C(14)-C(13)-H(13)	119.7
C(13)-C(14)-C(9)	120.43(18)
C(13)-C(14)-H(14)	119.8
C(9)-C(14)-H(14)	119.8

Symmetry transformations used to generate equivalent atoms:

#1 -x+1,-y+2,-z

Table 4. Anisotropic displacement parameters ($Å^2 x\ 10^3$)for 5fjc2_0m. The anisotropic displacement factor exponent takes the form: $-2\pi^2[\ h^2 a^{*2} U^{11} + ... + 2\ h\ k\ a^*\ b^*\ U^{12}\ ]$

	U^{11} U^{22}	U^{33}	U^{23}	U^{13}	U^{12}
Rh	12(1) 14(1)	14(1)	5(1)	3(1)	6(1)
C(1)	15(1) 12(1)	19(1)	4(1)	6(1)	5(1)
O(1)	23(1) 24(1)	17(1)	9(1)	0(1)	8(1)
C(2)	15(1) 19(1)	15(1)	8(1)	-1(1)	3(1)
O(2)	22(1) 29(1)	24(1)	9(1)	10(1)	15(1)
O(3)	16(1) 17(1)	14(1)	6(1)	4(1)	9(1)
O(4)	14(1) 17(1)	14(1)	6(1)	3(1)	7(1)
C(3)	26(1) 29(1)	17(1)	9(1)	5(1)	14(1)
C(4)	17(1) 17(1)	15(1)	6(1)	4(1)	7(1)
C(5)	15(1) 17(1)	16(1)	6(1)	2(1)	7(1)
C(6)	12(1) 10(1)	15(1)	5(1)	2(1)	1(1)
C(7)	14(1) 17(1)	18(1)	6(1)	3(1)	7(1)
C(8)	13(1) 10(1)	17(1)	5(1)	4(1)	3(1)
C(9)	14(1) 12(1)	15(1)	3(1)	3(1)	3(1)
C(10)	19(1) 16(1)	19(1)	7(1)	5(1)	7(1)
C(11)	23(1) 20(1)	16(1)	6(1)	6(1)	6(1)
C(12)	20(1) 18(1)	20(1)	2(1)	8(1)	6(1)
C(13)	19(1) 17(1)	25(1)	5(1)	4(1)	10(1)
C(14)	17(1) 16(1)	17(1)	5(1)	2(1)	6(1)

Table 5. Hydrogen coordinates (x 10^4) and isotropic displacement parameters ($Å^2$x 10^3) for 5fjc2_0m.

	x	y	z	U(eq)
H(3A)	7105	7838	5222	35
H(3B)	6738	9579	6006	35
H(3C)	8506	9651	5467	35
H(4A)	6435	10087	4073	19
H(4B)	5039	8266	3823	19
H(5A)	8358	8687	3016	19
H(5B)	7023	6865	2807	19
H(7)	7947	6703	585	19
H(10)	6020	6136	-3437	22
H(11)	7314	4677	-5090	24
H(12)	9194	3234	-4649	25
H(13)	9732	3215	-2562	25
H(14)	8474	4691	-896	21

Table 6. Torsion angles [°] for 5fjc2_0m.

C(2)-Rh-C(1)-O(1)	106(6)
O(4)-Rh-C(1)-O(1)	147(5)
O(3)-Rh-C(1)-O(1)	-77(6)
Rh#1-Rh-C(1)-O(1)	12(6)
C(1)-Rh-C(2)-O(2)	109(15)
O(4)-Rh-C(2)-O(2)	-71(15)
O(3)-Rh-C(2)-O(2)	34(16)
Rh#1-Rh-C(2)-O(2)	-157(15)
C(2)-Rh-O(3)-C(8)	-109.1(13)
C(1)-Rh-O(3)-C(8)	176.75(15)
O(4)-Rh-O(3)-C(8)	-4.02(14)
Rh#1-Rh-O(3)-C(8)	82.13(13)
C(2)-Rh-O(4)-C(6)	-178.94(14)
C(1)-Rh-O(4)-C(6)	140(3)
O(3)-Rh-O(4)-C(6)	3.91(14)
Rh#1-Rh-O(4)-C(6)	-85.05(13)
C(3)-C(4)-C(5)-C(6)	177.71(16)
Rh-O(4)-C(6)-C(7)	-0.9(3)
Rh-O(4)-C(6)-C(5)	179.23(11)
C(4)-C(5)-C(6)-O(4)	-0.8(2)
C(4)-C(5)-C(6)-C(7)	179.26(16)
O(4)-C(6)-C(7)-C(8)	-4.2(3)
C(5)-C(6)-C(7)-C(8)	175.72(17)
Rh-O(3)-C(8)-C(7)	1.0(3)
Rh-O(3)-C(8)-C(9)	-178.40(10)
C(6)-C(7)-C(8)-O(3)	4.1(3)
C(6)-C(7)-C(8)-C(9)	-176.51(17)
O(3)-C(8)-C(9)-C(14)	-162.49(17)
C(7)-C(8)-C(9)-C(14)	18.0(3)
O(3)-C(8)-C(9)-C(10)	16.4(2)
C(7)-C(8)-C(9)-C(10)	-163.11(17)
C(14)-C(9)-C(10)-C(11)	-0.8(3)
C(8)-C(9)-C(10)-C(11)	-179.69(17)
C(9)-C(10)-C(11)-C(12)	0.3(3)
C(10)-C(11)-C(12)-C(13)	0.6(3)
C(11)-C(12)-C(13)-C(14)	-1.0(3)
C(12)-C(13)-C(14)-C(9)	0.5(3)
C(10)-C(9)-C(14)-C(13)	0.4(3)

C(8)-C(9)-C(14)-C(13)	179.30(17)

Symmetry transformations used to generate equivalent atoms:

#1 -x+1,-y+2,-z

B.3 [Rh(bap)(CO)(PPh_3)]

Table 1. Crystal data and structure refinement for 5fjc1_0m.

Identification code	5fjc1_0m	
Empirical formula	C30 H26 O3 P Rh	
Formula weight	568.39	
Temperature	293(2) K	
Wavelength	0.71073 Å	
Crystal system	Triclinic	
Space group	P-1	
Unit cell dimensions	a = 8.9967(3) Å	α= 90.051(2)°.
	b = 15.7725(5) Å	β= 94.536(2)°.
	c = 19.3044(7) Å	γ = 104.963(2)°.
Volume	2637.48(15) $Å^3$	
Z	4	
Density (calculated)	1.431 Mg/m^3	
Absorption coefficient	0.737 mm^{-1}	
F(000)	1160	
Crystal size	0.23 x 0.12 x 0.05 mm^3	
Theta range for data collection	1.06 to 28.37°.	
Index ranges	-12<=h<=12, -21<=k<=21, -25<=l<=25	
Reflections collected	64974	
Independent reflections	13157 [R(int) = 0.0408]	
Completeness to theta = 28.37°	99.8 %	
Absorption correction	Semi-empirical from equivalents	
Max. and min. transmission	0.9641 and 0.8488	
Refinement method	Full-matrix least-squares on F^2	
Data / restraints / parameters	13157 / 79 / 651	
Goodness-of-fit on F^2	1.060	
Final R indices [I>2sigma(I)]	R1 = 0.0436, wR2 = 0.1055	
R indices (all data)	R1 = 0.0676, wR2 = 0.1192	
Largest diff. peak and hole	1.880 and -0.788 $e.Å^{-3}$	

Table 2. Atomic coordinates (x 10^4) and equivalent isotropic displacement parameters ($Å^2$x 10^3) for 5fjc1_0m. U(eq) is defined as one third of the trace of the orthogonalized U^{ij} tensor.

	x	y	z	U(eq)
Rh(1)	9437(1)	3284(1)	779(1)	42(1)
P(1)	7659(1)	2023(1)	511(1)	41(1)
O(1)	11062(3)	4445(2)	1044(1)	55(1)
O(2)	10060(3)	3401(2)	-212(1)	46(1)
O(3)	8616(6)	3108(3)	2220(2)	111(2)
C(1A)	14464(9)	5698(7)	1201(8)	95(3)
C(1B)	14544(17)	6000(20)	830(20)	102(6)
C(2)	12929(5)	5779(3)	951(3)	76(1)
C(3)	11897(4)	4936(2)	631(2)	54(1)
C(4)	11953(5)	4760(3)	-71(2)	55(1)
C(5)	11086(4)	4035(2)	-454(2)	47(1)
C(6)	11356(5)	3929(3)	-1193(2)	56(1)
C(7)	11914(6)	4647(4)	-1607(3)	77(1)
C(8)	12207(7)	4525(5)	-2292(3)	97(2)
C(9)	11948(8)	3701(6)	-2564(3)	111(2)
C(10)	11401(8)	2993(5)	-2176(3)	112(2)
C(11)	11117(6)	3099(4)	-1477(3)	80(1)
C(12)	8903(6)	3168(3)	1658(2)	64(1)
C(13)	5668(4)	2117(2)	395(2)	50(1)
C(14)	5284(5)	2790(3)	736(2)	61(1)
C(15)	3754(6)	2859(4)	653(3)	83(2)
C(16)	2667(6)	2271(4)	241(3)	87(2)
C(17)	3044(6)	1610(4)	-100(3)	91(2)
C(18)	4540(5)	1529(3)	-22(3)	70(1)
C(19)	7615(4)	1169(2)	1150(2)	44(1)
C(20)	6310(5)	490(3)	1232(2)	57(1)
C(21)	6362(6)	-163(3)	1703(3)	71(1)
C(22)	7702(6)	-150(3)	2098(2)	71(1)
C(23)	8992(5)	515(3)	2025(2)	65(1)
C(24)	8959(5)	1166(3)	1555(2)	54(1)
C(25)	7887(4)	1491(2)	-303(2)	43(1)
C(26)	8425(5)	750(3)	-305(2)	65(1)
C(27)	8636(7)	387(4)	-934(3)	91(2)
C(28)	8314(6)	739(3)	-1554(3)	74(1)
C(29)	7781(6)	1474(3)	-1549(2)	71(1)

C(30)	7565(5)	1848(3)	-933(2)	63(1)
Rh(2)	3960(1)	8252(1)	3864(1)	47(1)
P(2)	4428(1)	7021(1)	4296(1)	40(1)
O(4)	3569(3)	9394(2)	3456(1)	58(1)
O(6)	5100(5)	7805(3)	2555(2)	94(1)
O(5)	3236(3)	8587(2)	4771(2)	58(1)
C(31A)	1657(15)	9928(9)	5855(5)	119(4)
C(31B)	1160(20)	9170(20)	5896(10)	133(6)
C(32)	2638(8)	9377(4)	5681(3)	98(2)
C(33)	2951(5)	9314(3)	4935(2)	65(1)
C(34)	2959(5)	9993(3)	4484(2)	63(1)
C(35)	3219(4)	10010(2)	3791(2)	50(1)
C(36)	3142(5)	10790(2)	3358(2)	54(1)
C(37)	3878(6)	10910(3)	2754(2)	68(1)
C(38)	3797(7)	11604(3)	2333(3)	85(2)
C(39)	2986(8)	12192(3)	2519(3)	88(2)
C(40)	2289(7)	12089(3)	3117(3)	84(2)
C(41)	2363(6)	11393(3)	3545(3)	66(1)
C(42)	4639(5)	7978(3)	3069(3)	64(1)
C(43)	6462(4)	7097(2)	4551(2)	45(1)
C(44)	6915(5)	6605(3)	5077(2)	60(1)
C(45)	8465(5)	6657(3)	5244(3)	72(1)
C(46)	9564(5)	7190(3)	4894(3)	76(1)
C(47)	9144(5)	7683(4)	4368(3)	85(2)
C(48)	7585(5)	7642(3)	4196(3)	68(1)
C(49)	3799(4)	6063(2)	3709(2)	41(1)
C(50)	2439(5)	5973(3)	3282(2)	56(1)
C(51)	1874(5)	5241(3)	2855(3)	70(1)
C(52)	2659(6)	4600(3)	2841(3)	72(1)
C(53)	3993(6)	4678(3)	3256(2)	66(1)
C(54)	4565(4)	5410(2)	3692(2)	50(1)
C(55)	3490(4)	6624(2)	5081(2)	42(1)
C(56)	3799(5)	7169(3)	5675(2)	55(1)
C(57)	3048(6)	6906(3)	6268(2)	66(1)
C(58)	1994(5)	6105(3)	6275(2)	64(1)
C(59)	1697(5)	5556(3)	5700(2)	61(1)
C(60)	2435(4)	5818(2)	5108(2)	49(1)

Table 3. Bond lengths [Å] and angles [°] for 5fjc1_0m.

Rh(1)-C(12)	1.797(4)
Rh(1)-O(2)	2.032(2)
Rh(1)-O(1)	2.060(3)
Rh(1)-P(1)	2.2376(9)
P(1)-C(19)	1.823(4)
P(1)-C(25)	1.830(4)
P(1)-C(13)	1.831(4)
O(1)-C(3)	1.263(5)
O(2)-C(5)	1.289(4)
O(3)-C(12)	1.133(5)
C(1A)-C(2)	1.463(8)
C(1A)-H(1A1)	0.9600
C(1A)-H(1A2)	0.9600
C(1A)-H(1A3)	0.9600
C(1A)-H(2D)	1.5115
C(1B)-C(2)	1.443(13)
C(1B)-H(1B1)	0.9600
C(1B)-H(1B2)	0.9600
C(1B)-H(1B3)	0.9600
C(2)-C(3)	1.511(5)
C(2)-H(2A)	0.9700
C(2)-H(2B)	0.9700
C(2)-H(2C)	0.9703
C(2)-H(2D)	0.9695
C(3)-C(4)	1.390(6)
C(4)-C(5)	1.382(6)
C(4)-H(4)	0.9300
C(5)-C(6)	1.482(5)
C(6)-C(11)	1.376(7)
C(6)-C(7)	1.395(6)
C(7)-C(8)	1.391(7)
C(7)-H(7)	0.9300
C(8)-C(9)	1.357(9)
C(8)-H(8)	0.9300
C(9)-C(10)	1.352(9)
C(9)-H(9)	0.9300
C(10)-C(11)	1.411(7)
C(10)-H(10)	0.9300

C(11)-H(11)	0.9300
C(13)-C(14)	1.380(5)
C(13)-C(18)	1.386(6)
C(14)-C(15)	1.405(6)
C(14)-H(14)	0.9300
C(15)-C(16)	1.363(8)
C(15)-H(15)	0.9300
C(16)-C(17)	1.361(8)
C(16)-H(16)	0.9300
C(17)-C(18)	1.382(6)
C(17)-H(17)	0.9300
C(18)-H(18)	0.9300
C(19)-C(24)	1.388(5)
C(19)-C(20)	1.390(5)
C(20)-C(21)	1.381(6)
C(20)-H(20)	0.9300
C(21)-C(22)	1.371(7)
C(21)-H(21)	0.9300
C(22)-C(23)	1.365(7)
C(22)-H(22)	0.9300
C(23)-C(24)	1.376(6)
C(23)-H(23)	0.9300
C(24)-H(24)	0.9300
C(25)-C(26)	1.376(5)
C(25)-C(30)	1.382(6)
C(26)-C(27)	1.389(6)
C(26)-H(26)	0.9300
C(27)-C(28)	1.363(7)
C(27)-H(27)	0.9300
C(28)-C(29)	1.365(7)
C(28)-H(28)	0.9300
C(29)-C(30)	1.376(6)
C(29)-H(29)	0.9300
C(30)-H(30)	0.9300
Rh(2)-C(42)	1.788(5)
Rh(2)-O(5)	2.032(3)
Rh(2)-O(4)	2.067(3)
Rh(2)-P(2)	2.2387(9)
P(2)-C(55)	1.826(4)
P(2)-C(49)	1.827(4)

P(2)-C(43)	1.830(3)
O(4)-C(35)	1.285(4)
O(6)-C(42)	1.164(6)
O(5)-C(33)	1.282(5)
C(31A)-C(32)	1.445(9)
C(31A)-H(31A)	0.9600
C(31A)-H(31B)	0.9600
C(31A)-H(31C)	0.9600
C(31A)-H(32D)	1.3024
C(31B)-C(32)	1.379(12)
C(31B)-H(31D)	0.9600
C(31B)-H(31E)	0.9600
C(31B)-H(31F)	0.9600
C(32)-C(33)	1.498(6)
C(32)-H(32A)	0.9700
C(32)-H(32B)	0.9700
C(32)-H(32C)	0.9701
C(32)-H(32D)	0.9692
C(33)-C(34)	1.380(6)
C(34)-C(35)	1.376(6)
C(34)-H(34)	0.9300
C(35)-C(36)	1.501(5)
C(36)-C(37)	1.376(6)
C(36)-C(41)	1.383(6)
C(37)-C(38)	1.376(6)
C(37)-H(37)	0.9300
C(38)-C(39)	1.382(7)
C(38)-H(38)	0.9300
C(39)-C(40)	1.348(8)
C(39)-H(39)	0.9300
C(40)-C(41)	1.387(6)
C(40)-H(40)	0.9300
C(41)-H(41)	0.9300
C(43)-C(48)	1.375(6)
C(43)-C(44)	1.378(5)
C(44)-C(45)	1.387(6)
C(44)-H(44)	0.9300
C(45)-C(46)	1.348(7)
C(45)-H(45)	0.9300
C(46)-C(47)	1.369(7)

C(46)-H(46)	0.9300
C(47)-C(48)	1.400(6)
C(47)-H(47)	0.9300
C(48)-H(48)	0.9300
C(49)-C(54)	1.381(5)
C(49)-C(50)	1.395(5)
C(50)-C(51)	1.378(6)
C(50)-H(50)	0.9300
C(51)-C(52)	1.375(7)
C(51)-H(51)	0.9300
C(52)-C(53)	1.368(6)
C(52)-H(52)	0.9300
C(53)-C(54)	1.389(6)
C(53)-H(53)	0.9300
C(54)-H(54)	0.9300
C(55)-C(60)	1.380(5)
C(55)-C(56)	1.398(5)
C(56)-C(57)	1.386(6)
C(56)-H(56)	0.9300
C(57)-C(58)	1.370(7)
C(57)-H(57)	0.9300
C(58)-C(59)	1.373(6)
C(58)-H(58)	0.9300
C(59)-C(60)	1.378(5)
C(59)-H(59)	0.9300
C(60)-H(60)	0.9300

C(12)-Rh(1)-O(2)	179.08(17)
C(12)-Rh(1)-O(1)	90.84(15)
O(2)-Rh(1)-O(1)	89.39(10)
C(12)-Rh(1)-P(1)	88.15(14)
O(2)-Rh(1)-P(1)	91.62(7)
O(1)-Rh(1)-P(1)	178.99(8)
C(19)-P(1)-C(25)	103.44(16)
C(19)-P(1)-C(13)	104.77(17)
C(25)-P(1)-C(13)	103.01(17)
C(19)-P(1)-Rh(1)	114.39(12)
C(25)-P(1)-Rh(1)	114.86(12)
C(13)-P(1)-Rh(1)	114.93(12)
C(3)-O(1)-Rh(1)	125.8(3)

C(5)-O(2)-Rh(1)	126.8(2)
C(2)-C(1A)-H(1A1)	109.5
C(2)-C(1A)-H(1A2)	109.5
H(1A1)-C(1A)-H(1A2)	109.5
C(2)-C(1A)-H(1A3)	109.5
H(1A1)-C(1A)-H(1A3)	109.5
H(1A2)-C(1A)-H(1A3)	109.5
C(2)-C(1A)-H(2D)	38.0
H(1A1)-C(1A)-H(2D)	96.5
H(1A2)-C(1A)-H(2D)	145.4
H(1A3)-C(1A)-H(2D)	81.5
C(2)-C(1B)-H(1B1)	109.5
C(2)-C(1B)-H(1B2)	109.5
H(1B1)-C(1B)-H(1B2)	109.5
C(2)-C(1B)-H(1B3)	109.5
H(1B1)-C(1B)-H(1B3)	109.5
H(1B2)-C(1B)-H(1B3)	109.5
C(1B)-C(2)-C(1A)	34.4(14)
C(1B)-C(2)-C(3)	118.2(10)
C(1A)-C(2)-C(3)	113.0(5)
C(1B)-C(2)-H(2A)	75.6
C(1A)-C(2)-H(2A)	109.0
C(3)-C(2)-H(2A)	109.0
C(1B)-C(2)-H(2B)	128.7
C(1A)-C(2)-H(2B)	109.0
C(3)-C(2)-H(2B)	109.0
H(2A)-C(2)-H(2B)	107.8
C(1B)-C(2)-H(2C)	110.1
C(1A)-C(2)-H(2C)	135.8
C(3)-C(2)-H(2C)	108.3
H(2A)-C(2)-H(2C)	40.3
H(2B)-C(2)-H(2C)	70.2
C(1B)-C(2)-H(2D)	103.7
C(1A)-C(2)-H(2D)	73.7
C(3)-C(2)-H(2D)	108.6
H(2A)-C(2)-H(2D)	137.1
H(2B)-C(2)-H(2D)	39.3
H(2C)-C(2)-H(2D)	107.4
O(1)-C(3)-C(4)	126.0(4)
O(1)-C(3)-C(2)	115.2(4)

C(4)-C(3)-C(2)	118.8(4)
C(5)-C(4)-C(3)	127.0(4)
C(5)-C(4)-H(4)	116.5
C(3)-C(4)-H(4)	116.5
O(2)-C(5)-C(4)	124.9(4)
O(2)-C(5)-C(6)	115.2(4)
C(4)-C(5)-C(6)	119.8(4)
C(11)-C(6)-C(7)	118.3(4)
C(11)-C(6)-C(5)	119.5(4)
C(7)-C(6)-C(5)	122.1(4)
C(8)-C(7)-C(6)	120.7(6)
C(8)-C(7)-H(7)	119.7
C(6)-C(7)-H(7)	119.7
C(9)-C(8)-C(7)	120.1(6)
C(9)-C(8)-H(8)	120.0
C(7)-C(8)-H(8)	120.0
C(10)-C(9)-C(8)	120.6(6)
C(10)-C(9)-H(9)	119.7
C(8)-C(9)-H(9)	119.7
C(9)-C(10)-C(11)	120.5(6)
C(9)-C(10)-H(10)	119.8
C(11)-C(10)-H(10)	119.8
C(6)-C(11)-C(10)	119.9(5)
C(6)-C(11)-H(11)	120.1
C(10)-C(11)-H(11)	120.1
O(3)-C(12)-Rh(1)	177.7(5)
C(14)-C(13)-C(18)	119.3(4)
C(14)-C(13)-P(1)	118.9(3)
C(18)-C(13)-P(1)	121.8(3)
C(13)-C(14)-C(15)	119.0(5)
C(13)-C(14)-H(14)	120.5
C(15)-C(14)-H(14)	120.5
C(16)-C(15)-C(14)	120.5(5)
C(16)-C(15)-H(15)	119.8
C(14)-C(15)-H(15)	119.8
C(17)-C(16)-C(15)	120.7(4)
C(17)-C(16)-H(16)	119.6
C(15)-C(16)-H(16)	119.6
C(16)-C(17)-C(18)	119.6(5)
C(16)-C(17)-H(17)	120.2

C(18)-C(17)-H(17)	120.2
C(17)-C(18)-C(13)	120.9(5)
C(17)-C(18)-H(18)	119.5
C(13)-C(18)-H(18)	119.5
C(24)-C(19)-C(20)	117.8(4)
C(24)-C(19)-P(1)	119.0(3)
C(20)-C(19)-P(1)	123.1(3)
C(21)-C(20)-C(19)	120.7(4)
C(21)-C(20)-H(20)	119.7
C(19)-C(20)-H(20)	119.7
C(22)-C(21)-C(20)	120.5(4)
C(22)-C(21)-H(21)	119.8
C(20)-C(21)-H(21)	119.8
C(23)-C(22)-C(21)	119.5(4)
C(23)-C(22)-H(22)	120.2
C(21)-C(22)-H(22)	120.2
C(22)-C(23)-C(24)	120.6(4)
C(22)-C(23)-H(23)	119.7
C(24)-C(23)-H(23)	119.7
C(23)-C(24)-C(19)	121.0(4)
C(23)-C(24)-H(24)	119.5
C(19)-C(24)-H(24)	119.5
C(26)-C(25)-C(30)	118.4(4)
C(26)-C(25)-P(1)	121.4(3)
C(30)-C(25)-P(1)	120.1(3)
C(25)-C(26)-C(27)	119.5(4)
C(25)-C(26)-H(26)	120.2
C(27)-C(26)-H(26)	120.2
C(28)-C(27)-C(26)	122.0(5)
C(28)-C(27)-H(27)	119.0
C(26)-C(27)-H(27)	119.0
C(27)-C(28)-C(29)	118.3(4)
C(27)-C(28)-H(28)	120.9
C(29)-C(28)-H(28)	120.9
C(28)-C(29)-C(30)	120.9(4)
C(28)-C(29)-H(29)	119.6
C(30)-C(29)-H(29)	119.6
C(29)-C(30)-C(25)	120.9(4)
C(29)-C(30)-H(30)	119.5
C(25)-C(30)-H(30)	119.5

C(42)-Rh(2)-O(5)	178.59(17)
C(42)-Rh(2)-O(4)	91.68(14)
O(5)-Rh(2)-O(4)	87.84(11)
C(42)-Rh(2)-P(2)	87.47(12)
O(5)-Rh(2)-P(2)	92.99(8)
O(4)-Rh(2)-P(2)	178.85(9)
C(55)-P(2)-C(49)	102.50(16)
C(55)-P(2)-C(43)	102.72(16)
C(49)-P(2)-C(43)	104.87(16)
C(55)-P(2)-Rh(2)	115.77(11)
C(49)-P(2)-Rh(2)	114.64(11)
C(43)-P(2)-Rh(2)	114.75(12)
C(35)-O(4)-Rh(2)	126.6(2)
C(33)-O(5)-Rh(2)	128.0(3)
C(32)-C(31A)-H(31A)	109.5
C(32)-C(31A)-H(31B)	109.5
H(31A)-C(31A)-H(31B)	109.5
C(32)-C(31A)-H(31C)	109.5
H(31A)-C(31A)-H(31C)	109.5
H(31B)-C(31A)-H(31C)	109.5
C(32)-C(31A)-H(32D)	40.9
H(31A)-C(31A)-H(32D)	99.6
H(31B)-C(31A)-H(32D)	145.5
H(31C)-C(31A)-H(32D)	76.4
C(32)-C(31B)-H(31D)	109.5
C(32)-C(31B)-H(31E)	109.5
H(31D)-C(31B)-H(31E)	109.5
C(32)-C(31B)-H(31F)	109.5
H(31D)-C(31B)-H(31F)	109.5
H(31E)-C(31B)-H(31F)	109.5
C(31B)-C(32)-C(31A)	48.6(11)
C(31B)-C(32)-C(33)	122.5(10)
C(31A)-C(32)-C(33)	117.8(6)
C(31B)-C(32)-H(32A)	60.3
C(31A)-C(32)-H(32A)	107.9
C(33)-C(32)-H(32A)	107.9
C(31B)-C(32)-H(32B)	129.6
C(31A)-C(32)-H(32B)	107.9
C(33)-C(32)-H(32B)	107.9
H(32A)-C(32)-H(32B)	107.2

C(31B)-C(32)-H(32C)	104.9
C(31A)-C(32)-H(32C)	134.2
C(33)-C(32)-H(32C)	108.0
H(32A)-C(32)-H(32C)	53.2
H(32B)-C(32)-H(32C)	56.2
C(31B)-C(32)-H(32D)	106.4
C(31A)-C(32)-H(32D)	61.6
C(33)-C(32)-H(32D)	107.1
H(32A)-C(32)-H(32D)	144.0
H(32B)-C(32)-H(32D)	53.1
H(32C)-C(32)-H(32D)	107.2
O(5)-C(33)-C(34)	124.6(4)
O(5)-C(33)-C(32)	113.5(4)
C(34)-C(33)-C(32)	121.9(4)
C(35)-C(34)-C(33)	127.2(4)
C(35)-C(34)-H(34)	116.4
C(33)-C(34)-H(34)	116.4
O(4)-C(35)-C(34)	125.0(4)
O(4)-C(35)-C(36)	113.8(3)
C(34)-C(35)-C(36)	121.2(4)
C(37)-C(36)-C(41)	118.8(4)
C(37)-C(36)-C(35)	118.8(4)
C(41)-C(36)-C(35)	122.4(4)
C(36)-C(37)-C(38)	120.5(5)
C(36)-C(37)-H(37)	119.8
C(38)-C(37)-H(37)	119.8
C(37)-C(38)-C(39)	120.2(5)
C(37)-C(38)-H(38)	119.9
C(39)-C(38)-H(38)	119.9
C(40)-C(39)-C(38)	119.7(5)
C(40)-C(39)-H(39)	120.1
C(38)-C(39)-H(39)	120.1
C(39)-C(40)-C(41)	120.6(5)
C(39)-C(40)-H(40)	119.7
C(41)-C(40)-H(40)	119.7
C(36)-C(41)-C(40)	120.2(5)
C(36)-C(41)-H(41)	119.9
C(40)-C(41)-H(41)	119.9
O(6)-C(42)-Rh(2)	179.1(5)
C(48)-C(43)-C(44)	118.3(3)

C(48)-C(43)-P(2)	119.4(3)
C(44)-C(43)-P(2)	122.2(3)
C(43)-C(44)-C(45)	120.8(4)
C(43)-C(44)-H(44)	119.6
C(45)-C(44)-H(44)	119.6
C(46)-C(45)-C(44)	120.7(5)
C(46)-C(45)-H(45)	119.6
C(44)-C(45)-H(45)	119.6
C(45)-C(46)-C(47)	119.6(4)
C(45)-C(46)-H(46)	120.2
C(47)-C(46)-H(46)	120.2
C(46)-C(47)-C(48)	120.4(5)
C(46)-C(47)-H(47)	119.8
C(48)-C(47)-H(47)	119.8
C(43)-C(48)-C(47)	120.1(4)
C(43)-C(48)-H(48)	119.9
C(47)-C(48)-H(48)	119.9
C(54)-C(49)-C(50)	118.8(3)
C(54)-C(49)-P(2)	123.2(3)
C(50)-C(49)-P(2)	118.0(3)
C(51)-C(50)-C(49)	120.3(4)
C(51)-C(50)-H(50)	119.9
C(49)-C(50)-H(50)	119.9
C(52)-C(51)-C(50)	120.2(4)
C(52)-C(51)-H(51)	119.9
C(50)-C(51)-H(51)	119.9
C(53)-C(52)-C(51)	120.4(4)
C(53)-C(52)-H(52)	119.8
C(51)-C(52)-H(52)	119.8
C(52)-C(53)-C(54)	119.9(4)
C(52)-C(53)-H(53)	120.1
C(54)-C(53)-H(53)	120.1
C(49)-C(54)-C(53)	120.6(4)
C(49)-C(54)-H(54)	119.7
C(53)-C(54)-H(54)	119.7
C(60)-C(55)-C(56)	118.2(4)
C(60)-C(55)-P(2)	122.7(3)
C(56)-C(55)-P(2)	119.1(3)
C(57)-C(56)-C(55)	120.5(4)
C(57)-C(56)-H(56)	119.8

C(55)-C(56)-H(56)	119.8
C(58)-C(57)-C(56)	119.9(4)
C(58)-C(57)-H(57)	120.1
C(56)-C(57)-H(57)	120.1
C(57)-C(58)-C(59)	120.3(4)
C(57)-C(58)-H(58)	119.8
C(59)-C(58)-H(58)	119.8
C(58)-C(59)-C(60)	120.0(4)
C(58)-C(59)-H(59)	120.0
C(60)-C(59)-H(59)	120.0
C(59)-C(60)-C(55)	121.1(4)
C(59)-C(60)-H(60)	119.4
C(55)-C(60)-H(60)	119.4

Symmetry transformations used to generate equivalent atoms:

Table 4. Anisotropic displacement parameters ($Å^2 x\ 10^3$)for 5fjc1_0m. The anisotropic displacement factor exponent takes the form: $-2\pi^2[\ h^2 a^{*2} U^{11} + ... + 2\ h\ k\ a^*\ b^*\ U^{12}\ ]$

	U^{11}	U^{22}	U^{33}	U^{23}	U^{13}	U^{12}
Rh(1)	43(1)	38(1)	46(1)	-1(1)	10(1)	7(1)
P(1)	38(1)	37(1)	49(1)	1(1)	8(1)	10(1)
O(1)	55(2)	48(2)	54(2)	-3(1)	4(1)	0(1)
O(2)	43(1)	48(1)	46(1)	0(1)	9(1)	9(1)
O(3)	168(4)	93(3)	60(2)	-13(2)	49(2)	3(3)
C(1A)	68(4)	95(6)	112(8)	-4(5)	-16(4)	8(4)
C(1B)	74(8)	102(11)	112(11)	5(10)	-5(9)	-3(9)
C(2)	62(3)	59(3)	96(3)	-2(2)	1(2)	-2(2)
C(3)	44(2)	46(2)	69(3)	2(2)	3(2)	8(2)
C(4)	48(2)	49(2)	67(3)	6(2)	15(2)	7(2)
C(5)	44(2)	50(2)	53(2)	13(2)	11(2)	19(2)
C(6)	48(2)	67(3)	56(2)	9(2)	11(2)	20(2)
C(7)	85(3)	86(3)	72(3)	30(3)	23(3)	40(3)
C(8)	99(4)	137(6)	72(4)	42(4)	31(3)	53(4)
C(9)	120(5)	160(7)	62(4)	7(4)	37(3)	41(5)
C(10)	137(6)	120(5)	74(4)	-24(4)	42(4)	15(4)
C(11)	92(4)	84(4)	61(3)	-2(3)	23(3)	11(3)
C(12)	83(3)	46(2)	56(3)	-7(2)	18(2)	3(2)
C(13)	43(2)	42(2)	68(3)	9(2)	11(2)	17(2)
C(14)	64(3)	51(2)	74(3)	7(2)	18(2)	22(2)
C(15)	84(4)	84(4)	106(4)	22(3)	31(3)	59(3)
C(16)	54(3)	92(4)	128(5)	31(4)	14(3)	37(3)
C(17)	48(3)	91(4)	134(5)	7(4)	-9(3)	24(3)
C(18)	46(2)	62(3)	101(4)	-6(2)	-3(2)	17(2)
C(19)	47(2)	40(2)	47(2)	-1(2)	8(2)	11(2)
C(20)	52(2)	51(2)	64(3)	5(2)	5(2)	7(2)
C(21)	71(3)	58(3)	76(3)	19(2)	9(2)	2(2)
C(22)	96(4)	57(3)	60(3)	16(2)	7(3)	22(3)
C(23)	70(3)	67(3)	61(3)	6(2)	-3(2)	27(2)
C(24)	51(2)	52(2)	57(2)	1(2)	4(2)	11(2)
C(25)	39(2)	39(2)	50(2)	-5(2)	2(2)	8(1)
C(26)	86(3)	65(3)	55(3)	-1(2)	11(2)	40(2)
C(27)	128(5)	86(4)	79(4)	-14(3)	16(3)	62(4)
C(28)	78(3)	84(3)	60(3)	-22(3)	5(2)	21(3)
C(29)	74(3)	89(3)	45(2)	-3(2)	-6(2)	18(3)

C(30)	69(3)	63(3)	61(3)	2(2)	1(2)	24(2)
Rh(2)	46(1)	39(1)	56(1)	8(1)	4(1)	14(1)
P(2)	32(1)	38(1)	49(1)	6(1)	2(1)	10(1)
O(4)	80(2)	44(2)	55(2)	5(1)	6(1)	24(1)
O(6)	138(3)	96(3)	70(2)	28(2)	41(2)	58(3)
O(5)	64(2)	53(2)	62(2)	9(1)	12(1)	23(1)
C(31A)	150(8)	132(8)	94(6)	5(6)	44(6)	59(7)
C(31B)	146(10)	143(11)	106(9)	-7(10)	44(9)	22(10)
C(32)	130(4)	104(4)	71(3)	-1(3)	27(3)	47(3)
C(33)	74(3)	71(3)	56(2)	7(2)	12(2)	26(2)
C(34)	79(3)	54(2)	62(3)	-1(2)	6(2)	28(2)
C(35)	52(2)	43(2)	57(2)	3(2)	0(2)	16(2)
C(36)	60(2)	40(2)	58(2)	-3(2)	-8(2)	12(2)
C(37)	97(4)	51(2)	60(3)	5(2)	9(2)	24(2)
C(38)	132(5)	57(3)	71(3)	11(2)	14(3)	31(3)
C(39)	134(5)	47(3)	84(4)	9(2)	-6(4)	29(3)
C(40)	113(4)	57(3)	91(4)	-3(3)	-8(3)	43(3)
C(41)	81(3)	53(2)	69(3)	3(2)	1(2)	25(2)
C(42)	71(3)	48(2)	77(3)	29(2)	10(2)	22(2)
C(43)	33(2)	43(2)	58(2)	-2(2)	-1(2)	9(1)
C(44)	43(2)	59(2)	78(3)	10(2)	-2(2)	14(2)
C(45)	51(2)	73(3)	93(4)	1(3)	-16(2)	23(2)
C(46)	36(2)	78(3)	113(4)	-16(3)	-8(2)	18(2)
C(47)	38(2)	105(4)	103(4)	11(3)	10(2)	3(2)
C(48)	44(2)	80(3)	74(3)	18(2)	5(2)	7(2)
C(49)	40(2)	41(2)	42(2)	7(1)	4(1)	8(1)
C(50)	50(2)	55(2)	63(3)	2(2)	-5(2)	15(2)
C(51)	60(3)	67(3)	72(3)	-4(2)	-15(2)	3(2)
C(52)	83(3)	56(3)	70(3)	-12(2)	-7(3)	9(2)
C(53)	79(3)	49(2)	71(3)	-1(2)	8(2)	20(2)
C(54)	49(2)	48(2)	53(2)	4(2)	2(2)	15(2)
C(55)	37(2)	45(2)	45(2)	5(2)	1(1)	15(2)
C(56)	54(2)	54(2)	55(2)	4(2)	-4(2)	12(2)
C(57)	82(3)	78(3)	41(2)	0(2)	1(2)	28(3)
C(58)	68(3)	78(3)	50(2)	18(2)	13(2)	23(2)
C(59)	60(2)	58(2)	62(3)	14(2)	13(2)	10(2)
C(60)	46(2)	48(2)	54(2)	3(2)	8(2)	10(2)

Table 5. Hydrogen coordinates (x 10^4) and isotropic displacement parameters ($Å^2$x 10^3) for 5fjc1_0m.

	x	y	z	U(eq)
H(1A1)	15060	6247	1408	143
H(1A2)	14972	5547	819	143
H(1A3)	14366	5248	1542	143
H(1B1)	15058	6551	1056	152
H(1B2)	14649	6046	338	152
H(1B3)	15000	5550	1010	152
H(2A)	13038	6235	608	91
H(2B)	12442	5958	1337	91
H(2C)	12482	6257	812	91
H(2D)	12936	5743	1453	91
H(4)	12649	5175	-308	66
H(7)	12092	5213	-1424	92
H(8)	12580	5008	-2564	116
H(9)	12149	3623	-3022	133
H(10)	11211	2432	-2371	135
H(11)	10769	2610	-1209	96
H(14)	6026	3192	1017	73
H(15)	3481	3310	880	100
H(16)	1657	2322	192	105
H(17)	2298	1214	-384	109
H(18)	4795	1074	-252	84
H(20)	5393	475	968	68
H(21)	5480	-614	1752	85
H(22)	7733	-591	2414	85
H(23)	9901	527	2295	78
H(24)	9850	1611	1507	65
H(26)	8647	494	111	78
H(27)	9007	-112	-931	109
H(28)	8453	484	-1971	89
H(29)	7560	1726	-1967	85
H(30)	7198	2348	-940	76
H(31A)	1588	9932	6348	179
H(31B)	645	9702	5624	179
H(31C)	2087	10515	5707	179

CRYSTALLOGRAPHIC FRACTIONAL COORDINATES

H(31D)	1213	9254	6391	199
H(31E)	655	8572	5773	199
H(31F)	594	9549	5673	199
H(32A)	2177	8788	5833	117
H(32B)	3622	9587	5951	117
H(32C)	3157	8999	5946	117
H(32D)	3121	9975	5840	117
H(34)	2767	10495	4669	76
H(37)	4434	10520	2628	82
H(38)	4290	11677	1924	102
H(39)	2922	12656	2232	106
H(40)	1753	12489	3244	101
H(41)	1888	11332	3960	79
H(44)	6172	6233	5323	72
H(45)	8749	6321	5601	87
H(46)	10600	7221	5009	91
H(47)	9899	8048	4123	102
H(48)	7308	7983	3841	81
H(50)	1912	6408	3285	68
H(51)	961	5180	2575	84
H(52)	2280	4111	2547	86
H(53)	4516	4241	3247	79
H(54)	5473	5462	3974	60
H(56)	4514	7713	5672	66
H(57)	3259	7271	6662	79
H(58)	1478	5933	6670	77
H(59)	997	5009	5710	73
H(60)	2220	5445	4719	59

Table 6. Torsion angles [°] for 5fjc1_0m.

C(12)-Rh(1)-P(1)-C(19)	-42.4(2)
O(2)-Rh(1)-P(1)-C(19)	136.70(14)
O(1)-Rh(1)-P(1)-C(19)	-48(5)
C(12)-Rh(1)-P(1)-C(25)	-161.8(2)
O(2)-Rh(1)-P(1)-C(25)	17.26(15)
O(1)-Rh(1)-P(1)-C(25)	-167(5)
C(12)-Rh(1)-P(1)-C(13)	78.9(2)
O(2)-Rh(1)-P(1)-C(13)	-102.01(16)
O(1)-Rh(1)-P(1)-C(13)	74(5)
C(12)-Rh(1)-O(1)-C(3)	-177.2(3)
O(2)-Rh(1)-O(1)-C(3)	3.7(3)
P(1)-Rh(1)-O(1)-C(3)	-172(26)
C(12)-Rh(1)-O(2)-C(5)	-106(10)
O(1)-Rh(1)-O(2)-C(5)	-1.5(3)
P(1)-Rh(1)-O(2)-C(5)	178.5(3)
Rh(1)-O(1)-C(3)-C(4)	-4.5(6)
Rh(1)-O(1)-C(3)-C(2)	176.4(3)
C(1B)-C(2)-C(3)-O(1)	130(2)
C(1A)-C(2)-C(3)-O(1)	91.9(9)
C(1B)-C(2)-C(3)-C(4)	-49(2)
C(1A)-C(2)-C(3)-C(4)	-87.2(9)
O(1)-C(3)-C(4)-C(5)	2.0(7)
C(2)-C(3)-C(4)-C(5)	-179.0(4)
Rh(1)-O(2)-C(5)-C(4)	-0.2(5)
Rh(1)-O(2)-C(5)-C(6)	177.3(2)
C(3)-C(4)-C(5)-O(2)	0.7(6)
C(3)-C(4)-C(5)-C(6)	-176.7(4)
O(2)-C(5)-C(6)-C(11)	-28.7(5)
C(4)-C(5)-C(6)-C(11)	148.9(4)
O(2)-C(5)-C(6)-C(7)	154.1(4)
C(4)-C(5)-C(6)-C(7)	-28.3(6)
C(11)-C(6)-C(7)-C(8)	0.5(7)
C(5)-C(6)-C(7)-C(8)	177.7(4)
C(6)-C(7)-C(8)-C(9)	0.1(9)
C(7)-C(8)-C(9)-C(10)	0.2(11)
C(8)-C(9)-C(10)-C(11)	-1.2(11)
C(7)-C(6)-C(11)-C(10)	-1.5(8)
C(5)-C(6)-C(11)-C(10)	-178.7(5)

C(9)-C(10)-C(11)-C(6)	1.8(10)
O(2)-Rh(1)-C(12)-O(3)	73(16)
O(1)-Rh(1)-C(12)-O(3)	-32(11)
P(1)-Rh(1)-C(12)-O(3)	148(11)
C(19)-P(1)-C(13)-C(14)	100.0(3)
C(25)-P(1)-C(13)-C(14)	-152.1(3)
Rh(1)-P(1)-C(13)-C(14)	-26.4(4)
C(19)-P(1)-C(13)-C(18)	-79.7(4)
C(25)-P(1)-C(13)-C(18)	28.2(4)
Rh(1)-P(1)-C(13)-C(18)	153.9(3)
C(18)-C(13)-C(14)-C(15)	0.2(6)
P(1)-C(13)-C(14)-C(15)	-179.5(3)
C(13)-C(14)-C(15)-C(16)	-0.1(7)
C(14)-C(15)-C(16)-C(17)	-0.3(9)
C(15)-C(16)-C(17)-C(18)	0.6(9)
C(16)-C(17)-C(18)-C(13)	-0.5(9)
C(14)-C(13)-C(18)-C(17)	0.1(7)
P(1)-C(13)-C(18)-C(17)	179.8(4)
C(25)-P(1)-C(19)-C(24)	97.7(3)
C(13)-P(1)-C(19)-C(24)	-154.7(3)
Rh(1)-P(1)-C(19)-C(24)	-28.0(3)
C(25)-P(1)-C(19)-C(20)	-79.3(3)
C(13)-P(1)-C(19)-C(20)	28.3(4)
Rh(1)-P(1)-C(19)-C(20)	155.0(3)
C(24)-C(19)-C(20)-C(21)	0.0(6)
P(1)-C(19)-C(20)-C(21)	177.0(4)
C(19)-C(20)-C(21)-C(22)	0.1(7)
C(20)-C(21)-C(22)-C(23)	0.1(8)
C(21)-C(22)-C(23)-C(24)	-0.5(7)
C(22)-C(23)-C(24)-C(19)	0.6(7)
C(20)-C(19)-C(24)-C(23)	-0.4(6)
P(1)-C(19)-C(24)-C(23)	-177.5(3)
C(19)-P(1)-C(25)-C(26)	-19.3(4)
C(13)-P(1)-C(25)-C(26)	-128.2(3)
Rh(1)-P(1)-C(25)-C(26)	106.1(3)
C(19)-P(1)-C(25)-C(30)	163.0(3)
C(13)-P(1)-C(25)-C(30)	54.0(4)
Rh(1)-P(1)-C(25)-C(30)	-71.7(3)
C(30)-C(25)-C(26)-C(27)	0.3(7)
P(1)-C(25)-C(26)-C(27)	-177.6(4)

C(25)-C(26)-C(27)-C(28)	-0.5(9)
C(26)-C(27)-C(28)-C(29)	0.5(9)
C(27)-C(28)-C(29)-C(30)	-0.4(8)
C(28)-C(29)-C(30)-C(25)	0.2(7)
C(26)-C(25)-C(30)-C(29)	-0.1(6)
P(1)-C(25)-C(30)-C(29)	177.7(4)
C(42)-Rh(2)-P(2)-C(55)	-162.8(2)
O(5)-Rh(2)-P(2)-C(55)	18.50(15)
O(4)-Rh(2)-P(2)-C(55)	155(4)
C(42)-Rh(2)-P(2)-C(49)	-43.77(19)
O(5)-Rh(2)-P(2)-C(49)	137.56(15)
O(4)-Rh(2)-P(2)-C(49)	-86(4)
C(42)-Rh(2)-P(2)-C(43)	77.7(2)
O(5)-Rh(2)-P(2)-C(43)	-100.95(16)
O(4)-Rh(2)-P(2)-C(43)	36(4)
C(42)-Rh(2)-O(4)-C(35)	-170.9(3)
O(5)-Rh(2)-O(4)-C(35)	7.8(3)
P(2)-Rh(2)-O(4)-C(35)	-129(4)
C(42)-Rh(2)-O(5)-C(33)	61(6)
O(4)-Rh(2)-O(5)-C(33)	-9.0(4)
P(2)-Rh(2)-O(5)-C(33)	170.2(4)
Rh(2)-O(5)-C(33)-C(34)	6.1(7)
Rh(2)-O(5)-C(33)-C(32)	-172.4(4)
C(31B)-C(32)-C(33)-O(5)	-95.7(17)
C(31A)-C(32)-C(33)-O(5)	-152.3(8)
C(31B)-C(32)-C(33)-C(34)	85.8(18)
C(31A)-C(32)-C(33)-C(34)	29.1(11)
O(5)-C(33)-C(34)-C(35)	2.1(8)
C(32)-C(33)-C(34)-C(35)	-179.5(5)
Rh(2)-O(4)-C(35)-C(34)	-3.7(6)
Rh(2)-O(4)-C(35)-C(36)	175.1(2)
C(33)-C(34)-C(35)-O(4)	-3.2(8)
C(33)-C(34)-C(35)-C(36)	178.0(4)
O(4)-C(35)-C(36)-C(37)	-19.9(5)
C(34)-C(35)-C(36)-C(37)	159.0(4)
O(4)-C(35)-C(36)-C(41)	160.4(4)
C(34)-C(35)-C(36)-C(41)	-20.7(6)
C(41)-C(36)-C(37)-C(38)	-2.1(7)
C(35)-C(36)-C(37)-C(38)	178.2(4)
C(36)-C(37)-C(38)-C(39)	0.7(8)

C(37)-C(38)-C(39)-C(40)	0.8(9)
C(38)-C(39)-C(40)-C(41)	-0.7(9)
C(37)-C(36)-C(41)-C(40)	2.1(7)
C(35)-C(36)-C(41)-C(40)	-178.2(4)
C(39)-C(40)-C(41)-C(36)	-0.7(8)
O(5)-Rh(2)-C(42)-O(6)	28(28)
O(4)-Rh(2)-C(42)-O(6)	98(24)
P(2)-Rh(2)-C(42)-O(6)	-81(24)
C(55)-P(2)-C(43)-C(48)	-157.8(3)
C(49)-P(2)-C(43)-C(48)	95.3(4)
Rh(2)-P(2)-C(43)-C(48)	-31.4(4)
C(55)-P(2)-C(43)-C(44)	24.2(4)
C(49)-P(2)-C(43)-C(44)	-82.6(4)
Rh(2)-P(2)-C(43)-C(44)	150.7(3)
C(48)-C(43)-C(44)-C(45)	0.0(7)
P(2)-C(43)-C(44)-C(45)	177.9(4)
C(43)-C(44)-C(45)-C(46)	-0.1(7)
C(44)-C(45)-C(46)-C(47)	-0.1(8)
C(45)-C(46)-C(47)-C(48)	0.4(8)
C(44)-C(43)-C(48)-C(47)	0.4(7)
P(2)-C(43)-C(48)-C(47)	-177.6(4)
C(46)-C(47)-C(48)-C(43)	-0.6(8)
C(55)-P(2)-C(49)-C(54)	-86.8(3)
C(43)-P(2)-C(49)-C(54)	20.2(4)
Rh(2)-P(2)-C(49)-C(54)	146.9(3)
C(55)-P(2)-C(49)-C(50)	90.2(3)
C(43)-P(2)-C(49)-C(50)	-162.8(3)
Rh(2)-P(2)-C(49)-C(50)	-36.1(3)
C(54)-C(49)-C(50)-C(51)	0.4(6)
P(2)-C(49)-C(50)-C(51)	-176.8(3)
C(49)-C(50)-C(51)-C(52)	-0.8(7)
C(50)-C(51)-C(52)-C(53)	0.9(8)
C(51)-C(52)-C(53)-C(54)	-0.4(8)
C(50)-C(49)-C(54)-C(53)	0.0(6)
P(2)-C(49)-C(54)-C(53)	177.1(3)
C(52)-C(53)-C(54)-C(49)	0.0(7)
C(49)-P(2)-C(55)-C(60)	-7.2(3)
C(43)-P(2)-C(55)-C(60)	-115.8(3)
Rh(2)-P(2)-C(55)-C(60)	118.3(3)
C(49)-P(2)-C(55)-C(56)	175.4(3)

C(43)-P(2)-C(55)-C(56)	66.8(3)
Rh(2)-P(2)-C(55)-C(56)	-59.0(3)
C(60)-C(55)-C(56)-C(57)	-0.7(5)
P(2)-C(55)-C(56)-C(57)	176.8(3)
C(55)-C(56)-C(57)-C(58)	0.0(6)
C(56)-C(57)-C(58)-C(59)	1.1(7)
C(57)-C(58)-C(59)-C(60)	-1.4(7)
C(58)-C(59)-C(60)-C(55)	0.6(6)
C(56)-C(55)-C(60)-C(59)	0.4(5)
P(2)-C(55)-C(60)-C(59)	-177.0(3)

Symmetry transformations used to generate equivalent atoms:

Table 7. Hydrogen bonds for 5fjc1_0m [Å and °].

D-H...A	d(D-H)	d(H...A)	d(D...A)	<(DHA)
C(16)-H(16)...O(2)#1	0.93	2.58	3.358(5)	141.5
C(56)-H(56)...O(5)	0.93	2.60	2.958(5)	103.6

Symmetry transformations used to generate equivalent atoms:

#1 x-1,y,z

B.4 [Rh(bab)(CO)(PPh$_3$)]

Table 1. Crystal data and structure refinement for 6fms2.

Identification code	6fms2	
Empirical formula	C31 H28 O3 P Rh	
Formula weight	582.41	
Temperature	293(2) K	
Wavelength	0.71069 Å	
Crystal system	Monoclinic	
Space group	P 21/c	
Unit cell dimensions	a = 10.034(5) Å	α= 90.000(5)°.
	b = 26.771(5) Å	β= 101.746(5)°.
	c = 9.918(5) Å	γ = 90.000(5)°.
Volume	2608.4(19) Å^3	
Z	4	
Density (calculated)	1.483 Mg/m^3	
Absorption coefficient	0.747 mm^{-1}	
F(000)	1192	
Crystal size	0.17 x 0.10 x 0.02 mm^3	
Theta range for data collection	1.52 to 26.25°.	
Index ranges	-9<=h<=12, -33<=k<=33, -12<=l<=12	
Reflections collected	20242	
Independent reflections	5273 [R(int) = 0.0994]	
Completeness to theta = 26.25°	99.9 %	
Absorption correction	Semi-empirical from equivalents	
Max. and min. transmission	0.9852 and 0.8835	
Refinement method	Full-matrix least-squares on F^2	
Data / restraints / parameters	5273 / 201 / 380	
Goodness-of-fit on F^2	1.105	
Final R indices [I>2sigma(I)]	R1 = 0.0709, wR2 = 0.1283	
R indices (all data)	R1 = 0.1124, wR2 = 0.1441	
Largest diff. peak and hole	1.273 and -0.802 e.Å^{-3}	

Table 2. Atomic coordinates (x 10^4) and equivalent isotropic displacement parameters ($Å^2$x 10^3) for 6fms2. U(eq) is defined as one third of the trace of the orthogonalized U^{ij} tensor.

	x	y	z	U(eq)
Rh	4385(1)	1330(1)	5835(1)	18(1)
P	2771(2)	739(1)	5557(2)	19(1)
O(1)	5721(4)	1924(2)	6071(4)	22(1)
C	5332(7)	1039(3)	7355(8)	32(2)
O	6016(6)	844(2)	8276(6)	59(2)
C(1)	5744(6)	2284(3)	5232(6)	24(1)
C(2A)	4834(8)	2362(4)	3978(8)	27(2)
C(3A)	3728(9)	2054(5)	3480(9)	24(2)
C(4A)	2847(10)	2177(5)	2052(9)	29(2)
C(5A)	2865(13)	1775(6)	1067(10)	43(3)
C(6A)	1893(14)	1891(7)	-352(11)	58(4)
O(2A)	3339(9)	1669(4)	4064(8)	24(2)
C(2B)	4904(19)	2274(11)	3922(19)	26(3)
C(3B)	4000(30)	1901(13)	3350(30)	25(3)
C(4B)	3160(40)	1984(15)	1880(30)	30(3)
C(5B)	3120(50)	1551(18)	1000(30)	40(4)
C(6B)	2080(50)	1630(20)	-390(30)	45(6)
O(2B)	3660(30)	1509(12)	3930(30)	25(3)
C(11)	3086(6)	131(3)	6397(6)	20(2)
C(12)	3420(6)	107(3)	7835(7)	25(2)
C(13)	3612(7)	-351(3)	8492(7)	31(2)
C(14)	3512(7)	-790(3)	7753(8)	32(2)
C(15)	3188(6)	-767(3)	6334(7)	28(2)
C(16)	2976(6)	-316(3)	5664(7)	24(2)
C(21)	1246(6)	962(3)	6111(6)	22(2)
C(22)	453(6)	662(3)	6771(6)	23(2)
C(23)	-697(6)	857(3)	7151(7)	29(2)
C(24)	-1091(7)	1339(4)	6818(7)	36(2)
C(25)	-308(7)	1646(3)	6156(7)	37(2)
C(26)	860(7)	1456(3)	5804(7)	30(2)
C(31)	2179(6)	588(2)	3741(6)	19(1)
C(32)	796(6)	602(3)	3090(6)	21(2)
C(33)	423(7)	504(3)	1690(7)	25(2)
C(34)	1387(7)	388(3)	933(7)	27(2)
C(35)	2735(7)	361(3)	1564(7)	36(2)

CRYSTALLOGRAPHIC FRACTIONAL COORDINATES				
C(36)	3132(7)	468(3)	2970(7)	30(2)
C(41)	6853(7)	2660(3)	5700(7)	31(2)
C(42)	7130(9)	3046(4)	4935(9)	54(3)
C(43)	8245(9)	3362(3)	5381(9)	52(2)
C(44)	9048(9)	3278(3)	6631(8)	44(2)
C(45)	8791(9)	2919(4)	7452(10)	53(2)
C(46)	7685(8)	2609(3)	6988(8)	43(2)

Table 3. Bond lengths [Å] and angles [°] for 6fms2.

Rh-C	1.790(7)
Rh-O(2B)	1.94(3)
Rh-O(1)	2.062(4)
Rh-O(2A)	2.063(8)
Rh-P	2.2408(19)
P-C(31)	1.824(6)
P-C(11)	1.827(7)
P-C(21)	1.828(7)
O(1)-C(1)	1.277(8)
C-O	1.150(8)
C(1)-C(2B)	1.398(17)
C(1)-C(2A)	1.401(10)
C(1)-C(41)	1.501(9)
C(2A)-C(3A)	1.391(10)
C(2A)-H(2A)	0.9300
C(3A)-O(2A)	1.281(9)
C(3A)-C(4A)	1.545(10)
C(4A)-C(5A)	1.455(13)
C(4A)-H(4A1)	0.9700
C(4A)-H(4A2)	0.9700
C(5A)-C(6A)	1.572(12)
C(5A)-H(5A1)	0.9700
C(5A)-H(5A2)	0.9700
C(6A)-H(6A1)	0.9600
C(6A)-H(6A2)	0.9600
C(6A)-H(6A3)	0.9600
C(2B)-C(3B)	1.390(17)
C(2B)-H(2B)	0.9300
C(3B)-O(2B)	1.279(17)
C(3B)-C(4B)	1.547(17)
C(4B)-C(5B)	1.44(2)
C(4B)-H(4B1)	0.9700
C(4B)-H(4B2)	0.9700
C(5B)-C(6B)	1.56(2)
C(5B)-H(5B1)	0.9700
C(5B)-H(5B2)	0.9700
C(6B)-H(6B1)	0.9600
C(6B)-H(6B2)	0.9600

C(6B)-H(6B3)	0.9600
C(11)-C(16)	1.392(9)
C(11)-C(12)	1.399(9)
C(12)-C(13)	1.383(10)
C(12)-H(12)	0.9300
C(13)-C(14)	1.377(10)
C(13)-H(13)	0.9300
C(14)-C(15)	1.380(10)
C(14)-H(14)	0.9300
C(15)-C(16)	1.374(10)
C(15)-H(15)	0.9300
C(16)-H(16)	0.9300
C(21)-C(22)	1.386(9)
C(21)-C(26)	1.393(10)
C(22)-C(23)	1.387(9)
C(22)-H(22)	0.9300
C(23)-C(24)	1.371(11)
C(23)-H(23)	0.9300
C(24)-C(25)	1.391(11)
C(24)-H(24)	0.9300
C(25)-C(26)	1.387(10)
C(25)-H(25)	0.9300
C(26)-H(26)	0.9300
C(31)-C(36)	1.378(9)
C(31)-C(32)	1.407(8)
C(32)-C(33)	1.388(9)
C(32)-H(32)	0.9300
C(33)-C(34)	1.375(9)
C(33)-H(33)	0.9300
C(34)-C(35)	1.371(9)
C(34)-H(34)	0.9300
C(35)-C(36)	1.400(9)
C(35)-H(35)	0.9300
C(36)-H(36)	0.9300
C(41)-C(42)	1.345(11)
C(41)-C(46)	1.382(10)
C(42)-C(43)	1.400(11)
C(42)-H(42)	0.9300
C(43)-C(44)	1.353(11)
C(43)-H(43)	0.9300

C(44)-C(45)	1.319(12)
C(44)-H(44)	0.9300
C(45)-C(46)	1.388(11)
C(45)-H(45)	0.9300
C(46)-H(46)	0.9300

C-Rh-O(2B)	163.2(12)
C-Rh-O(1)	91.1(2)
O(2B)-Rh-O(1)	91.5(9)
C-Rh-O(2A)	178.5(3)
O(2B)-Rh-O(2A)	15.9(10)
O(1)-Rh-O(2A)	88.0(2)
C-Rh-P	92.4(2)
O(2B)-Rh-P	86.4(8)
O(1)-Rh-P	174.52(13)
O(2A)-Rh-P	88.6(2)
C(31)-P-C(11)	104.1(3)
C(31)-P-C(21)	104.2(3)
C(11)-P-C(21)	103.4(3)
C(31)-P-Rh	111.1(2)
C(11)-P-Rh	121.3(2)
C(21)-P-Rh	111.1(2)
C(1)-O(1)-Rh	127.3(4)
O-C-Rh	174.8(7)
O(1)-C(1)-C(2B)	120.2(14)
O(1)-C(1)-C(2A)	126.6(7)
C(2B)-C(1)-C(2A)	10.5(12)
O(1)-C(1)-C(41)	114.5(6)
C(2B)-C(1)-C(41)	124.7(14)
C(2A)-C(1)-C(41)	118.9(7)
C(3A)-C(2A)-C(1)	123.7(8)
C(3A)-C(2A)-H(2A)	118.1
C(1)-C(2A)-H(2A)	118.1
O(2A)-C(3A)-C(2A)	127.7(7)
O(2A)-C(3A)-C(4A)	114.6(7)
C(2A)-C(3A)-C(4A)	117.7(7)
C(5A)-C(4A)-C(3A)	112.0(8)
C(5A)-C(4A)-H(4A1)	109.2
C(3A)-C(4A)-H(4A1)	109.2
C(5A)-C(4A)-H(4A2)	109.2

C(3A)-C(4A)-H(4A2)	109.2
H(4A1)-C(4A)-H(4A2)	107.9
C(4A)-C(5A)-C(6A)	111.4(9)
C(4A)-C(5A)-H(5A1)	109.3
C(6A)-C(5A)-H(5A1)	109.3
C(4A)-C(5A)-H(5A2)	109.3
C(6A)-C(5A)-H(5A2)	109.3
H(5A1)-C(5A)-H(5A2)	108.0
C(5A)-C(6A)-H(6A1)	109.5
C(5A)-C(6A)-H(6A2)	109.5
H(6A1)-C(6A)-H(6A2)	109.5
C(5A)-C(6A)-H(6A3)	109.5
H(6A1)-C(6A)-H(6A3)	109.5
H(6A2)-C(6A)-H(6A3)	109.5
C(3A)-O(2A)-Rh	126.1(5)
C(3B)-C(2B)-C(1)	128(2)
C(3B)-C(2B)-H(2B)	116.0
C(1)-C(2B)-H(2B)	116.0
O(2B)-C(3B)-C(2B)	127.9(17)
O(2B)-C(3B)-C(4B)	113.8(15)
C(2B)-C(3B)-C(4B)	117.9(17)
C(5B)-C(4B)-C(3B)	113(2)
C(5B)-C(4B)-H(4B1)	108.9
C(3B)-C(4B)-H(4B1)	108.9
C(5B)-C(4B)-H(4B2)	108.9
C(3B)-C(4B)-H(4B2)	108.9
H(4B1)-C(4B)-H(4B2)	107.7
C(4B)-C(5B)-C(6B)	111(2)
C(4B)-C(5B)-H(5B1)	109.5
C(6B)-C(5B)-H(5B1)	109.5
C(4B)-C(5B)-H(5B2)	109.5
C(6B)-C(5B)-H(5B2)	109.5
H(5B1)-C(5B)-H(5B2)	108.1
C(5B)-C(6B)-H(6B1)	109.5
C(5B)-C(6B)-H(6B2)	109.5
H(6B1)-C(6B)-H(6B2)	109.5
C(5B)-C(6B)-H(6B3)	109.5
H(6B1)-C(6B)-H(6B3)	109.5
H(6B2)-C(6B)-H(6B3)	109.5
C(3B)-O(2B)-Rh	124.3(18)

C(16)-C(11)-C(12)	118.0(6)
C(16)-C(11)-P	122.7(5)
C(12)-C(11)-P	119.3(5)
C(13)-C(12)-C(11)	120.2(7)
C(13)-C(12)-H(12)	119.9
C(11)-C(12)-H(12)	119.9
C(14)-C(13)-C(12)	121.1(7)
C(14)-C(13)-H(13)	119.4
C(12)-C(13)-H(13)	119.4
C(13)-C(14)-C(15)	118.8(7)
C(13)-C(14)-H(14)	120.6
C(15)-C(14)-H(14)	120.6
C(16)-C(15)-C(14)	120.9(7)
C(16)-C(15)-H(15)	119.6
C(14)-C(15)-H(15)	119.6
C(15)-C(16)-C(11)	121.0(6)
C(15)-C(16)-H(16)	119.5
C(11)-C(16)-H(16)	119.5
C(22)-C(21)-C(26)	119.5(6)
C(22)-C(21)-P	123.3(6)
C(26)-C(21)-P	117.2(5)
C(21)-C(22)-C(23)	120.0(7)
C(21)-C(22)-H(22)	120.0
C(23)-C(22)-H(22)	120.0
C(24)-C(23)-C(22)	120.2(7)
C(24)-C(23)-H(23)	119.9
C(22)-C(23)-H(23)	119.9
C(23)-C(24)-C(25)	120.5(7)
C(23)-C(24)-H(24)	119.7
C(25)-C(24)-H(24)	119.7
C(26)-C(25)-C(24)	119.3(8)
C(26)-C(25)-H(25)	120.4
C(24)-C(25)-H(25)	120.4
C(25)-C(26)-C(21)	120.4(7)
C(25)-C(26)-H(26)	119.8
C(21)-C(26)-H(26)	119.8
C(36)-C(31)-C(32)	118.9(6)
C(36)-C(31)-P	118.5(5)
C(32)-C(31)-P	122.7(5)
C(33)-C(32)-C(31)	119.6(6)

C(33)-C(32)-H(32)	120.2
C(31)-C(32)-H(32)	120.2
C(34)-C(33)-C(32)	120.8(6)
C(34)-C(33)-H(33)	119.6
C(32)-C(33)-H(33)	119.6
C(35)-C(34)-C(33)	120.1(6)
C(35)-C(34)-H(34)	120.0
C(33)-C(34)-H(34)	120.0
C(34)-C(35)-C(36)	119.9(7)
C(34)-C(35)-H(35)	120.1
C(36)-C(35)-H(35)	120.1
C(31)-C(36)-C(35)	120.8(6)
C(31)-C(36)-H(36)	119.6
C(35)-C(36)-H(36)	119.6
C(42)-C(41)-C(46)	116.2(7)
C(42)-C(41)-C(1)	124.4(7)
C(46)-C(41)-C(1)	119.3(7)
C(41)-C(42)-C(43)	122.0(8)
C(41)-C(42)-H(42)	119.0
C(43)-C(42)-H(42)	119.0
C(44)-C(43)-C(42)	118.6(8)
C(44)-C(43)-H(43)	120.7
C(42)-C(43)-H(43)	120.7
C(45)-C(44)-C(43)	122.1(9)
C(45)-C(44)-H(44)	118.9
C(43)-C(44)-H(44)	118.9
C(44)-C(45)-C(46)	118.4(9)
C(44)-C(45)-H(45)	120.8
C(46)-C(45)-H(45)	120.8
C(41)-C(46)-C(45)	122.6(8)
C(41)-C(46)-H(46)	118.7
C(45)-C(46)-H(46)	118.7

Symmetry transformations used to generate equivalent atoms:

Table 4. Anisotropic displacement parameters ($Å^2 x\ 10^3$)for 6fms2. The anisotropic displacement factor exponent takes the form: $-2\pi^2[\ h^2 a^{*2} U^{11} + ... + 2\ h\ k\ a^*\ b^*\ U^{12}\ ]$

	U^{11}	U^{22}	U^{33}	U^{23}	U^{13}	U^{12}
Rh	17(1)	25(1)	11(1)	2(1)	1(1)	-1(1)
P	16(1)	29(1)	12(1)	1(1)	2(1)	-1(1)
O(1)	21(2)	25(3)	17(2)	1(2)	0(2)	-3(2)
C	27(4)	35(5)	30(4)	10(4)	-3(3)	-14(3)
O	52(4)	69(5)	43(4)	28(3)	-21(3)	-23(3)
C(1)	21(3)	32(3)	20(3)	4(2)	3(2)	-7(3)
C(2A)	20(3)	35(4)	25(3)	10(3)	-1(2)	-7(3)
C(3A)	18(3)	33(5)	21(3)	10(3)	1(2)	-4(3)
C(4A)	20(4)	35(6)	27(3)	9(3)	-5(3)	-5(4)
C(5A)	52(5)	46(7)	26(3)	5(4)	-1(4)	4(5)
C(6A)	53(7)	84(11)	30(4)	-1(6)	-10(4)	-13(8)
O(2A)	19(4)	31(5)	21(3)	7(3)	1(3)	-4(3)
C(2B)	21(5)	34(5)	23(4)	10(4)	-1(4)	-8(4)
C(3B)	19(5)	34(5)	20(4)	11(4)	-1(4)	-7(4)
C(4B)	29(5)	37(6)	20(4)	9(4)	-3(4)	-5(5)
C(5B)	47(8)	44(8)	23(5)	4(6)	-5(6)	5(8)
C(6B)	55(11)	57(13)	18(8)	0(8)	-4(8)	8(12)
O(2B)	19(6)	33(7)	21(5)	10(5)	1(5)	-6(5)
C(11)	14(3)	30(4)	16(3)	3(3)	5(3)	-1(3)
C(12)	17(3)	43(5)	15(3)	-1(3)	4(3)	2(3)
C(13)	26(4)	47(5)	21(4)	12(4)	8(3)	-1(4)
C(14)	27(4)	31(5)	40(5)	10(4)	11(3)	5(3)
C(15)	24(4)	31(4)	29(4)	-5(3)	6(3)	-4(3)
C(16)	17(3)	38(5)	17(3)	4(3)	4(3)	-2(3)
C(21)	16(3)	39(4)	7(3)	-5(3)	-4(2)	-1(3)
C(22)	15(3)	38(4)	16(3)	1(3)	1(3)	1(3)
C(23)	15(3)	52(5)	19(4)	-1(3)	2(3)	-7(3)
C(24)	17(3)	66(6)	24(4)	5(4)	4(3)	13(4)
C(25)	40(5)	48(5)	27(4)	10(4)	14(4)	17(4)
C(26)	25(4)	41(5)	27(4)	10(3)	10(3)	11(3)
C(31)	20(3)	24(4)	10(3)	8(3)	1(3)	-2(3)
C(32)	19(3)	32(4)	15(3)	5(3)	6(3)	2(3)
C(33)	23(3)	31(4)	18(4)	2(3)	-7(3)	-3(3)
C(34)	28(4)	43(5)	10(3)	-3(3)	2(3)	-4(3)
C(35)	29(4)	64(6)	16(4)	-12(4)	5(3)	-7(4)

CRYSTALLOGRAPHIC FRACTIONAL COORDINATES						
C(36)	17(3)	52(5)	20(4)	-7(3)	3(3)	-5(3)
C(41)	35(4)	36(5)	21(4)	6(3)	4(3)	-9(4)
C(42)	61(6)	63(7)	30(5)	8(4)	-13(4)	-11(5)
C(43)	60(6)	48(6)	45(5)	7(4)	1(4)	-24(5)
C(44)	53(5)	37(5)	35(5)	-5(4)	-8(4)	0(4)
C(45)	50(5)	56(6)	47(6)	-6(5)	-3(4)	-14(5)
C(46)	43(5)	51(6)	31(4)	-1(4)	-1(4)	-14(4)

Table 5. Hydrogen coordinates (x 10^4) and isotropic displacement parameters ($Å^2$x 10^3) for 6fms2.

	x	y	z	U(eq)
H(2A)	4978	2636	3449	33
H(4A1)	1916	2236	2147	34
H(4A2)	3181	2481	1705	34
H(5A1)	2584	1466	1437	51
H(5A2)	3787	1731	926	51
H(6A1)	1903	1615	-968	87
H(6A2)	2198	2188	-742	87
H(6A3)	984	1941	-212	87
H(2B)	4957	2550	3365	32
H(4B1)	2235	2073	1931	35
H(4B2)	3546	2262	1458	35
H(5B1)	2865	1260	1475	48
H(5B2)	4021	1492	817	48
H(6B1)	2269	1390	-1053	67
H(6B2)	2162	1959	-716	67
H(6B3)	1174	1574	-241	67
H(12)	3514	399	8352	30
H(13)	3811	-363	9449	37
H(14)	3661	-1096	8202	38
H(15)	3111	-1061	5824	34
H(16)	2757	-309	4707	29
H(22)	692	330	6959	28
H(23)	-1204	659	7633	35
H(24)	-1887	1462	7037	43
H(25)	-566	1976	5951	45
H(26)	1388	1658	5359	36
H(32)	135	675	3595	26
H(33)	-490	517	1257	31
H(34)	1125	328	-7	33
H(35)	3384	272	1059	43
H(36)	4049	458	3389	36
H(42)	6564	3105	4084	65
H(43)	8429	3624	4829	63
H(44)	9806	3480	6920	53

CRYSTALLOGRAPHIC FRACTIONAL COORDINATES				
H(45)	9337	2875	8321	63
H(46)	7495	2357	7566	51

Table 6. Torsion angles [°] for 6fms2.

C-Rh-P-C(31)	-141.6(3)
O(2B)-Rh-P-C(31)	21.6(12)
O(1)-Rh-P-C(31)	89.1(14)
O(2A)-Rh-P-C(31)	37.4(4)
C-Rh-P-C(11)	-18.9(4)
O(2B)-Rh-P-C(11)	144.3(12)
O(1)-Rh-P-C(11)	-148.2(13)
O(2A)-Rh-P-C(11)	160.0(4)
C-Rh-P-C(21)	102.9(3)
O(2B)-Rh-P-C(21)	-94.0(12)
O(1)-Rh-P-C(21)	-26.4(14)
O(2A)-Rh-P-C(21)	-78.2(4)
C-Rh-O(1)-C(1)	173.3(5)
O(2B)-Rh-O(1)-C(1)	9.9(13)
O(2A)-Rh-O(1)-C(1)	-5.6(6)
P-Rh-O(1)-C(1)	-57.4(16)
O(2B)-Rh-C-O	27(9)
O(1)-Rh-C-O	-71(8)
O(2A)-Rh-C-O	-22(21)
P-Rh-C-O	113(8)
Rh-O(1)-C(1)-C(2B)	-8.0(11)
Rh-O(1)-C(1)-C(2A)	2.0(9)
Rh-O(1)-C(1)-C(41)	-179.8(4)
O(1)-C(1)-C(2A)-C(3A)	1.7(12)
C(2B)-C(1)-C(2A)-C(3A)	57(7)
C(41)-C(1)-C(2A)-C(3A)	-176.5(8)
C(1)-C(2A)-C(3A)-O(2A)	2.0(15)
C(1)-C(2A)-C(3A)-C(4A)	-177.7(8)
O(2A)-C(3A)-C(4A)-C(5A)	-61.8(11)
C(2A)-C(3A)-C(4A)-C(5A)	118.0(10)
C(3A)-C(4A)-C(5A)-C(6A)	176.4(9)
C(2A)-C(3A)-O(2A)-Rh	-8.5(14)
C(4A)-C(3A)-O(2A)-Rh	171.2(6)
C-Rh-O(2A)-C(3A)	-41(16)
O(2B)-Rh-O(2A)-C(3A)	-94(4)
O(1)-Rh-O(2A)-C(3A)	8.6(8)
P-Rh-O(2A)-C(3A)	-175.7(8)
O(1)-C(1)-C(2B)-C(3B)	-1(2)

C(2A)-C(1)-C(2B)-C(3B)	-131(8)
C(41)-C(1)-C(2B)-C(3B)	170(2)
C(1)-C(2B)-C(3B)-O(2B)	6(4)
C(1)-C(2B)-C(3B)-C(4B)	178.9(19)
O(2B)-C(3B)-C(4B)-C(5B)	-51(4)
C(2B)-C(3B)-C(4B)-C(5B)	135(3)
C(3B)-C(4B)-C(5B)-C(6B)	171(3)
C(2B)-C(3B)-O(2B)-Rh	-1(5)
C(4B)-C(3B)-O(2B)-Rh	-174(2)
C-Rh-O(2B)-C(3B)	-104(4)
O(1)-Rh-O(2B)-C(3B)	-5(3)
O(2A)-Rh-O(2B)-C(3B)	72(4)
P-Rh-O(2B)-C(3B)	170(3)
C(31)-P-C(11)-C(16)	5.1(6)
C(21)-P-C(11)-C(16)	113.8(5)
Rh-P-C(11)-C(16)	-120.8(5)
C(31)-P-C(11)-C(12)	-173.3(5)
C(21)-P-C(11)-C(12)	-64.6(5)
Rh-P-C(11)-C(12)	60.8(5)
C(16)-C(11)-C(12)-C(13)	-0.9(9)
P-C(11)-C(12)-C(13)	177.5(5)
C(11)-C(12)-C(13)-C(14)	1.6(10)
C(12)-C(13)-C(14)-C(15)	-1.4(10)
C(13)-C(14)-C(15)-C(16)	0.5(10)
C(14)-C(15)-C(16)-C(11)	0.1(10)
C(12)-C(11)-C(16)-C(15)	0.1(9)
P-C(11)-C(16)-C(15)	-178.3(5)
C(31)-P-C(21)-C(22)	97.1(6)
C(11)-P-C(21)-C(22)	-11.5(6)
Rh-P-C(21)-C(22)	-143.2(5)
C(31)-P-C(21)-C(26)	-80.8(6)
C(11)-P-C(21)-C(26)	170.6(5)
Rh-P-C(21)-C(26)	38.9(5)
C(26)-C(21)-C(22)-C(23)	-1.6(9)
P-C(21)-C(22)-C(23)	-179.5(5)
C(21)-C(22)-C(23)-C(24)	3.1(10)
C(22)-C(23)-C(24)-C(25)	-3.1(11)
C(23)-C(24)-C(25)-C(26)	1.6(11)
C(24)-C(25)-C(26)-C(21)	-0.1(11)
C(22)-C(21)-C(26)-C(25)	0.1(10)

P-C(21)-C(26)-C(25)	178.1(5)
C(11)-P-C(31)-C(36)	-80.2(6)
C(21)-P-C(31)-C(36)	171.8(6)
Rh-P-C(31)-C(36)	52.0(6)
C(11)-P-C(31)-C(32)	101.6(6)
C(21)-P-C(31)-C(32)	-6.5(6)
Rh-P-C(31)-C(32)	-126.3(5)
C(36)-C(31)-C(32)-C(33)	-1.2(10)
P-C(31)-C(32)-C(33)	177.1(5)
C(31)-C(32)-C(33)-C(34)	0.8(11)
C(32)-C(33)-C(34)-C(35)	0.9(11)
C(33)-C(34)-C(35)-C(36)	-2.1(12)
C(32)-C(31)-C(36)-C(35)	-0.1(11)
P-C(31)-C(36)-C(35)	-178.4(6)
C(34)-C(35)-C(36)-C(31)	1.7(12)
O(1)-C(1)-C(41)-C(42)	174.6(8)
C(2B)-C(1)-C(41)-C(42)	3.3(15)
C(2A)-C(1)-C(41)-C(42)	-7.0(12)
O(1)-C(1)-C(41)-C(46)	-3.9(10)
C(2B)-C(1)-C(41)-C(46)	-175.2(12)
C(2A)-C(1)-C(41)-C(46)	174.6(8)
C(46)-C(41)-C(42)-C(43)	3.6(14)
C(1)-C(41)-C(42)-C(43)	-174.9(8)
C(41)-C(42)-C(43)-C(44)	-1.2(15)
C(42)-C(43)-C(44)-C(45)	-2.0(15)
C(43)-C(44)-C(45)-C(46)	2.3(15)
C(42)-C(41)-C(46)-C(45)	-3.3(13)
C(1)-C(41)-C(46)-C(45)	175.3(8)
C(44)-C(45)-C(46)-C(41)	0.5(14)

Symmetry transformations used to generate equivalent atoms:

Table 7. Hydrogen bonds for 6fms2 [Å and °].

D-H...A	d(D-H)	d(H...A)	d(D...A)	<(DHA)
C(13)-H(13)...O#1	0.93	2.57	3.416(9)	151.0
C(26)-H(26)...O(2A)	0.93	2.55	3.352(11)	144.6
C(46)-H(46)...O(1)	0.93	2.37	2.709(9)	101.0

Symmetry transformations used to generate equivalent atoms:

#1 -x+1,-y,-z+2

B.5 [Rh(bav)(CO)(PPh_3)]

Table 1. Crystal data and structure refinement for 6fms1_0m.

Identification code	6fms1_0m	
Empirical formula	C32 H30 O3 P Rh	
Formula weight	596.44	
Temperature	293(2) K	
Wavelength	0.71069 Å	
Crystal system	Monoclinic	
Space group	P 21/c	
Unit cell dimensions	a = 10.261(5) Å	α= 90.000(5)°.
	b = 25.393(5) Å	β= 102.444(5)°.
	c = 10.793(5) Å	γ = 90.000(5)°.
Volume	2746.1(19) $Å^3$	
Z	4	
Density (calculated)	1.443 Mg/m^3	
Absorption coefficient	0.711 mm^{-1}	
F(000)	1224	
Crystal size	0.33 x 0.28 x 0.28 mm^3	
Theta range for data collection	1.60 to 28.37°.	
Index ranges	-9<=h<=13, -33<=k<=33, -14<=l<=14	
Reflections collected	27483	
Independent reflections	6865 [R(int) = 0.0316]	
Completeness to theta = 28.37°	99.8 %	
Absorption correction	Semi-empirical from equivalents	
Max. and min. transmission	0.8257 and 0.7991	
Refinement method	Full-matrix least-squares on F^2	
Data / restraints / parameters	6865 / 0 / 335	
Goodness-of-fit on F^2	1.207	
Final R indices [I>2sigma(I)]	R1 = 0.0613, wR2 = 0.1246	
R indices (all data)	R1 = 0.0671, wR2 = 0.1279	
Largest diff. peak and hole	2.836 and -1.940 $e.Å^{-3}$	

Table 2. Atomic coordinates (x 10^4) and equivalent isotropic displacement parameters ($Å^2$x 10^3) for 6fms1_0m. U(eq) is defined as one third of the trace of the orthogonalized U^{ij} tensor.

	x	y	z	U(eq)
Rh	5594(1)	1412(1)	4018(1)	20(1)
P	7214(1)	803(1)	4301(1)	18(1)
O(1)	4223(3)	2023(1)	3828(3)	24(1)
O(2)	6528(3)	1723(1)	5706(3)	30(1)
C(1)	4155(4)	2382(2)	4637(4)	23(1)
C(2)	5042(5)	2444(2)	5799(5)	27(1)
C(3)	6153(5)	2130(2)	6256(4)	26(1)
C(4)	7030(5)	2261(2)	7529(5)	28(1)
C(5)	6960(5)	1826(2)	8467(5)	28(1)
C(6)	7864(5)	1949(2)	9785(5)	36(1)
C(7)	7825(7)	1512(3)	10725(6)	54(2)
C	4742(4)	1117(2)	2545(5)	26(1)
O	4154(4)	938(2)	1619(4)	47(1)
C(11)	7655(4)	589(2)	5944(4)	22(1)
C(12)	6610(5)	463(2)	6541(5)	35(1)
C(13)	6879(6)	290(2)	7780(6)	43(1)
C(14)	8190(6)	243(2)	8454(5)	38(1)
C(15)	9239(5)	373(2)	7885(4)	28(1)
C(16)	8967(4)	542(2)	6633(4)	22(1)
C(21)	8772(4)	1062(2)	3997(4)	18(1)
C(22)	9074(4)	1591(2)	4257(4)	22(1)
C(23)	10247(4)	1806(2)	4034(4)	26(1)
C(24)	11133(4)	1496(2)	3554(4)	26(1)
C(25)	10843(4)	966(2)	3301(4)	26(1)
C(26)	9670(4)	750(2)	3525(4)	24(1)
C(31)	6983(4)	188(2)	3392(4)	20(1)
C(32)	6756(4)	216(2)	2066(4)	24(1)
C(33)	6581(5)	-245(2)	1345(5)	29(1)
C(34)	6622(5)	-728(2)	1928(5)	35(1)
C(35)	6849(5)	-759(2)	3236(6)	37(1)
C(36)	7033(5)	-301(2)	3968(5)	30(1)
C(41)	3001(4)	2756(2)	4259(5)	24(1)
C(42)	2527(5)	3051(2)	5161(5)	27(1)
C(43)	1397(5)	3362(2)	4810(5)	31(1)
C(44)	735(5)	3386(2)	3545(5)	32(1)

C(45)	1211(5)	3115(2)	2646(5)	34(1)
C(46)	2352(5)	2798(2)	3016(5)	30(1)

Table 3. Bond lengths [Å] and angles [°] for 6fms1_0m.

Rh-C	1.805(5)
Rh-O(2)	2.027(3)
Rh-O(1)	2.074(3)
Rh-P	2.2429(13)
P-C(11)	1.817(5)
P-C(21)	1.823(4)
P-C(31)	1.833(4)
O(1)-C(1)	1.274(5)
O(2)-C(3)	1.291(5)
C(1)-C(2)	1.391(6)
C(1)-C(41)	1.505(6)
C(2)-C(3)	1.391(6)
C(2)-H(2)	0.9300
C(3)-C(4)	1.508(6)
C(4)-C(5)	1.510(7)
C(4)-H(4A)	0.9700
C(4)-H(4B)	0.9700
C(5)-C(6)	1.554(7)
C(5)-H(5A)	0.9700
C(5)-H(5B)	0.9700
C(6)-C(7)	1.511(8)
C(6)-H(6A)	0.9700
C(6)-H(6B)	0.9700
C(7)-H(7A)	0.9600
C(7)-H(7B)	0.9600
C(7)-H(7C)	0.9600
C-O	1.143(6)
C(11)-C(16)	1.396(6)
C(11)-C(12)	1.402(6)
C(12)-C(13)	1.377(8)
C(12)-H(12)	0.9300
C(13)-C(14)	1.389(8)
C(13)-H(13)	0.9300
C(14)-C(15)	1.390(7)
C(14)-H(14)	0.9300
C(15)-C(16)	1.388(6)
C(15)-H(15)	0.9300
C(16)-H(16)	0.9300

C(21)-C(22)	1.392(6)
C(21)-C(26)	1.392(6)
C(22)-C(23)	1.389(6)
C(22)-H(22)	0.9300
C(23)-C(24)	1.385(6)
C(23)-H(23)	0.9300
C(24)-C(25)	1.395(6)
C(24)-H(24)	0.9300
C(25)-C(26)	1.390(6)
C(25)-H(25)	0.9300
C(26)-H(26)	0.9300
C(31)-C(36)	1.383(6)
C(31)-C(32)	1.401(6)
C(32)-C(33)	1.394(6)
C(32)-H(32)	0.9300
C(33)-C(34)	1.376(7)
C(33)-H(33)	0.9300
C(34)-C(35)	1.383(8)
C(34)-H(34)	0.9300
C(35)-C(36)	1.396(7)
C(35)-H(35)	0.9300
C(36)-H(36)	0.9300
C(41)-C(46)	1.368(7)
C(41)-C(42)	1.396(6)
C(42)-C(43)	1.386(6)
C(42)-H(42)	0.9300
C(43)-C(44)	1.390(7)
C(43)-H(43)	0.9300
C(44)-C(45)	1.363(7)
C(44)-H(44)	0.9300
C(45)-C(46)	1.407(7)
C(45)-H(45)	0.9300
C(46)-H(46)	0.9300

C-Rh-O(2)	177.98(19)
C-Rh-O(1)	91.99(16)
O(2)-Rh-O(1)	88.68(13)
C-Rh-P	92.13(13)
O(2)-Rh-P	87.30(10)
O(1)-Rh-P	174.93(9)

C(11)-P-C(21)	103.90(19)
C(11)-P-C(31)	104.1(2)
C(21)-P-C(31)	103.25(19)
C(11)-P-Rh	111.14(15)
C(21)-P-Rh	112.31(14)
C(31)-P-Rh	120.56(14)
C(1)-O(1)-Rh	127.1(3)
C(3)-O(2)-Rh	126.5(3)
O(1)-C(1)-C(2)	125.3(4)
O(1)-C(1)-C(41)	115.0(4)
C(2)-C(1)-C(41)	119.8(4)
C(1)-C(2)-C(3)	125.6(4)
C(1)-C(2)-H(2)	117.2
C(3)-C(2)-H(2)	117.2
O(2)-C(3)-C(2)	126.7(4)
O(2)-C(3)-C(4)	114.6(4)
C(2)-C(3)-C(4)	118.6(4)
C(3)-C(4)-C(5)	110.1(4)
C(3)-C(4)-H(4A)	109.6
C(5)-C(4)-H(4A)	109.6
C(3)-C(4)-H(4B)	109.6
C(5)-C(4)-H(4B)	109.6
H(4A)-C(4)-H(4B)	108.2
C(4)-C(5)-C(6)	111.2(4)
C(4)-C(5)-H(5A)	109.4
C(6)-C(5)-H(5A)	109.4
C(4)-C(5)-H(5B)	109.4
C(6)-C(5)-H(5B)	109.4
H(5A)-C(5)-H(5B)	108.0
C(7)-C(6)-C(5)	111.7(5)
C(7)-C(6)-H(6A)	109.3
C(5)-C(6)-H(6A)	109.3
C(7)-C(6)-H(6B)	109.3
C(5)-C(6)-H(6B)	109.3
H(6A)-C(6)-H(6B)	107.9
C(6)-C(7)-H(7A)	109.5
C(6)-C(7)-H(7B)	109.5
H(7A)-C(7)-H(7B)	109.5
C(6)-C(7)-H(7C)	109.5
H(7A)-C(7)-H(7C)	109.5

H(7B)-C(7)-H(7C)	109.5
O-C-Rh	177.2(4)
C(16)-C(11)-C(12)	118.8(4)
C(16)-C(11)-P	123.7(3)
C(12)-C(11)-P	117.6(4)
C(13)-C(12)-C(11)	120.3(5)
C(13)-C(12)-H(12)	119.8
C(11)-C(12)-H(12)	119.8
C(12)-C(13)-C(14)	120.4(5)
C(12)-C(13)-H(13)	119.8
C(14)-C(13)-H(13)	119.8
C(13)-C(14)-C(15)	120.2(5)
C(13)-C(14)-H(14)	119.9
C(15)-C(14)-H(14)	119.9
C(16)-C(15)-C(14)	119.4(5)
C(16)-C(15)-H(15)	120.3
C(14)-C(15)-H(15)	120.3
C(15)-C(16)-C(11)	120.9(4)
C(15)-C(16)-H(16)	119.5
C(11)-C(16)-H(16)	119.5
C(22)-C(21)-C(26)	119.1(4)
C(22)-C(21)-P	118.6(3)
C(26)-C(21)-P	122.4(3)
C(23)-C(22)-C(21)	120.6(4)
C(23)-C(22)-H(22)	119.7
C(21)-C(22)-H(22)	119.7
C(24)-C(23)-C(22)	120.2(4)
C(24)-C(23)-H(23)	119.9
C(22)-C(23)-H(23)	119.9
C(23)-C(24)-C(25)	119.5(4)
C(23)-C(24)-H(24)	120.2
C(25)-C(24)-H(24)	120.2
C(26)-C(25)-C(24)	120.2(4)
C(26)-C(25)-H(25)	119.9
C(24)-C(25)-H(25)	119.9
C(25)-C(26)-C(21)	120.4(4)
C(25)-C(26)-H(26)	119.8
C(21)-C(26)-H(26)	119.8
C(36)-C(31)-C(32)	119.0(4)
C(36)-C(31)-P	122.4(4)

C(32)-C(31)-P	118.5(3)
C(33)-C(32)-C(31)	120.1(4)
C(33)-C(32)-H(32)	119.9
C(31)-C(32)-H(32)	119.9
C(34)-C(33)-C(32)	120.3(5)
C(34)-C(33)-H(33)	119.8
C(32)-C(33)-H(33)	119.8
C(33)-C(34)-C(35)	119.9(5)
C(33)-C(34)-H(34)	120.0
C(35)-C(34)-H(34)	120.0
C(34)-C(35)-C(36)	120.2(5)
C(34)-C(35)-H(35)	119.9
C(36)-C(35)-H(35)	119.9
C(31)-C(36)-C(35)	120.4(5)
C(31)-C(36)-H(36)	119.8
C(35)-C(36)-H(36)	119.8
C(46)-C(41)-C(42)	118.3(4)
C(46)-C(41)-C(1)	120.2(4)
C(42)-C(41)-C(1)	121.5(4)
C(43)-C(42)-C(41)	120.8(5)
C(43)-C(42)-H(42)	119.6
C(41)-C(42)-H(42)	119.6
C(42)-C(43)-C(44)	119.8(5)
C(42)-C(43)-H(43)	120.1
C(44)-C(43)-H(43)	120.1
C(45)-C(44)-C(43)	120.1(5)
C(45)-C(44)-H(44)	119.9
C(43)-C(44)-H(44)	119.9
C(44)-C(45)-C(46)	119.5(5)
C(44)-C(45)-H(45)	120.3
C(46)-C(45)-H(45)	120.3
C(41)-C(46)-C(45)	121.4(5)
C(41)-C(46)-H(46)	119.3
C(45)-C(46)-H(46)	119.3

Symmetry transformations used to generate equivalent atoms:

Table 4. Anisotropic displacement parameters ($Å^2 x\ 10^3$)for 6fms1_0m. The anisotropic displacement factor exponent takes the form: $-2\pi^2[\ h^2 a^{*2} U^{11} + ... + 2\ h\ k\ a^*\ b^*\ U^{12}\ ]$

	U^{11}	U^{22}	U^{33}	U^{23}	U^{13}	U^{12}
Rh	14(1)	20(1)	26(1)	-9(1)	3(1)	-1(1)
P	14(1)	20(1)	22(1)	-3(1)	4(1)	-1(1)
O(1)	20(2)	19(2)	34(2)	-9(1)	7(1)	2(1)
O(2)	21(2)	34(2)	34(2)	-12(2)	0(1)	3(1)
C(1)	18(2)	22(2)	31(2)	-3(2)	10(2)	-3(2)
C(2)	24(2)	26(2)	32(2)	-9(2)	6(2)	0(2)
C(3)	24(2)	24(2)	29(2)	-3(2)	4(2)	-1(2)
C(4)	26(2)	23(2)	33(2)	-2(2)	0(2)	1(2)
C(5)	24(2)	27(2)	34(2)	2(2)	5(2)	-1(2)
C(6)	33(3)	45(3)	29(3)	5(2)	4(2)	7(2)
C(7)	69(4)	56(4)	37(3)	12(3)	8(3)	20(3)
C	24(2)	17(2)	34(2)	-2(2)	0(2)	10(2)
O	54(2)	38(2)	37(2)	-17(2)	-20(2)	20(2)
C(11)	22(2)	23(2)	22(2)	-1(2)	8(2)	-2(2)
C(12)	27(2)	38(3)	41(3)	1(2)	14(2)	-4(2)
C(13)	46(3)	43(3)	47(3)	14(3)	28(3)	0(3)
C(14)	52(3)	39(3)	27(2)	9(2)	18(2)	4(2)
C(15)	32(2)	28(2)	24(2)	1(2)	5(2)	2(2)
C(16)	22(2)	21(2)	23(2)	-3(2)	7(2)	-2(2)
C(21)	13(2)	23(2)	18(2)	1(2)	0(1)	-1(2)
C(22)	19(2)	26(2)	19(2)	-3(2)	2(2)	-1(2)
C(23)	25(2)	24(2)	28(2)	-4(2)	5(2)	-8(2)
C(24)	17(2)	31(2)	29(2)	2(2)	4(2)	-6(2)
C(25)	20(2)	27(2)	31(2)	2(2)	8(2)	3(2)
C(26)	21(2)	21(2)	28(2)	2(2)	5(2)	1(2)
C(31)	12(2)	20(2)	27(2)	-5(2)	5(2)	0(2)
C(32)	21(2)	20(2)	31(2)	-2(2)	7(2)	0(2)
C(33)	25(2)	31(2)	31(2)	-10(2)	5(2)	-1(2)
C(34)	29(3)	26(2)	47(3)	-14(2)	4(2)	0(2)
C(35)	38(3)	19(2)	51(3)	1(2)	5(2)	2(2)
C(36)	25(2)	25(2)	37(3)	4(2)	4(2)	2(2)
C(41)	21(2)	15(2)	37(2)	-1(2)	12(2)	-1(2)
C(42)	28(2)	25(2)	27(2)	-1(2)	4(2)	0(2)
C(43)	28(2)	28(2)	39(3)	-2(2)	8(2)	6(2)
C(44)	29(2)	28(2)	38(3)	4(2)	2(2)	6(2)

CRYSTALLOGRAPHIC FRACTIONAL COORDINATES						
C(45)	34(3)	28(2)	41(3)	4(2)	9(2)	2(2)
C(46)	30(2)	25(2)	35(3)	-1(2)	11(2)	2(2)

Table 5. Hydrogen coordinates (x 10^4) and isotropic displacement parameters ($Å^2$x 10^3) for 6fms1_0m.

	x	y	z	U(eq)
H(2)	4878	2718	6315	33
H(4A)	6740	2590	7838	34
H(4B)	7945	2304	7441	34
H(5A)	7242	1497	8150	34
H(5B)	6044	1784	8555	34
H(6A)	8776	1999	9692	43
H(6B)	7570	2275	10108	43
H(7A)	6949	1492	10901	81
H(7B)	8465	1583	11497	81
H(7C)	8038	1183	10375	81
H(12)	5729	496	6099	41
H(13)	6181	205	8167	51
H(14)	8365	123	9288	45
H(15)	10116	348	8340	34
H(16)	9669	624	6247	26
H(22)	8486	1801	4583	26
H(23)	10438	2160	4208	31
H(24)	11916	1641	3402	31
H(25)	11435	755	2981	31
H(26)	9483	396	3359	28
H(32)	6722	541	1667	29
H(33)	6435	-225	465	35
H(34)	6497	-1034	1442	42
H(35)	6879	-1086	3630	44
H(36)	7190	-324	4847	35
H(42)	2974	3038	6007	32
H(43)	1084	3553	5420	38
H(44)	-35	3588	3311	39
H(45)	785	3140	1796	41
H(46)	2672	2612	2401	35

Table 6. Torsion angles [°] for 6fms1_0m.

C-Rh-P-C(11)	-138.1(2)
O(2)-Rh-P-C(11)	39.98(19)
O(1)-Rh-P-C(11)	77.6(11)
C-Rh-P-C(21)	106.0(2)
O(2)-Rh-P-C(21)	-75.93(18)
O(1)-Rh-P-C(21)	-38.3(11)
C-Rh-P-C(31)	-16.0(2)
O(2)-Rh-P-C(31)	162.1(2)
O(1)-Rh-P-C(31)	-160.3(11)
C-Rh-O(1)-C(1)	173.8(4)
O(2)-Rh-O(1)-C(1)	-4.3(4)
P-Rh-O(1)-C(1)	-41.8(13)
C-Rh-O(2)-C(3)	-106(5)
O(1)-Rh-O(2)-C(3)	3.2(4)
P-Rh-O(2)-C(3)	-179.9(4)
Rh-O(1)-C(1)-C(2)	3.1(6)
Rh-O(1)-C(1)-C(41)	-176.7(3)
O(1)-C(1)-C(2)-C(3)	0.9(8)
C(41)-C(1)-C(2)-C(3)	-179.3(4)
Rh-O(2)-C(3)-C(2)	-0.9(7)
Rh-O(2)-C(3)-C(4)	178.4(3)
C(1)-C(2)-C(3)-O(2)	-2.2(8)
C(1)-C(2)-C(3)-C(4)	178.6(4)
O(2)-C(3)-C(4)-C(5)	-65.2(5)
C(2)-C(3)-C(4)-C(5)	114.2(5)
C(3)-C(4)-C(5)-C(6)	179.6(4)
C(4)-C(5)-C(6)-C(7)	-178.8(5)
O(2)-Rh-C-O	81(11)
O(1)-Rh-C-O	-28(10)
P-Rh-C-O	155(10)
C(21)-P-C(11)-C(16)	-12.4(4)
C(31)-P-C(11)-C(16)	95.4(4)
Rh-P-C(11)-C(16)	-133.4(3)
C(21)-P-C(11)-C(12)	167.8(4)
C(31)-P-C(11)-C(12)	-84.4(4)
Rh-P-C(11)-C(12)	46.9(4)
C(16)-C(11)-C(12)-C(13)	-0.8(8)
P-C(11)-C(12)-C(13)	179.0(4)

C(11)-C(12)-C(13)-C(14)	0.5(9)
C(12)-C(13)-C(14)-C(15)	0.5(9)
C(13)-C(14)-C(15)-C(16)	-1.2(8)
C(14)-C(15)-C(16)-C(11)	1.0(7)
C(12)-C(11)-C(16)-C(15)	0.0(7)
P-C(11)-C(16)-C(15)	-179.7(3)
C(11)-P-C(21)-C(22)	-88.6(4)
C(31)-P-C(21)-C(22)	163.0(3)
Rh-P-C(21)-C(22)	31.6(4)
C(11)-P-C(21)-C(26)	90.9(4)
C(31)-P-C(21)-C(26)	-17.5(4)
Rh-P-C(21)-C(26)	-148.9(3)
C(26)-C(21)-C(22)-C(23)	0.9(6)
P-C(21)-C(22)-C(23)	-179.6(3)
C(21)-C(22)-C(23)-C(24)	-0.3(7)
C(22)-C(23)-C(24)-C(25)	-0.3(7)
C(23)-C(24)-C(25)-C(26)	0.2(7)
C(24)-C(25)-C(26)-C(21)	0.4(7)
C(22)-C(21)-C(26)-C(25)	-0.9(6)
P-C(21)-C(26)-C(25)	179.6(3)
C(11)-P-C(31)-C(36)	5.6(4)
C(21)-P-C(31)-C(36)	113.9(4)
Rh-P-C(31)-C(36)	-119.8(3)
C(11)-P-C(31)-C(32)	-174.0(3)
C(21)-P-C(31)-C(32)	-65.7(4)
Rh-P-C(31)-C(32)	60.6(4)
C(36)-C(31)-C(32)-C(33)	0.2(6)
P-C(31)-C(32)-C(33)	179.8(3)
C(31)-C(32)-C(33)-C(34)	0.4(7)
C(32)-C(33)-C(34)-C(35)	-0.5(7)
C(33)-C(34)-C(35)-C(36)	0.2(8)
C(32)-C(31)-C(36)-C(35)	-0.5(7)
P-C(31)-C(36)-C(35)	179.9(4)
C(34)-C(35)-C(36)-C(31)	0.4(8)
O(1)-C(1)-C(41)-C(46)	-18.6(6)
C(2)-C(1)-C(41)-C(46)	161.6(4)
O(1)-C(1)-C(41)-C(42)	158.6(4)
C(2)-C(1)-C(41)-C(42)	-21.2(6)
C(46)-C(41)-C(42)-C(43)	2.5(7)
C(1)-C(41)-C(42)-C(43)	-174.8(4)

C(41)-C(42)-C(43)-C(44)	-0.8(7)
C(42)-C(43)-C(44)-C(45)	-1.5(8)
C(43)-C(44)-C(45)-C(46)	2.0(8)
C(42)-C(41)-C(46)-C(45)	-2.0(7)
C(1)-C(41)-C(46)-C(45)	175.3(4)
C(44)-C(45)-C(46)-C(41)	-0.2(8)

Symmetry transformations used to generate equivalent atoms:

Table 7. Hydrogen bonds for 6fms1_0m [Å and °].

D-H...A	d(D-H)	d(H...A)	d(D...A)	<(DHA)
C(22)-H(22)...O(2)	0.93	2.57	3.339(6)	140.5
C(24)-H(24)...O(1)#1	0.93	2.51	3.395(5)	159.7

Symmetry transformations used to generate equivalent atoms:

#1 x+1,y,z

Abstract.

β-diketones $PhCOCH_2COR$, prepared with lithium diisopropaylamide under Schlenk conditions, were complexed to rhodium(I) to form dicarbonylrhodium(I) and monocarbonylphosphinerhodium(I) complexes (Ph = phenyl).

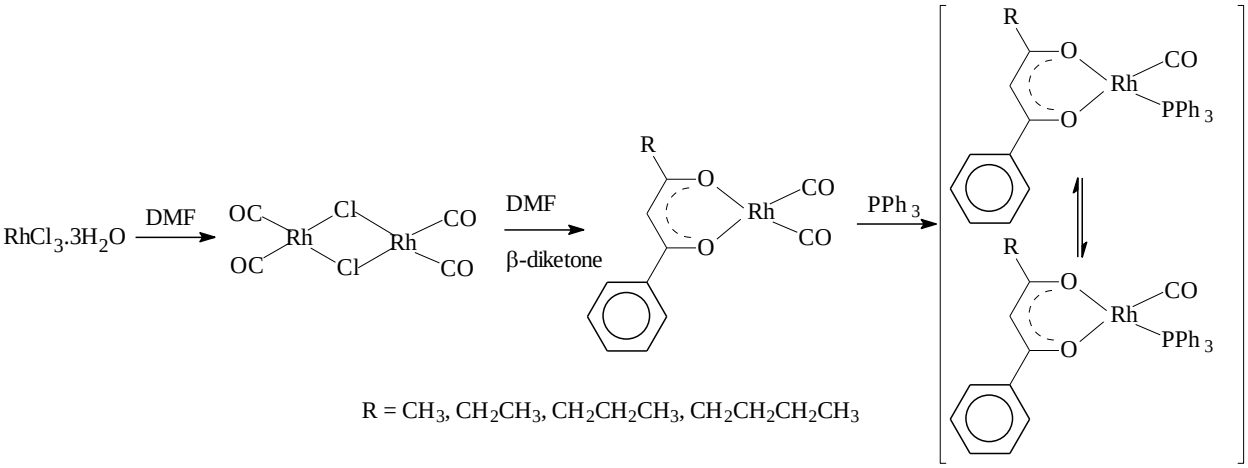

The $pK_a^{/}$ values of the β-diketones and group electronegativities of the R substituents is determined as (R, $pK_a^{/}$, χ_R) = (CH_3, 8.81, 2.21), (CH_2CH_3, 9.28, 2.31), ($CH_2CH_2CH_3$, 9.17, 2.41) and ($CH_2CH_2CH_2CH_3$, 9.25, 2.22). The equilibrium constant between the keto and enol tautomers of the β-diketones is determined as K_c = [keto]/[enol] = 0.084 (Hba), 0.122 (Hbap), 0.087 (Hbab) and 0.086 (Hbav) respectively.

^1H NMR studies indicated that all [Rh(PhCOCHCOR)(CO)(PPh_3)] complexes with an unsymmetrical β-diketonato ligand, are composed of two isomers in a thermodynamic equilibrium with each other. Chemical kinetics of the oxidative addition of methyl iodide to rhodium(I)carbonyl centers has significant implications in catalysis, especially when followed by methyl migration to give the acyl derivative[1]. This oxidative addition reaction to the [Rh(PhCOCHCOR)(CO)(PPh_3)] complexes was followed, utilizing UV/VIS, IR, ^1H and ^{31}P NMR techniques. Three consecutive sets of reactions involving isomers of at least two distinctly different classes of Rh^{III}-alkyl and two different classes of Rh^{III}-acyl species were observed. The second Rh^{III}-acyl species is not generally observed.

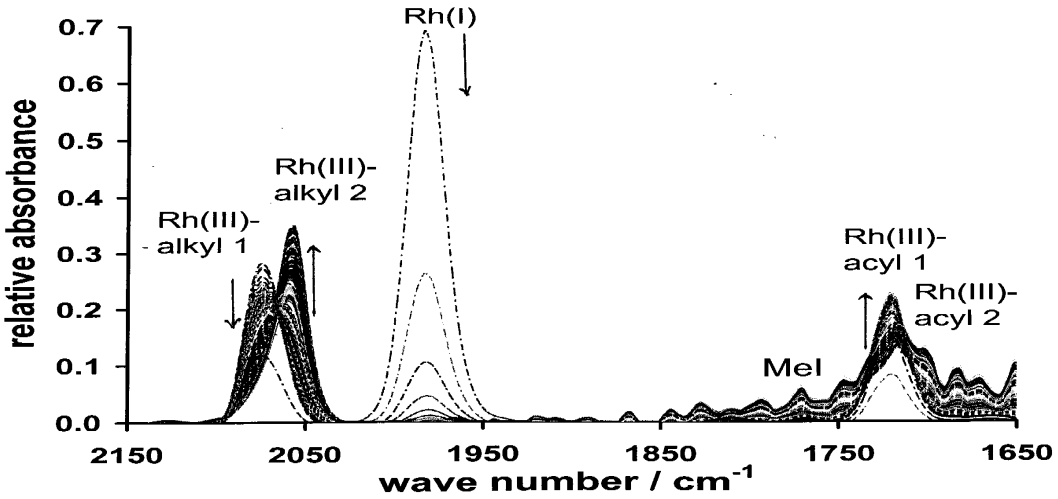

A general reaction sequence for the oxidative addition of iodomethane to all [Rh(β-diketonato)(CO)(PPh_3)] complexes is:

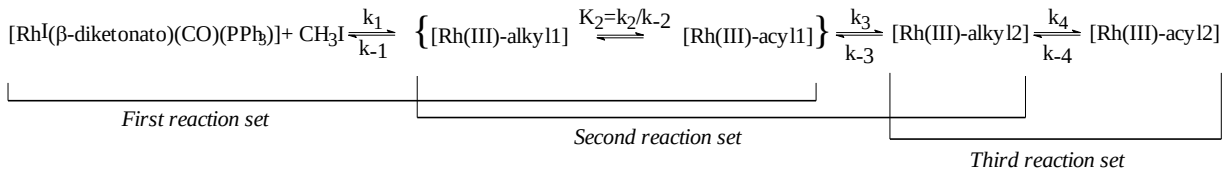

The significant and rare feature of the crystal structure of [Rh(bap)(CO)(PPh_3)], where two crystals, the *cis* and the *trans* isomers are found in the same crystal lattice was solved crystallographically.

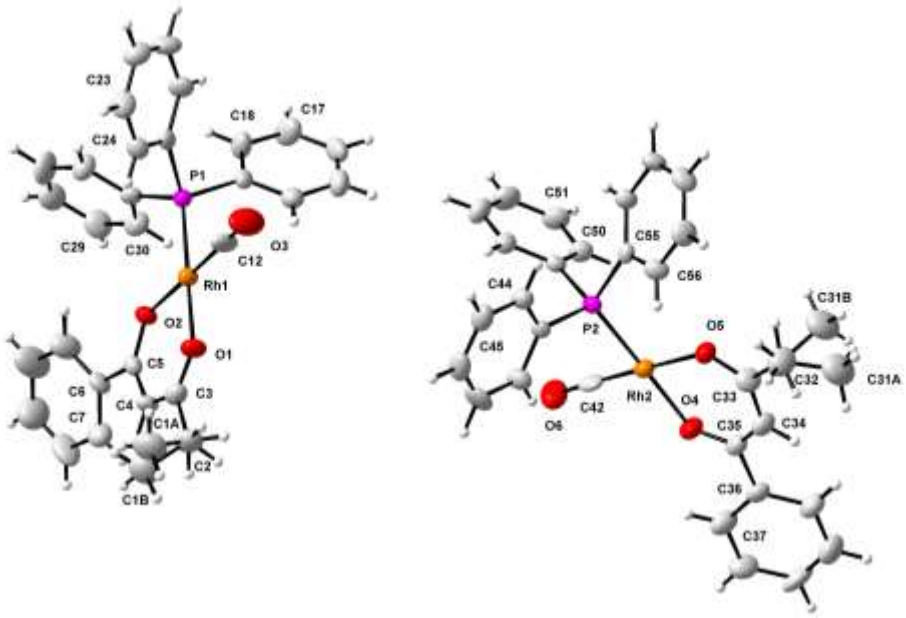

Keywords

β-diketone, rhodium(I), oxidative addition, p$K_a^{/}$, group electronegativity, crystallography.

Opsomming.

β-diketone $PhCOCH_2COR$, is berei met lithium diisopropaylamied onder Schlenk kondisies, is gekomplekseer met rodium(I) om dikarbonielrodium(I) en monokarbonielfosfienrodium(I) komplekse te vorm (Ph = feniel).

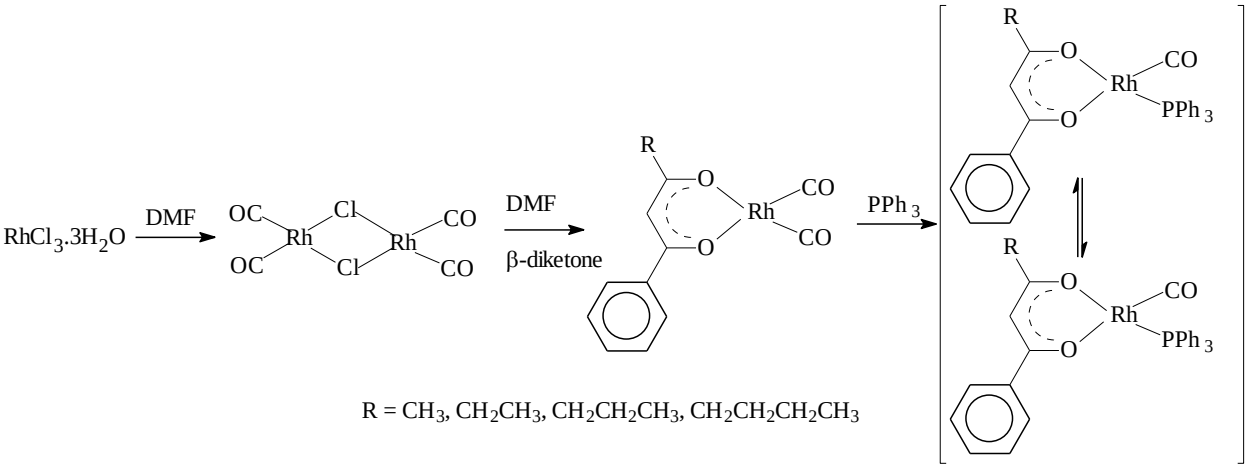

Die $pK_a^{/}$ waardes van die β-diketone en die groep elektron-negatiwiteite van die R groepe is bereken as (R, $pK_a^{/}$, χ_R) = (CH_3, 8.81, 2.21), (CH_2CH_3, 9.28, 2.31), ($CH_2CH_2CH_3$, 9.17, 2.41) and ($CH_2CH_2CH_2CH_3$, 9.25, 2.22). Die ewewigskonstante tussen die keto en enol tautomere van die β-diketone is bereken as K_c = [keto]/[enol] = 0.084 (Hba), 0.122 (Hbap), 0.087 (Hbab) en 0.086 (Hbav) respektiewelik.

^{1}H-KMR-studies het aangetoon dat alle [Rh(PhCOCHCOR)(CO)(PPh_3)] komplekse met 'n onsimmetriese β-diketonato ligand, uit minstens twee isomere in 'n termodinamiese ewewig met mekaar, bestaan. Die chemiese kinetika van die oksidatiewe addisie van metieljodied aan rodium(I)-karboniel komplekse het verreikende implikasies in katalise, in besonder indien opgevolg word deur metiel migrasie om die asiel kompleks te gee[1]. Die oksidatiewe addisie reaksie aan [Rh(PhCOCHCOR)(CO)(PPh_3)] komplekse deur middel van infra-rooi, UV/sigbaar, ^{1}H-KMR en ^{31}P-KMR-spektroskopie ondersoek. Drie opeenvolgende reaksies wat ten minste twee verkillende klasse van Rh^{III}-alkiel en twee verkillende klasse van Rh^{III}-asiel spesies behels, is waargeneem. Die tweede Rh^{III}-asiel spesie word nie algemeen waargeneem nie.

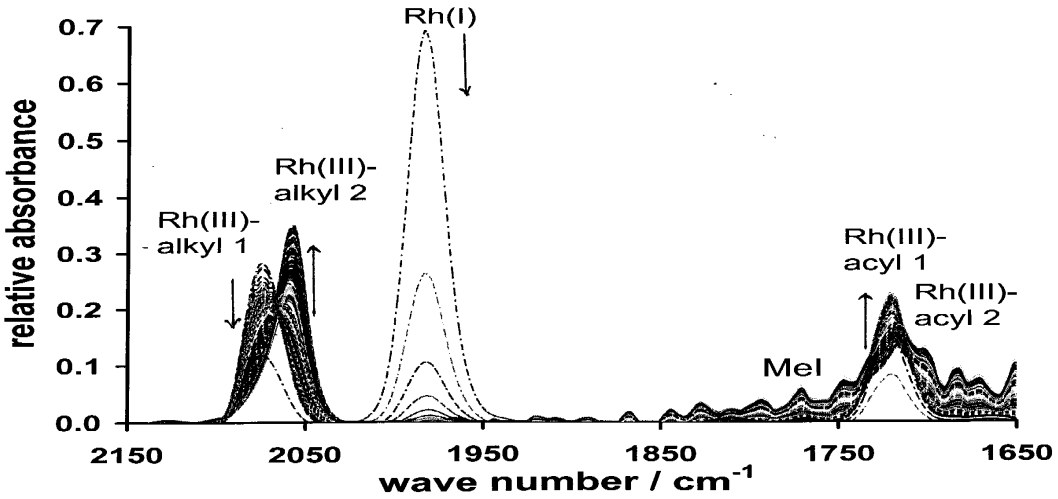

'n Algemene reaksieskema vir die oksidatiewe addisie van metieljodied aan alle [Rh(β-diketonato)(CO)(PPh_3)] komplekse is:

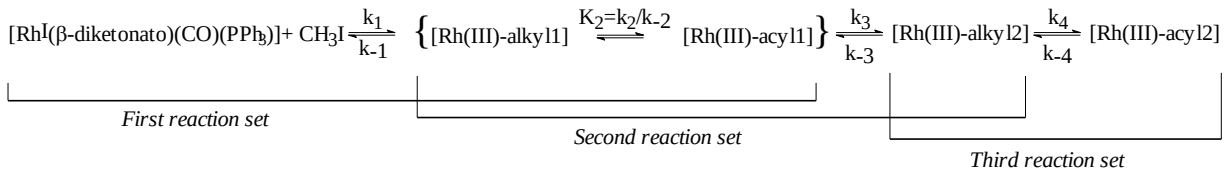

Die impak en rariteit van die kristal struktuur van [Rh(bap)(CO)(PPh_3)] is dat twee kristalle, die *cis* en die *trans* isomere in dieselfde eenheidsel kristallografies gevind is.